INVESTIGATING ORGANIC MATTER-MINERAL INTERACTIONS AT THE MOLECULAR SCALE: AN INTEGRATED FIELD AND LABORATORY STUDY

by

Chunmei Chen

A dissertation submitted to the Faculty of the University of Delaware in partial fulfillment of the requirements for the degree of Doctor of Philosophy in Plant and Soil Sciences

Fall 2013

ProQuest LLC.
789 East Eisenhower Parkway
P.O. Box 1346
Ann Arbor, MI 48106 - 1346

INVESTIGATING ORGANIC MATTER-MINERAL INTERACTIONS AT THE MOLECULAR SCALE: AN INTEGRATED FIELD AND LABORATORY STUDY

by

Chunmei Chen

Approved: _____
Blake C. Mayers, Ph.D.
Chair of the Department of Plant and Soil Sciences

Approved: _____
Mark Regier, Ph.D.
Dean of the College of Agricultural and Natural Resources

Approved: _____
James G. Richards, Ph.D.
Vice Provost for Graduate and Professional Education

I certify that I have read this dissertation and that in my opinion it meets the academic and professional standard required by the University as a dissertation for the degree of Doctor of Philosophy.

Signed: _____

Donald L.Sparks, Ph.D.
Professor in charge of dissertation

I certify that I have read this dissertation and that in my opinion it meets the academic and professional standard required by the University as a dissertation for the degree of Doctor of Philosophy.

Signed: _____

Kyungsoo Yoo, Ph.D.
Member of dissertation committee

I certify that I have read this dissertation and that in my opinion it meets the academic and professional standard required by the University as a dissertation for the degree of Doctor of Philosophy.

Signed: _____

Anthony Aufdenkampe, Ph.D.
Member of dissertation committee

I certify that I have read this dissertation and that in my opinion it meets the academic and professional standard required by the University as a dissertation for the degree of Doctor of Philosophy.

Signed: _____

Peter Leinweber, Ph.D.
Member of dissertation committee

ACKNOWLEDGMENTS

Pursuit of my doctoral degree in the United States has been both a hard and rewarding experience. The research would not be possible without the encouragement, support, and collaboration of numerous individuals.

I am most appreciative to my advisor, Dr. Donald L. Sparks for the opportunity of pursuing my Ph.D. in his research group. I have greatly benefited from his professional advice, excellent mentorship and support. Much of my work within and beyond this thesis would be impossible without his caring, patience and guidance. I am grateful to my committee members: Dr. Kyungsoo Yoo and Dr. Anthony Aufdenkampe for providing me help with field site selections and sampling, as well as numerous valuable advice and enlightening discussions. I can still remember the days of digging soil pits in the Stroud watershed with Dr. Yoo and Dr. Aufdenkampe . I have also benefited from the knowledge that Dr. Yoo taught me to characterize soils in the field. Many thanks are due to my committee member: Dr. Peter Leinweber, for his kind help with Py-FIMS analysis and data interpretation, as well as valuable suggestions on my research.

I have had the pleasure to work at National Laboratories and would like to acknowledge those with whom I have worked. I would like to particularly thank Drs. Jay Dynes, Jian Wang, and Tom Regier at the Canadian Light Source for their

patience, tutorials, help and guidance in STXM and NEXAFS experiments and data processing. I cannot thank enough Dr. Ravi Kukkadapu at the Environmental Molecular Science Laboratory of Pacific National Laboratory, for his help on Mössbauer analysis and valuable discussions on Mössbauer data interpretation. A portion of this research was done at beamlines X11A and X27A (NSLS), 4-1, 4-3, and 11-2 (SSRL), and 5.3.2 (ALS). I am grateful for the use of the facilities and support provided by the staff members at these beamlines.

I would like to thank my wonderful group members; my research would not have been possible without their support and assistance. Special acknowledgement is due to Jerry Hendricks for assistance with travelling arrangements and the laboratory supplies I needed. I also thank the staff of the Department of Plant and Soil sciences for their help: Amy Broadhurst, Kathy Fleischut, Sue Biddle, and t laboratory technicians Cathy Olsen and Karen Gartley in the UD Soil Testing Laboratory.

I am deeply thankful to my parents, who strongly supported me and provided me continuous love and understanding as I pursued this degree in Delaware, which is so far away from them. Although we are physically distant, our bonds became strengthened during my doctoral studies. Finally I would like to give my special thanks to my husband, who has supported me in countless ways. We have been through a lot of unexpected, difficult times, as we moved to Delaware for our Ph.D. studies. He is always standing by me with positive thinking and cheering me up during those hard times. I feel so lucky to be with him.

TABLE OF CONTENTS

LIST OF TABLES

LIST OF FIGURES

ABSTRACT

Intimate association of organic matter (OM) with soil mineral phases has been acknowledged as a fundamental mechanism for stabilizing organic compounds against biological degradation, controlling the long-term sequestration of organic matter in terrestrial ecosystems. However, the fundamental nature of the interactions between OM and soil mineral components is not well understood. Since both the organic and mineral phases of soils are involved, the extent to which OM interacts with minerals depends on both mineralogical properties as well as the composition of OM involved. Landscape topographic positions have important impacts on biogeochemical C and mineral cycling processes, and thus affect OM-mineral interaction.

We applied NEXAFS spectroscopy and Py-FIMS to characterize organic matter in soils obtained from a pasture hillslope. Results showed that the recalcitrant aromatic C and lignin was enriched in the subsoils and poorly-drained footslope locations. In addition, organic compounds had a greater thermal stability in the subsoils and poorly-drained footslope locations. STXM coupled with NEXAFS spectroscopy was used to investigate C associations with Ca, Fe, Al and Si species in pasture soils at the nanometer scale. Good C-Ca spatial correlations were found for soil clay fractions with no $CaCO_3$, suggesting a strong role of Ca in organo-mineral assemblage formation. C showed similar correlation with Fe to Al & Si, implying a

similar association of Fe oxides and aluminosilicates in organo-mineral assemblages. Iron oxides are important for OM-mineral interactions because of their abundance and reactivity. Iron is susceptible to redox variations along landscape gradients over a wide range of spatial scales. We applied Fe K-edge EXAFS and Mössbauer spectroscopy to characterize Fe mineral phases in a floodplain soil profile with spatially sharp redox gradients. Results showed that the permanent reducing conditions led to a strong reduction in the structural Fe(III) in the phyllosilicates, in addition to a complete reductive dissolution of Fe(III) oxides. Therefore the importance of Fe oxides in OM-mineral interaction should be expected to decrease in the low-redox conditions.

Poorly-crystalline Fe oxy-hydroxide ferrihydrite, because of its high surface area, is of particular importance in OM retention. Organic matter-ferrihydrite complexes can be formed by either adsorption or coprecipitation. We compared these interactions by preparing OM-ferrihydrite complexes at varying C:Fe ratios using dissolved organic matter extracted from a forest litter layer. Our study clearly demonstrated that coprecipiation could result in greater C retention capacity and C stability than adsorption. Iron EXAFS measurements revealed that coprecipitation of OM with Fe led to the formation of OM-Fe(III) cation complexes in the solid phase by suppressing ferrihydrite formation, which might be related to a significantly greater organic carbon retention for coprecipitation than adsorption. Formation of strong complexes between carboxyl C functional groups and ferrihydrite via a ligand exhange mechanism was evidenced by FTIR and C (1s) NEXAFS analysis for both adsorption and coprecipitation.

The ripening of ferrihydrite to more stable and hence less reactive phases such as goethite is catalyzed by surface reaction with aqueous Fe(II). While ferrihydrite within most natural environments contains high concentrations of co-precipitated organic matter, little is known regarding the impact of this OM on the reactivity of ferrihydrite. We explored the extent, pathways and products of Fe(II)-induced secondary mineralization of OM-Fe coprecipitates by reacting aqueous Fe(II) (0.2 and 2.0 mM) with ferrihydrite containing a range of coprecipitated OM loadings (0-21% C). Results demonstrated that OM copreciptated with ferrihydrite resulted in diminished secondary mineralization and preservation of ferrihydrite. Goethite formation and magnetite nucleation were inhibited by the coprecipitated OM.

Chapter 1

INTRODUCTION

1.1 Literature Review

1.1.1 The Role of Soil Organic Matter in the Global Carbon Cycle

Interest in soil organic matter (SOM) continues to ramp up, with the ongoing concern about steadily increasing levels of atmospheric CO_2. The amount of organic matter (OM) stored in soils represents one of the largest reservoirs of organic carbon on a global scale (Schlesinger, 1995). Globally, soils and surface litter store 2-3 times the amount of carbon (C) present in atmospheric CO_2 (Houghton, 2005). Consequently, any change in the size and the turnover rate of soil C pools may potentially alter the atmospheric CO_2 concentration and the global climate. Soil respiration, which integrates below-ground plant and microbially derived CO_2, is one of the largest annual transfers in the global C budget. The annual global CO_2 flux from soils is estimated to average (± S.D.) 68± 4 Pg C/ yr (Raich and Schlesinger, 1992). Managing soils to increase their carbon storage capacity has been proposed as a means to reduce the rise of CO_2 concentrations in the atmosphere. Increasing soil C storages also improves soil fertility and productivity, and thus provides a clear win-win

situation. Appropriate action, however, requires an understanding of mechanisms governing the long-term residence time of organic matter (OM) in soils. The mechanisms for C stabilization in soils are still not well understood and the ultimate potential for C stabilization in soils is unknown.

1.1.2 Soil Organic Matter Stabilization Mechanisms

Three major mechanisms have been proposed for soil organic stabilization process (Baldock and Skjemstad, 2000; Sollins et al., 1996; von Lützow et al., 2006). They are: (1) the innate stability (recalcitrance) of the organic matter; (2) physical stabilization related to the accumulation of OM due to establishing of physical barriers between microbes and enzymes and their substrates as aggregates form, and (3) stabilization of the organic matter through interaction with the soil or sediment matrix, especially with mineral components.

1.1.2.1 Recalcitrance of Soil Organic Matter

Recalcitrance relates to the preservation of OM caused by structures inherently stable against biochemical decay such as condensed and lignin-derived aromatic carbons, melanoidins, some tannins or aliphatic compounds (Krull et al., 2003; Poirier et al., 2003). Organic matter may range in size and complexity from simple monomers or organic acids to mixtures of complex biopolymers aggregated together in the form of cellular debris. In addition, the chemical structure of each component biomolecule, whether simple or complex, can vary along a continuum of decomposition. Molecular

properties that influence decomposition rates of natural substrates are molecule size, polarity, ether-bridges, quaternary C-atoms, three-fold substituted N-linkages, phenyl- and heterocyclic N-groups as well as long-chain (hydrophobic) hydrocarbons (Ottow, 1997). The turnover of simple monomers such as glucose and amino acids could occurs within hours or days, while polymers (e.g. polysaccharides, proteins) have long turnover times, e.g., weeks (von Lützow et al., 2006). The polymers most resistant to degradation contain aromatic rings, such as lignin and a range of polymethylenic molecules, such as lipids and waxes, curtin and suberin (Derenne & Largeau, 2001). Many laboratory and field investigations show that these components are selectively preserved during the initial phase of degradation of plant residues (Kalbitz et al., 2003a, 2003b).

Fire can create a range of complex, highly condensed aromatic chemicals collectively known as black carbon. Black carbon comprises up to 40% of total SOM in grasslands and boreal forests (Preston et al., 2006). Fire-derived carbon was suspected to be more stable in soil than other organic matter because of its fused aromatic ring structures and the old radiocarbon ages of fire residues isolated from soil (Schmidt et al., 2000).Black carbon has an estimated residence time in the order of 500–10 000 years in soils (Skjemstad et al., 1998; Schmidt et al., 2002). Due to this apparent long residence time, the formation of charred OM is regarded as a carbon stabilization process that results in effective carbon retention in the soil (Swift, 2001). However, data on the turnover times or the age of charred OM in soils is still lacking. Therefore, the ‘true’ recalcitrance of charred OM in soils is still not understood.

The molecular structure of biomass and organic material has long been thought to determine long-term decomposition rates in the mineral soil. However, using compound-specific isotopic analysis, molecules predicted to persist in soils (such as lignins or plant lipids) have been shown to turn over more rapidly than the bulk organic matter (Fig.1.1, reviewed by Schmidt et al., 2011; Marschner. et al., 2008; Amelung et al., 2008). Therefore, the initial stages of litter decomposition could not explain the persistence of organic compounds in soils for centuries to millennia. Instead, stabilization through interactions with soil minerals is increasing recognized as the most important factor.

1.1.2.2 Spatial Inaccessibility

Organic matter could be physically occluded and therefore protected by aggregation, because C mineralization is enhanced when soil aggregates are disrupted (Six et al., 2000; Six et al., 2002b). Occlusion could occur via abiotic mechansims such as the formation of networks of Fe- and Al-oxides or hydroxides (Mayer et al., 2004). However, soil biota is strongly involved in the process of occlusion of OM by aggregation (Oades, 1993; Six et al., 2002b). Microbial cells, secretions, root exudates and faunal mucus act as cementing agents and are also occluded within the aggregates (von Lützow et al., 2006). Fungal hyphae and roots could cause larger plant residues occluded within macroaggregates (von Lützow et al., 2006).

Occluded OM is spatially protected against decomposition due to: (i) reduced access for the microorganisms and their enzymes; (ii) reduced diffusion of enzymes

into the intra-aggregate space; and (iii) restricted aerobic decomposition due to reduced diffusion of oxygen and water. The pore-size distribution in soils primarily controls the above processes.

Adequate quantities of available water and oxygen are required to optimize the processes of decomposition and mineralization. Since the total amount of pore space and the pore size distribution of the soil matrix control the availability of water and oxygen, these soil architectural properties exert a control over decomposition. Changes in the pore size distribution towards a greater proportion of large pores, such as noted in progressing from a clay to sand, accelerated C mineralization (Franzluebbers, 1999). The pore size distribution of soils also controsl the ability of decomposer organisms to reach potential organic substrates. With increasing clay content, the proportion of the total porosity found in small pores increases, and the potential stabilization of OM against biological attack due to the exclusion of decomposer organisms increases (Baldock and Skjemstad, 2000).

Turnover of OM in macroaggregates is much faster than in smaller aggregates (Six et al., 2002b; John et al., 2005), but the exact mechanisms are not clear yet. More studies combining an analysis of OM structure and OM turnover within aggregate fractions could enhance an understanding of the contribution of OM occlusion to SOC stabilization.

1.1.2.3 Interaction between Organic Matter and Soil Minerals

There is a growing acceptance that interactions with soil minerals may be the most important overarching stabilization mechanism for soil organic matter (Fig.1.2, reviewed by Schmidt et al., 2011). These are inter-molecular interactions between OM and either inorganic soil components or other OM that decrease the rate of decomposition. Evidence for stabilization of OM by binding to mineral surfaces, comes from the fact that soil OM in fine silt and clay fractions is older (Quideau et al.,2001; Eusterhues et al., 2003) or has a longer turnover time (Balesdent, 1996; Ludwig et al., 2003). Kalbitz et al. (2005) showed that sorption of soluble OM to subsoil material (B_w horizon) decreased OM mineralization by 20–30% compared with mineralization in the soil solution. There is a need for a detailed mechanistic understanding of the effect of adsorption on OM decomposition mechanisms and rates.

Interaction Mechanisms

Various mechanisms have been proposed for OM interactions with mineral surfaces, i.e. ligand exchange, polyvalent cation bridges, and weak interactions, such as hydrophobic interactions including van der Waals forces and H-bonding (von Lützow et al., 2006).

Ligand exchange between simple coordinated OH groups on mineral surfaces, carboxyl groups and phenolic OH groups of OM is one important mechanism for the formation of strong organo-mineral associations, e.g. Fe–O–C bonds (Gu et al., 1994). Ligand exchange between reactive inorganic hydroxyls (OH groups of Fe, Al and Mn-

oxides and edge sites of phyllosilicates) and organic carboxyl and phenolic OH groups is predominant in acids soils rich in minerals with protonated hydroxyl groups (Shen, 1999). Kaiser and Guggenberger (2003) found that DOM rich in carboxyl- and aromatic-C forms strong complexes with Al and Fe oxides via ligand exchange in acid subsoils

Organic anions are normally repelled from negatively charged surfaces in soils, but binding occurs when polyvalent cations are present on the exchange sites Polyvalent cations are able to maintain neutrality at the surface by neutralizing both the charge on the negatively charged surface (e.g. in clay minerals) and the acidic functional group of the OM (e.g. COO^-) and thus act as a bridge between two charged sites. The major polyvalent cations present in soil are Ca^{2+} and Mg^{2+} in neutral and alkaline soils and Fe^{3+} and Al^{3+} in acid soils. The bonding efficiency of OM on phyllosilicates by cation bridges is weaker compared with ligand exchange on Al and Fe hydroxides (Benke et al., 1999; Kaiser & Zech, 2000).

Hydrophobic interactions are driven by the exclusion of non-polar residues (e.g. aromatic or alkyl C) from water (entropy-related interactions) to force the non-polar groups together (von Lützow et al., 2006). Van der Waals forces (electrostatic forces) can operate between atoms or non-polar molecules due to a temporarily fluctuating dipole moment arising from a brief shift of orbital electrons to one side of one atom or molecule. This creates a similar shift in adjacent atoms or molecules (von Lützow et al., 2006). In the case of hydrogen bonds, a hydrogen atom with a positive

partial charge interacts with partially negatively charged O or N atoms (von Lützow et al., 2006).

Most often information on the binding mechanisms is obtained from theoretical considerations, processes found in short-term laboratory experiments, or from statistical correlations. Further studies are needed to directly investigate the specific binding mechanisms found in organomineral associations isolated from soils using high-resolution spectroscopic techniques

Types of Mineral Surfaces Involved in the OM Interactions

Three types of functional surface sites on minerals can be distinguished, which offer different bonding possibilities to OM (Kögel-Knabner et al., 2008). Their availability is assumed to control area density as well as the strength of the bonds formed: (1) single coordinated hydroxyl groups are common on Fe and Al oxides, allophone, and imogolite and the edges of layer silicates; (2) siloxane groups with permanent layer charge due to isomorphic substitution. In soils, these siloxane groups are present on some 2:1-layer-type phyllosilicates, such as vermiculite, illite, and smectite; and (3) siloxane groups without layer charge. This type occurs in both 2:1-layer-type (talc, pyrophyllite) and in 1:1-type minerals (kaolinite group).

Schulten and Leinweber (2000) compiled literature data to deduce possible effects of clay mineralogy on the organic carbon contents of organic-mineral clay fractions (Table 1.1). Results showed that fractions rich in kaolinite often had small organic carbon contents (Table 1.1). Comparatively large organic carbon contents appeared to be characteristic for chlorite-rich clay fractions, which was attributed to

low pH favoring the formation of secondary chlorites and inhibits the decomposition of organic matter. The simultaneous formation of poorly crystalline pedogenic oxides which have a large surface area could be also possible. In general, the data in Table 1.1 indicates that the binding capacity of different clay minerals for organic matter may vary, depending on factors such as clay content, chemical and biological soil properties, vegetation, etc.

Strong protection of OM was generally correlated with the presence of hydroxylated mineral phases in acidic soil environments (Kögel-Knabner et al., 2008). The presence of oxy-hydroxides of Al and Fe and increases in surface charge density, originating from either isomorphic substitution or pH-dependent charges, will increase the reactivity of the mineral surface and the potential adsorptive and protective capacities (Baldock and Skjemstad, 2000). In a wide range of different soils, organic matter concentration often correlates with the content of Fe oxides and/or clay (Eusterhues et al., 2003) or Fe oxides and short-range order Al silicates (Kleber et al., 2005; Mikutta et al., 2006). Strong correlations exist between the mineral-bound OC and the Fe oxide content in subsoils (Fig. 1.3, reviewed by Kögel-Knabner et al., 2008; Eusterhues et al., 2005). By selective extraction of crystalline pedogenic oxides using dithionite/citrate/bicarbonate (DCB) it was showed that 40–70% of organic carbon in syrosem-regosol-cambisol soil associations of the Bolivian Andes was bound by pedogenic Al and Fe oxides (Leinweber and Schulten 1994). Collectively these results strongly suggest that OM is predominantly associated with Fe &Al oxides and short-range order Al silicates. Such minerals provide large reactive surface

areas (Eusterhues et al., 2005), which renders them most suitable for interaction with OM either via sorption interactions or coprecipitation. Moreover, there is evidence that the pedogenic oxides also influence the composition and stability of the organic matter. A Pyrolysis and field ionization mass spectrometry (Py-FIMS) study carried out with silt and clay fractions before and after extraction with DCB, indicated a general destabilization of SOM and preferential extraction of some SOM compounds by removal of the pedogenic oxides. It was concluded that lipids, lignin dimers and alkylaromatics were more intensively bound to pedogenic oxides than other SOM compounds (Schulten and Leinweber 1995).

The mineralogy, surface charge characteristics, and precipitation of amorphous Fe and Al oxides on clay mineral surfaces give clay minerals a capacity to interact with OM. Kaiser & Guggenberger (2003) demonstrated that sorption occurs preferentially at reactive sites such as edges, rough surfaces, micropores or small mesopores. Micropores are sites of increased reactivity, and thus well suited for sorptive interactions with organic compounds (Kaiser and Guggenberger, 2003; Mikutta et al., 2004). OM can bind strongly to micropore openings that decrease desorbability and the oxidative removal of OM (Kaiser and Guggenberger, 2007). Kaiser and Guggenberger (2003) hypothesized that the molecules adsorbed first might be strongly stabilized by multiple ligand attachments. At higher surface loadings, sorption can then take place with fewer ligand attachments, which leaves part of the molecule not attached to the surface and thus rendersOM more susceptible to degradation.

Interaction of Metal Ions with Organic Substances

The interaction of soil OM with metal ions is well known. However, little information is available about the effect of metal binding on soil OM stability or about the mechanisms involved. Metal ions that have been considered as potentially stabilizing for soil OM are Ca^{2+}, Al^{3+}, Fe^{3+}, and heavy metals (Baldock & Skjemstad, 2000). Organic substances can bind to silicate surfaces via $Ca^{2+,}$ Al^{3+} and Fe^{3+} bridges. Dissolved organic matter (DOM) in soils can be precipitated by metal ions such as Al^{3+} and Fe^{3+}. Larger DOM molecules, which are potentially recalcitrant, preferentially are uptake by precipitation while small molecules remain in solution (Blaser et al., 1999; Nierop et al., 2002; Schwesig et al., 2003). To our knowledge, the mechanisms and stability of DOM-metal coprecipitates is not well understood.

1.1.3 Soil Fe-redox Cycling

As the most abundant transition metal on the Earth's surface, iron plays a particularly important role in environmental biogeochemistry. The oxidized form of iron (Fe(III)) is soluble under extremely acidic conditions but Fe(III) precipitates as Fe(III) (hydr)oxides in near-neutral pH environments. Many nutrients, trace elements, and organic compounds strongly sorb to these Fe(III) oxides. Iron is a redox sensitive element and therefore is subject to oxidation and reduction depending on redox conditions (Fig.1.4). Iron-redox cycling takes place across a wide range of subsurface and near-surface environments, potentially encompassing millimeter-to-decameter (or more) spatial scales. A common ingredient in all such environments is the presence of

a redox transition zone (or boundary environment). Under reducing conditions, Fe(III) (hydr)oxides can be reduced abiotically, e.g., by sulfide (Afonso and Stumm, 1992). In addition, Fe(III) minerals may serve as terminal electron acceptors to dissimilatory iron-reducing bacteria. These organisms, which are ubiquitous in freshwater and marine environments, are able to couple the cytoplasmic oxidation of organic compounds or hydrogen to the extracellular reduction of poorly soluble Fe(III) minerals, hence gaining energy for growth via electron transport phosphorylation (DiChristina et al., 2005). Reduction of Fe(III) minerals produces soluble Fe(II) and a wide range of secondary minerals, including Fe(II) minerals (e.g., vivianite ($Fe_3(PO_4)_2$) and siderite (Fe- CO_3), Fe(III) minerals (e.g., goethite), and mixed Fe(II)-Fe(III) minerals e.g., magnetite(Fe_3O_4) and greenrusts (Fe(II)-Fe(III) layered double hydroxides) (Borch et al., 2011). Reductive dissolution of Fe (hydr)oxides due to reducing conditions often leads to the release of large quantities of dissolved organic matter into soil solution (Hagedorn et al., 2000). Studies investigating the dynamics of dissolved organic matter release in wetlands under field condition report positive correlations between dissolved organic matter and Fe(II) (Hagedorn et al., 2000; Gruau et al., 2004). This suggests that establishment of reducing soil conditions could be a key factor in enhancing the release of organic matter which is originally associated with Fe oxides.

Input of an oxidant such as oxygen or nitrate drives Fe(II) chemical oxidation, thereby generating Fe(III) [e.g. in the form of Fe(III) oxyhydroxides at circumneutral pH]. Oxidation of Fe(II) may be also mediated by aerobic and anaerobic bacteria.

Microbial Fe(II) oxidation is common in low pH environments where chemical oxidation is not favorable (Borch et al., 2010). Under near-neutral pH conditions, aerobic Fe(II)-oxidizing bacteria have to compete with the rapid chemical oxygenation of Fe(II). Therefore, they thrive mainly at low levels of oxygen typically encountered at oxic-anoxic interfaces (Druschel et al., 2008), e.g., around plant roots in waterlogged soils. Phototrophic and nitrate-dependent Fe(II)-oxidizing bacteria mediate Fe(II) oxidation in neutrophilic, anoxic environments, where nitrite and Mn(IV) oxides can serve as chemical oxidants for Fe(II) (Kappler and Straub, 2005). Since OM is present in soil solutions, oxidation of Fe(II) to Fe(III) (hydr)oxides could lead to adsorption and coprecipitation of OM and therefore affect soil C storage and stabilization. The coprecipitation of Fe and dissolved organic matter (DOM) is common in soil, sediments, surface water and subsurface aquifers, systems that experience significant variation in either redox or pH conditions (Fuller et al., 1993; Pokrovsky and Schott, 2002). These interactions are hypothesized to play a role in immobilizing DOM and stabilizing it against microbial degradation, as well as controlling the structure and reactivity of natural Fe (hydr)oxides (von Luetzow et al., 2006; Eusterhues et al., 2008). Studies of OM-ferrihydrite coprecipitation have found that coprecipitation of ferrihydrite with DOM lowered its crystallinity and decreased the magnetic ordering temperature, the magnetic hyperfine field and particle size, compared to organic-free synthetic ferrihydrite (Schwertmann et al., 2005; Eusterhues et al.,2008). Therefore, the reactivity of natural ferrihydrites will often differ from their synthetic counterparts, formed in the absence of OM. However, data on the effect

of Fe-OM coprecipitation on C storage and stability and also the reactivity of ferrihydrite is lacking.

1.2 Objectives and Hypthesis

The role of carbon (C)-mineral interactions in the long-term accumulation of soil organic matter (OM) is increasingly recognized as a key process in terrestrial C cycling. However, the specific mineral phases or the mechanisms for the formations of the C-mineral complex are largely unknown. Redox changes, as a consequence of varying landscape topographic positions, will have important impacts on biogeochemical C and mineral cycling processes. Whereas the chemical composition of soil OM has been subject to numerous studies, little is known about whether the composition of soil organic matter also varies with landscape topographic positions and drainage regimes. Iron (Fe) oxides are of particular importance in soils because of their abundance and high reactive surface area. Iron oxides with short-range crystal order and small particle sizes contain more reactive high surface area compared to other bulk Fe-oxides. Fe is susceptible to redox variations along landscape gradients over a wide range of spatial scales. Fe (III) minerals predominate in well-drained upland soils, while under poorly-drained conditions at lowland locations, floodplains and streams reductive dissolution of Fe (III) minerals occurs. The soil redox conditions affect not only the amount but also mineralogical composition of Fe mineral phases. Since both the organic matter and mineral phases of soils are involved

in OM-mineral complex formation, differences in both mineralogy and organic matter composition could lead to differences in organo-mineral complexes.

Ferrihydrite, an amorphous Fe oxyhydroxide, ubiquitously occurs in soils and sediments. Ferrihydrite, with its high surface area and intrinsic reactivity, serves as an important sink for organic matter. Organic matter-ferrihydrite complexes could be formed by adsorption and coprecipitation. In natural environments, ferrihydrite often forms in the presence of dissolved organic matter, which leads to coprecipitation of organic matter (OM) with ferrihydrite. The coprecipitation of Fe and dissolved organic matter is common in soils and sediment that experience fluctuating pH and redox conditions. However, in contrast to adsorption studies, the coprecipitation process has received relatively little attention. Little is known about the amount, nature and stability of the coprecipitated OM in natural environments. Association of OM with ferrihydrite may also affect the structure and reactivity of the ferrihydrite. Studies of OM-ferrihydrite coprecipitation have found that coprecipitation of ferrihydrite with DOM lowered its crystallinity and particle size. However, the role of OM coprecipitation on ferrihydrite reactivity is not well understood.

Accordingly, the specific objectives of this study are:

(1) To investigate soil organic matter molecular composition under varying landscape topographic positions; (Chapter 2)

(2) To assess the interactions of C and C forms with soil minerals at the molecular scale; (Chapter 3)

(3) To characterize Fe speciation along the redox gradients; (Chapter 4)

(4) To compare the ferrihydrite-OM complexes formation via adsorption and coprecipitateion with DOM extracts from a forest litter layer; (Chapter 5 & 6)

(5) To investigate iron-organic matter coprecipitation impacts on the structure and reactivity of ferrihydrite. (Chapter 7)

REFERENCES

Afonso, M. D.; Stumm, W., Reductive dissolution of iron(III) (hydr)oxides by hydrogen-sulfide. *Langmuir* **1992**, 8, 1671-675.

Amelung, W.; Brodowski, S.; Sandhage-Hofmann, A.; Bol, R., Combining biomarker with stable isotope analysis for assessing the transformation and turnover of soil organic matter. *Adv. Agron*. **2008,** 100, 155-250.

Baldock, J. A.; Skjemstad, J. O., Role of the soil matrix and minerals in protecting natural organic materials against biological attack. *Org. Geochem.* **2000**, 31, 697-710.

Balesdent, J., The significance of organic separates to carbon dynamics and its modeling in some cultivated soils. *Eur. J. Soil Sci.* **1996,** 47, 485-493.

Blaser, P.; Heim, A.; Luster, J., Total luminescence spectroscopy of NOM-typing samples and their aluminium complexes. *Environment International* **1999,** 25, 285-293.

Benke, M. B.; Mermut, A. R.; Shariatmadari, H., Retention of dissolved organic carbon from vinasse by a tropical soil, kaolinite, and Fe oxides. *Geoderma* **1999,** 91, 47-63.

Borch, T.; Kretzschmar, R.; Kappler, A.; Van Cappellen, P.; Ginder-Vogel, M.; Voegelin, A.; Campbell, K. M., Biogeochemical Redox Processes and their Impact on Contaminant Dynamics. *Environ. Sci. Technol.* **2010,** *44*, 15-23.

Derenne, S.; Largeau, C., A review of some important families of refractory macromolecules: composition, origin, and fate in soils and sediments. *Soil Sci.* **2001,** 166, 833-847.

DiChristina, T. J.; Fredrickson, J. K.; Zachara, J., Enzymology of electron transport: Energy generation with geochemical consequences. In Molecular Geomicrobiology; Mineralogical Society of America: Chantilly, VA, **2005,** 59, 27-52.

Druschel, G. K.; Emerson, D.; Sutka, R.; Suchecki, P.; Luther III, G. W., Low-oxygen and chemical kinetic constraints on the geochemical niche of neutrophilic iron(II) oxidizing microorganisms. *Geochim. Cosmochim. Acta* **2008,** 72, 3358-3370.

Eusterhues, K.; Rumpel, C.; Kleber, M.; Kögel-Knabner, I., Stabilization of soil organic matter by interactions with minerals as revealed by mineral dissolution and oxidative degradation. *Org. Geochem.* **2003,** 34, 1591-1600.

Eusterhues, K.; Rumpel, C., Kögel-Knabner, I., Organomineral associations in sandy acid forest soils: importance of specific surface area, iron oxides and micropores. *Eur. J. Soil Sci.* **2005,** 56, 753-763.

Eusterhues, K.; Wagner, F. E.; Häusler, W.; Hanzlik, M.; Knicker, H.; Totsche, K. U.; Kögel-Knabner, I.; Schwertmann, U., Characterization of ferrihydrite-soil organic matter coprecipitates by X-ray diffraction and Mössbauer. *Environ. Sci. Technol.* **2008,** 42, 7891-7897.

Franzluebbers, A. J., Microbial activity in response to water-filled pore space of variably eroded southern Piedmont soils. *Appl. Soil Ecol.* **1999,** 11, 91-101.

Fuller, C. C.; Davis, J. A.; Waychunas, G. A., Surface-chemistry of ferrihydrite. 2. Kinetics of arsenate adsorption and coprecipitation. *Geochim. Cosmochim. Acta* **1993,** 57, 2271-2282.

Gu, B. H., Schmitt, J.; Chen, Z.; Liang, L. Y.; McCarthy, J. F., Adsorption and desorption of natural organic matter on iron oxide: mechanisms and models. *Environ. Sci. Technol.* **1994,** 28, 38-46.

Gruau, G.; Dia, A.; Olivie-Lauquet, G.; Davranche, M.; Pinay, G., Controls on the distribution of rare earth elements in shallow groundwaters. *Water Res*. **2004,** 38, 3576-3586.

Hagedorn, F.; Kaiser, K.; Feyen, H.; Schleppi, P., Effect of redox conditions and flow processes on the mobility of dissolvedorganic carbon and nitrogen in a forest soil. *J. Environ. Qual*. **2000,** 29, 288-297.

Houghton, R.A., The comtemporary carbon cycle. In: Schlesinger, W.H. (Ed.). Biogeochemistry, Elsevier-Pergammon, Oxford, **2005**, 473-513.

John, B.; Yamashita, T.; Ludwig, B.; Flessa, H., Storage of organic carbon in aggregate and density fractions of silty soils under different types of land use. *Geoderma* **2005,** 128, 63-79.

Kaiser, K.; Guggenberger, G., Mineral surfaces and soil organic matter. *Eur. J. Soil Sci.* **2003,** 54, 219-236.

Kaiser, K.; Guggenberger, G., Sorptive stabilization of organic matter by microporous goethite: sorption into small pores vs. surface complexation. *Eur. J. Soil Sci.* **2007,** 53, 639-644.

Kaiser, K.; Zech, W., Dissolved organic matter sorption by mineral constituents of subsoil clay fractions. *J. Plant Nutr. Soil Sci.* **2000,** 163, 531-535.

Kalbitz, K.; Schmerwitz, J.; Schwesig, D.; Matzner, E., Biodegradation of soil-derived dissolved organic matter as related to its properties. *Geoderma* **2003a,** 113, 273-291.

Kalbitz, K.; Schwesig, D.; Schmerwitz, J.; Kaiser, K.; Haumaier, L.; Glaser, B.; Ellerbrock, R.; Leinweber, P., Changes in properties of soil-derived dissolved organic matter induced by biodegradation. *Soil Biol. Biochem.* **2003b,** 35, 1129-1142.

Kalbitz, K.; Schwesig, D.; Rethemeyer, J.; Matzner, E., Stabilization of dissolved organic matter by sorption to the mineral soil. *Soil Biol. Biochem.* **2005,** 37, 1319-1331.

Kappler, A.; Straub, K. L., Geomicrobiological cycling of iron. *Rev. Mineral. Geochem.* **2005**, 59, 85-108.

Kleber, M.; Mikutta, R.; Torn, M. S.; Jahn, R., Poorly crystalline mineral phases protect organic matter in acid subsoil horizons. *Eur. J. Soil Sci.* **2005,** 56, 717-725.

Krull, E. S.; Baldock, J. A.; Skjemstad, J. O., Importance of mechanisms and processes of the stabilization of soil organic matter for modeling carbon turnover. *Funct. Plant Biol.* **2003,** 30, 207-222.

Leinweber, P; Schulten, H. R., Zur Bedeutung pedogener Oxide für die Bindung organischer Substanzen. *Mitt. Dtsch. Bodenkd. Ges.* **1994,** 74, 383-386.

Ludwig, B.; John, B.; Ellerbrock, R.; Kaiser, M.; Flessa, H., Stabilization of carbon from maize in a sandy soil in a long-term experiment. *Eur. J. Soil Sci.* **2003,** 54, 117-126.

Marschner, B., How relevant is recalcitrance for the stabilization of organic matter in soils? *J. Plant Nutr. Soil Sci.* **2008,** 171, 91-110.

Mayer, L. M.; Schick, L. L.; Hardy, K. R.; Wagal, R.; McCarthy, J. Organic matter in small mesopores in sediments and soils. *Geochim. Cosmochim. Acta* **2004,** 68, 3868-3872.

Mikutta, R.; Kleber, M.; Torn, M. S.; Jahn, R., Stabilization of soil organic matter: Association with minerals or chemical recalcitrance? *Biogeochem.* **2006,** 77, 25-56.

Mikutta, C.; Lang, F.; Kaupenjohann, M., Soil organic matter clogs mineral pores: Evidence from H-1-NMR and N-2 adsorption. *Soil Sci. Soc. Am. J.* **2004,** 68, 1853-1862.

Nierop, K. G. J.; Jansen, B.; Verstraten, J. A., Dissolved organic matter, aluminium and iron interactions: precipitation induced by metal/carbon ratio, pH and competition. *Sci. Total Environ.* **2002,** 300, 201-211.

Oades, J. M., The role of biology in the formation, stabilization and degradation of soil structure. *Geoderma* **1993,** 56, 377-400.

Ottow, J. C. G., Abbaukinetik und Persistenz von Fremdstoffen in Böden. Organische Natur- und Fremdstoffe. In: Umweltbiotechnologie (eds J. C. G. Ottow & W. Bidlingmaier), **1997**, 103-104.

Parton, W. J., Ecosystem model comparisons: science or fantasy world? In: Evaluation of Soil Organic Matter Models (eds D. S. Powlson, P. Smith & J. U. Smith), **1996**, 133-142. Springer-Verlag, Berlin.

Preston, C. M.; Schmidt, M. W. I., Black (pyrogenic) carbon: a synthesis of current knowledge and uncertainties with special consideration of boreal regions. *Biogeosciences* **2006,** 3, 397-420.

Poirier, N.; Derenne, S.; Balesdent, J.; Mariotti, A.; Massiot, D.; Largeau, C., Isolation and analysis of the non-hydrolysable fraction of a forest soil and an arable soil (Lacade´ e, southwest France). *Eur. J. Soil Sci*. **2003,** 54: 243-255.

Pokrovsky, O.S.; Schott, J., Iron colloids/organic matter associated transport of major and trace elements in small boreal rivers and their estuaries (NW Russia). *Chem. Geol.* **2002,** 190, 141-179.

Quideau, S. A.; Chadwick, O. A.; Trumbore, S. E.; Johnson-Maynard, J. L.; Graham, R. C.; Anderson, M. A., Vegetation control on soil organic matter dynamics. *Org. Geochem.* **2001,** 32, 247-252.

Raich, J. W.; Schlesinger, W. H., The global carbon dioxide flux in soil respiration and its relationship to vegetation and climate. *Tellus B* **1992,** 44, 81-99.

Schlesinger, W. H., An overview of the C cycle. In: Soils and Global Change (eds R. Lal, J. Kimble, J. Levin & B. A. Stewart), Lewis Publishers, Boca Raton, FL, **1995,** 9-26.

Schmidt, M. W. I.; Noack, A. G., Black carbon in soils and sediments: analysis, distribution, implications, and current challenges. *Glob. Biogeochem. Cycles* **2000,** 14, 777-794.

Schmidt, M. W. I.; Skjemstad, J. O.; Jäger, C., Carbon isotope geochemistry and nanomorphology of soil black carbon: black chernozemic soils in central Europe originate from ancient biomass burning. *Glob. Biogeochem. Cycles* **2002,** 16, DOI: **10.1129/2002GB001939.**

Schmidt, M. W. I.; Torn, M. S.; Abiven, S.; Dittmar, T.; Guggenberger, G.; Janssens, I. A.; Kleber, M.; Kögel-Knabner, I.; Lehmann, J.; Manning, D. A. C.; Nannipieri, P.; Rasse, D. P.; Weiner, S.; Trumbore, S. E., Persistence of soil organic matter as an ecosystem property. *Nature* **2011,** 478, 49-56.

Schulten, H. R.; Leinweber, P., Dithionite-citrate-bicarbonate-extractable organic matter in particle-size fractions of a Haplaquoll. *Soil Sci Soc Am J.* **1995,** 59: 1019-1027.

Schulten, H. R.; Leinweber, P., New insights into organic-mineral particles: composition, properties and models of molecular structure. *Biol. Fertil. Soils,* **2000,** *30, 399-432.*

Schwertmann, U.; Wagner, F.; Knicker, H., Ferrihydrite-humic associations: Magnetic hyperfine interactions. *Soil Sci. Soc. Am. J.* **2005,** 69, 1009-1015.

Schwesig, D.; Kalbitz, K.; Matzner, E., Effects of aluminium on the mineralization of dissolved organic carbon derived from forest floors. *Eur. J. Soil Sci.* **2003,** 54, 311-322.

Shen, Y. H., Sorption of natural dissolved organic matter on soil. *Chemosphere* **1999,** 38, 1505-1515.

Six, J.; Elliott, E. T.; Paustian, K., Soil macroaggregate turnover and microaggregate formation: a mechanism for C sequestration under no-tillage agriculture. *Soil Bio. Biochem.* **2000,** 32, 2099-2103.

Six, J.; Feller, C.; Denef, K.; Ogle, S. M.; de Moraes Sa, J. C.; Albrecht, A., Soil organic matter, biota and aggregation in temperate and tropical soils - effects of no-tillage. *Agronomie* **2002,** 22, 755-775.

Skjemstad, J. O.; Janik, L. J.; Taylor, J. A., Non-living soil organic matter: what do we know about it? *Aust. J. Exp. Agric.* **1998,** 38, 667-680.

Sollins, P.; Homann, P.; Caldwell, B. A., Stabilization and destabilization of soil organic matter: mechanisms and controls. *Geoderma* **1996,** 74, 65-105.

Swift, R. S., Sequestration of carbon by soil. *Soil Sci.* **2001**, 166, 858-871.

Von Lützow, M.; Kögel-Knabner, I.; Ekschmitt, K.; Matzner, E.; Guggenberger, G.; Marschner, B.; Flessa, H., Stabilization of organic matter in temperate soils: mechanisms and their relevance under different soil conditions-a review**.** *Eur. J. Soil Sci.* **2006,** 57, 426-445**.**

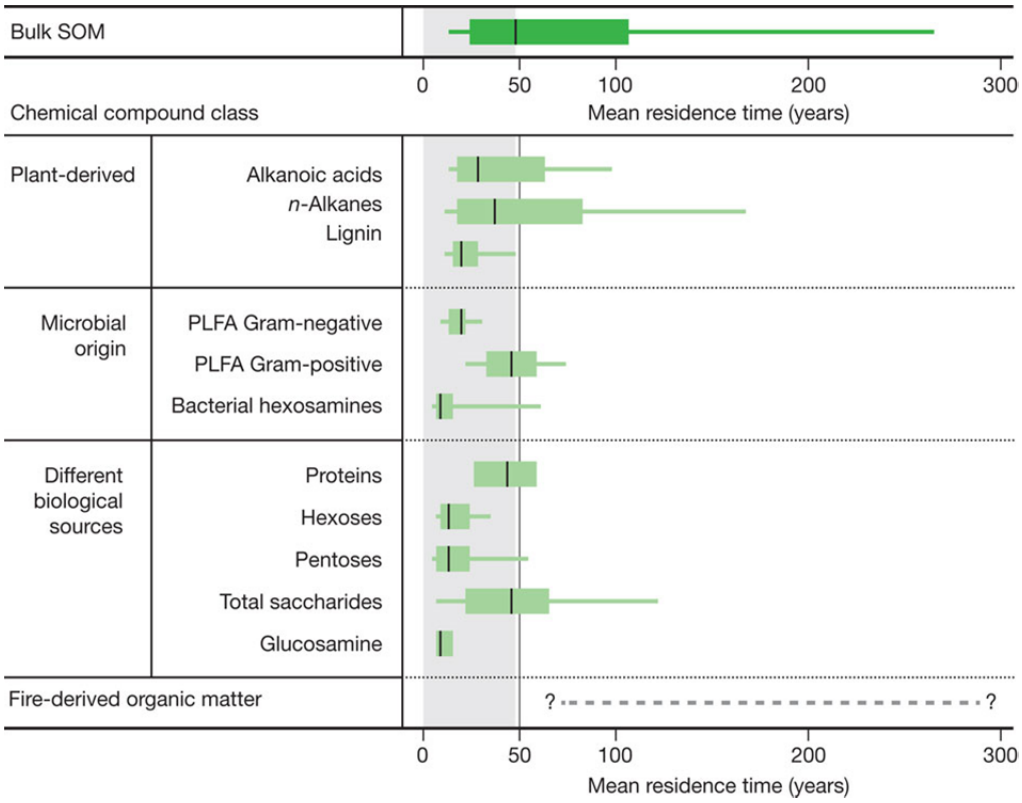

Figure 1.1 Molecular structure does not control long-term decomposition of soil organic matter (Adapted from Schmidt et al., 2011).

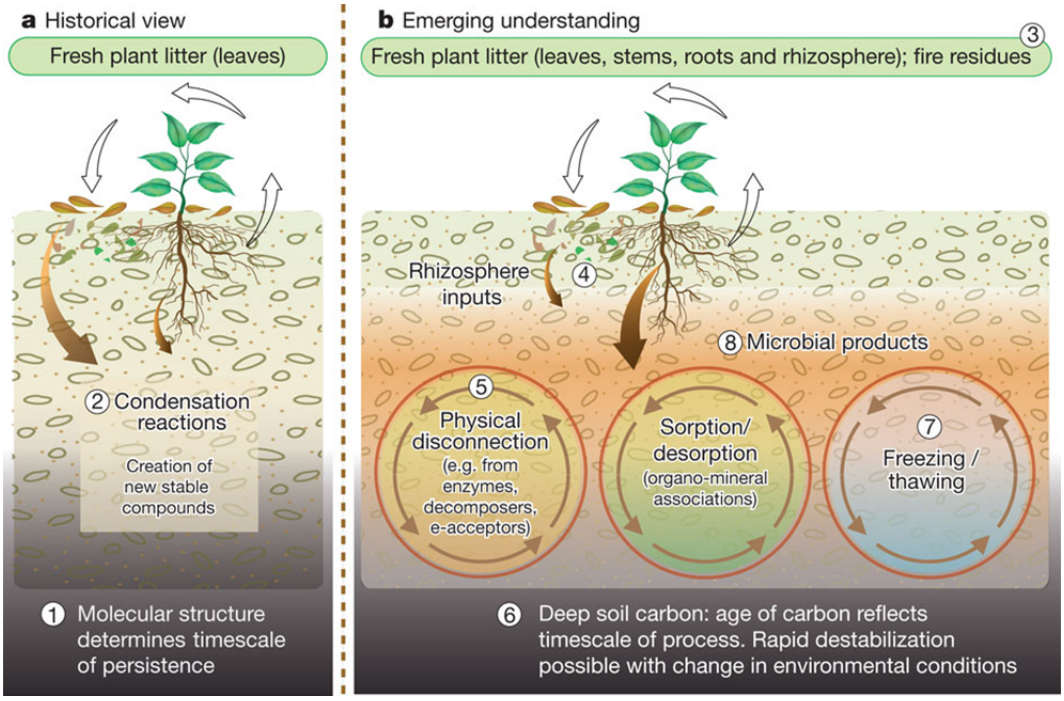

Figure 1.2 A synopsis of all eight insights, contrasting historical and emerging views of soil carbon cycling. (Adapted from Schmidt et al., 2011).

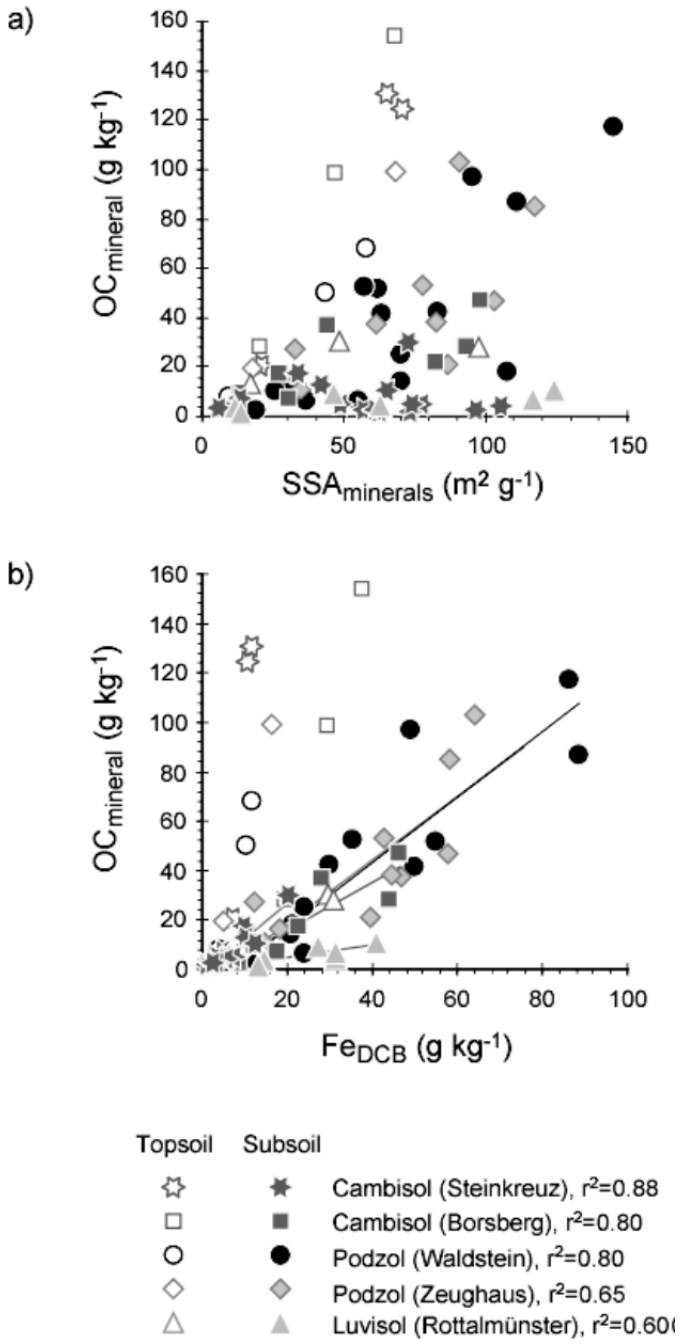

Figure 1.3 Relation between mineral-bound OM and (a) specific surface area or (b) Fe oxide content (Adapted from Kögel-Knabner et al., 2008).

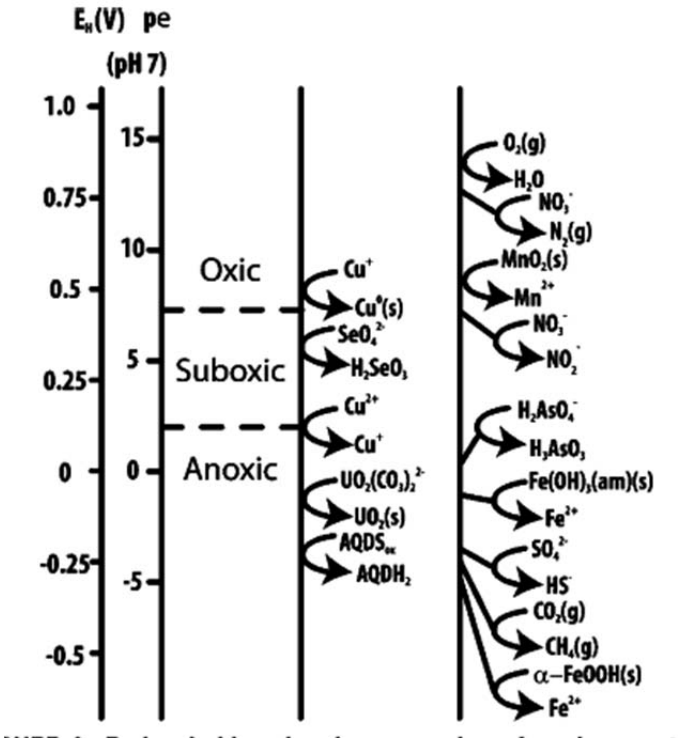

Figure 1.4 Redox ladder showing examples of environmentally relevant redox couples (Adapted from Borch et al., 2010).

Table 1.1 Clay contents, predominant clay minerals and organic carbon (C_{org}) contents of organic-mineral clay fractions (Compiled by Schulten and Leinweber, 2000).

Clay (%)	Predominant clay minerals	C_{org} (%)
60	Smectite	2
39	Kaolinite and smectite	1–2
32	Allophane	13–14
6	Smectite, less vermiculite	6
17	Chlorite (vermiculite, illite)	11
3–15	Illite (vermiculite)	4–16
8	Smectite	15
17–18	Kaolinite	2–3
8–45	Chlorite-mixed layers	1–20
45	Smectite	2
17	Kaolinite and illite	2–6
45	Smectite and illite	7–9
46	Palygorskite	3–7
69	Smectite	1–2
8	Illite, less smectite	4–6
9	Chlorite-mixed layers	8–11
9	Illite (quartz, feldspars, smectite)	8–9
2	Smectite	6–17
28	Smectite/vermiculite	2–5

Chapter 2

NEXAFS AND PYROLYSIS-FIMS STUDY OF SOIL ORGANIC MATTER COMPOSITION ALONG A PASTURE HILLSLOPE: EFFECTS OF SOIL DEPTH AND LANDSCAPE TOPOGRAPHIC POSITIONS

2.1 Abstract

The characteristics of soil organic matter strongly vary with soil depth and landscape topographic position. In this study, we used synchrotron-based near-edge x-ray absorption fine structure (NEXAFS) spectroscopy and pyrolysis-field ionization mass spectrometry (Py-FIMS) to characterize organic matter in soils obtained from different landscape positions at three soil depths (0-15, 15-25 and 25-35 cm) along a pasture hillslope. Carbon NEXAFS spectra demonstrated aromatic C was relatively enriched in the subsoils. The relative abundance of recalcitrant lignin increased with soil depth, followed by a decreasing percentage of lipid-like compounds, based on Py-FIMS analysis. Large proportions of aromatic C and lignin were found in the footlsope location, compared to the summit. The Py-FIMS thermal evolution curve showed that the carbohydrates, N-containing compounds (heterocyclic nitrogen, nitriles and amides), and phenols and lignin monomers were more thermally stable in the subsoil and footslope location, whereas the thermal stability of recalcitrant alkylaromatics and lignin dimers remained relatively unchanged with soil depth and hillsope location.

2.2 Introduction

Organic carbon bound to minerals is considered relatively stable (Torn et al., 1997, Kalbitz et al., 2005; Mikutta et al., 2006) and it controls the long-term organic matter sequestration in soils. Organic matter stabilization by minerals has been envisioned as a combined effect of the chemical properties of minerals (surface area and charge) and the composition of the OM involved, with an aromatic structure being most resistant to microbial decomposition (Kalbitz et al., 2005; Mikutta et al., 2007). Organic matter (OM) in soils is a mixture of a diverse range of organic compounds that have variable chemical composition and turnover rates (Kölbl and Kögel-Knabner, 2004). The composition of soil organic matter (SOM) is largely influenced by the nature of OM inputs, management practices, diagnostic horizons, and the extent of chemical and physical protection offered to the decomposing organic materials (Baldock and Skjemstad, 2000; Baldock et al., 1992; Chan, 2001).

Soil properties exhibit pronounced differences at different landscape topographic positions. These differences have been linked to translocation of soil particles and water redistribution toward downslope locations (Gregorich and Anderson, 1985; Pennock and de Jong, 1990; Pennock et al., 1994; Verity and Anderson, 1990). Many studies have reported increases in the organic C and N contents in the depressional areas, which may be attributed to the accumulation of eroded organic matter-rich sediments in low-lying landscape positions (Jenny, 1980). Whereas the chemical composition of soil OM has been subject to numerous studies, little is known about the structural changes of SOM as a function of landscape

topographic positions. The components of soil organic matter might vary with drainage regions at different landscape positions. Lignin is a recalcitrant organic compound and the decomposition of lignin primarily depends on the supply of O_2 (Williams and Yavitt, 2003). Thus water accumulation may inhibit lignin decomposition at the depressional positions, where O_2 levels in the soil solution are limited, therefore enriching SOM in lignin materials (Benner et al., 1984; Gleixner et al., 2001; Kogel-Knabner, 2002). In addition, lipids to be associated with clay fractions in soils have been noted by a number of authors (Mahieu et al., 1999; Schmidt et al., 2000; Mao et al., 2007), and therefore downslope translocation of fine particles could be enriched in lipids.

Recent carbon inventories have shown that subsoils (B and C horizons) can store significant amounts of SOM (Swift, 2001; Lorenz and Lal, 2005). Carbon retained in subsoils may be more stable than that in the surface soil due to the differences in the quantity, source, composition, and environmental conditions (Rumpel and Kogel-Knabner, 2011). Plant litter or shoots contributes the majority of organic matter to the surface soil horizons and degrades progressively with soil depth. In comparison, subsoil receives a large proportion of inputs from root residues (including exudates), and translocation of dissolved or particulate organic matter (Lorenz and Lal, 2005; Rasse et al., 2006). Temperature, moisture, and soil microbial activities, critical factors determining SOM decomposition rates on a regional scale, also vary with depth in a soil profile (Gill and Burke, 2002; Taylor et al.,2002).There is limited information on the chemistry and stability of OM in the subsurface soils

(Rumpel and Kogel-Knaber, 2011). Aromatic carbon measured with solid-state ^{13}C nuclear magnetic resonance (NMR) was reported to increase with soil depth (Fox et al., 1994). Collectively, a better understanding of the characteristics of SOM in subsurface horizons is important to improve modeling of organic matter turnover and storage on a landscape scale (Viaud et al., 2010).

Characterizing SOM is challenging because of the intermixture of organic and mineral components in soils. Researchers have employed alkaline solution to extract humic fractions from soils for several decades. However, this approach could produce artifacts and the humic substances extracted are not representative of SOM (Kleber and Johnson, 2011). In this study, we combined two approaches to characterize SOM: (i) applying synchrotron-based NEXAFS spectroscopy and classifying carbon into functional groups based on spectral features corresponding to specific compound classes, and (ii) using analytical pyrolysis coupled with mass spectrometry, where soils are thermally degraded in the absence of O_2, and the volatilized monomeric products are characterized using mass spectrometry (Schulten, 1996; Schulten and Schnitzer, 1997). Our specific objectives were to characterize the characteristics of SOM at different soil depths and landscape topographic positions along a pasture hillslope.

2.3 Materials and Methods

2.3.1 Field Sampling

Our field site is located within the long-term 725-ha research watershed upstream of the Stroud Water Research Center (SWRC) in southeastern PA (39º53'N, 75º47'E). The 3rd-order watershed forms the headwaters of the White Clay Creek and is an intensive study site for the established Christina River Basin Critical Zone Observatory. Currently, 23% of the watershed is covered with forests (Newbold, 1997). Approximately 52% of the watershed area is in pasture for horses and cattle, and 22% is tilled primarily for maize, soybeans and winter wheat or hayed (alfalfa).The remaining land (~3%) is in residential use, a commercial catering establishment, and the Stroud Water Research Center (Newbold, 1997). The watershed is underlain by highly metamorphosed sedimentary rocks containing gneisses, schists, quartzites, and marbles (Sloto, 1994). The soils are primarily Typic Hapludults (Newbold, 1997). Soil samples were collected from the summit, backslope and footslope of a pasture hillslope with an angle of 15°, at soil depths of 0-15 (A horizon), 15-25 (B horizon) and 25-35 cm (B-horizon), respectively. The pasture has been used for at least 50 yrs. The same plant species at this site are critical to the study because they minimize the influence of primary organic sources on the chemical variability of organic matter. The soil samples represented well and poorly drained areas.

2.3.2 Clay Fraction Separation

The bulk soil samples were air-dried, and roots and visible plant material were removed. The >2 mm fraction was removed by dry sieving. The clay fraction separation was performed according to Amelung et al. (1998). Briefly, thirty grams of soil were ultrasonically treated with an energy input of 60 J mL^{-1} using a probe type sonicator at a soil/water ratio of 1:5 (w/v). The coarse sand fraction (>250 μm) was removed by wet sieving. To completely disperse the remaining suspension, ultrasonication was again applied with an energy input of 440 J mL^{-1}at a soil/water ratio of 1:10 (w/v). The clay-sized fraction (<2 μm) was separated from the silt and sand sized separates by repeated centrifugation. The clay fractions were then freeze-dried. Total C and N content of bulk soils and clay fractions were analyzed by dry combustion with a C/N elemental analyzer.

2.3.3 NEXAFS Spectroscopy

C NEXAFS measurements were conducted at the SGM beamline located at the Canadian Light Source synchrotron (CLS), Saskatoon, Canada. The samples were subjected to routine sample preparation developed by SGM beamline scientists before acquisition of C (1s) NEXAFS spectra. Thin films of samples were prepared by homogeneously mixing 1mg of the finely ground sample material in 1ml of DI water and by transferring 1μl of aqueous sample on gold coated silicon wafers attached to a 10-mm diameter stainless steel sample holder. The thin film was air dried at room temperature. The sample holder was inserted into the high vacuum X-ray absorption

chamber on beamline ID11-1, which is equipped with a spherical grating monochromator (SGM). C (1s) NEXAFS spectra of the samples were collected using a photodiode and recorded from 270 to 320 eV in steps of 0.1eV using a dwell time of 500 ms. Exit slit gap was 50 µm. Background measurements were collected by measuring an empty gold-coated silicon wafer. A Ti filter was used in the beamline to reduce the effects of 2nd oxygen in the pre-edge region. In order to minimize beam damage to organic matter, we collected only one spectrum from one spot. At least four to six spectra were collected from each sample and averaged. . The C NEXAFS spectra were energy calibrated using the 1s $\rightarrow \pi^*_{C=O}$ transition of glutaric acid at 288.6 eV (Kim et al., 2003).

2.3.4 Pyrolysis Field Ionization Mass Spectrometry

Soils were dried, milled with a mortar and pestle, transferred to quartz capsules, and pyrolyzed at temperatures ranging from 110 to 700°C in steps of 20°C in the direct inlet of a Finnigan MAT 900 mass spectrometer (Finnigan MAT, Bremen, Germany). Across the full temperature range, 91 scans were recorded for masses ranging from 15 to 900 *m*/*z*; ion intensities were normalized on a sample weight basis (i.e., ion counts per milligram of soil). These were combined to produce a single thermogram of total ion intensity (TII) and a single summed and averaged mass spectrum. A detailed description of the Py-FIMS method and the statistical treatment of TII and weight normalization was given by Sorge et al. (1993).

2.4 Results and Discussion

2.4.1 Soil C and N content

The C and N content generally decreased with soil depth in three locations (Table 2.1). The atomic C/N ratio also decreased from soil depth of 0-15 cm to 25-35cm (Table 2.1), indicating the degradation of SOM with soil depth. The footslope soils contained slightly lower C content than the summit and backslope soils (Table 2.1). Total C and N content was significantly greater in the clay fractions than in the unfractionated, whole-soil samples (Table2.1). The atomic C/N ratios of the clay-fraction SOM tended to less than those of the whole-soil SOM (Table 2.1), perhaps reflecting a greater degree of humification in the SOM associated with clay. By combining C content data with soil clay content data, 44-67% of total C was associated with soil clay fractions (Table 2.1), indicating the important role of clay particles in soil C storage. A greater contribution of clay-associated C to total C was found in the footslope than in the summit and backslope, due to a higher clay content in the footslope (Table 2.1). This could be a result of downslope transport of soil fine particles.

2.4.2 Carbon NEXAFS Spectroscopy

The SGM beamline at CLS is a bulk beamline, and with a beam spot size of 1000 μm × 100 μm, allows one to perform bulk near-edge X-ray absorption fine structure (NEXAFS) analyses on soil samples. Another great advantage of this

technique is that it allows one to characterize in-situ soil organic matter without extraction. Soil organic matter extraction techniques are controversial, and may cause alterations and artifacts.

Figure 2.1 shows C K-edge NEXAFS spectra for the soils from three hillslope locations at soil depths of 0-15 and 15-25 cm. Resonances corresponding to C functional groups were identified as (Wan et al., 2007; Lehmann et al., 2008): aromatic C at 285.5 eV, aliphatic C at 287.4 eV, carboxylic C at 288.6 eV and polysaccharides at 289.5 eV. There is no peak at 290.3 eV (Fig.2.1), which is indicative of inorganic carbonate, indicating that all the C in the studied soils is organic. In general, all the spectra in Fig.2.1 exhibited major features for aromatic and carboxylic C, as those from spectra of various soil samples (Wan et al., 2007; Lehmann et al., 2008), but differed in relative intensity. The relative intensity of the aromatic C peak was greater at a soil depth of 15-25 cm than at a soil depth of 0-15cm (Fig.2.1), suggesting that the recalcitrant aromatic C is preserved in the subsoil. Notably, compared to the summit and backslope soil, the footslope soil was enriched in aromatic C. These results suggest a selective preservation of recalcitrant aromatic C in the footslope soil. Based on field observations, the footslope soil experiences a poorly-drained condition after heavy rainfall. Due to periodic O_2 deficiency, decomposition of aromatic lignin material may be limited at the footlsope soil, thus causing enrichment in the aromatic C compounds.

2.4.3 Pyrolysis-Field Ionization Mass Spectrometry

2.4.3.1 Soil Organic Compound Classes

The summed and averaged Py-FIMS spectra and respective thermograms of total ion intensity (TII, upper right) are presented in Fig.2.2. Except for the sample from footslope at a soil depth of 25-35 cm, all the other samples showed two volatilization peaks at 320 °C and 420 °C (Fig.2.2). In the thermograms, the ratio between the first (320 °C) and the second (420 °C) volatilization maxima was much lower in the subsoils than in the top 0-15 cm soils (Fig.2.2a-e). In addition, the first volatilization peak at 320 °C disappeared and only one peak at 420 °C was found in the sample from the footslope at a soil depth of 25-25 cm (Fig. 2.2f). These results indicate a higher thermal stability of SOM from deeper soil layers, probably resulting from stronger C-C or C-mineral bonding.

The spectra of soils from depths of 0-15cm and 15-25cm in both the summit and footslope soils were dominated by sugar peaks at m/z 82/84 96 110 126 from hexoses (Fig.2.2 a-d), whereas the sample from the footlsope at a soil depth of 25-35 cm was dominated by phenols and lignin monomers and alkylaromatics at m/z 94 156 178 184 196 210 218 (Fig.2.2f). The spectra of soils from depth of 0-15 cm were nearly indistinguishable between the summit and footslope soil (Fig.2.2a-b), because they are dominated by grass vegetation. A homologous series of alkenes at m/z 252 266 280 294 308 336 was found in all the other samples except for the sample from the footslope at a soil depth of 25-35 cm (Fig.2.2). The dominant peaks for grass roots

are at m/z 194/208, which were observed in soils from soil depths of 0-15 and 15-25 cm but absent in soils from 25-35cm (Fig.2.2). In addition, the samples from soil depths of 0-15 cm and 15-25 cm also received inputs of fresh plant materials, indicated by octacosanol/nonacosanol at m/z 392/406 from epicuticular waxes (Fig.2.2a-d). Interestingly, both samples from a soil depth of 0-15cm and one sample from the summit at 15-25 cm showed intense markers of aminosugars at m/z 125, 137 and 167 from bacterial cell walls (Fig.2.2a-c), which were not found in soils from a soil depth of 25-35 cm (Fig.2.2e-f). This indicated a higher soil microbial activity in the top 25 cm. Collectively, input of fresh plant materials and grass roots and the abundance of bacteria is significantly greater in the soils from the top 0-25 cm. Fontaine et al. (2007) suggested that C in deep soil layers is protected from decomposition due to the lack of fresh plant residues to stimulate microbial activity.

The Py-FIMS spectra can be evaluated by grouping characteristic biomarker *m*/*z* signals into compound classes (Schulten, 1996). The results of this compound class evaluation are shown in Table 2.2. For Py-FIMS analysis, the signals for lignin compounds include alkylaromatics, phenols and lignin monomers, and lignin dimers, while the signals for lipid-type compounds contained lipids, alkanes, alkenes, n-alkyl esters, sterols and fatty acids. Organic matter in these pasture soils primarily contained the following compound classes (in order of abundance): alkylaromatics > phenols and lignin monomers > N-containing compounds > lipids = carbohydrates. This composition is comparable with previous Py-FIMS analyses (Sleutel et al., 2007). Soil organic matter composition generally varies with soil depth and landscape topographic

positions (Table 2.2). Despite a decrease in the relative amount of lignin dimers, the proportions of lignin significantly increased with increasing soil depth in general because of the much greater abundance of alkylaromtics and phenols and lignin monomers in the deeper soils (Table 2.2). Lignin compounds have been considered highly recalcitrant and resistant against microbial decomposition since only a limited group of fungi (white rot fungi) is capable of completely decomposing lignin to CO_2 (Kögel-Knabner 2002). Since lignin is more abundant in roots than in shoots (Rasse et al., 2005), and root biomass contributes strongly to subsoil organic matter, it is reasonable to expect an increasing lignin percentage in the subsoil. Subsoil lignin could be also stabilized by association with soil minerals such as Fe and Al oxides, since many studies have shown that the recalcitrant aromatic C compounds are preferentially sorbed by Fe and Al oxides (e.g. Gu et al., 1995; Chorover and Amistadi, 2001). These results indicate that lignin is a significant stable fraction of subsoil organic matter and therefore lignin compounds may be very important with regards to carbon storage in the subsoil environment. By comparison, the proportions of lipid products including lipids, alkanes, alkenes, n-alkyl esters, sterols and fatty acids, strongly decreased with soil depth (Table 2.2). Lipid-like compounds such as sterols and fatty acids are major organic components of fresh plant biomass and microorganisms (e.g. Gregorich et al., 1996; Kögel-Knabner, 2002). Because plant biomass inputs and microbial activity generally decreases with soil depth, one could expect a decreasing percentage of lipids with increasing soil depth. These data also suggest that lipids are not preferentially preserved in the subsoil horizons in grassland

ecosystems. Although lipids are somewhat thermodynamically stable, recent evidence has shown that lipid-type materials are not persistent in the long-term in soils (Guggenberger et al., 1994; Gleixner et al., 1999). Therefore, these compounds may represent soil organic matter stabilized in the medium term.

Landcape topographic positions also impact soil organic matter composition. The pronounced differences in the chemical composition between the summit and footslope were much greater percentages of lignin compounds (alkylaromatics, phenols and lignin monomers) found in the footslope than in the summit at soil depths of 15-25 cm and 25-35 cm, while no significant difference was found for soil organic matter composition between the summit and footslope at a soil depth of 0-15cm (Table 2.2). Lignin is a significant component of organic matter in the anaerobic environment, as decomposition of lignin primarily depends on the supply of oxygen (Williams and Yavitt, 2003). The knowledge of lignin transformation in soils and sediments, recently reviewed by Thevenot et al (2010), is mainly based on aerobic systems and uses the abundance of syringyl, guaiacyl and *p*-hydroxyphenyl moieties, oxygen functionality and chain length reduction of alkyl side-chains, and demethoxylation. The footslope soil is often under poorly-drained conditions. Decomposition of lignin in low-redox environments is slow in the absence of certain species of fungi that require aerobic conditions. Therefore, the poorly-drained conditions at footslope position, where O_2 in the soil solution is limited, could inhibit lignin decomposition and thus enrich soil organic matter in lignin compounds (Benner et al., 1984; Gleixner et al., 2001; Kogel-Knabner, 2002). No difference in the

proportions of lignin compounds among landscape positions at a soil depth of 0-15cm (Table 2.2) is probably due to the fact that surface soil organic matter is largely controlled by grass vegetation. In addition, N-containing compounds (heterocyclic nitrogen, nitriles and amides) and carbohydrates did not differ among landscape positions or soil depths (Table 2.2).

2.4.3.2 Thermal Stability of Selected Soil Organic Compound Classes:

One of the great advantages of Py-FIMS over other methods lies in the temperature-dependent volatilization of organic molecules which gives an indication of the stability of the chemical bonds involved. Temperature-resolved Py-FIMS gives an indication of the thermal energy required for the evolution of individual biomarkers of SOM. Higher thermal stability has been correlated with higher resistance to biodegradation (Leinweber et al., 2009) and increased protection of OM by the solid phase. Plante et al. (2005) found that thermal properties of clay associated OM are related to biological decomposition. Consequently, the volatilization at higher pyrolysis temperatures indicates a stronger biological stabilization.

Figure 2.3 illustrates the thermal evolution of carbohydrates, N-containing compounds (heterocyclic nitrogen, nitriles and amides), phenols and lignin monomers, lignin dimers, and lkylaromatics. In general, the sequences of summed ion intensity of these compound classes, plotted versus the pyrolysis temperature, resulted in characteristic curves of either bimodal or gaussian-like shape (Fig.2.3). The bimodal thermogram curve reflects the different OM bond strength. The volatilization of

organic matter at lower temperatures is associated with weak organic bonds. The high temperature volatilization in contrast is indicative of a thermally stable fraction with strong organic-mineral or organic-organic bonds. At soil depths of 0-15 cm and 15-25 cm, a majority of carbohydrates and N-containing compounds (heterocyclic nitrogen, nitriles and amides) was volatile at lower temperature (330-350 °C) (Fig.2.3a-c), while lignin dimers and alkylaromatics showed most intensive volatilization at high pyrolysis temperature (430-460°C) (Fig.2.3e-f). This indicates that carbohydrates and N-containing compounds are more labile organic matter in the topsoils as a result of weak C-C or C-mineral bonds, whereas alkylaromatics and lignin dimers, thermally resistant up to high temperature, are stabilized fractions of soil organic compounds. The volatilization curves of phenols and lignin monomers showed one major peak at 340 °C and a second at 470 °C at soil depths of 0-15 cm and 15-25 cm (Fig.2.3d), indicating phenols and lignin monomers contained both labile and stable organic compounds due to different C-C or C-mineral bonding strengths.

As soil depth increases from 0-25 cm to 25-35 cm, the major peak of carbohydrates and N-containing compounds (heterocyclic nitrogen, nitriles and amides) shifted toward higher temperatures (Fig.2.3a-c), indicating increased thermal energy for these compounds released from soils. The peak temperature for carbohydrates shifted by 30 K and 80 K at the summit and footslope, respectively (Fig.2.3a). In comparison to carbohydrates, a greater shift of N-containing compounds heterocyclic nitrogen, nitriles and amides) was characterized at 80 K and 120 K higher temperatures at the summit and footslope, respectively (Fig.2.3b-c). The thermal

evolution curves of phenols and lignin monomers showed that a ratio of the high temperature volatilization peak to the low temperature volatilization peak increased with soil depth (Fig.2.3d). In addition, the high temperature volatilization peak shifted to a 20 K higher temperature for the footslope soil from a soil depth of 25-35 cm (Fig.2.3d). These results indicate that the stability of organic matter changes with soil depth, with increasing stability in deeper horizons. These organic substances are either stabilized by C-C bonds in organic matter or more strongly bound to the mineral matrix. The latter follows from the shift of evolution maxima toward higher temperatures with significant lower amounts of C associated with soil minerals in deeper soils. Therefore it seems that organic mineral bonds contributed to the spectra. And the strong organic-mineral binds could have a pronounced protection of OM in the subsoil. This confirms the conclusion of Kaiser and Guggenberger (2003) that potential OM stabilization at mineral surfaces is limited to those OM molecules that sorb to surfaces with small surface loading. According to Kaiser and Guggenberger (2003, 2007), at higher OM loadings at the mineral surface, less organic ligands per organic molecule are involved in the bonding, making the organic molecules more flexible and extending more into the soil solution, thus making them more susceptible for microbial decomposition. Sollins et al. (2006) and Kleber et al. (2007) provide an alternative explanation stating a zonal structure for OM associated with mineral surfaces, with the outer layers of the OM having a more rapid turnover than the inner ones. A greater shift of major peaks of carbohydrates, N containing compounds and phenols and lignin monomers toward high temperatures was found in the footslope

than in the summit (Fig.2.3a-d), implying that landscape positions influence the stability of the OM, with increasing stability displayed at depressional locations. There were noo temperature shifts for lignin dimers and alkylaromatics as soil depth increased (Fig.2.3e-f), indicating that some organic constituents, e.g lignin, are thermally resistant up to high temperatures which was observed in the previous studies (Schulten, et al ., 1993, Schulten and Leinweber, 1999), and are of little diagnostic value for the investigation of organic-mineral bonds.

2.5 Conclusions

The goal of this study was to apply NEXAFS and Py-FIMS to examine the changes in SOM composition along a pasture hillslope. These two techniques were able to reveal common trends among soil depths and landscape topographic locations. The relative amount of recalcitrant aromatic C compounds and lignin materials including alkylaromatics, phenols and lignin dimers increased with soil depth, while the proportions of lipid-like compounds such as alkanes, alkenes, n-alkyl esters, sterols and fatty acids decreased with soil depth. A greater contribution of clay associated C to total C was found in the footslope than in the summit, due to accumulation of clay particles in footslope as a result of erosion and deposition. In addition, the footslope soil was enriched in recalcitrant aromatic C compounds and lignin materials including alkylaromatics and phenols and lignin monomers. N-containing compounds did not show variations with soil depth and hillslope location.

Py-FIMS thermal evolution curves provide valuable information on the thermal stability of specific organic compound classes. It was shown that at a soil depth of 0-25cm, alkylaromatics and lignin dimers, thermally resistant up to high temperatures, were stabilized fractions of soil organic compounds, while carbohydrates and N-containing compounds were more labile organic matter. As soil depth increased from 0-25 cm to 25-35 cm, the thermal stability of carbohydrates and N-containing compounds was significantly increased probably as a result of stronger C-mineral bonds, while alkylaromatics and lignin dimers did not show variations in thermal stability with soil depth. Pheonls and lignin monomers, containing both labile and stable forms of organic matter, showed increasing stability at deeper soils. The thermal stability of carbohydrates, N-containing compounds, and phenols and lignin monomers changed with landscape position, with increasing stability in depressional landscape positions. In conclusion, our study suggests that organic compounds are more recalcitrant and stable in the subsoil and depressional locations.

REFERENCES

Amelung, W.; Zech, W.; Zhang, X.; Follett, R. F.; Tiessen, H.; Knox, E.; Flach, K. W., Carbon, nitrogen, and sulfur pools in particle-size fractions as influenced by climate. *Soil Sci. Soc. Am. J.* **1998**, 62, 171-181.

Baldock, J. A.; Oades, J. M.; Waters, A. G.; Peng, X.; Vassallo, A. M.; Wilson, M. A., Aspects of the chemical structure of soil organic materials as revealed by solid-state ^{13}C NMR spectroscopy. *Biogeochem.***1992**, 16, 1-42.

Baldock, J. A.; Skjemstad, J. O., Role of the soil matrix and minerals in protecting natural organic materials against biological attack. *Org. Geochem.* **2000**, 31, 697-710.

Benner, R.; Maccubin, A. E.; Hodson, R. E., Anaerobic biodegradation of the lignin and polysaccharide components of ligocellulose and synthetic lignin by sediment microflora. *Appl. Environ. Microbiol.* **1984**, 47, 998-1004.

Chan, K. Y., Soil particulate organic carbon under different land use and management. *Soil Use Manage.* **2001**, 17, 217-221.

Chorover, J.; Amistad, M. K., Reaction of forest floor organic matter at goethite, birnessite and smectite surfaces. *Geochim. Cosmochim. Acta* **2001**, 65(1), 95-109.

Fontaine, S.; Barot, S.; Barre, P.; Bdioui, N.; Mary, B.; Rumpel. C., Stability of organic carbon in deep soil layers controlled by fresh carbon supply. *Nature* **2007**, 450, 277-280.

Fox, C. A.; Preston, C. M.; Fyfe, C. A., Micromorphological and 13C NMR characterization of a humic, lignic, and histic folisol from British Columbia. *Can. J. Soil Sci.* **1994**, 74, 1-15.

Gill, R. A.; Burke, I. C., Influence of soil depth on the decomposition of *Bouteloua gracilis* roots in the shortgrass steppe. *Plant Soil* **2002**, 241, 233-242.

Gleixner, G.; Bol, R.; Alesdent, J. B., Molecular insight into soil carbon turnover. *Rapid Commun. Mass Sp.* **1999**, 13, 1278-1283.

Gleixner, G.; Czimczik, C. I.; Kramer, C.; Lühker, B.; Schmidt, M. W. I., Plant compounds and their turnover and stabilization as soil organic matter. In: Schulze, E.-D., Heimann, M., Harrison, S., Holland, E., Lloyd, J., et al. (Eds.), Global Biogeochemical Cycles in the Climate System. Academic Press, San Diego, **2001**, 201-215.

Gregorich, E. G.; Anderson, D. W., The effects of cultivation and erosion onsoils of four toposequences in the Canadian prairies. *Geoderma* **1985**, 36, 343-54.

Gregorich, E.G.; Monreal, C.M.; Schnitzer, M.; Schulten, H.R., Transformation of plant residues into soil organic matter: Chemical characterization of plant tissue, isolated soil fractions, and whole soils. *Soil Sci.* **1996**, 161, 680-693.

Gu, B.H.; Schmitt, J.; Chen, Z.; Liang, L.Y.; McCarthy, J. F., Adsorption and desorption of natural organic matter on iron oxide: mechanisms and models. *Environ. Sci. Technol.* **1994**, 28, 38-46.

Guggenberger, G.; Christensen, B.T.; Zech, W., Land use effects on the composition of organic matter in soil particle size separates: I. Lignin and carbohydrate signature. *Eur. J. Soil Sci*. **1994**, 45, 449-458.

Jenny, H., The Soil Resource, Origin and Behaviour, Springer-Verlag, New York. **1980**.

Williams, C. J.; Yavitt, J. B., Botanical composition of peat and degree of peat decomposition in three temperate peatlands. *Ecoscience* **2003**,10, 85-95.

Kaiser, K., Sorption of natural organic matter fractions to goethite (α-FeOOH): Effect of chemical composition as revealed by liquid-state 13C NMR and wet chemical analysis. *Org. Geochem*. **2003,** 34, 1569-1579.

Kaiser, K.; Guggenberger, G., Mineral surfaces and soil organic matter. *Eur. J. Soil Sci.* **2003**, 54(2), 219-236.

Kaiser, K.; Guggenberger, G., Sorptive stabilization of organic matter by microporous goethite: sorption into small pores vs. surface complexation. *Eur. J. Soil Sci.* **2007**, 58 (1), 45-59.

Kalbitz, K.; Schwesig, D.; Rethemeyer, J.; Matzner, E., Stabilization of dissolved organic matter by sorption to the mineral soil. *Soil Biol*. *Biochem*. **2005**, 37, 1319-1331.

Kim, J. S.; Ree, M.; Lee, W. S.; Oh, W.; Baek, S.; Lee, B.; Shin, T. J.; Kim, K. J.; Kim, B.; Luning, J., NEXAFS spectroscopy study of the surface properties of zinc glutarate and its reactivity with carbon dioxide and propylene oxide. *J. Catal.* **2003**, 218, 386-395.

Kleber, M.; Johnson, M. G., Advances in understanding the molecular structure of soil organic matter: Implications for interactions in the environment. *Adv*. *Agron*. **2010**, 106, 77-142.

Kleber, M.; Sollins, P.; Sutton, R., A conceptual model of organo-mineral interactions in soils: self-assembly of organic molecular fragments into zonal structures on mineral surfaces. *Biogeochem.* **2007**, 85, 9-24.

Kögel-Knabner, I., The macromolecular organic composition of plant and microbial residues as inputs to soil organic matter. *Soil Biol. Biochem.* **2002**, 34, 139-162.

Kölbl, A.; Kögel-Knabner, I., Content and composition of particulate organic matter in arable cambisols of different texture. *J. Plant Nutr. Soil Sc.* **2004**, 167, 45-53.

Mahieu, N.; Powlson, D. S.; Randall, E. W., Statistical analysis of published carbon-13 CPMAS NMR spectra of soil organic matter. *Soil Sci*. *Soc*. *Am*. J. **1999**, 63, 307-319.

Lehmann, J.; Solomon, D.; Kinyang, J.; Dathe, L.; Wirick, S.; Jacobsen, S., Spatial complexity of soil organic matter forms at nanometer scales. *Nature Geosci*. **2008**, 1, 238-242.

Leinweber, P.; Walley, F.; Kruse, J.; Jandl, G.; Eckhardt, K. U.; Blyth, R. I. R.; Regier, T., Cultivation Affects Soil Organic Nitrogen: Pyrolysis-Mass Spectrometry and Nitrogen K-edge XANES Spectroscopy Evidence. *Soil Sci. Soc. Am. J.* **2009**, 73, 82-92.

Lorenz, K.; Lal, R., The depth distribution of soil organic carbon in relation to land use and management and the potential of carbon sequestration in sub-soil horizons. *Adv*. *Agron*. **2005**, 88, 36-66.

Mao, J. D.; Fang, X. W.; Rohr, K. S.; Carmo, A. M.; Hundal, L.S.; Thompson, M. L., Molecular-scale heterogeneity of humic acid in particle-size fractions of two Iowa soils. *Geoderma* **2007**, 140, 17-29.

Mikutta, R.; Kleber, M.; Torn, M.S.; Jahn, R., Stabilization of soil organic matter: Association with minerals or chemical recalcitrance? *Biogeochem.* **2006**, 77(1), 25-56.

Mikutta, R.; Mikutta, C.; Kalbitz, K.; Scheel, T.; Kaiser, K.; Jahn, R., Biodegradation of forest floor organic matter bound to minerals via different binding mechanisms. *Geochim. Cosmochim. Acta* **2007**, 71, 2569-2590.

Newbold, J. D.; Bott, R. L.;Kaplan L. A.; Sweeney, B. W.; Vannote, R. L., Organic matter dynamics in White Clay Creek, Pennsylvania, USA. *J. North Am. Benthol. Soc*. **1997**, 16(1), 46-50.

Omoike, A.; Chorover, J., Adsorption to goethite of extracellular polymeric substances from Bacillus subtilis. *Geochim*. *Cosmochim*. *Acta* **2006***,* 70, 827-838.

Pennock, D. J.; Anderson, D. W.; Jong, E. de., Landscape scale changes in indicators of soil quality due to cultivation in Saskatchewan, Canada. *Geoderma* **1994**, 64(1-2), 1-19.

Plante, A. F.; Fernández, J. M.; Haddix, M. L.; Steinweg, J. M.; Conant, R. T., Biological, chemical and thermal indices of soil organic matter stability in four grassland soils. *Soil Biol. Biochem.* **2011**, 43, 1051-1058.

Plante, A. F.; Pernes, M.; Chenu, C., Changes in clay-associated organic matter quality in a C depletion sequence as measured by differential thermal analyses. *Geoderma* **2005**, 129, 186-199.

Rasse, D. P.; Mulder, J.; Moni, C.; Chenu, C., Carbon turnover kinetics with depth in a French loamy soil. *Soil Sci*. *Soc*. *Am*. *J*. **2006**, 70:2097-2105.

Rumpel, C.; Kogel-Knaber, I., Deep soil organic matter-A key but poorly understood component of terrestrial C cycle. *Plant Soil* **2011**, 338:143-158.

Safari Sinegani, A. A.; Emtiazi, G.; Shariatmadari, H., Sorption and immobilization of cellulase on silicate clay minerals, *J*. *Colloid Interf. Sci*. **2005, 290**, 39-44.

Schmidt, M. W. I.; Knicker, H.; Kogel-Knabner, I., Organic matter accumulating in Aeh and Bh horizons of a Podzol - chemical characterization in primary organo-mineral associations. *Org. Geochem.* 2000, 31, 727-734.

Schulten, H. R., Direct pyrolysis-mass spectrometry of soils: a novel tool in agriculture, ecology, forestry, and soil science. In: Yamasaki S, Boutton TW (eds) Mass spectrometry of soils. Dekker, *New York*, **1996**, 373-436.

Schulten, H. R.; Leinweber, P., Thermal stability and composition of mineral-bound organic matter in density fractions of soil. *Eur. J. Soil Sci.* **1999,** 50, 237-248.

Schulten, H. R.; Schnitzer, M., Chemical model structures for soil organic matter and soils. *Soil Sci.* **1997**, 162, 115-130.

Sleutel, S.; Kader, M. A.; Leinweber, P.; D'Haene, K.; De Neve, S., Tillage management alters surface soil organic matter composition: A pyrolysis mass Spectroscopy study. *Soil Sci. Soc. Am. J.* **2007**, 71, 1620-1628.

Sloto, R. A., Geology, hydrology, and ground water quality of Chester County, Pennsylvania, Chester County Water Resources Authority Water- Resource Report 2. **1994**.

Sollins, P.; Homann, P.; Caldwell, B. A., Stabilization and destabilization of soil organic matter: mechanisms and controls. *Geoderma* **1996**, 74, 65-105.

Sollins, P.; Swanston, C.; Kleber, M.; Filley, T.; Kramer, M.; Crow, S.; Caldwell, BA.; Lajtha, K.; Bowden, R., Organic C and N stabilization in a forest soil: Evidence from sequential density fractionation. *Soil Biol. Biochem.* **2006**, 38, 3313-3324.

Sorge, C.; Muller, R.; Leinweber, P.; Schulten, H. R., Pyrolysis-mass spectrometry of whole soils, soil particle-size fractions, litter materials and humic substances: Statistical evaluation of sample weight, residue, volatilized matter and total ion intensity. *Fresenius J. Anal. Chem*. **1993**, 346, 697-703.

Swift, R. S. Sequestration of carbon by soil. *Soil Sci*. **2001**, 166, 858-871.

Taylor, J.P.; Wilson, B.; Mills, M. S.; Burns, R. G., Comparison of microbial numbers and enzymatic activities in surface soils and subsoils using various techniques. *Soil Biol. Biochem*. **2002**, 34, 387-401.

Thevenot, M., Dignac, M. F., Rumpel, C., Fate of lignins in soils: A review. *Soil Biol. Biochem.* **2010**, 42(8), 1200-1211.

Torn, M. S.; Trumbore, S. E.; Chadwick, O. A.; Vitousek, P. M.; Hendricks, D. M., Mineral control of soil organic carbon storage and turnover. *Nature* **1997**, 389, 170-173.

Verity, G. E.; Anderson, D. W., Soil erosion effects on soil quality and yield. *Can. J. Soil Sci.* **1990**, 70, 471-484.

Viaud, V.; Angers, D.; Walter, C., Toward landscape-scale modeling of soil organic matter dynamics in agroecosystems. *Soil Sci. Soc. Am. J.* **2010**, 74, 1847-1860.

von Lützow, M.; Kögel-Knabner, I.; Ekschmitt, K.; Matzner, E.; Guggenberger, G.; Marschner, B.; Flessa, H., Stabilization of organic matter in temperate soils: mechanisms and their relevance under different soil conditions-a review. *Eur. J. Soil Sci.* **2006, 57, 426-445.**

Wan, J. M.; Tyliszczak, T.; Tokunaga, T. K., Organic carbon distribution, speciation, and elemental correlations with soil micro aggregates: applications of STXM and NEXAFS spectroscopy. *Geochim. Cosmochim. Acta* **2007**, 71(22), 5439-5449.

Table 2.1 C and N content and atomic C/N ratio in bulk soils and their clay fractions, clay content and percentage of clay-associated C in total C.

Landscape Location	Soil depth (cm)	C content (%)		N content (%)		Atomic C/N ratio		Clay content (%)	Fraction of clay-associated C in total C (%)
		Whole soil	Clay fraction	Whole soil	Clay fraction	Whole soil	Clay fraction		
Summit	0-15	3.06	7.26	0.33	0.93	10.82	7.81	20	47
	15-25	1.75	4.91	0.20	0.64	10.21	7.67	20	56
	25-35	0.66	1.81	0.08	0.25	9.63	7.24	20	55
Backslope	0-15	2.87	7.03	0.31	0.87	10.80	8.08	18	44
	15-25	1.65	4.75	0.19	0.62	10.13	7.66	18	52
	25-35	0.63	1.73	0.08	0.24	9.19	7.21	17	47
Footslope	0-15	2.76	6.87	0.28	0.84	11.50	8.18	24	60
	15-25	1.59	4.43	0.18	0.60	10.31	7.38	24	67
	25-35	0.52	1.38	0.07	0.19	8.67	7.26	25	66

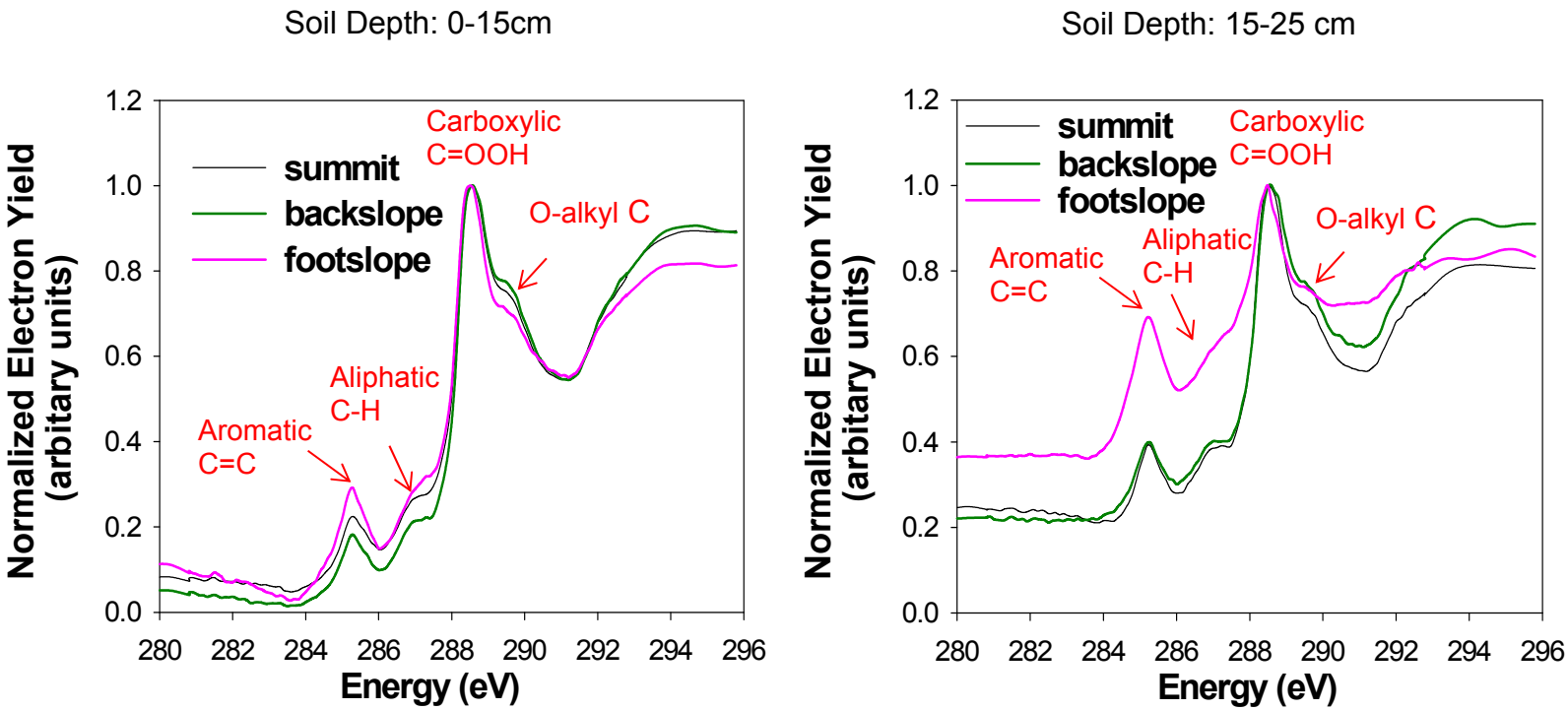

Figure 2.1 C (1s) NEXAFS spectra of soil organic matter from different hillslope locations at soil depths of 0-15 and 15-25 cm.

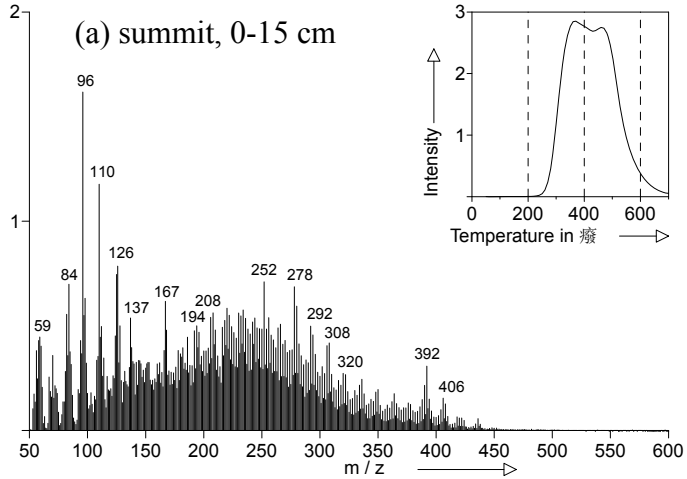
(a) summit, 0-15 cm
Intensity
Temperature in 癈
m / z

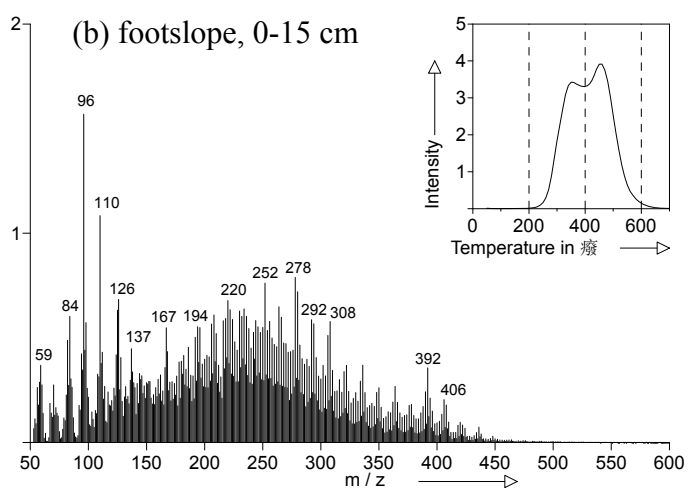
(b) footslope, 0-15 cm
Intensity
Temperature in 癈
m / z

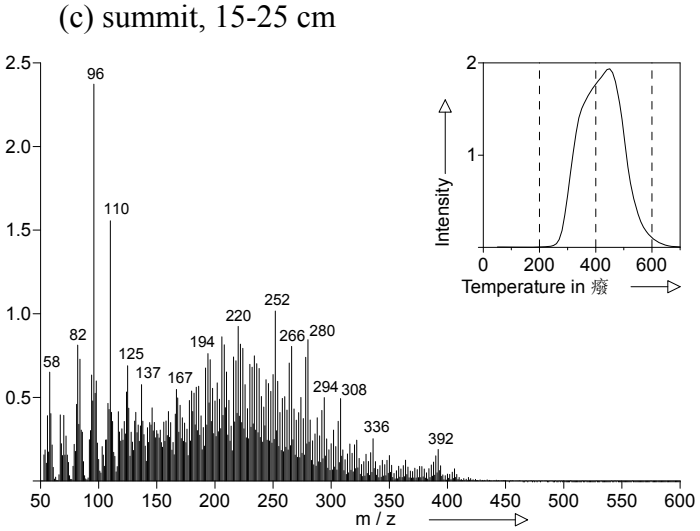
(c) summit, 15-25 cm
Intensity
Temperature in 癈
m / z

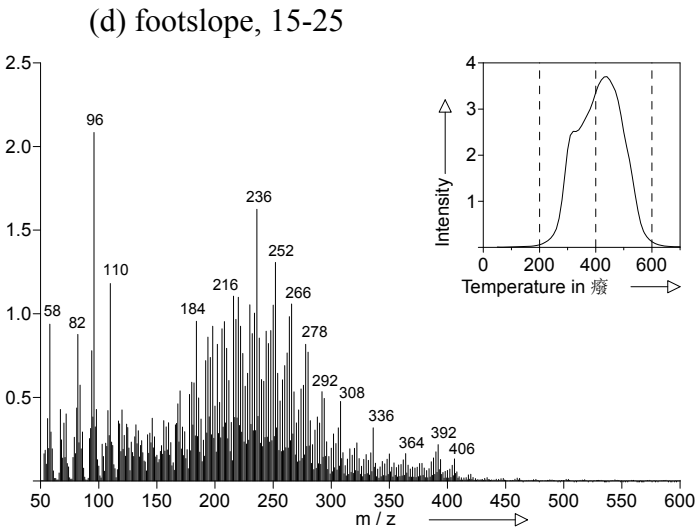
(d) footslope, 15-25
Intensity
Temperature in 癈
m / z

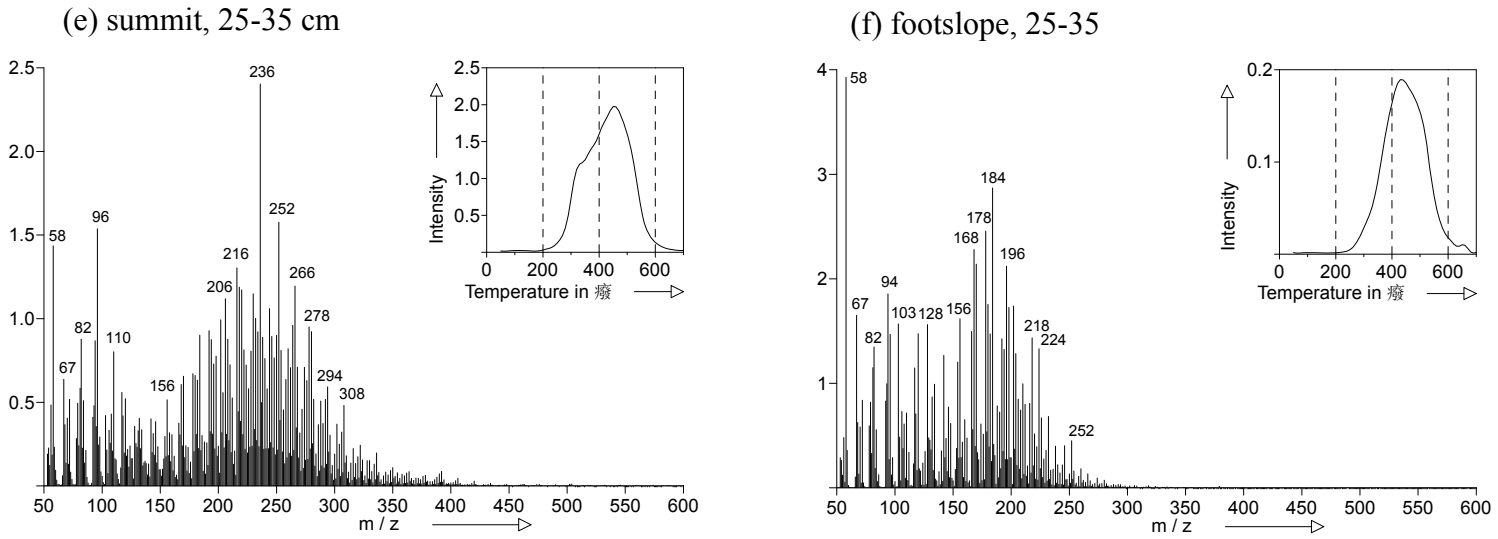

Figure 2.2 Summed and averaged pyrolysis–field ionization mass spectra and thermograms of total ion intensity (TII, inset) of summit and footslope soils obtained from three soil depths of 0-15, 15-25 and 25-35 cm.

Table 2.2 Compound class groups of marker signals from pyrolysis-field ionization mass spectrometry of summit and footslope soils obtained from three soil depths of 0-15, 15-25 and 25-35 cm.

Location	Soil Depth (cm)	EX1	EX2	EX3	EX4	EX5	EX6	EX7	EX8	EX10	Lignin	Lipids	N-containing compounds
		% of total ion intensity											
Summit	0-15	7.9	8.9	3.4	6.9	10	9	1.7	3.7	1	22.3	9.6	12.7
	15-25	8.6	11	3.5	6.3	12.8	8.8	1	3.3	0.6	27.3	7.9	12.1
	25-35	5.9	14.8	1.7	5.2	15.7	8.7	0.4	3.1	0.5	32.2	6.1	11.8
Footslope	0-15	7.1	8.7	3.9	8.2	10.9	8.2	2.2	2.9	1.5	23.5	11.9	11.1
	15-25	7	15.3	1.5	5.6	14.1	7.9	1.2	3	1.1	30.9	7.9	10.9
	25-35	7.8	21	0.5	3.4	23.1	8.5	0	3.5	0.1	44.6	3.5	12

EX1: Carbohydrates; EX2: Phenols and lignin monomers; EX3: Lignin dimers; EX4: Lipids, alkanes, alkenes, fatty acids, n-alkyl esters; EX5: Alkyl aromatics; EX6: Heterocyclic nitrogen and nitriles; EX7: Sterols; EX8: Amides (amino acids, peptides and aminosugars; EX10: Free fatty acids C16 to C34.
Lignin: EX2+EX3+EX5; Lipids: EX4+EX7+EX10; N-containing compounds: EX6+EX8.

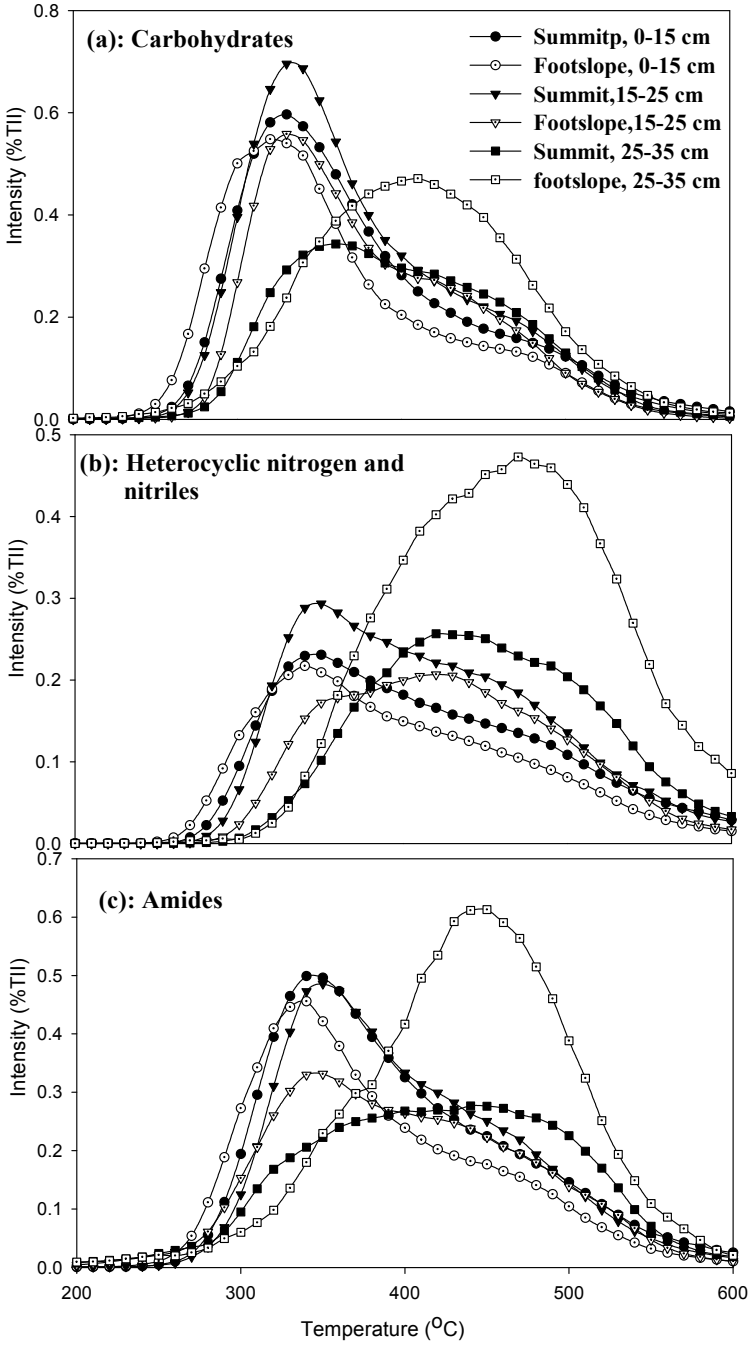
(a): Carbohydrates
Summitp, 0-15 cm
Footslope, 0-15 cm
Summit,15-25 cm
Footslope,15-25 cm
Summit, 25-35 cm
footslope, 25-35 cm
(b): Heterocyclic nitrogen and nitriles
(c): Amides
Intensity (%TII)
Temperature (°C)

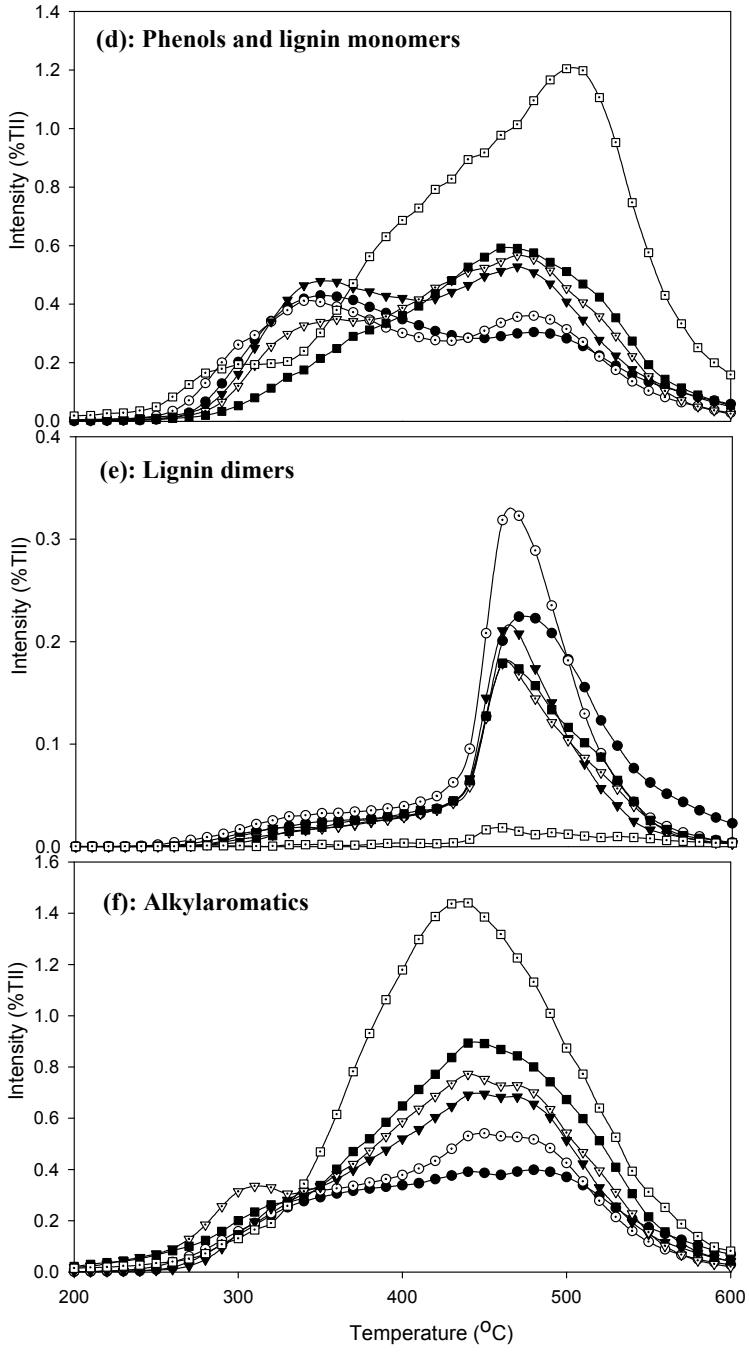

Figure 2.3 Pyrolysis thermograms of (a) carbohydrates, (b) heterocyclic nitrogen and nitriles, (c) amides, (d) phenols and lignin monomers, (e) lignin dimers, and (f) alkylaromatics from summit and footslope soils at soil depths of 0-15, 15-25 and 25-35 cm. Peaks at higher temperatures indicate higher thermal stability.

Chapter 3

SOFT X-RAY SPECTROMICROSCOPY STUDY OF MINERAL-ORGANIC MATTER ASSOCIATIONS IN PASTURE SOIL CLAY FRACTIONS

3.1 Abstract

There is a growing acceptance that associations with soil minerals may be the most important overarching stabilization mechanism for soil organic matter. However, direct investigation of organo-mineral associations has been hampered by a lack of methods that can simultaneously characterize organic matter (OM) and soil minerals. In this study, STXM-NEXAFS spectroscopy at the C 1s, Ca 2p, Fe 2p, Al 1s and Si 1s edges was used to investigate C associations with Ca, Fe, Al and Si species in soil clay fractions from an upland pasture hillslope. Bulk techniques including C and N NEXAFS, Fe K-edge EXAFS spectroscopy and XRD were applied to provide supplementary information. Results demonstrated that carbon was associated with Ca, Fe, Al, and Si with no seperate phase in soil clay particles. In the soil clay particles, the pervasive C forms were aromatic C, carboxyl C and polysaccharides over surfaces with the relative abundance of carboxyl C and polysaccharides varing spatially at the submicron scale. Only limited regions in the soil clay particles had aliphatic C. Good C-Ca spatial correlations were found for soil clay particles and $CaCO_3$ was not present, suggesting a strong role of Ca in organomineral assemblage formation. Fe EXAFS showed that about 50% of the total Fe in soils was contained in Fe(III) oxides,

whereas Fe-bearing aluminosilicates (vermiculite and illite) accounted for another 50%. Fe(III) oxides in the soil were mainly crystalline goethite and hematite, with lesser amounts of poorly-crystalline ferrihydrite. XRD revealed that soil clay aluminosilicates were hydroxy-interlayered vermiculite, illite and kaolinite. C showed similar correlation with Fe to Al and Si, implying similar associations of Fe(III) oxides and aluminosilicates with organic matter in organo-mineral associations. These direct microscopic determinations can help improve understanding of organo-mineral interactions in soils.

3.2 Introduction

Soil organic matter (OM) represents the largest terrestrial carbon (C) reservoir on a global scale. The soil's ability to accumulate and retain C has received increasing interest, as the concerns about climate change grow. Intimate association of OM with mineral phases has been acknowledged as a fundamental mechanism for stabilizing organic compounds against biological degradation (Torn et al., 1997; Baldock et al., 2001; Lützow et al., 2006), controlling the long-term sequestration of organic matter in terrestrial ecosystems. However, the fundamental nature of the interactions between OM and soil mineral components is not well understood. Since both the organic and mineral phases of soils are involved, the extent to which OM interacts with minerals depends on both the physical and chemical properties of the mineral fraction as well as on the morphology and chemical structure of the organic material (Baldock et al., 2001; Kaiser, 2003; Kaiser & Guggenberger, 2000; Mikutta et al., 2007).

Mineral surfaces in soils are dominated by the soil clay fraction (<2 μm). This fraction is a mixture of aluminosilicates, oxides, and hydroxides, and, in some soil types, short–range ordered minerals like allophane and imogolite. Iron and aluminum (oxy) hydroxides are particularly effective in sorbing and stabilizing OC in soils (Kaiser & Guggenberger, 2000; Kaiser et al, 2002; Kiem & Kögel-Knabner, 2002; Wiseman & Püttmann, 2009). Studies have shown that stable OC is well correlated with amorphous and poorly crystalline Al and Fe minerals in soils (Torn et al., 1997; Mikutta et al., 2005). The aluminosilicate clay minerals can also help preserve organic matter (Chorover & Amistadi, 2001). However, metal oxides may have better sorptive potential on a weight basis (mg C g^{-1}) than aluminosilicates (Mikutta et al., 2007; Kaiser et al., 1996; Kaiser & Zech., 19993), due to their large specific surface area with a high density of surface functional groups. Mikutta et al (2007), for instance, examined the adsorption of dissolved organic carbon (DOC) on mineral surfaces and found that goethite adsorbed more carbon than aluminosilicates (pyrophyllite and vermiculite).

Specific compounds bearing certain chemical functional groups may be responsible for binding to specific mineral surfaces (Kleber et al., 2007) and form very stable organic carbon pools with long turnover times. The relationship between soil mineral components and the chemistry of bound OM has been suggested using chemical fractionation of OM after sorption with different minerals (Chorover & Amistadi, 2001; Kaiser 2003; Gu et al., 1994; Wang & Xing, 2005; Kang & Xing, 2008; Namjesnik-Dejanovic et al., 2000). It has been shown that OM rich in aromatic

moieties and carboxyl groups is preferentially adsorbed on Al and Fe oxides (Kaiser 2003; Gu et al., 1994), while aliphatic fractions are preferentially adsorbed by clay minerals (Wang & Xing, 2005). However, Kang and Xing (2008) found that aliphatic fractions were preferentially adsorbed by goethite, while Namjesnik-Dejanovic et al. (2000) found more aromatic fractions of fulvic acid were preferentially adsorbed onto clay. The composition of OM stabilized by specific minerals has also been suggested by analyzing OM in mineralogically diverse density or size fractions of soils (Larid et al., 2001; Kahle et al., 2003; Kleber et al., 2004). However, a straightforward evaluation of a mineralogical control can, however, be compromised by the fact that OM in different soil fractions is subjected to different degrees of microbial transformations, which may mask the mineral-induced speciation. Therefore, the role of minerals on OM composition remains an open question.

As discussed above, most of the information on mineral-organic interactions was derived from indirect methods and/or macroscopic observations. Therefore there is a need to relate these laboratory results to natural processes and directly investigate the associations of OM with specific minerals in natural soils using high spatial resolution and state-of-the-art spectroscopic techniques. However, this is challenging because there are few techniques that can simultaneously characterize soil organic matter and soil minerals. Scanning Transmission X-ray Microscopy (STXM), combined with Near Edge X-ray Absorption Fine Structure spectroscopy (NEXAFS) is a powerful method for analyses of C functional group distribution in soils and sediments at the nanoscale (Schumacher et al., 2005; Lehmann et al., 2007 2008; Wan

et al., 2007). Not only is the spatial distribution of OM important, but also the specific association with certain minerals. However, most synchrotron-based soft X-ray spectroscopic analyses do not provide enough flux at higher energies to quantify Al and Si, which are the major elements in soil clay minerals. To our knowledge, only one paper has been published so far showing the spatial association of C with Fe, Al, Si, Ca and K in soils (Wan et al., 2007). In this study, some associations between OM and mineral cations were obscured by the presence of very thick particles. Further research is needed to more clearly investigate the spatial association of C with different mineral phases. In addition to using STXM to map C species, Ca, Fe, Al and Si were also speciated and mapped. Our objectives were to: (i) determine the spatial distribution of the major cations (Ca, Fe, Al and Si) and their speciation in soil clay fractions; (ii) determine the spatial arrangement of C and its correlation with cation (Ca, Fe, Al and Si) species in soil clay fractions; and (iii) investigate the spatial distribution of C functional groups and their associations with the mineral phases within the soil clay fractions.

3.3 Experimental Section

3.3.1 Sampling Sites

Our field site is located within the long-term 725-ha research watershed upstream of the Stroud Water Research Center (SWRC) in southeastern PA (39º53'N, 75º47'E). The 3rd-order watershed forms the headwaters of the White Clay Creek and

is an intensive study site for the established Christina River Basin Critical Zone Observatory (CRB-CZO). The watershed is underlain by highly metamorphosed sedimentary rocks containing gneisses, schists, quartzites, and marbles (Sloto, 1994). The soils are primarily Typic Hapludults (Newbold et al., 2007). Soil samples were collected from the summit and footslope of a pasture hillslope with an angle of 13°, at soil depths of 0-15 cm (A horizon). The pasture has been established for at least 50 yrs.

We specifically examined clay-sized organo-mineral associations isolated from the soils. We chose the clay fractions because a majority of particulate organic matter was removed from this fraction. Our choice of clay fractions was additionally motivated by the technical difficulty in making thin sections of soil samples and possible alteration of C speciation during preparation of thin sections. In this study, the soil clay fractions were simply analyzed with STXM without any alteration.

3.3.2 Clay Fraction Separation

The bulk soil samples were air-dried, and roots and visible plant material were removed. The >2mm fraction was removed by dry sieving. The clay fraction separation was performed according to Amelung et al. (1998). Briefly, thirty grams of soil were ultrasonically treated with an energy input of 60 J mL^{-1} using a probe type sonicator at a soil/water ratio of 1:5 (w/v). The coarse sand fraction (>250 μm) was removed by wet sieving. To completely disperse the remaining suspension, ultrasonication was again applied with an energy input of 440 J mL^{-1}at a soil/water

ratio of 1:10 (w/v). The sand fraction (>53 μm) was removed by wet sieving the clay-sized fraction (<2 μm) was separated from the silt and sand sized separates by repeated centrifugation. The clay fractions were then freeze-dried.

3.3.3 Scanning Transmission X-ray microscope (STXM)

Samples for STXM analysis were prepared by depositing 1-2 μl of an aqueous suspension (1 mg of the clay fraction mixed with 1 ml deionized-distilled water)onto a Si_3N_4 window (75 nm thick), which was then air-dried. The samples were analyzed at STXM spectromicroscopy beamline 10ID-1 at the Canadian Light Source (CLS), a 2.9 GeV third-generation synchrotron source (Kaznatcheev et al., 2007). The beamline is equipped with an APPLE II type elliptically polarizing undulator (EPU), which provides circularly polarized light (up to 1000 eV) and linearly polarized light (130-2500 eV). All measurements were performed using a 25 nm Fresnel zone plate, which provided a maximum spatial resolution of ~30 nm and the samples were kept under 1/6 atm of He during data collection.

The samples were raster scanned in STXM with synchronized detection of transmitted X-rays to generate images. Chemical imaging and NEXAFS spectra were obtained using image sequence scans (i.e., stacks) over a range of photon energies at a specific element edge. The C 1s, Ca 2p, Fe 2p, Al 1s and Si 1s data were collected (in that order) over the same areas in order to identify the associations of OC with specific soil mineral phases. The stack measurements for each element were obtained with dwell times of 1-1.5 ms and with pixel sizes from 40-80 nm.

3.3.4 Data Analysis

The aXis2000 software package was used for image and spectra processing (Hitchcock, 2000).The image sequences were aligned and then converted to optical density (OD=ln (I_0/I)) by using the transmitted flux through the sample (I) and the incident flux measured in an empty region adjacent to the analyzed particles (I_0), to correct for the absorbance by the silicon nitride membranes. According to Lambert Beer's law, the optical density (OD) is directly proportional to the amount (thickness) of the individual compound in the X-ray beam path.

The C distribution map was obtained by subtracting below-edge OD map from its above-edge OD map. The C thickness estimate was obtained by dividing OD values by the product RE$\cdot\mu\cdot f\cdot\rho$, where RE is the resonance enhancement factor, μ is the difference between the mass absorption coefficient above and below the absorption edge, f is the mass fraction of the element within the solid phase, and ρ is the solid phase density (Table A.1, Wan et al., 2007). The distribution of Ca, Fe, Al and Si was mapped by the difference between two images, one measured at the energy of a strong characteristic absorption feature and the other measured at an energy below the onset of absorption for the specific element. The image difference map was made quantitative by converting the change in the optical density (ΔOD) scale to effective thickness (in nm) using a scale factor determined from the linear absorbance (optical density per nm) for a specific compound at the top photon energies. The energies and scaling factor used for the quantification of the image difference maps (on-resonance minus off-resonance) for each element are listed in Table A.2.

For the spatial analyses of C, Ca, Fe, Al and Si species, principle component analysis (PCA) and cluster analysis (CA) were carried out on image sequence data for each individual element. The image sequence data were orthogonalized and noise-filtered by principal component analysis. Significant components were determined based on observations of the eigenvalues, eigenimage, and eigenspectra (Lerotic et al., 2005). Cluster analysis was used to identify sample regions with similar spectral properties. Singular value decomposition (SVD) was performed to calculate target maps and corresponding fitted target spectra from the spectra obtained by cluster analysis.

3.4 Results and Discussion

3.4.1 Soil C Content and Clay Mineralogy

In general, the footslope soils contained lower C content than the summit soils but the difference was very small (Table A.3). C content was significantly greater in the clay fractions than in the sand and silt fractions. In combination with particle size distribution data shown in Table A.3, 47-60% of total C is in the clay fractions (Table A.3), indicating the important role of clay particles in soil C storage. A greater contribution of clay-associated C to total C was found in the footslope than in the summit soil, due to a higher clay content in the footslope soil (Table A.4) as a result of erosion and deposition.

The predominate clay minerals in the soils were hydroxy-interlayered vermiculite (HIV), illite and kaolinite based on X-ray diffraction (XRD) results (Table A.5). Compared to the summit soil, the footslope soil contained a larger fraction of kaolinite followed by a lower percentage of hydroxy-interlayered vermiculite, implying that the footslope soil might have experienced a greater degree of chemical weathering than the summit soil.

3.4.2 Mapping Carbon and Carbon Functional Group Distribution

The fine-scale spatial distribution of total C and its functional groups was only obtained for the thin regions from the summit and footslope soil clay particles (Fig.3.1). For the thick regions of the clay particles, there was a dip (reversed peak) in the C 1s NEXAFS spectra at around 284.5 eV (Fig.A.3). The dip (reversed peak) at 284.5 eV is due to the thick sample combined with beamline carbon contamination dip at this energy, which causes the ratio between the very low transmitted counts and the incident counts to deviate from linear behavior in terms of the OD scale at other energies. It was argued that the dip at 284.5 eV could lead to the distortion of the rest of the spectra, which is likely to change peak ratios and the calculation of OD values. Therefore, we excluded the thick regions of the particles for C spatial distribution and speciation.

Figure 3.1A-B displays the fine-scale spatial C distribution in the summit and footslope soil clay particles. The C thickness in the soil clay particles varied at the nanometer scale, similar to earlier findings for soil microaggregates (Wan et al.,

2007). The maximum C thickness in the summit and footslope soil particles was 245 and 216 nm, respectively, with the average C thickness in the summit and footslope soil particles 68 and 48nm, respectively. The thicker C in the summit soil than in the footslope soil is consistent with the higher C content found for the summit soil compared to the footslope soil (Table A.3).

Investigation of the fine scale spatial heterogeneity of organic matter forms in soil clay particles was achieved using principle component (PCA) and cluster analysis (CA) of all NEXAFS spectra for each pixel, as shown in Figure 3.1C-D. C 1s NEXAFS spectra of the distinct regions are presented in Figure 3.1E-F. Functional groups in the spectra and resonance peak energies used to characterize the organic carbon species were taken from a compilation of the published literature (Schumacher et al., 2005; Lehmann et al., 2007 2008; Wan et al., 2007). The resonance peak at energy level 285.5 eV represents 1s $\rightarrow\pi^*$ C=C of aromatic C. The peak at 287.4 eV is assigned to 1s $\rightarrow\pi^*$ transitions of C-H and is referred to as aliphatic C. The strong peak at 288.6 eV is attributed to a 1s $\rightarrow\pi^*_{C=O}$ transition of carboxyl C and the peak at 289.5 eV corresponds to the 1s$\rightarrow$3p, $\sigma^*$of C-OH groups, primarily representing polysaccharides.

The compositional chemistry of organic C displayed fine-scale heterogeneity (Fig.3.1C-F). The cluster maps displayed various regions with distinctively discernible C 1s NEXAFS spectral features (Fig.3.1C-F). PCA-CA analysis identified three (red, green, and blue) and two (green, blue) regions within the clay particles from the summit and footlsope soils, respectively. The red region was the only location on these

clay particles having a peak at 287.4 eV for aliphatic C (Fig.3.1C and 3.1E). This is in contrast to a previous study which has shown that organic matter in soil fine fractions is dominated by long-chain aliphatic molecules in the topsoil horizons based on NMR analysis (Kögel-Knabner et al., 2008). In addition to aliphatic C (287.4 eV), the C 1s NEXAFS spectrum from the red region showed strong resonances at 285.5 eV for aromatic C and 289.5 eV for polysaccharides and a small peak at 288.6 eV for carboxylic C. This type of spectrum has not been commonly observed in soils. This C 1s NEXAFS spectral signatures and peak positions recorded from the red region were similar to the spectral features observed from fungi (Liang et al, 2006), implying that organic matter in this red region could originate from soil microorganisms and their metabolites. The aromatic C in this region may be derived from proteinaceous cell wall components or melanin-like compounds that can be synthesized by fungi. Melanins are considered recalcitrant due to their aromatic structure (Kögel-Knabner, 2002; Knicker, 2004), although their fate and decomposition in soils remains unknown. Aliphatic C is generally attributed to cell wall lipids. Aliphatic-C of CH, CH_2 and CH_3 groups may form non-polar termini that confer hydrophobic properties and lead to hydrophobic interaction between organic C and minerals. The presence of resonances in the aliphatic-C chain together with carboxyl and O-alkyl C suggested the occurrence of C forms in phospholipid fatty acids or chitin (Solomon et al., 2005; Kinyangi et al., 2006) that may be from microbial residues. The strong O-alkyl C absorption bands appeared at 289.5 eV, representing mainly microbial polysaccharides in intimate association with minerals in the clay fractions, could be direct evidence

that such structures can be stabilized by organomineral complexes in soils. Oades (1984) suggested that polysaccharides can be produced in situ by fungi and bacteria in soils and exist as a gel or fibrillae. Polysaccharides can be either encapsulated by the clay minerals or act as cementing agents binding clay minerals to the microbial structure (Oades, 1984; Lützow et al., 2006). Microbially secreted polysaccharides are often negatively charged and they can adsorb strongly to negatively charged clay mineral surfaces through polyvalent cation bridging (Chenu, 1995). Polysaccharides can also be adsorbed to clay minerals through week bonds such as hydrogen bonding and van der Waals forces.

Both green and blue spectra showed a resonance at 285.5 eV aromatic C regions, followed by a steep rise to a peak at 288.6 eV (carboxylic C) and a peak at 289.5 eV for polysaccharides (Fig.3.1E-F). The spectral types were seen in both the summit and footslope soils. Spectra of this type have been reported for organic matter in organo-mineral assemblage (Solomon et al., 2012) and Fe oxides associated organic matter (Keiluweit et al., 2012). The relative abundance of carboxyl and O-alkyl C showed prominent difference between the green and blue spectra for both the summit and footslope soil clay particles. Compared to the green spectra, the blue spectra showed a strong decrease of O-alkyl C abundance associated with polysaccharides, with a simultaneous increase in carboxyl C corresponding to proteinaceous materials (Fig.3.1E-F). These results suggest that the fraction of microbially derived material is least in the blue region with a simultaneous increase in protenaceous materials. Both

the summit and footslope soils lacked a peak at 290.3 eV indicative of carbonate (Fig.3.1E-F), indicating that all the carbon was organic in nature

3.4.3 Mapping and Speciation of Major Cations (Ca, Fe, Al and Si)

Calcium. The distribution of total Ca in the summit and footslope soil clay particles is displayed in the Ca image difference maps (Fig.3.2A-B). Ca displayed heterogeneous distribution in both soils. The maximum thickness of the Ca in the summit and footslope soil particles was 24 and 18 nm, respectively, with the average Ca thickness in the summit and footslope soil particles being 4.6 and 3.4 nm, respectively. PCA-CA analysis identified only one type of Ca 2p NEXAFS spectra for both summit and footslope soil clay particles. The Ca 2p spectra collected from the summit and footslope soil clay particles, showed two major peaks near 349.3 eV and 352.6 eV, respectively, along with small peaks near 348.2 eV and 351.4 eV (Fig. 3.2C). Compared to several Ca-containing reference compounds such as calcite, $CaHPO_4 \cdot 2H_2O$ and sorbed Ca^{2+} to extracellular polymers (EPS), Ca in the soils showed similar spectra to those of $CaHPO_4 \cdot 2H_2O$ and sorbed Ca on EPS (Fig.3.2C), suggesting that the soil Ca was sorbed as organic Ca and/or calcium phosphate and there was no calcium carbonate in these soils. This suggestion is also supported by the C 1s NEXAFS spectra, which clearly showed the absence of carbonate in the studied soils. The pH of the investigated soils (pH = 5.5-5.7) may not lead to the accumulation of $CaCO_3$ compounds, since the stable pH for Calcite is around 8.4 (Cailleau et al., 2005).

Iron. Figure 3.3A-B presents the Fe image difference map ($OD_{709.8}$-OD_{704}) showing the distribution of Fe in the footslope and summit soil clay particles. The maximum thickness of the Fe in the summit and footslope soil clay particles was 120 nm, with the average Fe thickness in the summit and footslope soil clay particles being 33 and 25 nm, respectively. Fe 2p NEXAFS spectra provide information on the oxidation state of Fe (van Aken and Liebscher, 2002). The Fe 2p NEXAFS spectra from all the samples showed multiple peaks at the Fe L_3- (708.2 and 709.8 eV) and L_2- (721.0 and 723.0 eV) edges (Fig.3.3D). The Fe oxidation state could be determined from the shape of the Fe L_3 $2p_{3/2}$ signal that has two main peaks, with the peak at 708.2 eV being the strongest for Fe(II) species and that at 709.8 eV the strongest for Fe(III) species (Dynes et al., 2006; Hitchcock et al., 2009), as seen in the $FeCl_3 \cdot 6H_2O$ and $FeCl_2 \cdot 4H_2O$ reference spectra (Fig.3.3D). PCA-CA analysis suggested that there was only one type of Fe 2p NEXAFS spectrum in the summit soil clay particles, while there were two regions (red and green) with distinct Fe 2p NEXAFS spectra in the footslope soil clay particles (Fig.3.3C-D). In the summit soil clay particles and the red region of the footslope soil clay particles, as the observed intensity ratio between the 709.8-eV and 708.2-eV peak mimics that of the Fe(III) standard (Fig.3.3D), it appears that the mineralogy of the summit soils and the red region of footslope soils are dominated by Fe(III). Although the 709.8-eV peak was also the most intense in the spectrum from the green region, the Fe 2p spectrum from the green region showed increased intensity ratio between the 708.2-eV and 709.8-eV peak, compared to that from the red region (Fig.3.3D). This indicates that the green region also contained

some Fe(II) in addition to Fe(III), possibly from a mixed valance Fe(II)-Fe(III) mineral. Collectively, the footslope soil contained mainly Fe(III), and only a small amount of Fe(II). The footslope soil is periodically under poorly-drained conditions. The periodical low-redox conditions could drive reductive transformation of Fe(III) minerals into Fe(II)-bearing solids.

It is impossible to ambiguously differentiate Fe(III)-containing oxides, alumininosilicates and organic compounds based on Fe 2p NEXAFS. Therefore we employed a more quantitative method, extended X-ray absorption spectroscopy (EXAFS), to determine Fe speciation. Fe K-edge EXAFS spectra are presented in Fig.A.4 and the results of least-squares best fits summarized in Table A.7. In both soils, ~46-50% of the total Fe was bound to Fe(III)-bearing aluminosilicates, with vermiculite contributing 30-35% of the total Fe and the remainder due to illite. Although XRD analysis showed almost equivalent amounts of vermiculite and illite in soil clay fractions (Table A.5), the Fe EXAFS data demonstrated that a higher percentage of total Fe is from vermiculite than from illite. This is probably due to the fact that vermiculite contains a much higher percentage of Fe in the structure than illite (Birkeland, 1999). Fe(III) oxides accounted for the other 50-54% of total Fe. Up to 40% of the total Fe was contained in the crystalline Fe(III) oxides, with 16-22% in hematite and 18-23% in goethite, whereas poorly crystalline Fe(III) oxides such as 2-line ferrihydrite only accounted for 10-15% of the total Fe. The footslope soil contained a slightly higher percentage of ferrihydrite than the summit soil, but the difference was very small.

Aluminum. The distribution of Al in the summit and footslope soils is displayed in Figure A.5A-B. The maximum thickness of the Al in the summit and footslope soil particles was 353 and 394 nm, respectively, with the average Al thickness in the summit and footslope soil particles of 48 and 66 nm, respectively. The Al 1s NEXAFS is a useful technique for probing the bonding and symmetry of the local environment around Al atoms (IIdefonse et al., 1998; Doyle et al., 1999; Shaw et al., 2009). It has been shown to be particularly powerful in differentiating six-fold (coordination number (CN)=6) and four-fold (CN=4) coordination environments for Al atoms. For Al compounds with CN=6 such as gibbsite and kaolinite, their spectra generally have two main maxima near 1567and 1570 eV (IIdefonse et al., 1998; Shaw et al., 2009). Al compounds with CN=4 have a strong single-edge maximum near 1565 eV (IIdefonse et al., 1998; Shaw et al., 2009). For Al compounds with mixed coordination number, e.g. illite (CN=4 and 6), there are three main maxima near 1565, 1567, and 1570 eV (IIdefonse et al., 1998; Shaw et al., 2009). PCA analysis suggested two regions (red and green) with distinct Al NEXAFS spectra for the summit and footslope soils, respectively (Fig.A.5C-E). All the Al NEXAFS spectra from soils contained a slight shoulder near 1565.6 eV, a peak near 1567.7 eV and the most pronounced peak near 1570.4 eV (Fig.A.5E), indicating there was mainly six-fold coordinated Al with a slight amount of four-fold coordinated Al in these soils. These results are in agreement with XRD data which showed that there was a mixture of kaonilite with six-fold Al, and hydroxy-interlayerred vermiculite and illite with mixed four-fold and six-fold Al. The Al 1s spectra were similar in both the red and green

regions, except the Al spectra recorded from the green region showed increased intensity of the 1570.4-eV peaks increased relative to the 1567.7-eV peak when compared to the green region (Fig.A.5E). As observed by Shaw et al. (2009), the peak near 1570 eV is substantially more intense relative to the peak near 1567 eV for kaolinite (1:1 aluminosilicates) when compared to 2:1 aluminosilicates such as illite. It was demonstrated that the intensity of the 1570-eV peak increased relative to the peak 1567-eV peak with an increase in the amount of Al in the silicate (Neuville et al., 2004). Kaolinite with 1:1 structure contains relatively more Al than 2:1 phyllosilicates like illite and verimiculte. Therefore, the increase in the 1570.4-eV peak relative to the 1567.7-eV peak for spectra recorded from the green region, in comparison to that from the red region, were attributed to a greater abundance of kaolinite with six-fold Al.

Silicon. The distribution of Si in the summit and footslope soil clay particles is shown in Figure 3.4A-B.The maximum thickness of Si in the summit and footslope soil particles was 810 and 800 nm, respectively, with the average Si thickness in the summit and footslope soil particles of 140 and 120 nm, respectively. PCA-CA analysis suggested two regions (red and green) with distinct Si 1s spectra for the summit and footslope soils, respectively (Fig.3.4C-E). The Si 1s spectra collected from the green region showed distinctive peaks at 1846.4 (i), 1850.4 (ii) and 1857.1 eV (iv). These spectral features resembled the Si 1s spectra of aluminosilicate ($Si_4O_{10}^{4-}$- Q^3) minerals such as kaolinite, illite and muscovite (Shaw et al., 2009). Aluminosilicates including kaolinite, illite, vermiculite and muscovite, are characterized by dioctahedral, Al-rich layers which have similar Si 1s spectra. Therefore, it is impossible to tease them apart

base on Si 1s NEXAFS spectra. 2:1:1 type aluminosilicates such as chlorite were absent in these soils, since the Si 1s spectral features recorded from these minerals are distinctively different from the Si 1s spectra collected from these soils. These results agree with XRD findings. Si 1s spectra from the red region were characterized by the peak shifted to a higher energy (1846.7 eV) and the appearance of the peak (iii) at 1854.6 eV, which is similar to the spectrum for quartz (Shaw et al., 2009).

3.4.4 Correlation between Elements

To show explicitly the spatial relationship between the elements, each elemental distribution map (total C, Ca, Fe, Al and Si) was aligned to common reference features and overlayed. The correlation between C and other major cations (Ca, Fe, Al, Si) was only performed on the thin regions of the summit and footslope soil clay particles, while the correlation among the major cations including Ca, Fe, Al and Si was carried out on whole images. The color-coded composite maps are shown in Figure A.7-8 for the summit and footslope soil clay particles. To determine the correlation coefficients among the different elements, elemental thickness values on a pixel-by-pixel basis were compared. Plots of elemental correlations are shown in Figure A.9-10 and the correlation coefficients in Table 3.1.

Comparing the C map to cation distribution maps showed all C was associated with the major cations Ca, Fe, Al and Si and there was no discrete phase of C (Fig.A.7). Organic matter can adsorb onto mineral surfaces via various mechanisms: i.e. ligand exchange, polyvalent cation bridges, and weak interactions, such as

hydrophobic interactions including van der Waals forces and H-bonding (Baldock et al., 2001; Lützow et al., 2006). In addition, organic matter can enter into small pores of soil minerals such as Fe(III) oxides including goethite and ferrihydrite (Kaiser & Guggenberger, 2007). The physical protection of organic matter by occlusion within small clay aggregates is another possible process in these soils. Although a majority of particulate organic matter is excluded from the clay fraction, the possibility of particulate organic matter in the clay fractions could not be excluded from STXM images. Therefore organic matter in the organo-mineral assemblages could be adsorbed, occluded or particulate OM.

Based on correlation plots, carbon showed the highest correlation with calcium in both soils (Fig.A.9 & Table 3.1). Carbonate was not observed in the soils based on the C and Ca NEXAFS analysis, hence we infer that the majority of the carbon is organic in nature rather than occurring as a carbonate. The good C-Ca correlations might suggest Ca plays an important role in organomineral assemblage formation in these soils. Organic anions are normally repelled from negatively charged surfaces in soils. Calcium can facilitate binding of organic compounds to permanently negatively-charged siloxane surfaces or to the hydroxyls of aluminosilicates and oxides via "cation bridging". In these soils, Ca was moderately well correlated with Fe, Al and Si (Table 3.1), suggesting that Ca could form bridges between organic matter and iron oxides as well as aluminosilicate minerals. Batch experiments have shown that Ca increases the sorption of OM to minerals (goethite, vermiculite, and pyrophyllite) (Mikutta et al (2007; Varadachari et al., 2000; Weng et al., 2005). In particular,

Mikutta et al (2007) found that sorption of OM to vermiculite is mainly due to the formation of "Ca^{2+} bridges" and the bridges reduced the bioavailability of clay-bound OM. Ca ions are also known to bind to negatively charged functionalities originating from microbial polysaccharides via polyvalent cation bridges (Lützow et al., 2006). Dissolved organic matter can also be precipitated by metal ions such as Ca^{2+} and thus organic matter- Ca cation precipitates might also be present in the soils. Organic-metal cation (such as Ca^{2+}) complexation has been considered potentially stabilizing for soil OM. Therefore, the good C-Ca correlation could also be a result of Ca-bearing organic compounds in soils. In addition, Ca NEXAFS suggested the possible presence of Ca phosphate compounds which might be important in organomineral interactions, since it has been observed that organic biomolecules containing proteins and extracellular polymeric substances are intimately associated with Ca phosphate compounds (Benzarara et al., 2004). Although no definite conclusion can be made on the interactive mechanisms of organic matter, calcium and minerals, our results imply an important role of calcium in organo-mineral associations.

The color-composite maps of three cations (Fe, Al and Si) (Fig.A.8) and correlation between Fe and Al & Si (Fig.A.10 & Table 3.1) showed that Fe was associated with Al and Si. This is probably attributed to the fact that in these soils, aluminosilicate minerals, which consist mainly of Al and Si, also contain different amounts of Fe in their structure. This is also supported by Fe EXAFS results, which showed Fe(III)-containing aluminosilicates, including vermiculite and illite, contributed up to 45-50% of the total Fe (Fig.A.4 & Table A.7). Combining the

dithionite-citrate extraction data with the total digestion results for the soil clay fractions, Fe content in the aluminosilicate structures (Fe_t-Fe_d) was 3.35% and 3% in the summit soil and footslope soils, respectively (Table A.6). Noticeably, there was no discrete particles containing Fe that was in association with Al and Si in soil clay fractions (Fig.A.8), suggesting that Fe oxides, including goethite, hematite and ferrihydrite, exhibit coatings on the aluminosilicate minerals. These may also contribute to the correlation of Fe with Al and Si.

The C-Fe correlation plot could reflect C associations with Fe(III) oxides and with Fe(III)-containing aluminosilicate minerals. STXM elemental maps from both the summit and footslope soils displayed similar correlations of C with Fe to Al and Si (Fig.A.9 & Table 3.1), suggesting an equivalent role of Fe(III) oxides and Fe(III)-containing aluminosilicates in organomineral assemblage formation. This is in contrast to previous field soil studies which showed a strong positive correlation between C and Fe oxide content (Kaiser et al, 2002; Kiem & Kögel-Knabner, 2002), and to batch DOM sorption studies which have found that oxides were better sorbents than aluminosilicate clay minerals (Kaiser et al., 1996; Mikutta et al., 2007). In these investigated soils, based on the ratio of oxalate extracted Fe to dithionite extracted Fe, 20-34% of the Fe(III) oxides were amorphous while a majority of the Fe(III) oxides were crystalline minerals in the investigated soils (Table A.6). This is consistent with the Fe EXAFS results, which showed most of the Fe(III) oxides were crystalline goethite and hematite and there was much less poorly-crystalline ferrihydrite (Fig.A.4 & Table A.7). This is probably why we observed a similar correlation of C with Fe to

Al and Si, since amorphous and poorly crystalline minerals (e.g. ferrihydrite) are more powerful for stabilizing OC in the soils (1). The low Fe(III) oxide content in the soils (Table A.6) and the presence of about 50% total Fe in aluminosilicates (Table A.6-7), might also contribute to these results. Ideally, in order to clearly investigate the role of specific Fe(III) oxides in C-mineral associations in soils, further study on soils with varying Fe oxide content and crystallinity is needed.

Carbon correlations with Al and Si were similar in the footslope soil, while carbon displayed a better correlation with Al than with Si in the summit soil (Fig.A.9 & Table 3.1). There was a very strong correlation between Al and Si particularly for the footslope soil (Fig.A.10 & Table 3.1), due to the predominant aluminosilicate minerals in the soil clay fractions. In the summit soil, there were also a few discrete quartz particles that contained Si but neither Al nor Fe. The presence of quartz particles, in addition to aluminosilicates, accounts for the poorer correlation between Al and Si in the summit soil than in the footslope soil. The molar ratios of Si/Al were calculated and plotted on the Al-Si correlation graphs (Fig.A.10). Vermiculite and illite are 2:1 type aluminosilicates with Si/Al molar ratio of 2, while kaolinite is 1:1 type aluminosilicate with Si/Al molar ratio equal to 1. The Si/Al ratio was 1.7 for the summit soil and 1.8 for the footslope soil, consistent with the XRD results that soil clay minerals are dominated by a mixture of 2:1 aluminosilicate minerals (hydroxy-interlayered vermiculite and illite) with Si/Al molar ratio of 2 and 1:1 aluninosilicate minerals (kaolinite) with Si/Al molar ratio of 1 (Table A.5).

3.5 Implications

Scanning transmission X-ray microscopy with high spatial resolution combined with NEXAFS represents the most direct way to observe organic matter-mineral interactions. It enables direct assessment of distribution and speciation of C and major cations and their associations in organomineral assemblages. Bulk techniques including Fe EXAFS, XRD, and C and N NEXAFS were also applied in this study to provide supplementary information. The C NEXAFS analyses clearly demonstrated that aromatic C=C, carboxyl C and polysaccharides were the pervasive C functional groups associated with soil mineral phases, with a spatial variability in the relative abundance of carboxyl C and polysaccharides on mineral surfaces at this submicron scale. Aliphatic C, generally from cell wall lipids, was localized in limited regions in the soil clay particles. This study suggests the importance of Ca in organo-(metal)-mineral interactions and/or organo-metal cation omplexation. The metal-rich mineral matrix was composed of Fe(III) oxides (hematite, goethite, and ferrihydrite), quartz and aluminosilicates including hydroxy-interlayered vermiculite, illite and kaolinite. Additionally, the mineralogical impact on C distribution was assessed. C was associated with both Fe(III) oxides and aluminosilicate minerals and C was similarly correlated with Fe, Al and Si. This study is among the first spectromicroscopic investigations of organo-mineral assemblages in soils. Overall, our results show progress towards examining, at the sub-micron-level, compositional chemistry and associative interactions between organic matter and natural minerals. Of particular interest is the need to expand this investigation by including soils with a

wider range of mineralogical composition and under different land uses. Such a study will help to develop a clearer understanding of specific C-mineral associations in a wide variety of soil types.

REFERENCES

Amelung, W.; Zech, W.; Zhang, X.; Follett, R. F.; Tiessen, H.; Knox, E.; Flach, K. W., Carbon, nitrogen, and sulfur pools in particle-size fractions as influenced by climate. *Soil* Sci. *Soc. Am. J.* **1998**, 62, 171-181.

Baldock, J. A.; Skjemstad, J. O., Role of the soil matrix and minerals in protecting natural organic materials against biological attack. *Org. Geochem*. **2000**, 31, 697-710.

Benzerara, K.; Yoon, T. H.; Tyliszczak, T.; Constantz, B.; Spormann, A. M; Brown, G. E., Scanning transmission X-ray microscopy study of microbial calcification. *Geobiology* **2004**, 2, 249-259.

Cailleau, G.; Braissant, O.; Dupraz, C.; Aragno, M.; Verrecchia, E.P., Biologically induced accumulations of $CaCO_3$ in orthox soils of Biga, Ivory Coast. *Catena* **2005**, 59, 1-17.

Chorover, J.; Amistadi, K., Reaction of forest floor organic matter at goethite, birnessite, and smectite surfaces. *Geochim. Cosmochim. Acta* **2001**, 65, 95-109.

Chenu, C., Extracellular polysaccharides: an interface between microorganisms and soil constituents. In: Huang, P.M., Berthelin, J., Bollag, J.-M., McGill, W.B., Page, A.L. (Eds.), Environmental Impact of Soil Component Interactions: Natural and Anthropogenic Organics. Lewis, Boca Raton, FL, **1995**, pp. 217-233.

Doyle, C. S.; Traina, S. J.; Ruppert, H.; Kendelewicz, T.; Rehr, J. J.; Brown, G. E., XANES studies at the Al K-edge of aluminium-rich surface phases in the soil environment. *J. Synchrotron Rad.* **1999**, 6, 621-623.

Dynes, J. J.; Tyliszczak, T.; Araki, T.; Lawrence, J. R.; Swerhone, G. D. W.; Leppard, G. G.; Hitchcock, A. P., Speciation and quantitative mapping of metal species in microbial biofilms using scanning transmission X-ray microscopy. *Environ. Sci. Technol*. **2006**, 40(5), 1556-1565.

Hitchcock, A. P., aXis-2000 is an IDL-based analytical package. **2000**. http://unicorn.mcmaster.ca.

Hitchcock, A. P.; Dynes, J. J.; Lawrence, R.; Obst, M.; Swerhone, G. D. W.; Korber, D. R.; Leppardi, G. G., Soft X-ray spectromicroscopy of nickel sorption in a natural river biofilm. *Geobiology* **2009**, 7, 432-453.

Ildefonse, P.D.; Cabaret, P.; Sainctavit, P.; Calas, G.; Flank, A.M.; Lagarde, P., Aluminum X-ray absorption near edge structure in model compounds and Earth's surface minerals. *Phys. Chem. Miner* **1998**, 25, 112-121.

Gu, B.; Schmitt, J.; Chen, Z.; Liang, L.; McCarthy, J. F., Adsorption and desorption of natural organic matter on iron oxide: mechanisms and models. *Environ. Sci. Technol.* 1994, 28, 38-46.

Kahle, M.; Kleber, M.; Torn, M. S.; Jahn, R., Carbon storage in coarse and fine clay fractions of illitic soils. *Soil Sci. Soc. Am. J.* **2003**, 67(6), 1732-1739.

Kaiser, K. Sorption of natural organic matter fractions to goethite (alpha-FeOOH): effect of chemical composition as revealed by liquid-state C-13 NMR and wet-chemical analysis. *Org. Geochem.* **2003**, 34(11), 1569-1579.

Kaiser, K.; Eusterhues, K.; Rumpel, C.; Guggenberger, G.; Kögel-Knabner, I., Stabilization of organic matter by soil minerals-investigations of density and particle-size fractions from two acid forest soils. *J. Plant Nutr. Soil Sci.* **2002**, 165, 451-459.

Kaiser, K.; Guggenberger, G., Sorptive stabilization of organic matter by microporous goethite: sorption into small pores vs. surface complexation. *Eur. J. Soil Sci.* 2007, 58, 45-59

Kaiser, K.; Guggenberger, G., The role of DOM sorption to mineral surfaces in the preservation of organic matter in soils. *Org. Geochem.* **2000**, 31, 711-725.

Kaiser, K.; Guggenberger, G.; Zech, W., Sorption of DOM and DOM fractions to forest soils. *Geoderma* 1996, 74, 281-303.

Kaiser, K.; Zech, W., Release of natural organic matter sorbed to oxides and a subsoil. *Soil Sci. Soc. Am. J.* 1999, 63(5), 1157-1166.

Kang, S.; Xing, B. S., Humic acid fractionation upon sequential adsorption onto goethite. *Langmuir* 2008, 24(6), 2525-2531.

Kaznatcheev, K.V.; Karunakaran, C.; Lanke, U.D.; Urquhart, S.G.; Obst, M.; Hitchcock, A.P., Soft X-ray spectromicroscopy beamline at the CLS: commissioning results. *Nucl. Instrum. Methods Phys. Res. Sect. A-Accel. Spectrom. Dect. Assoc. Equip.* **2007**, 582, 96-99.

Keiluweit ,M.; Bougoure, J.J.; Zeglin, L.H.; Myrold, D.D.; Weber, P.K.; Pett-Ridge, J.; Kleber, M.; Nico, P.S., Nano-scale investigation of the association of microbial nitrogen residues with iron (hydr) oxides in a forest soil O-horizon. *Geochim. Cosmochim. Acta* **2012**, 95, 213-226.

Kiem, R.; Kögel-Knabner, I., Refractory organic carbon in particle-size fractions of arable soils II: organic carbon in relation to mineral surface area and iron oxides infractions <6 µm. *Org. Geochem*. **2002**, 33(12), 1699-1713.

Kinyangi, J.; Solomon, D.; Liang, B.; Lerotic, M.; Wirick, S.; Lehmann, J., Nanoscale biogeocomplexity of the organo-mineral assemblage in soil: application of STXM microscopy and C 1s-NEXAFS spectroscopy. *Soil Sci. Soc. Am.* **2006**, 70, 1708-1718.

Knicker, H., Stabilization of N-compounds in soils and organic matter-rich sediments - what is the difference? *Mar. Chem.* **2004**, 92, 167-195.

Kleber, M.; Mertz, C.; Zikeli, S.; Knicker, H.; Jahn, R., Changes in surface reactivity and organic matter composition of clay subfractions with duration of fertilizer deprivation. *Eur. J. Soil Sci.* **2004**, 55(2), 381-391.

Kleber, M.; Sollins, P.; Sutton, R., A conceptual model of organo-mineral interactions in soils: self-assembly of organic molecular fragments into zonal structures of mineral surfaces. *Biogeochem.* 2007, 85, 9-24.

Kögel-Knabner, I.; Guggenberger G.; Kleber, M.; Kandeler, E.; Kalbitz, K.; Scheu, S.; Eusterhues, K.; Leinweber, P., organo-mineral associations in temperate soils: Integrating biology, mineralogy, and organic matter chemistry. *J. Plant Nutr. Soil Sci.* **2008**, 171, 61-82.

Kögel-Knabner, I., The macromolecular organic composition of plant and microbial residues as inputs to soil organic matter. *Soil Bio. Biochem.* **2002**, 34, 139-162.

Larid, D. A.; Martens, D. A.; Kingery, W.L., Nature of clay-humic complexes in an agricultural soil: I. Chemical, biochemical, and spectroscopic analyses. *Soil Sci. Soc. Am. J*. **2001**, 65(5), 1413-1418.

Lehmann, J.; Kinyangi, J.; Solomon, D., Organic matter stabilization in soil microaggregates: implications from spatial heterogeneity of organic carbon contents and carbon form. *Biogeochem.* **2007**, 85(1), 45-57.

Lehmann, J.; Solomon, D.; Kinyang, J.; Dathe, L.; Wirick, S.; Jacobsen, S., Spatial complexity of soil organic matter forms at nanometer scales. *Nature Geosci*. **2008**, 1, 238-242.

Lerotic, M.; Jacobsen, B.; Gillow, J. B., Cluster analysis in soft X-ray spectromicroscopy: Finding the patterns in complex specimens. *J. Electron Spectrosc. Relat. Phenom.* **2005**, 144-147C, 1137-1143.

Liang, B.; Lehmann, J.; Solomon, D.; Kinyangi, J.; Grossman, J.; O'Neill, B.; Skjemstad, J.O.; Thies, J.; Luizao, F.J.; Petersen, J.; Neves, E.G., Black carbon increases cation exchange capacity in soils. *Soil Sci. Soc. Am. J.* **2006**, 70, 1719-1730.

Lützow, V. M.; Kögel-Knabner, I.; Ekschmitt, K.; Matzner, E.; Guggenberger, G.; Marschner, B.; Flessa, H., Stabilization of organic matter in temperate soils: mechanisms and their relevance under different soil conditions - a review. *Eur. J. Soil Sci*. **2006**, 57, 426-445.

Mikutta, R.; Kleber, M.; Jahn, R., Poorly crystalline minerals protected organic carbon in clay subfractions from acid subsoil horizons. *Geoderma* **2005**, 128, 106-115.

Mikutta, R.; Mikutta, C.; Kalbitz, K.; Scheel, T.; Kaiser, K; Jahn, R., Biodegradation of forest floor organic matter bound to minerals via different binding mechanisms. *Geochim. Cosmochim. Acta* **2007**, 71, 2569-2590.

Namjesnik-Dejanovic, K.; Maurice, P. A.; Aiken, G. R.; Cabaniss, S.; Chin, Y. P.; Pullin, M. J. ,Adsorption and fractionation of a muck fulvic acid on kaolinite and goethite at pH 3.7, 6, and 8. *Soil Sci.* 2000, 165(7), 545-559.

Neuville, D.R; Cormier, L.; Massiot, D., Al environment in tectosilicates and peraluminous glasses: a 27Al MQ-MAS NMR, Raman, and XANES investigation. *Geochim. Cosmochim. Acta* **2004**, 68, 5071-5079.

Newbold, J. D.; Bott, R. L.; Kaplan L. A.; Sweeney, B. W.; Vannote, R. L., Organic matter dynamics in White Clay Creek, Pennsylvania, USA. *J. North Am. Benthological Soc*. **1997**, 16(1), 46-50.

Oades, J. M., Soil organic matter and structural stability: mechanisms and implications for management. *Plant and Soil* **1984**, 76, 319-337.

Schumacher, M.; Christl, I.; Scheinost, A. C.; Jacobsen, C.; Kretzschmar, R., Chemical heterogeneity of organic soil colloids investigated by scanning transmission X-ray microscopy and C-1s NEXAFS microspectroscopy. *Environ, Sci. Technol*. **2005**, 39(23), 9094-9100.

Shaw, S.A.; Peak, D.; Hendry, M.J., Investigation of acidic dissolution of mixed clays between pH 1.0 and 3.0 using Si and Al X-ray absorption near edge structure. *Geochim. Cosmochim. Acta* **2009**, 73, 4151-4165.

Sloto, R. A., Geology, hydrology, and ground water quality of Chester County, Pennsylvania, Chester County Water Resources Authority Water- Resource Report 2. **1994.**

Solomon, D.; Lehmann, J.; Harden, J.; Wang, J.; Kinyangi, J.; Heymann, K.; Karunakaran, C.; Lu, Y.S.; Wirick, S.; Jacobsen, C., Micro- and nano-environments of carbon sequestration: Multi-element STXM–NEXAFS spectromicroscopy assessment of microbial carbon and mineral associations. *Chem. Geol.* 2012, 329, 53-73.

Solomon, D.; Lehmann, J.; Kinyangi, J.; Liang, B.; Schäfer, T., Carbon K-edge NEXAFS and FTIR-ATR spectroscopic investigation of organic carbon speciation in soils. *Soil Sci. Soc. Am. J.* **2005**, 69, 107-119.

Torn, M. S.; Trumbore, S. E.; Chadwick, O. A.; Vitousek, P. M.; Hendricks, D.M., Mineral control of soil organic carbon storage and turnover. *Nature* **1997**, 389, 170-173.

van Aken, P.A.; Liebscher, B., Quantification of ferrous/ferric ratios in minerals: new evaluation schemes of Fe L2,3 electron energy-loss near-edge spectra. *Phys. Chem. Miner*. **2002**, 29, 188-200.

Varadachari, C.; Chattopadhyay, T.; Ghosh, K., The crystallo-chemistry of oxide-humus complexes. *Au. J. Soil Res.* **2000**, 38(4), 789-806.

Wan, J.M.; Tyliszczak, T.; Tokunaga, T. K., Organic carbon distribution, speciation, and elemental correlations with soil micro aggregates: applications of STXM and NEXAFS spectroscopy. *Geochim. Cosmochim. Acta* **2007**, 71(22), 5439-5449.

Wang, K. J.; Xing, B. S., Structural and sorption characteristics of adsorbed humic acid on clay minerals. *J. Environ. Qual.* 2005, 34(1), 342-349.

Weng, L. P.; Koopal, L. K.; Hiemstra, T.; Meeussen, J. C. L.; Van Riemsdijk, W. H., Interactions of calcium and fulvic acid at the goethite-water interface. *Geochim. Cosmochim. Acta* **2005**, 69(2), 325-339.

Wiseman, C. L. S.; Püttmann, W., Soil organic carbon and its sorptive preservation in central Germany. *Eur. J. Soil Sci*. **2005**, 56, 65-76.

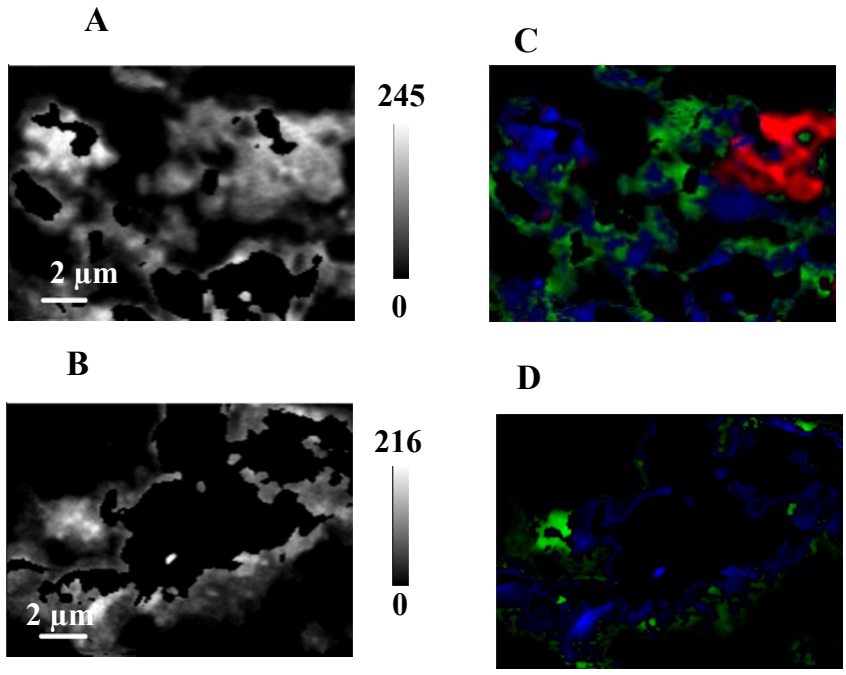
A
C
245
2 µm
0
B
D
216
2 µm
0

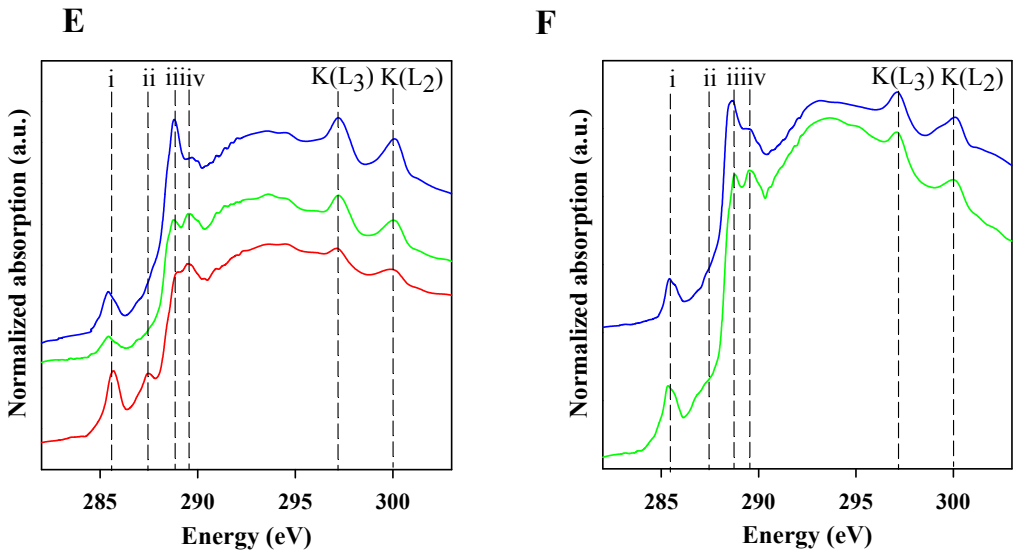

Figure 3.1 Carbon image difference maps (OD_{289}-OD_{282}) of the thin regions from the (A) summit and (B) footslope soil clay particles. The gray scale indicates thickness in nanometers. C 1s cluster indices map showing the distribution of C functional groups in the thin regions from the (C) summit soil clay particles, with three distinct regions (red, green, and blue) and (D) footslope soil clay particles, with two distinct regions (green and blue).The C 1s NEXAFS spectra were extracted from the regions in the cluster indices maps for the (E) summit and (F) footslope soil clay particles, respectively. Note the color of the spectra and the region's color from which they were extracted are the same. Spectra features identified by the vertical dashed lines correspond to (i) aromatic (C=C) (285.5 eV), (ii) aliphatic C-H(287.4eV), (iii) carboxylic (COOH) (288.6 eV), and (iv) polysaccharides C-OH(289.5 eV) functional groups. The peaks at higher energies are from K^+, and corresponding to its L_3 and L_2 edges.

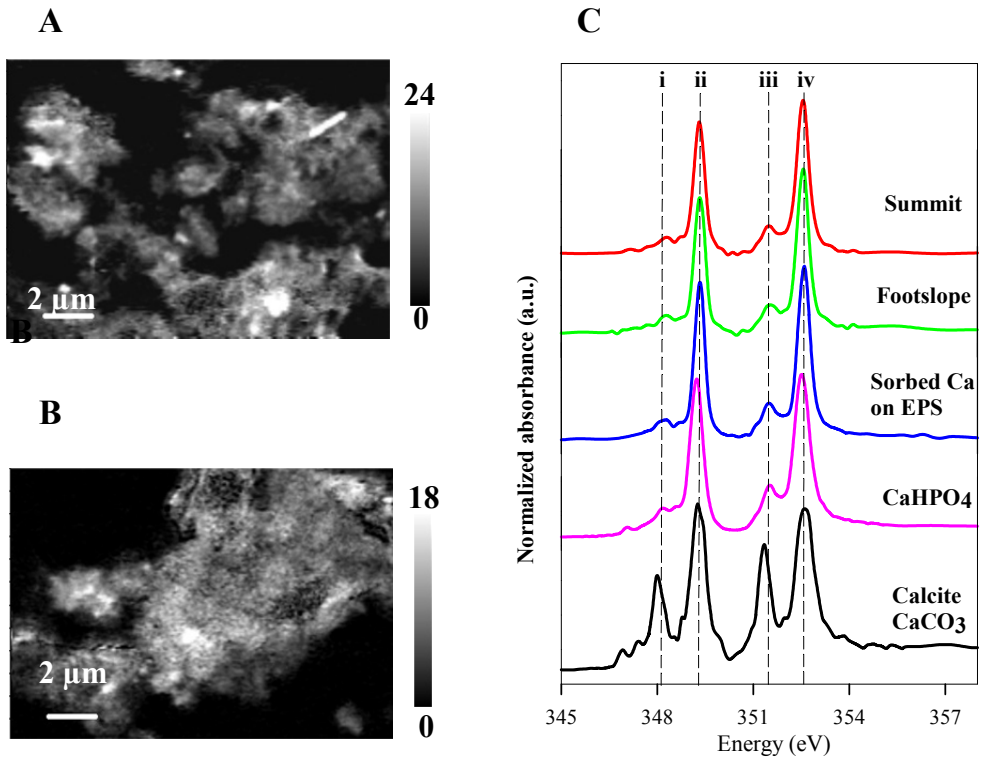

Figure 3.2 Ca image difference maps ($OD_{352.6}$-$OD_{350.3}$) of the (A) summit and (B) footslope soil clay particles. The gray scale indicates thickness in nanometers. (C) Ca 2p NEXAFS spectra of the summit and footslope soil clay particles, compared to the reference compounds $CaHPO_4 \cdot 2H_2O$, sorbed Ca on EPS, and calcite. The vertical dashed lines correspond to (i) 348.2, (ii) 349.3, (iii) 351.4, and (iv) 352.6 eV.

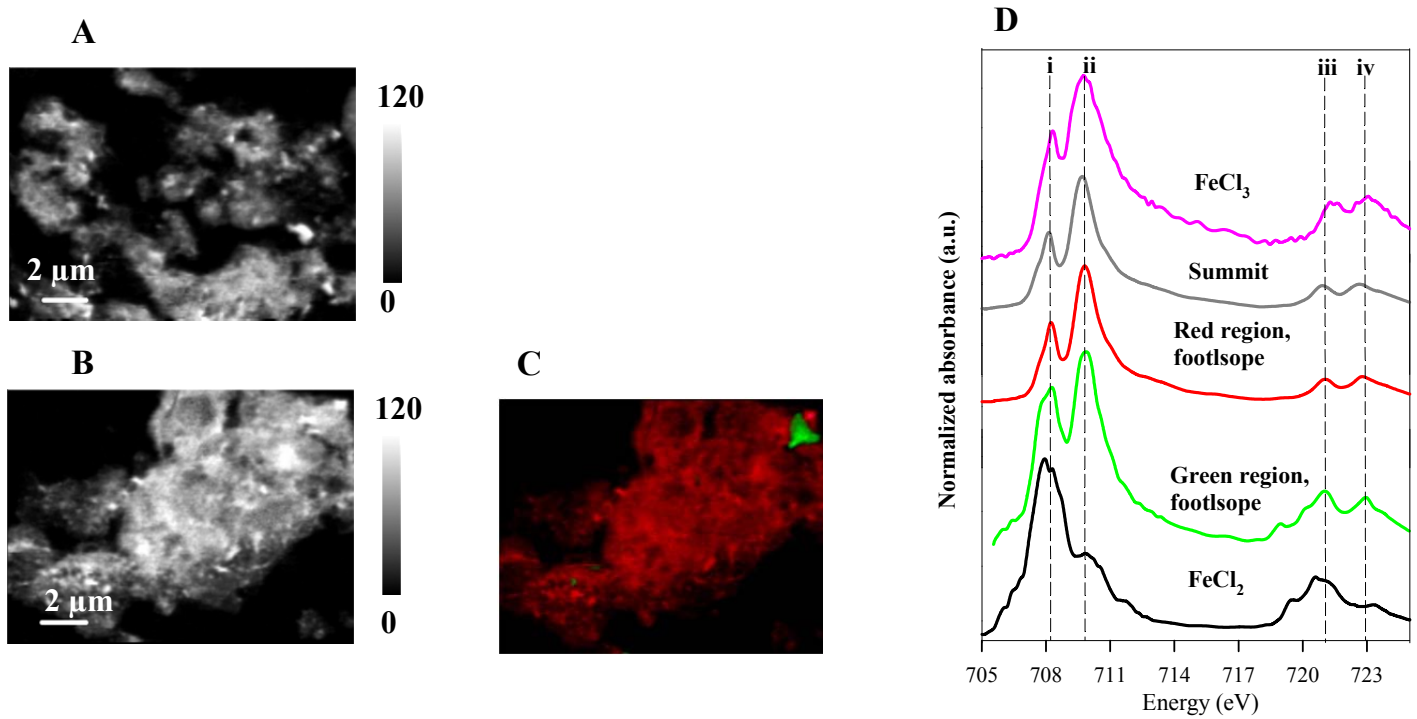

Figure 3.3 Fe image difference map ($OD_{709.8}$-OD_{704}) of the (A) summit and (B) footslope soil clay particles. The gray scale indicates thickness in nanometers. (C) Fe 2p cluster indices map showing the distribution of Fe species in the footslope soil clay particles, with two distinct regions (red and green). (D) Fe 2p NEXAFS spectra from the summit soil clay particles, and the red and green regions in the cluster indices map (as shown in Fig.3C) for the footlsope soil clay particles, compared to reference compounds $FeCl_3 \cdot 6H_2O$ and $FeCl_2 \cdot 4H_2O$. The vertical dashed lines correspond to (i) 708.2, (ii) 709.8, (iii) 721.0, and (iv) 723.0 eV.

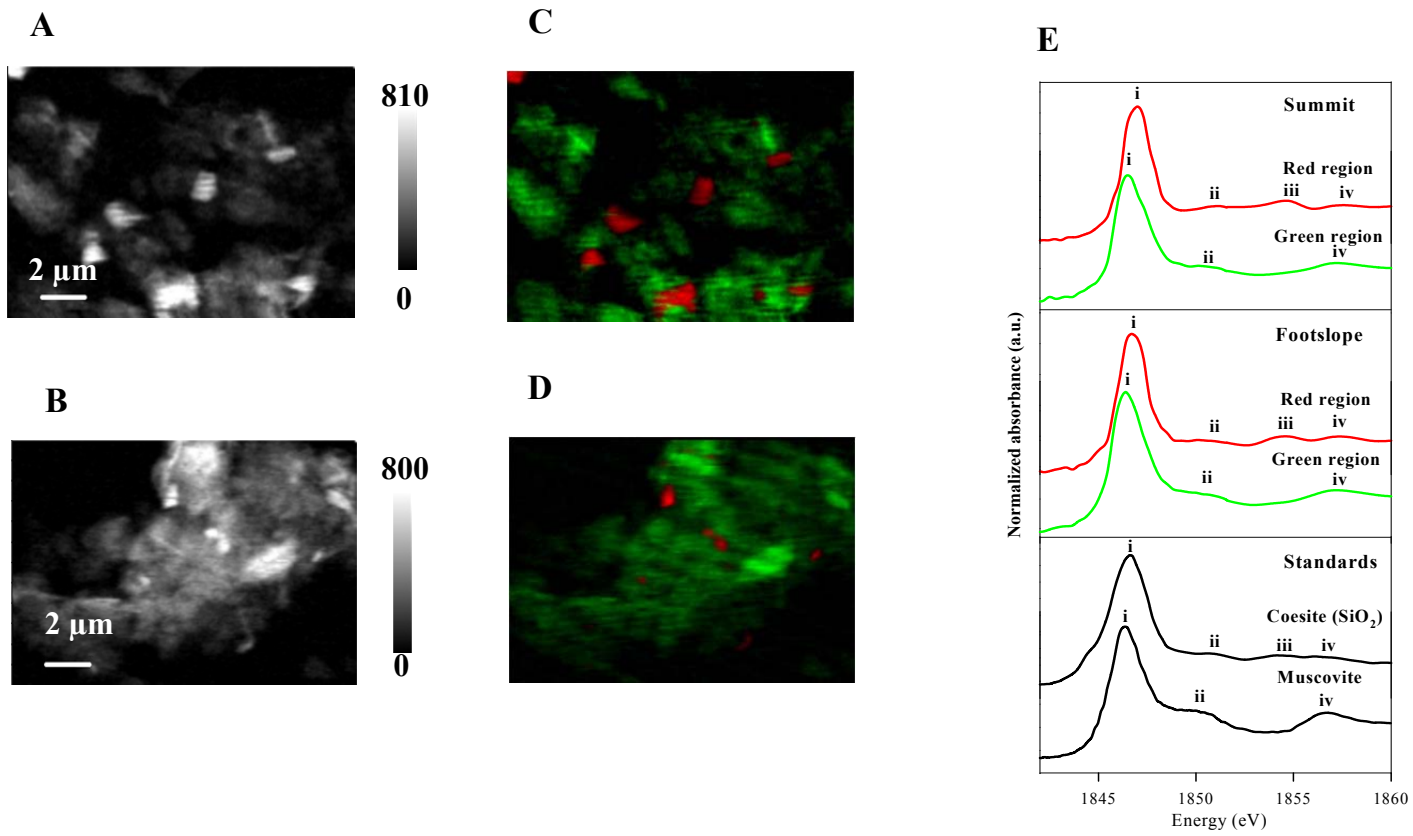

Figure 3.4 Total Si distribution map ($OD_{1846.4}$-OD_{1830}) of the (A) summit and (B) footslope soil clay particles. The gray scale indicates thickness in nanometers. Si 1s cluster indices map showing the distribution of Si species in the (C) summit and (D) footslope soil clay particles with two distinct regions (red and green), respectively. (E) The Si 1s NEXAFS spectra were extracted from the regions in the cluster indices maps for the summit and footslope soil clay particles, respectively, compared to the standards SiO_2 and muscovite. Note the color of the spectra and the region's color from which they were extracted are the same.

Table 3.1 Correlation coefficients from pairs of thickness values of different elements within distribution maps of the (A) summit and (B) footslope soil clay particles.

	Ca	Fe	Al	Si
(A) Summit				
C	0.87	0.64	0.64	0.54
Ca		0.70	0.71	0.60
Fe			0.77	0.49
Al				0.70
(B) Footslope				
C	0.89	0.75	0.71	0.71
Ca		0.74	0.72	0.72
Fe			0.78	0.77
Al				0.95

Chapter 4

SOIL IRON SPECIATION ALONG A FLOODPLAIN REDOX GRADIENT: A COMBINED EXAFS AND MöSSBAUER STUDY

4.1 Abstract

Properties of Fe mineral phases are poorly understood in soils with fluctuating water tables and variable redox conditions. The objective of this research was to apply Fe k-edge EXAFS and Mössbauer spectroscopy to characterize Fe-containing mineralogy in a floodplain soil profile with spatially sharp redox gradients. Redox conditions across the floodplain varied substantially from permanent reducing conditions in a pre-colonial buried wetland at a soil depth of 80-120cm, to oxidizing conditions within post-colonial sediments at a soil depth of 0-80 cm. Results showed that soil redox conditions had an important control on soil Fe mineralogy. Both EXAFS and Mössbauer analysis showed that the permanent reducing conditions led to a strong reduction in the structural Fe(III) in the phyllosilicates, in addition to a complete reductive dissolution of Fe(III) oxides. Mössbauer analysis showed that the mineralogical composition of Fe(III) oxides also varied with the redox levels, with oxides of smaller particle size abundant at lower redox levels. The relative abundance of ilmenite increased with decreasing redox levels, as shown by Mössbauer analysis.

4.2 Introduction

Iron is a redox-sensitive element and its high redox activity triggers many processes in terrestrial ecosystems such as mineral weathering, nutrient cycling, and contaminant mobility (Borch et al., 2010). Iron-bearing minerals in soils occur in a variety of phases such as Fe-oxyhydroxides (e.g. ferrihydrite, goethite), Fe-oxides (e.g. magnetite, hematite), or phyllosilicates (e.g. Fe-containing vermiculite or smectite) (Cornell and Schwertmann, 2003). The crystal mineral phase, size, surface charge and bonding environment of Fe governs its influence on ecosystem biogeochemistry such as toxicity of trace elements and cycling of organic compounds (Tebo and He, 1998; Myneni et al., 1997). Iron oxides with short-range crystal order and small particle sizes contain more reactive surface area compared to other bulk Fe-oxides (Cornell and Schwertmann, 2003; Bonneville et al., 2004). Association of organic matter with Fe minerals has been increasingly recognized as a major process for soil carbon stabilization (Chorover et al., 2007; Gu et al., 2004; Kaiser et al., 1997) by decreasing its susceptibility to microbial degradation (Keil et al., 1994; Mikutta et al., 2006). Fe is susceptible to redox variations along landscape gradients over a wide range of spatial scales. Fe (III) minerals predominate in well-drained upland soils, while under poorly-drained conditions at lowland locations, floodplains and streams reductive dissolution of Fe (III) minerals occurs. These redox fluctuations drive local mobilization of Fe^{2+} (aq) (Weber et al., 2006), which can be either removed from soil by leaching, reoxidiation and precipitation as Fe(III)-oxide coatings on soil mineral surfaces or incorporated into ferrous-bearing solids. Therefore the soil redox

conditions affect not only the amount but also mineralogical composition of Fe mineral phases. However, little research has been conducted on the mineralogy of Fe oxides in soils subjected to different redox conditions.

Assessment of Fe speciation requires the application of techniques capable of providing accurate and quantitative information on the types and abundance of Fe phases present. Spectroscopic tools such as Mössbauer and X-ray absorption spectroscopy (XAS) can provide this type of information for Fe. Mössbauer Spectroscopy is one of the most powerful methods to study iron mineralogy in soils and sediments (Thompson et al, 2011). It is capable of precise physical measurements of Fe nuclear energy levels, which facilitates detection of Fe coordination in short-order ranged Fe minerals. It is inherently a "bulk" spectroscopic technique, requiring >10 mg Fe for detection, and thus is ideal for integrated analysis of whole soil speciation changes. Iron K-edge extended X-ray adsorption fine structure (EXAFS) spectra have been shown to be useful in distinguishing among the multitude of different Fe-bearing minerals in soils and sediments (O'Day et al., 2004; Kiczka et al., 2011; Baker et al., 2010). O'Day et al. (2004) specifically addressed the utility of Fe K edge XAS to determine Fe speciation in mineral samples (soils and sediments) consisting of mixtures of Fe-bearing minerals, and concluded that this technique is capable of distinguishing between major classes of iron-bearing minerals (phosphates, oxides, etc.), with a practical detection limit of 5% atomic Fe. The present study employed both Mössbauer and XAS spectroscopy to characterize solid-phase iron

species in soils under different redox conditions. This study will enhance our understanding of biogeochemical Fe cycling in the natural environment.

4.3 Materials and Methods

4.3.1 Field Site and Sampling

We collected soil core samples under varying redox conditions from a floodplain within the long-term 725-ha research watershed upstream of the Stroud Water Research Center (SWRC) in southeastern PA (39º53'N,75º47'E). The 3rd-order watershed forms the headwaters of the White Clay Creek and is an intensive study site for the established Christina River Basin Critical Zone Observatory located in the Piedmont region of Southeastern Pennsylvania and northern Delaware. The watershed is underlain by highly metamorphosed sedimentary rocks containing gneisses, schists, quartzites, and marbles (Newbold, 1997). The soils are primarily Aquic Fragiudults in the riparian zones. The floodplain soil profile displays a visible C-rich buried A horizon interpreted to be a pre-colonial wetland (Walter & Merrits, 2008). The floodplain profiles demonstrats a distinctive heterogeneity in terms of soil composition, organic C content and redox environment. They vary from post-colonial legacy sediments, pre-colonial wetland, gravel, to the exposed bedrock (Fig.4.1). The interface between the anoxic pre-colonial wetland and valley-bottom gravel beds within the hyporheic zone should demonstrate significant redox gradients that can control the cycling of Fe and C. To minimize Fe oxidization, samples were loaded into

plastic flasks with dry ice. Sublimation of solid CO_2 in the flask yields positive CO_2 pressure, thus creating anoxic conditions and preventing sample oxidation via atmospheric O_2.

4.3.2 Soil Characterization

All soil samples were freeze-dried and sieved (<63 μm) in an O_2-free glove box. Particle-size distribution was determined by wet sieving and sedimentation using the pipette sampling technique. The soil pH was determined in DI water. Carbon and N content (CN analyzer) and total element concentrations using microwave digestion were determined. Specific surface areas of soil samples were analyzed by BET surface area and porosity analyzer after removing OM with H_2O_2. Oxalate-extractable Fe was determined by using the method of Schwertmann (1964) and dithionite-extractable Fe determined according to Mehra and Jackson (1960). Iron in the extracts was measured by ICP-AES.

4.3.3 Clay Mineralogy

The clay fraction (< 2 μm) was separated by wet sieving, gravity sedimentation and centrifugation (Jackson, 1979). Clay samples were saturated with Mg and K and mounted as slurries on glass slides for X-ray diffraction (XRD) analysis. The air-dried Mg-saturated samples were analyzed at 25 °C followed by glycerol solvation. The air-dried K-saturated samples were analyzed at 25 °C and then heated at 300 and 550 °C. All X-ray diffractograms were recorded with a Rigaku Miniflex X-ray diffractometer

equipped with CuKα radiation generated at 35 kV and 10 mA. The XRD patterns were recorded from 2 to 20° 2θ at a scanning speed of 0.5° 2θ min^{-1}.

4.3.4 EXAFS Spectroscopy

The speciation of Fe in soils was determined using synchrotron-based Fe K-edge extended X-absorption fine structure (EXAFS) spectroscopy. Using a linear combination fitting (LCF) approach, the sample spectra were evaluated by fitting them as a linear combination of reference spectra. In addition to crystalline compounds, EXAFS analysis also allows quantifying non-crystalline Fe species in soils, which would not be detectable with common analytical methods such as XRD. The Fe K-edge EXAFS spectra of sample and reference compounds were measured at beamline 4-1 at the Stanford Synchrotron Radiation Facility (SSRL). Fe K-edge EXAFS spectra were collected using a Si(220) phi = 0 monochromator crystal set at a slit size of 1 by10 mm. The monochromator was detuned 50% for harmonic rejection. Four to six scans of each sample were collected either in transmission mode using an ion chamber or fluorescence mode using a Lytle detector. The Sixpack program was used for standard background subtraction and edge-height normalization (Webb, 2005). Iron speciation in samples was quantified by least squares fitting (LCF) of k^3-weighted EXAFS oscillations in the 2–11$Å^{-1}$ range, to selected reference standards using the Sixpack program. LCF analysis of the sample spectra was initiated with the reference spectrum giving the lowest R-factor (Kelly et al., 2008). A best-fit involving n+1 components was only considered to be superior to the best n-component fit if the R-

factor decreased by more than 10% (relative). No energy shift was included in the LCF and the sum of the fitted fractions was not constrained (LCF data are presented normalized to 100%).

Reference Spectra. For the analysis of the Fe-K EXAFS spectra of soil clay fractions by linear combination fitting, the reference compounds listed below were considered.

Illite (IMt-1): from Source Clays Repository, Clay Minerals Society

Fe(III)-Oxalate ($Fe_2(C_2O_4)_3$): Aldrich 98% pure

Fe(III)-Citrate Hydrate ($C_6H_5FeO_7$): Aldrich 98% pure

Nontronite (NAu-1): from Source Clays Repository, Clay Minerals Society

Smectite (SWy-2): from Source Clays Repository, Clay Minerals Society

Vermiculite (VTx-1): from Source Clays Repository, Clay Minerals Society

Chlorite (CCa-2): from Source Clays Repository, Clay Minerals Society

Augite: from Stanford Mineral Collection

Biotite: from Stanford Mineral Collection

Ferrihydrite ($Fe(OH)_3$): synthesized from $Fe(NO_3)_3.9H_2O$ and KOH according to the 2-line ferrihydrite method of Schwertmann and Cornell (1991).

Goethite (FeOOH): synthesized from $Fe(NO_3)_3.9H_2O$ and KOH according to the method of Schwertmann and Cornell (1991).

Lepidocrocite (FeOOH): synthesized from $FeCl_2.4H_2O$ and NaOH according to the method of Schwertmann and Cornell (1991).

Hematite (Fe_2O_3): synthesized from $Fe(NO_3)_3.9H_2O$ according to the precipitation method of Schwertmann and Cornell (1991)

4.3.5 Mössbauer Spectroscopy

Mössbauer spectra were collected using either a WissEl Elektronik (Germany) or Web Research Company (St. Paul, MN) instrument that included a closed-cycle cryostat SHI-850 obtained from Janis Research 18 Company, Inc (Wilmington, MA), a Sumitomo CKW-21 He compressor unit, and an Ar-Kr proportional counter detector with WissEl setup or a Ritverc (St. Petersburg, Russia) NaI detection system. A ^{57}Co/Rh source (50-mCi to 75-mCi, initial strength) was used as the gamma energy source. With the WissEl setups, the transmitted counts were stored in a multichannel scalar (MCS) as a function of energy (transducer velocity) using a 1024-channel analyzer. In both the setups (WissEl and Web Research Company) the raw data were folded to 512 channels to provide a flat background and a zero-velocity position corresponding to the center shift (CS) of a metal Fe foil at room temperature (RT). Calibration spectra were obtained with a 25-μm-thick Fe foil (Amersham, England) placed in the same position as the samples to minimize any geometry errors. The Mössbauer data were modeled with Recoil^{TM} software (University of Ottawa, Canada) using a Voigt-based structural fitting routine (Rancourt and Ping, 1991). Sample preparation (type of sample holder, etc) is identical to the procedures reported in Peretyazhko et al. (Peretyazhko et al., 2012).

4.4 Results and Discussion

4.4.1 Basic Soil Properties

Figure 4.1 shows a photograph of the floodplain soil profile. Soil color is an indication of redox variations. The main feature of the soil is the significant depletion of Fe(III) oxides in the pre-colonial wetland, whereas a higher Fe(III) oxide content is shown in the post-colonial sediments and gravel.

Figure 4.2 shows the results of in-situ field monitoring of redox conditions. There is a significant redox gradient across the floodplain profile. Redox conditions ranged substantially from very reducing conditions (Eh< -50 mV) within the pre-colonial buried wetland to oxidizing conditions (averaged Eh > 600 mV) within the post-colonial deposits. Strongly reducing conditions (Eh< -50 mV) occurred in the pre-colonial buried wetland at a soil depth of 80-120 cm over entire measurements. In this permanently water-saturated horizon with its gray color, Fe(III) is thermodynamically not stable and Fe(III) oxides are virtually absent. Highest redox fluctuations occurred in the gravel layer, ranging from 400 to 600 mV. The Eh level of the gravel layer was between that of the pre-colonial buried wetland and post-colonial sediments.

Soil C content and particle size distribution also changed significantly along the floodplain profile, as presented in Table 4.1. Soil C content increased from ~1-1.4 % in the post-colonial sediments to 4.2% in the pre-colonial buried wetland. The high C concentration in the pre-colonial wetland is probably due to inhibited decomposition

of organic matter under strongly reducing conditions. Particle-size analysis showed that the soil samples ranged from 2.6 to 22.4 wt.% clay (Table 4.1). Samples from the top 0-20 cm were dominated by sand particles (77.8 wt.%) with 8.1 wt.% clay. As soil depth increased from 0-20 cm to 20-120 cm, the percentage of sand particles dropped dramatically to 28.6-41wt.%, followed by a significant increase in clay fractions to 18.3-22.4 wt.%. These results suggest soils from the floodplain surface are relatively new sandy deposits as a result of overbank flooding and the clay particles are formed in deeper horizons during pedogenesis. In the gravel layer, 93.2 wt.% of the particles were sands.

Soil Fe content varied substantially across the floodplain profile (Table 4.2). Soil Fe content dramatically decreased from 26.1-34.7 g/kg in the oxic post-colonial sediments to 16.0 g/kg in the strongly reduced pre-colonial wetland soils, indicating the reductive dissolution of Fe(III)-containing mineral phases. Fe content was lower in the gravel layer than in the pre-colonial wetland, because of a pronounced lower amount of clay particles present in the gravel layer (Table 4.2). For soils from the post-colonial deposits and gravel layer, dithionite-citrate extracted 28.3-38.9% of the total Fe, and oxalate extracted 43.3-55.3% of the total Fe, suggesting a majority of Fe(III) oxides in these soils was present in poorly crystalline phases that are subject to dissolution by oxalate, with a relatively small portion of total Fe in more crystalline mineral phases. The difference between total Fe and dithionite-citrate extractable Fe can be attributed to Fe bound in phyllosilicates. In the post-colonial sediments and

gravel layer, 44.7-56.7% of Fe was bound in phyllosiicates, while phyllosilicate-Fe contributed up to 84.4% of the total Fe in the pre-colonial wetland.

4.4.2 Fe K-edge EXAFS Spectroscopy

Fe K-edge EXAFS spectra are presented in Fig.4.3 and the results of least-squares best fits summarized in Table 4.3. In the pre-colonial sediments, about 41% of the total Fe wasbound to Fe(III)-bearing phyllosilicates, with verimuclite and illite contributing 31% and 10%, respectively. The greater proportions of Fe in vermiculite than in illite is in agreement with XRD analysis which showed that clay mineralogy in this soil is dominated by vermiculite with much lesser amounts of illite (Fig.B.1). About 9% of the total Fe in the legacy sediments was due to Fe(II)-bearing phyllosilicates (Table 4.3). However the proportion of total Fe in the Fe(II)-bearing phyllosilicates increased up to 56% in the strongly reduced pre-colonial wetland (Table 4.3). In gravel where the redox level was in between the pre-colonial wetland and post-colonial sediments, 22% of the total Fe was bound to Fe(II)-bearing phyllosilicates and this number was intermediate to the pre-colonial wetland and post-colonial sediments (Table 4.3). Therefore, these results indicate that the relative abundance of phyllosilicate-Fe(II) increased with decreasing redox levels. The transformation of Fe(III)-bearing phyllosilicates to Fe(II)-bearing phyllosilicates is dominated by direct structural modifications, probably including the reduction of Fe within the phyllosilicate structure, the partial release of Fe(II) from the phyllosilicate, and the precipitation of new clay minerals.

Based on linear combination fitting, Fe(III) oxides accounted for 43% of the total Fe in the post-colonial sediments, with 28% as ferrihydrite and 15% as goethite (Table 4.3). A greater contribution of ferrihydrite than goethite to total Fe is consistent with the selective chemical extractions, which showed that a majority of Fe(III) oxides in these soils was present in poorly crystalline phases. In the anoxic pre-colonial wetland, the Fe(III) oxides were not detectable (Table 4.3), indicating that the permanent reducing conditions led to a complete reductive dissolution of Fe(III) oxides. Critical redox potentials for the onset of soil Fe(III) reduction are at 150 to 200 mV at pH 6 to 7 (Cogger et al. 1992; Mansfeldt 2004; Patrick and Jugsujinda 1992). Thus, it is plausible to expect an absence of Fe(III) oxides in the wetland with an Eh < -50 mV over the time. In the gravel layer, 25% and 11% of the total Fe was present as ferrihydrite and goethite, respectively (Table 4.3). The Fe(III) oxides in the gravel layer might orginate from the oxidation and subsequent precipitation of Fe(II) leached from the anoxic pre-colonial wetland, which is just above the gravel layer (Fig.4.1). High concentrations of Fe(II) in soil water are caused by reductive dissolution of Fe(III)-containing minerals under reducing conditions from the pre-colonial wetland. As pointed out by Banning et al. (2009), when coming into contact with O_2, $Fe^{2+}$is rapidly immobilized by precipitation as Fe oxide. Ferrihydrite is intrinsically a short-range-ordered phase having very small particles of about 2 to 4 nm and poor crystallinity. It is assumed that ferrihydrite is often the first phase to form in soils, especially under rapid oxidative precipitation (Cornell and Schwertmann 2003; Schneider 1988). However, under oxidizing conditions metastable ferrihydrite is

gradually transformed to more thermodynamically stable and crystalline phases like goethite.

4.4.3 Mössbauer Spectroscopy

Fe-oxides are in ubiquitous in the subsurface. XRD which is commonly employed to characterize sediments, however, is not optimum if multiple oxide phases are present and the oxide content is below 1-2 wt.% or the phase is amorphous. Also, this technique is not suitable to gauge the effect of organic carbon association on oxides nor is suitable to characterize structural Fe (Fe_{oct} and Fe_{tet}) in clays and the redox state. Mössbauer spectroscopic technique is very sensitive to Fe structural changes and is particularly suitable for Fe-poor systems (Peretyazhko et al., 2012). Hence, Fe-oxide(s) that were not detected in XRD and Fe-EXAFS will be evident in Mössbauer spectroscopy. Despite this advantage, unambiguous characterization of soil Fe-oxides, however, is not straightforward because Fe-oxide distribution in soils and sediments is rather complex. Particle size, substitution of Fe by other elements (e.g., Al, Si, P) (Kukkadapu et al., 2001; Carlson and Schwertmann, 1981; Thibault et al., 2009), and/or organic matter associations (Eusterhues et al., 2008), affect magnetic properties. For example, Al-/Si-substituted ferrihydrite coprecipitated with organic matter may exist in soils and sediments. Fortunately, since magnetic properties are temperature dependent, insights into the nature of these Fe-oxides can be realized, to a good extent, by coupling Mössbauer data obtained at various temperatures to operationally defined selective chemical extraction data and complimentary

microscopic and spectroscopic data. This approach is needed because theoretically calculated Mössbauer parameters of small-particle/metal substituted/organic matter coated, Fe-oxides are not readily available. Also, this approach is found useful in characterizing systems where Fe-oxides are mixed with small amounts of carbonates (e.g., siderite, green rust), phosphates (e.g., vivianite), and sulfides (e.g., pyrite) (Kukkadapu et al., 2004; Qafoku et al., 2009; Peretyazhko et al., 2012), which are common in reduced soils.

Post-colonial Deposits (Oxic Sediments): A variable temperature measurement approach is used (as discussed before) to tease apart not only contributions of various Fe-oxides from each other but also to characterize phyllosilicate (PS) Fe (Figures 4.4a-d). In general, the characterization of Fe-oxides, is based on insights gained both from laboratory-synthesized single-phase oxides of various particle sizes [pure, metal substituted (e.g., Al, Si), and oxides coprecipitated with organic matter and complex sediments (Thompson et al., 2006; Peretyazhko et al., 2012; Fox et al., 2013).

At room temperature, ferrihydrite, small-particle (sp) goethite**,** and PS-Fe(III) display doublet feature characteristic of octahedral (also tetrahedral in PS) Fe with more or less similar parameters. The two sextets in the room temperature (RT) spectrum are due to large-particle/well-crystalline hematite and goethite (~10% total; Figure 4.4a). Mössbauer spectroscopic data generated below RT temperature provided some valuable information on the nature of the remaining oxide (Figures 4.4b-d). The Mössbauer spectral parameters/features of ferrihydrite, small particle (sp) goethite and

PS-Fe(III), are different below RT. For example, PS-Fe(III) exists as a doublet even at liquid He (4.5 K) temperature (Thompson et al., 2006, 2011). Ferrihydrite transforms from a doublet to a sextet below 77 K (Murad and Cashion, 2004) and the RT sp-goethite doublet exists as a sextet at 77 K (Janot et al., 1973). The well-defined sextet in the 77 K spectra (labeled nG1), thus, can be characterized as sp-goethite (to simplify modeling, large-particle goethite, and hematite, evident in the RT spectrum, were also included in this sextet) (Fig.4.4b). The increased sextet peak area from 77 K to 12 K could be assigned to ferrihydrite (labeled as nG2) (Fig.4.4c). However, it could also result from goethite with a smaller particle size or poorer crystallinity than nG1. Recently, Thompson *et al.,* (2006) assigned a more or less similar well-defined sextet in liquid He spectra (4.5 K) of sediments, to microcrystalline- and nano-goethite, respectively. Alternatively, the nG2 domain may be small goethite particles with substituted Al or Si and/or organic matter association. This assignment is also in line with the feature of pure ferrihydrite being different than ferrihydrite-OM coprecipitates (Eusterhues et al., 2008). Finally, for the sake of convenience, the well-defined sextets and the broad feature in < 77 K spectra were labeled as nG1 (relatively larger-particle size than nG2) and nG2, respectively (Fig.4.4c). More or less similar nG1 and nG2 contents in the <77 K spectra also implies these fractions to be independent domains (Fig.4.4c). Together, the spectral interpretations from these studies suggest that the post-colonial sediment contains at least two particle-size domains of Fe(III) oxides (in addition to small amounts of large-particle/crystalline goethite and hematite, Figure 4.4a). But it is not possible to tease goethite and

ferrihydrite apart based on Mössbauer analysis, because of the complex nature of the sediments.

Operationally, sp-oxides and poorly-crystalline Fe-oxides readily dissolve in oxalate. The spectral area of nG2 (smaller particle domain) that was 24% (based on 12 K spectrum, Fig.4.4c), however, was lower than the amount of Fe extracted by oxalate-extractable (39%, Table 4.2). This suggests that oxalate may also extract part of the oxides labeled as nG1. The sextet areas of 5 K data (Fig.4.4d) were not used for the calculations because the broad-feature may have some contribution from Fe-rich clays (e.g., illite, verimiculite) (Murad and Cashion, 2004). It is also possible that the difference is due to a different recoilless fraction of oxides and clays at this temperature (Stucki et al., 2007). Therefore, the 5 K spectrum was mainly shown to compare to reduced sediments (see section on pre-colonial wetland). As expected, the dithionite-citrate extractable Fe was higher (55% Fe_{tot}, Table 4.2) than oxalate, since almost all Fe-oxides dissolve in the dithionite-citrate reagent (Mehra and Jackson, 1960). The dithionite-citrate extractable Fe was similar to combined nG1 and nG2 (59%, 12 K spectrum) (Fig.4.4c).

Phyllosilicate-Fe(III) in illite and HIV exists as a doublet even at 4.2 K (liquid He). The Fe(III) doublet's Mössbauer spectral parameters are in agreement with this phyllosilicate suite (Murad and Cashion, 2004). The presence of multiple clays can be inferred from the modeled spectrum. A good fit was only realized with two Gaussian sites in the QSD distribution, suggesting the presence of at least two Fe(III) clay domains. Twenty nine percent of the total Fe was PS-Fe(III), while PS-Fe(II) was

~14% of the Fe_{tot} (Fig.4.4c). Modeling also suggested that this sample contained small amounts of ilmenite (4% of the total Fe), see RT and 77 K spectra (Fig.4.4a-b). Ilmenite contribution was not included in the 12 K and 5 K spectra because it exhibits a complex spectrum below 45 K due to magnetic ordering (Murad and Cashion, 2004).

Pre-colonial Wetland (Reduced Sediment): The Fe content of the sample was small (1.6 wt.%) and most Fe was bound to phyllosilicates (evident in the Fe-EXAFS). The absence of Fe-oxide(s) in the EXAFS analysis indicates that they are below the detection limits, if any present.

Reducing conditions had a significant effect on Fe mineralogy, which was evident from a comparison of the pre-colonial wetland Mössbauer spectra to the post-colonial sediment (compare Figs.4.4 and 4.5). Its phyllosilicate (PS) Fe(II) content was significantly higher than the post-colonial sediment, and the absence of sextet features in the 77 K spectrum indicates that the sediment was free of goethite (Fig.4.5b). Ferrihydrite and lepidocrocite are also not expected in the sample because they are readily bioavailable, which is in agreement with the 12 K spectrum that was devoid of sextet(s) (Fig.4.5c), and the Fe-EXAFS data. The Mössbauer spectroscopic data, therefore, unambiguously indicates that the sample is free of Fe-oxides or Fe-oxides present in the post-colonial sediment are absent in the reduced sediment. Although there was no Fe oxides detected in this reduced sediments based on Mössbauer and Fe-EXAFS, oxalate and dithionite-citrate still extracted 13-15% of the total Fe (Table 4.2). This suggests that oxalate and dithionite-citrate -reagents probably extracted Fe associated with organic matter (the sediment's OC content is ~

5 wt.% *vs.* 1 wt.% in the post-colonial sediment). The organic matter bonded Fe should be ferrous Fe, since this sediment was under permanent reducing conditions and the presence of organic matter bounded Fe(III) seems possible. Mössbauer spectral parameters also indicated that the Fe(II) was not due to siderite, magnetite or green rust. The fate of biogenic Fe(II), as a result of reductive dissolution of Fe-oxides, depends upon aqueous biogeochemical conditions and soil mineral composition. A lack of secondary Fe(II) minerals in the sediment (e.g., siderite, magnetite, green rust), despite the sediment being Fe-oxide free, thus seems consistent with the presence of organic matter-Fe(II) in the sediment.

The Fe(II) doublet feature, thus, is a combination of PS- and OM-Fe(II). Despite this, the Fe(II) doublet was not modeled into individual contributions because: a) Mössbauer parameters of Fe(II) associated with OC are not reported in the literature, to our knowledge, and b) the difficulty in resolving individual clay mineral contributions from each other. The reduced pre-colonial wetland soil also contained a greater percentage of ilmenite than the oxic post-colonial sediment (Fig. 4.5a-b). The difference in 77 K and 12 K spectral features is due to magnetic ordering of ilmenite at 12 K. Its high-energy in the peak 12 K spectrum was indicated by * in the Figure 4.5c insert. The spectrum was not modeled because the nature of ilmenite is uncertain (in terms of Fe and Ti contents) (Fig.4.5c). The 5 K spectral features were similar to the bioreduced Oakridge sediment that had a similar PS mineral suite (illite, HIV, and kaolinite) (Kukkadapu *et al.,* 2006), as the post-colonial sediment. By comparing the 12 K and 5 K spectra, broadening of the central feature and incipient sextet peaks

(indicated by +), evident in the 5 K spectrum (Fig.4.5c), is typical of highly reduced clays due to magnetic ordering of both Fe(II) and Fe(III)), while the Fe(II) doublet is typical of relatively less reduced clays. Finally, modeling of 5 K spectrum was not attempted because magnetic ordering of clays is not well documented in the literature.

Gravel (Partially Reduced Sediment): Mass balance data of the gravel layer indicated that its dithionite-citrate extractable Fe (49.8% of Fe_{tot}), and oxalate extractable Fe (36.7% of Fe_{tot}), was similar to that of the post-colonial sediments (Table 4.2). Despite this similarity, which implies a similar Fe-oxide suite and distribution in both the sediments, their Mössbauer spectral features were different (Figure 4.6). First, its ilmenite and PS-Fe(II) content was relatively higher than the post-colonial sediment (compare to Figure 4.4). However, their contents were significantly lower than in the pre-colonial wetland sediment (compare to Figure 4.5). Its PS-Fe(II) content, which was intermediate to the post-colonial sediment and pre-colonial wetland, is in agreement with its Eh level that was in between the post-colonial sediment and pre-colonial wetland. Clearly, the data also indicate that Eh levels have an impact on ilmenite content, with a higher abundance in the low-redox conditions. .

The temperature effects on spectral areas of sextets are significant**.** In the post-colonial sediment, the nG1 sextet had more or less similar spectral areas in the 77 K and 12 K spectra (Fig.4.4b-c). In the gravel sample, on the other hand, the sextet area due to nG1 increased significantly upon cooling the sample from 77 K to 12 K (Fig.4.6b-c)**.** This suggests that this sediment has a different domain of sp-Fe-oxide

than those present in the post-colonial sediment. Ferrihydrite/lepidocrocite that exists as a doublet at 77 K, transforms to a sextet at 12 K. This implied that a fraction of the 12 K well-defined sextet could be ferrihydrite/lepidocrocite or sp-goethite that is intermediate in particle size to nG1 and nG2. Based EXAFS spectra fitting, lepidocrocite was not detected in this soil (Table 4.3). Since particle size, metal substitutions, organic matter coatings, etc., are possible in soil Fe-oxides, unambiguous labeling of this fraction to a certain mineral (pure or modified) is not possible. Hence, this fraction was labeled as nG1, for simplicity.

Collectively, a comparison of Mössbauer spectra in the post-colonial sediment and gravel sample, indicates that even though their behavior towards various chemical reagents is similar, they differ considerably from each other in Fe-oxide suite distribution (due to different particle size domains), ilmenite and PS- Fe(II) contents. The Mössbauer study also suggests caution should be exercised in assigning a certain fraction of Fe-oxide of soil Fe-oxides to ferrihydrite, based on selective chemical extraction data (the same applies for Fe-EXAFS data). The EXAFS linear combination fitting estimates of components in complex natural samples are typically considered to be subject to absolute detection limits of ~10%, and relative errors may approach up to 25% (Ostergren et al., 1999; Roberts et al., 2002); However, for natural samples these percentages are difficult to quantify, especially for less-abundant species (Manceau et al., 2000). The standards used for linear combination fitting in this study include clay minerals containing substituted Fe, but the Fe contents of the standard clays may differ from the Fe contents of vermiculite, illite and augite in the soil clays.

Furthermore, the Fe contents of soil clay minerals may vary among samples. Thus, the linear combination fit percentages shown in Table 4.3 should only be viewed as approximations of the amount of total Fe in soil minerals. A complete mass-balance calculation is not possible

REFERENCES

Baker, L. L.; Strawn, D.; Vaughan, K.; McDaniel, P., XAS study of Fe mineralogy in chronosequence of soil clays formed in basaltic cinders. *Clays Clay Miner.* **2010**, 58(6), 772-782.

Banning, A.; Coldewey, W. G.; Gobel, P., A procedure to identify natural arsenic sources, applied in an affected area in North Rhine-Westphalia, Germany. *Environ. Geol.* **2009**, 57, 775-787.

Bonneville, S.; Van Cappellen, P.; Behrends, T., Microbial reduction of iron(III) oxyhydroxides: effects of mineral solubility and availability. *Chemi. Geol.* **2004**, 212, 255-268.

Borch, T.; Kretzschmar, R.; Kappler, A.; Van Cappellen, P.; Ginder-Vogel, M.; Voegelin, A.; Campbell, K. M., Biogeochemical Redox Processes and their Impact on Contaminant Dynamics. *Environ. Sci. Technol.* **2010,** *44*, 15-23.

Carlson, L.; Schwertmann, U., Natural ferrihydrites in surface deposits from Finland and their association with silica. *Geochim.Cosmochim. Acta* **1981**, 45, 421-429.

Cogger, C. G.; Kennedy, P. E.; Carlson, D. ,Seasonally saturated soils in the Puget Lowland II. Measuring and interpreting redox potentials. *Soil Sci***. 1992**, 154:50-58

Cornell, R. M.; Schwertmann, U., The iron oxides: characterization (ch. 7), R.M. Cornell, U. Schwertmann (Eds.), The Iron Oxides, VCH, New York, NY **2003**

Chorover, J.; Kretzschmar, R.; Garcia-Pichel, F.; Sparks, D. L., Soil biogeochemical processes within the critical zone. *Elements* **2007**, 3, 321-326.

Cornell, R.M., Schwertmann, U., The iron oxides: characterization. In: *The Iron Oxides,*R.M. Cornell and U. Schwertmann, Eds, VCH, New York, NY, **2003**.

Fox, P. M.; Davis, J. A.; Kukkadapu, R.; Singer, D. M.; Bargar, J.; Williams K. W., Abiotic U(VI) reduction by sorbed Fe(II) on natural sediments. *Geochim. Cosmochim. Acta* **2013**, 117, 266-282.

Eusterhues, K.; Wagner, F. E.; Häusler, W.; Hanzlik, M.; Knicker, H.; Totsche, K. U.; Kögel-Knabner, I.; Schwertmann, U., Characterization of Ferrihydrite-Soil Organic Matter Coprecipitates by X-ray Diffraction and Mössbauer Spectroscopy. *Environ. Sci. Technol.* **2008**, 48, 7891-7897.

Gu, B.; Schmitt, J.; Chen, Z.; Liang, L.; McCarthy, J. F., Adsorption and desorption of different organic matter fractions on iron oxide. *Geochim. Cosmochim. Acta* **1995**, 59, 219-229.

Jackson, M.L., Chemical Analysis — Advanced Course, 2nd edn.University of Wisconsin, College of Agric., Department of Soils, Madison, WI, **1979**.

Janot, C.; Gibert, H.; Tobias, C., Characterization of ferriferous kaolinites by Mössbauer spectrometry. *Bull. Soc. Fr. Mineral. Cristallogr.* **1973**, 96, 281-291.

Kaiser, K.; Guggenberger, G.; Haumaier, L.; Zech, W., Dissolved organic matter sorption on subsoils and minerals studied by 13C-NMR and DRIFT spectroscopy. *Eur. J. Soil Sci.* **1997**, 48, 301-310.

Keil, R. G.; Montlucon, D. B.; Prahl, F.R.; Hedges, J. I., Sorptive preservation of labile organic matter in marine sediments. *Nature* **1994**, 370, 549-552.

Kelly, S. D.; Hesterberg, D.; Ravel, B., Analysis of soils and minerals using X-ray absosrption spectroscopy. In Methods of Soil Analysis Part 5 – Mineralogical Methods (eds. A. L. Ulery and R. Drees). *Soil Sci. Soc. Am*. **2008**

Kostka, J. E.; Stucki, J. W.; Nealson, K. H.; Wu, J., Reduction of structural Fe(III) in smectite by a pure culture of *Shewanellaputrefaciens* strain MR-1. *Clays Clay Miner.* **1996**, 44 (4), 522-529.

Kiczka, M.; Wiederhold, J. G.; Frommer, J.; Voegelin, A.; Kraemer, K.; Bourdon, B.; Kretzschmar, R., Iron speciation and isotope fractionation during silicate weathering and soil formation in an alpine glacier forefieldchronosequence. *Geochim. Cosmochim. Acta* **2011**, 75, 5559-5573.

Kukkadapu, R. K.; Zachara, J. M.; Fredrickson, J. K.; McKinley, J. P.; Kennedy, D. W.; Smith, S. C.; Dong, H. L., Reductive biotransformation of Fe in shale-limestone saprolite containing Fe(III) oxides and Fe(II)/Fe(III) phyllosilicates. *Geochim. Cosmochim. Acta* **2006**, 70 (14), 3662-3676

Kukkadapu, R. K.; Zachara, J. M.; Fredrickson, J. K.; Kennedy, D. W., Biotransformation of synthetic 2-line silica-ferrihydrite coprecipitates by a

dissimilatory Fe(III)-reducing bacterium: Formation of carbonate green rust in the presence of phosphate. *Geochim. Cosmochim. Acta* **2004**, 68, 2799-2814.

Kukkadapu, R. K.; Zachara, J. M.; Smith, S. C.; Fredrickson, J. K.; Liu, C., Dissimilatory bacterial reduction of Al-substituted goethite in subsurface sediments. *Geochim. Cosmochim. Acta* **2001**, 65, 2913-2924.

Kukkadapu, R. K.; Zachara, J. M.; Fredrickson, J. K.; McKinley, J. P.; Kennedy, D. W.; Smith, S. C.; Dong, H. L., Reductive biotransformation of Fe in shale-limestone saprolite containing Fe(III) oxides and Fe(II)/Fe(III) phyllosilicates. *Geochim. Cosmochim. Acta* **2006**, 70, 3662-3676.

Manceau, A.; Lanson, B.; Schlegel, M. L.; Harge, J. C.; Musso, M.; Eybert-Berard, L.; Hazemann, J. L.; Chateigner, D.; Lamble, G. M., Quantitative Zn speciation in smelter-contaminated soils by EXAFS spectroscopy. *Am. J. Sci.* **2000**, 300, 289-343.

Mansfeldt, T., Redox potential of bulk soil and soil solution concentration of nitrate, manganese, iron, and sulfate in two Gleysols. *J. Plant Nutr. Soil Sci.* **2004**, 167:7–16

Mehra, O. P.; Jackson, M. L., Iron oxide removal from soils and clays by a dithionite–citrate system buffered with sodium bicarbonate. *Clays Clay Miner.* **1960**, 7, 317-327.

Mikutta, R.; Kleber, M.; Torn, M.S.; Jahn, R., Stabilization of soil organic matter: Association with minerals or chemical recalcitrance? *Biogeochem.* **2006**, 77, 25-56.

Murad, E.; Cashion, J., *Mössbauer spectroscopy of environmental materials and their industrial utilization*. Kluwer Academic Publishers, *Dordrecht*. **2004**.

Myneni, S. C. B.; Tokunaga, T. K.; Brown, G. E., Abiotic Se redox chemistry in the presence of Fe(II, III)-oxides. *Science* **1997**, 278, 1106-1109.

Newbold, J. D.; Bott, T. L.; Kaplan, L. A.; Sweeney, B. W.; Vannote, R. L., Organic matter dynamics in White Clay Creek, Pennsylvania, USA, *J. North Am. Benthol. Soc.* **1997**, 16(1), 46-50.

O'Day, P. A.; Rivera, N.; Root, R.; Carroll, S. A., X-ray absorption spectroscopic study of Fe reference compounds for the analysis of natural sediments. *Am. Min.* **2004**, 89, 572-585.

Patrick,W. H.; Jugsujinda, A., Sequential reduction and oxidation of inorganic nitrogen, manganese, and iron in flooded soil. *Soil Sci. Soc. Am. J.* **1992**, 56:1071-1073.

Peretyazhko, T.; Zachara, J. M.; Kukkadapu, R. K.; Heald, S. M.; Kutnyakov, I. V.; Resch, C. T.; Arey, B. W.; Wang, C. M.; Kovarik, L.; Phillips, J. L.; Moore, D. A., Pertechnetate (TcO4-) reduction by reactive ferrous iron forms in naturally anoxic, redox transition zone sediments from the Hanford Site, USA. *Geochim. Cosmochim. Acta* **2012**, 92:48-66.

Qafoku, N. P.; Kukkadapu, R. K.; McKinley, J. P.; Arey, B. W.; Kelly, S. D.; Wang, C. M.; Resch, C. T.; Long, P. E., Uranium in framboidal pyrite from a naturally bioreduced alluvial sediment. *Environ. Sci. Technol*. **2009**, 43, 8528-8534.

Rancourt, D. G.; Ping, J. Y., Voigt-based methods for arbitrary-shape static hyperfine parameter distributions in mossbauer spectroscopy. *Nucl. Instrum.mMethods Phys. Res., Sect. B* **1991**, 58, 85-97.

Roberts, D. R.; Scheinost, A. C.; Sparks, D. L., Zinc speciation in a smelter-contaminated soil profile using bulk and microspectroscopic techniques. *Environ. Sci. Technol.* **2002**, 36, 1742-1750.

Stucki, J. W.; Komadel, P.; Wilkinson, H. T., Microbial reduction of structural iron(III) in smectites. *Soil Sci. Soc. Am. J.* **1987**, 51 (6), 1663-1665.

Schwertmann, U.; Cornell, R. M., Iron oxides in the laboratory: Preparation and characterization, 137 p. Weinheim, *New York*. **1991**,

Schneider, W., Iron hydrolysis and the bio- chemistry of iron- The interplay of hydroxide and biogenic ligands. *Chimia* **1988**, 42, 9-20

Stucki, J. W.; Lee, K.; Goodman, B.; Kostka, J. E., Effects of in situ biostimulation on iron mineral speciation in a sub-surface soil. *Geochim. Cosmochim. Acta* **2007**, **71**, 835-843.

Tebo, B.M.; He, L.M., Microbially mediated oxidative precipitation reactions. In:*Mineral*-Water *Interfacial Reacions: Kinetics and Mechanisms,* D.L. Sparks and T.J. Grundl, Eds., *ACS symposium series* **1998**, 393-414.

Thibault, P. J.; Rancourt, D. G.; Evans, R. J.; Dutrizac, J. E., Mineralogical conformation of a near-P:Fe = 1:2 limiting stoichiometric ratio in colloidal P-bearing ferrihydrite-like hydrous ferric oxide. *Geochim.Cosmochim. Acta* **2009**, 73, 364-376.

Thompson, A.; Rancourt, D. G.; Chadwick, O. A.; Chorover, J., Iron solid-phase differentiation along a redox gradient in basaltic soils. *Geochim. Cosmochim. Acta* **2011**, 75(1), 119-133.

Thompson, A.; Chadwick, O. A.; Rancourt, D. G.; Chorover, J., Iron-oxide crystallinity increases during soil redox oscillations. *Geochim. Cosmochim. Acta* **2006,** 70, 1710-1727.

Walter, R. C.; Merritts, D. J., Natural Streams and the Legacy of Water-Powered Mills. *Science* **2008**, 319, 299-304.

Weber, K. A.; Achenbach, L. A.; Coates, J. D., Microorganisms pumping iron: anaerobic microbial iron oxidation and reduction. *Nat. Rev. Microbiol*. **2006**, 4, 752-764.

Webb, S. M., SIXPack a graphical user interface for XAS analysis using IFEFFIT. *Phys. Scr.* **2005**, T115.

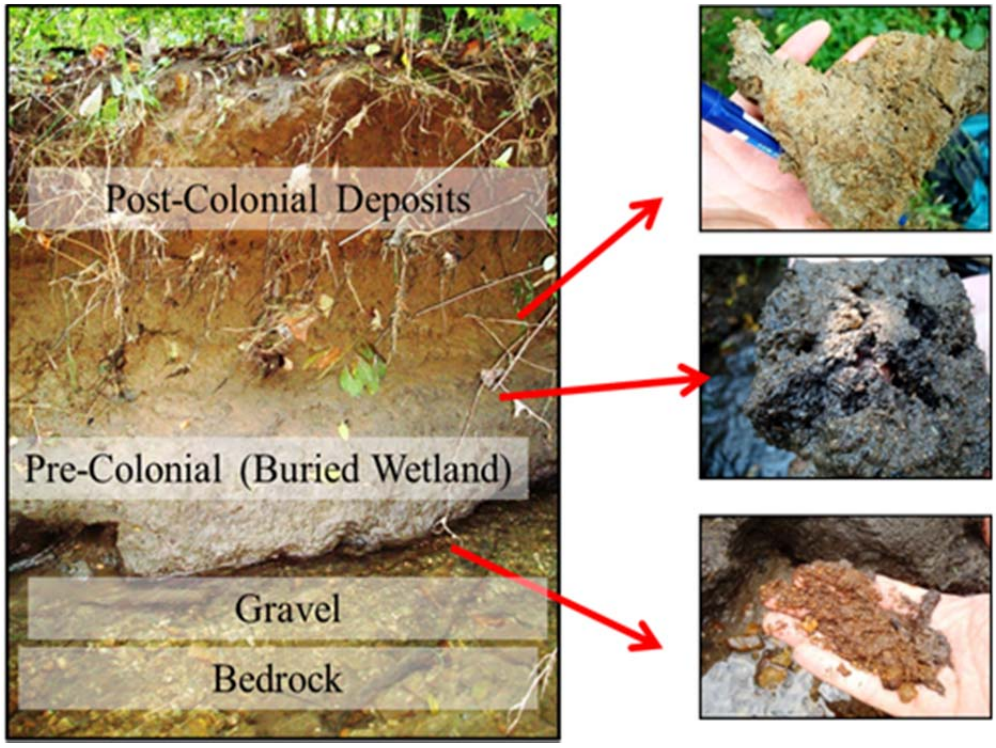

Figure 4.1 Photograph of the soil profile from the floodplain.

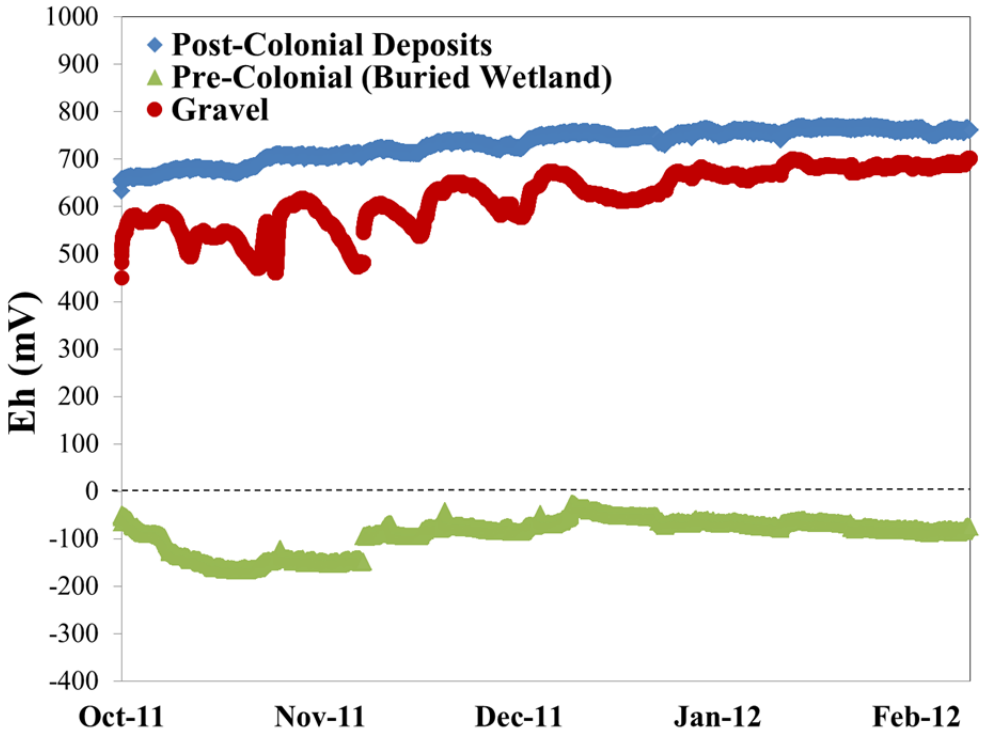

Figure 4.2 Continuous In-situ monitoring of redox potential in the floodplain soil profile.

Table 4.1 Soil C content and particle size distribution in the floodplain soil.

	Soil depth (cm)	C content (%)	Particle size distribution		
			Sand (%)	Silt (%)	Clay (%)
Post-colonial sediments	0-20	1.41	77.8	14.2	8.1
	20-40	1.26	41.0	40.7	18.3
	40-60	1.03	39.0	41.7	19.3
	60-80	1.09	28.6	49.0	22.4
Pre-colonial buried wetland	80-120	4.24	31.8	47.5	20.7
Gravel		0.83	93.2	4.2	2.6

Table 4.2 Soil Fe content from total digestion and selective chemical extractions in the floodplain soil.

	Soil depth (cm)	Total Fe content (g/kg)	Fe from selective extractions (g/kg)		Fraction of total Fe (%)	
			Oxalate	Dithionite Citrate	Oxalate	Dithionite Citrate
Post-colonial sediments	0-20	26.1	7.8	11.3	29.9	43.3
	20-40	33.6	9.5	15.0	28.3	44.6
	40-60	32.1	10.6	14.0	33.0	43.6
	60-80	34.7	13.5	19.2	38.9	55.3
Pre-colonial buried wetland	80-120	16.0	2.1	2.5	13.1	15.6
Gravel		13.1	4.8	6.5	36.6	49.6

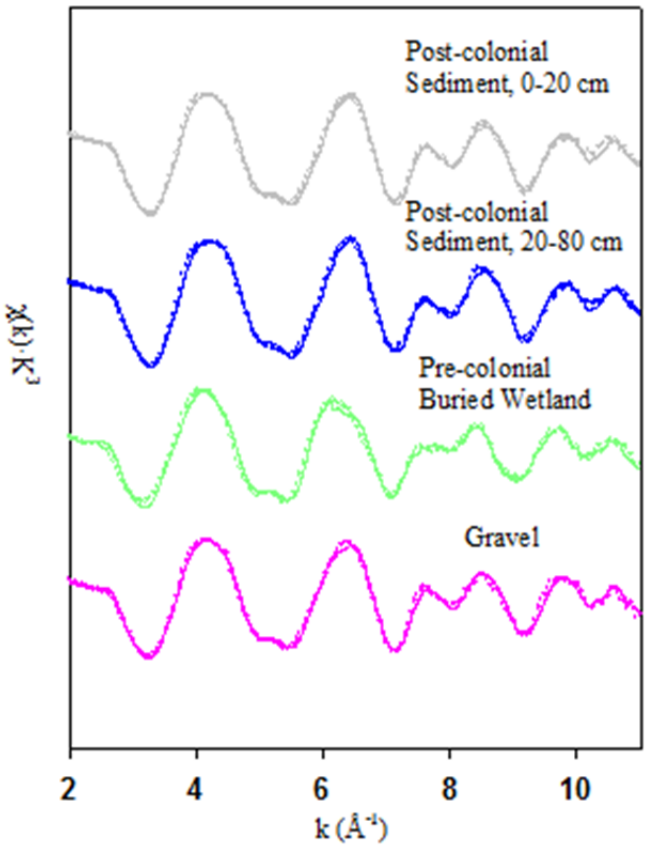

Figure 4.3 Iron k^3-weighted chi spectra of the floodplain soils. Solid lines are the collected data and dotted lines show the best linear combination fits.

Table 4.3 Summary of Fe mineralogy of floodplain soils based on EXAFS linear combination fitting over *k*-range 2–11Å^{-1}.

	Soil depth (cm)	Phyllosilicate Fe(III)		Phyllosilicate Fe(II)	Fe(III) oxides		Ilmenite	R-factor
		Vermiculite (%)	Illite (%)	Augite (%)	2-line ferrihydrite (%)	Goethite (%)		
Post-colonial sediments	0-20	32	10	9	26	14	9	0.0077
	20-80	31	10	8	28	15	8	0.0814
Pre-colonial buried wetland	80-120	20	16	54	ND	ND	10	0.0178
Gravel		24	12	20	25	11	8	0.0108

ND means non detectable.

.

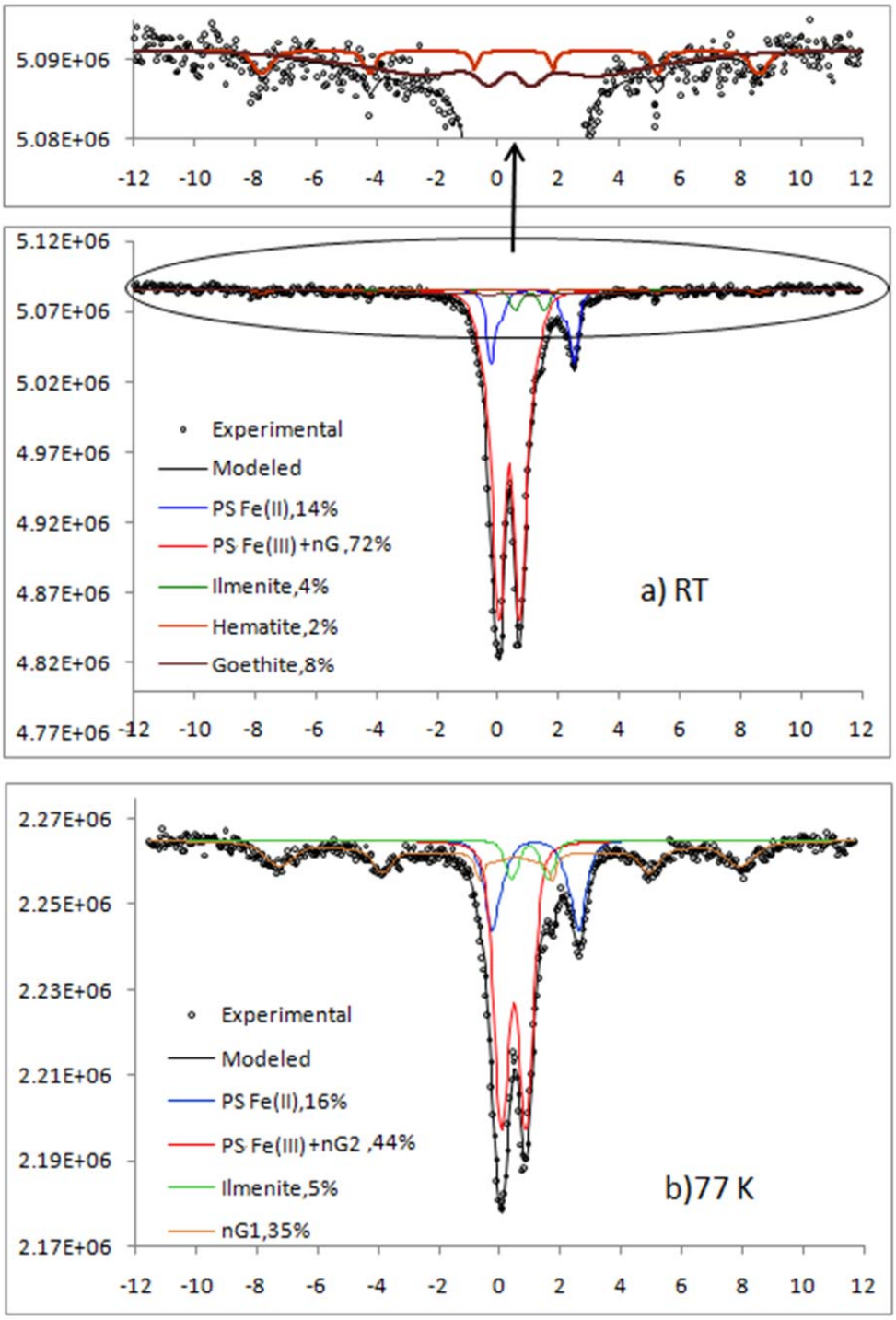
5.09E+06
5.08E+06
-12 -10 -8 -6 -4 -2 0 2 4 6 8 10 12
5.12E+06
5.07E+06
5.02E+06
4.97E+06
4.92E+06
4.87E+06
4.82E+06
4.77E+06
Experimental
Modeled
PS Fe(II),14%
PS Fe(III)+nG ,72%
Ilmenite,4%
Hematite,2%
Goethite,8%
a) RT
2.27E+06
2.25E+06
2.23E+06
2.21E+06
2.19E+06
2.17E+06
Experimental
Modeled
PS Fe(II),16%
PS Fe(III)+nG2 ,44%
Ilmenite,5%
nG1,35%
b)77 K

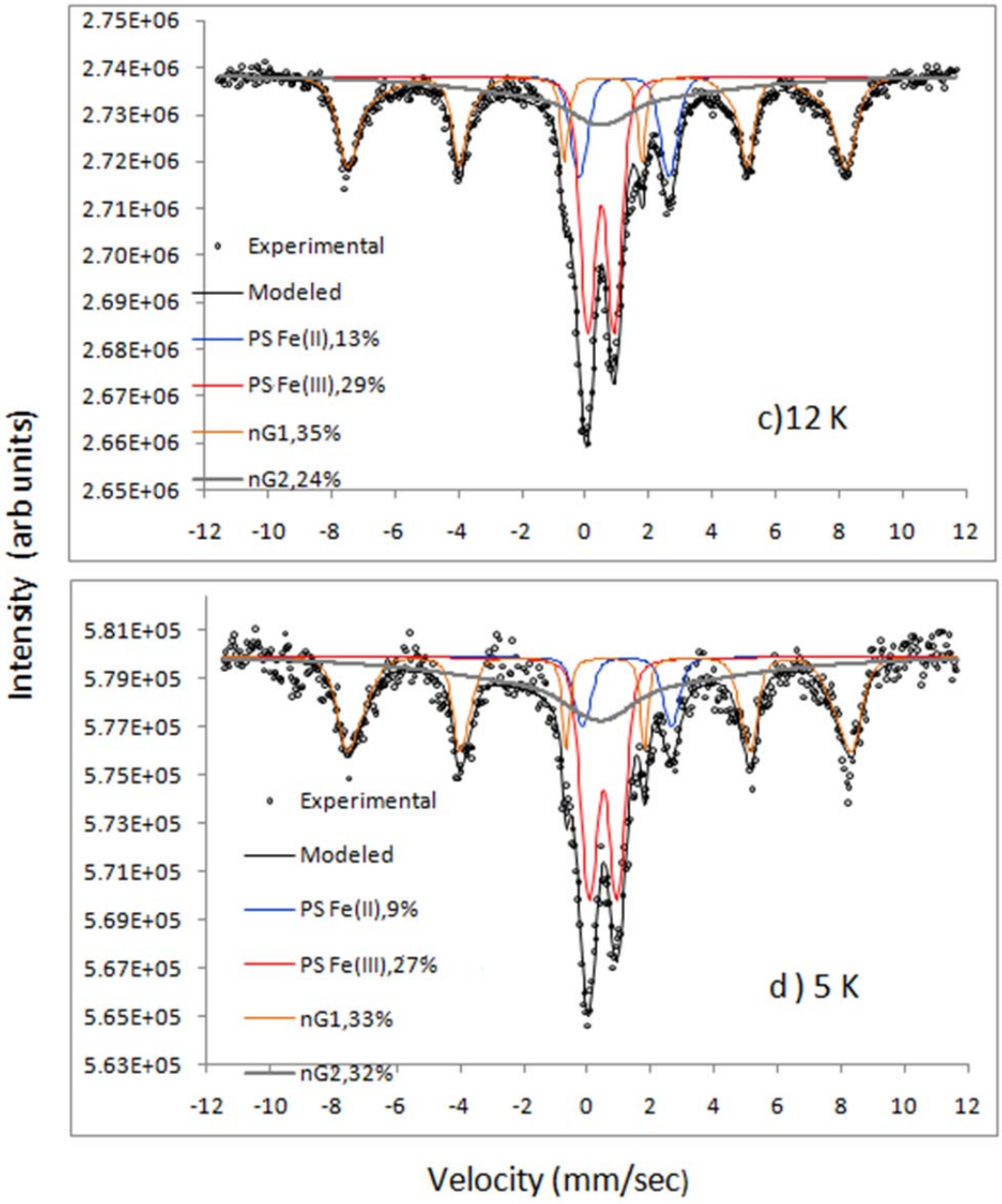

Figure 4.4 Mössbauer data of the post-colonial sediment at room temperature (RT), 77 k, 12 K and 5K.

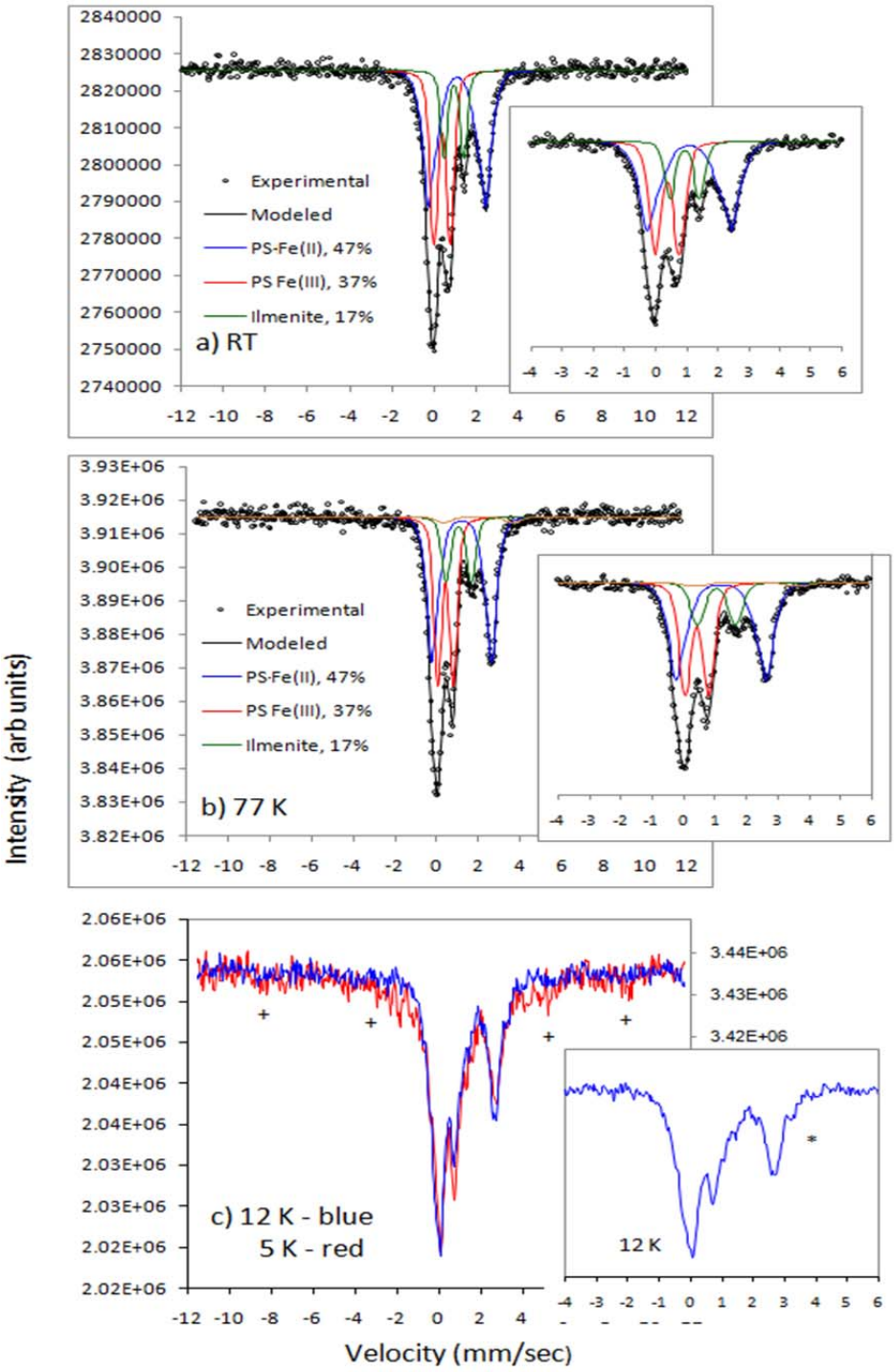

Figure 4.5 Mössbauer data of the pre-colonial buried wetland soil at room temperature (RT), 77 k, 12 K and 5K.

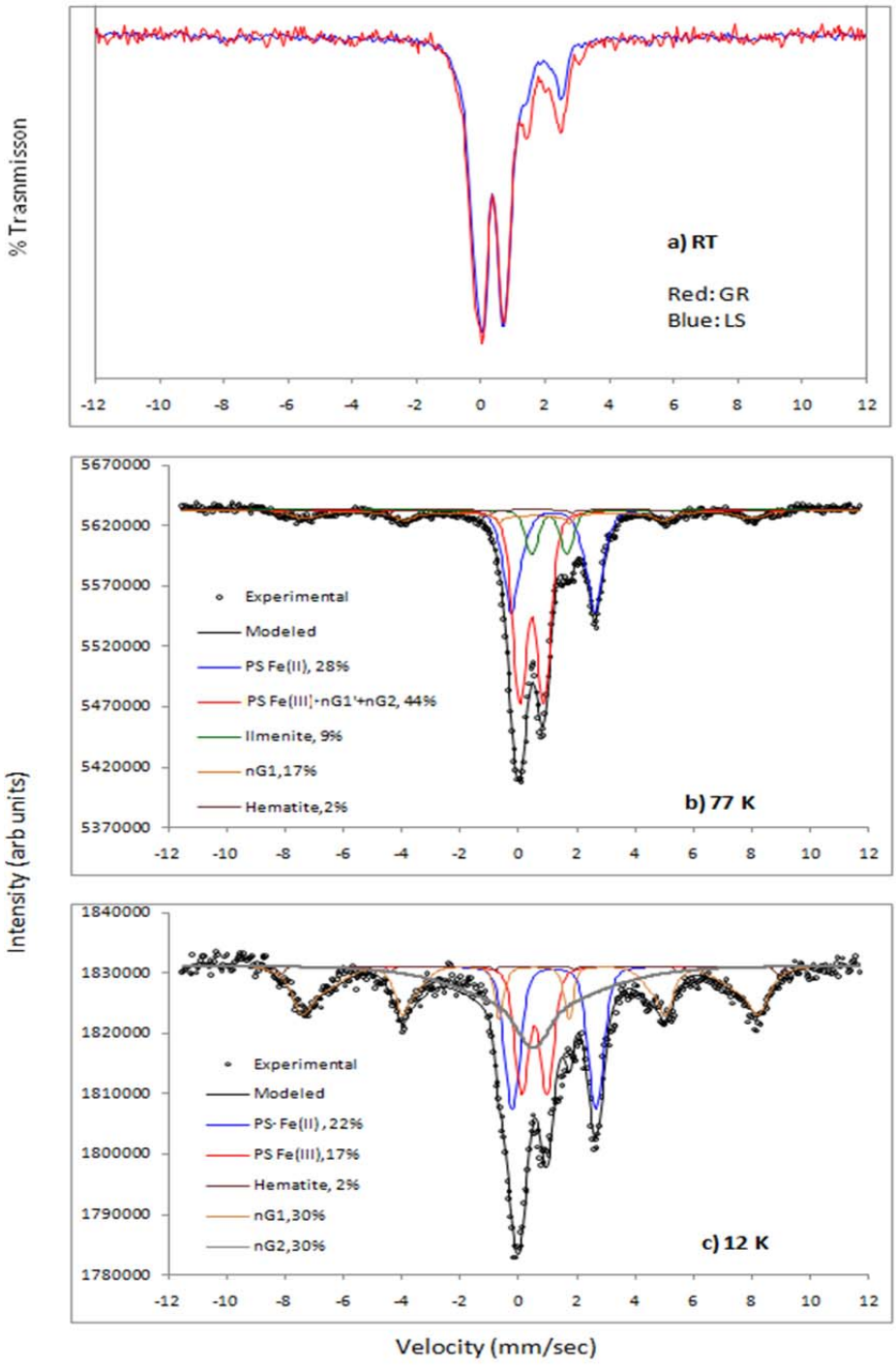

Figure 4.6 Mössbauer data of the gravel sediment at room temperature (RT), 77 k and 12 K. (GR, Gravel sediment; LS, Post-colonial sediment).

Chapter 5

RETENTIPN OF DISSOLVED ORGANIC MATTER BY ADSORPTION AND COPRECIPITATION WITH FERRIHYDRITE I: RETIONTION CAPACITY

5.1 Abstract

Poorly-crystalline ferrihydrite contributes significantly to organic matter (OM) complexation against microbial decay in soils and sediments. OM-ferrihydrite complexes can be formed by either adsorption or coprecipitation. In this study, we examined these interactions by preparing OM-ferrihydrite complexes at varying C:Fe ratios (0.05-5.36 g/g) using dissolved organic matter (DOM) extracts from a forest litter layer. We monitored organic carbon (OC) retention capacity, chemical fractionation of OM by UV-Vis spectroscopy, changes in specific surface area (SSA) and micro- and mesopore volumes of the OM-ferrihhydrite complexes by N_2 adsorption and desorption, and desorbability of the adsorbed and coprecipitated OM associated with these two processes. The results showed coprecipitation resulted in a greater maximum OC retention capacity of ca. 486 mg/g ferrihydrite or 3.38 mg C m^{-2} than adsorption (314 mg C/g or 1.64 mg C m^{-2}). Complete loss of micro- and mesopores was observed for adsorption, while coprecipitation led to complete loss of micropores but 78% maximum reduction in mesopore volumes. For both adsorption

and coprecipitation, ferrihydrite achieved almost complete coverage of OC at loadings of 0.88-0.97 mg C m^{-2}. Whereas UV-Vis spectroscopy showed preferential removal of high-molecular-weight, aromatic components by adsorption and coprecipitation at lower C/Fe ratios, no preference was observed at larger ones. Coprecipitation led to a more selective uptake of high-molecular-weight compounds than adsorption. Desorption of coprecipitated OC was much less than for the adsorbed OC at comparable OC loadings. Our study clearly demonstrated that coprecipiation could result in greater C retention capacity and C stability than adsorption. The STXM analysis demonstrated that at lower C loadings, C showed continuous homogenous distribution on ferrihydrite and C spatially correlated well with Fe, whereas there were localized concentrated C "hotspots" on ferrihydrite and the correlation between C and Fe was lower at higher C loadings.

5.2 Introduction

The formation of organo-mineral complexes is an important process in the soil carbon (C) cycle, stabilizing soil organic matter (OM) against microbial decay (Torn et al., 1997; Baldock & Skjemstad, 2000; von Lützow et al., 2006). Dissolved organic matter (DOM) is present in all ecosystems and occurs in forms that range from simple amino acids and carbohydrates to complex high-molecular-weight materials (Wershaw et al., 1996; Neff and Asner, 2001). The retention and also the stabilization of DOM in the mineral soil contribute substantially to total soil OM storage (Kalbitz and Kaiser,

2008). Therefore, changes in the retained amount and nature of OM or the degree of its stabilization can be of fundamental importance in the global C cycle.

Adsorption of DOM to mineral surfaces is an important and well-documented process for soil organic carbon (OC) stabilization in soils (Kaiser and Guggenberger, 2000, 2003, 2007; Schneider et al, 2010; Kalbitz et al, 2005). Fe oxides and hydroxides are major sorbents of DOM in many acidic and non-acidic soils (e.g. Kaiser and Guggenberger, 2000), retaining large proportions of the solid-phase OM (e,g., Shang & Tiessen, 1998; Eusterhues et al., 2005) and exerting a pronounced influence on OM stabilization. Poorly-crystalline Fe oxy-hydroxide ferrihydrite, because of its prevalence in the environment and high surface area, is of particular importance in DOM adsorption. The adsorptive stabilizing effect is likely due to multiple strong chemical bonds formed between organic molecules and mineral surfaces (Kaiser and Guggenberger, 2000). Multiple attachment of OM decreases the likelihood of desorption (e.g. Kaiser& Z ech, 1999) and degradation (e.g. Jones and Edwards, 1998; Mikutta et al, 2007). Mineral surfaces of Fe oxides are often dominated by micropores (< 2nm in diameter) and mesopores (2-50 nm in diameter), which may also contribute to the accumulation and stabilization of OM. Micropore entrances are regarded as preferential sorption sites for OM (Kaiser and Guggenberger, 2003). Molecules sorbed at the opening of mineral micropores are subjected to stronger multiple attachment, inhibiting organic compound removal from such pores (Kaiser and Guggenberger, 2003 2007). Some workers have also suggested that mineral mesopores play a major role in the sequestration and preservation of OM

in sediments by physical occlusion within mineral pores (Mayer, 1994; Zimmerman et al, 2004). Furthermore, the sorptive stabilization of OM also likely depends on the intrinsic stability of the adsorbed organic compounds (Kalbitz et al, 2005). Prior work focusing on DOM adsorption to iron and aluminum oxides and hydroxides has shown that DOM fractions with higher molecular weight, acidity and aromaticity tend to be preferentially adsorbed (Gu et al, 1995; Chorover and Amistadi, 2001). This likely contributes to the large adsorption-desorption hysteresis that is observed (Gu et al, 1995).

Another process potentially involved in the stabilization of soil organic carbon against microbial decay is coprecipitation of DOM by polyvalent cations, such as Fe and Al (Baldock and Skjemstad, 2000). In soils and sediments, amorphous Fe oxides like ferrihydrite often precipitate from solutions containing varying amounts of dissolved organic matter. This leads to coprecipitation of OM with ferrihydrite. Therefore OM-ferrihydrite coprecipitates represent an important class of structures in nature and may also contribute to the stabilization of organic matter. However, in contrast to adsorption studies, the coprecipitation process has received relatively little attention. Little is known about the amount, nature and stability of the coprecipitated OM in natural environments. A recent study by Henneberry et al (2012) showed no release of DOM from the OM-Fe coprecipitates after exposure to reducing conditions. This indicated that coprecipitation of natural complex organic matter may lead to long-term C sequestration. Moreover, comparative studies on the extent of adsorption

and coprecipitation and the impacts of such reactions on soil C stabilization are limited (Eusterhues et al., 2011).

In this study, we investigated ferrihydrite-OM complexes formed via adsorption and coprecipitation with DOM extracts from a forest litter layer. The primary objectives were to (1) quantify the OC loadings of the adsorptive complexes and coprecipitates, (2) determine the changes in N_2 accessible SSA, and micro- and mesopore volumes of the adsorptive complexes and coprecipitates with different amounts of OC to assess the association of OM with mineral surfaces and small pores, (3) characterize chemical fractionation processes associated with these two processes, and (4) compare the stability of the adsorbed and coprecipitated OC against desorption.

5.3 Materials and Methods

5.3.1 Materials

Dissolved organic matter used in the adsorption and coprecipitation experiments was extracted from field-fresh samples of a forest floor layer by mixing organic materials with deionized water for 24 h. The dominant tree species were beech (*Fagus grandifolia*), red and black oak (*Quercus rubra and Q. velutina*), and tulip poplar (*Liriodendron tulipifera*). The suspension was stirred periodically, centrifuged at 20000 g for 20 min and subsequently isolated by pressure filtration through 0.2-µm polysulfone membrane filters. The extraction was carried out just before the

experiments. The DOC concentration of the stock solution was 750 mg C L^{-1} determined by a TOC analyzer (Apollo 9000HS). We prepared 15 initial solutions ranging from 7.5 to 750 mg C L^{-1} for the adsorption and coprecipitation experiments by diluting the extract with DI water.

Ferrihydrite was synthesized by neutralization of a $Fe(NO_3)_3$ solution by slow addition of NaOH until pH of 7 was reached (Schwertmann and Cornell, 2000). The amorphous structure of ferrihydrite was confirmed by X-ray diffraction (Rigaku, Japan). The product had a specific surface area (SSA) of 280 m^2 g^{-1}, and micro- and mesopore volumes of 0.038 and 0.047 cm^3 g^{-1}, respectively.

5.3.2 Adsorption and Coprecipitation Experiments

Batch adsorption experiments were conducted by adding 200ml of a DOM solution containing 7.5-750 mg C L^{-1} to 0.05 g of the synthetic ferrihydrite, producing C:Fe mass ratios ranging between 0.05-5.36 (0.03 -3 mg C/ 1 mg FeOOH). The suspensions were adjusted to pH values of 4 and 7 by adding NaOH or HCl. The initial pH of 4.0 is close to the pH at which maximum adsorption of OM is observed on ferrihydrite. For coprecipitation, 0.2 g $Fe(NO_3)_3 \cdot 9H_2O$ was mixed with 200ml of a DOM solution containing 7.5-750 mg C L^{-1}, generating the same C:Fe mass ratios of 0.05-5.35 (g/g) as in the adsorption experiment. The pH of the suspensions was then raised from ~2.2-2.4 to 7 using 0.1 M NaOH. A solid to solution ratio of 1:4000 (w/v) was necessary to achieve maximum adsorption and coprecipitation. All experiments were conducted in triplicate at room temperature.

After 24 h of shaking adsorption and coprecipitation suspensions on a shaker at 60 rpm, the suspensions were centrifuged at 2000 g for 30 minutes. The supernatant was removed and pressure filtered through 0.2-μm polysulfone membrane filters. The filtrates were analyzed for DOC with an Apollo 9000HS TOC Analyzer, Fe by ICP-AES and pH. The possibility of DOM-vessel interaction and/or microbial degradation of DOM was excluded by verifying the TOC of a DOM solution not reacted with ferrihydrite. The DOC concentration without added ferrihydrite did not change during a similar equilibration period. The mass of adsorbed or coprecipitated OC was calculated by the difference between DOC concentrations in the initial and the equilibrated solutions. The settled material was washed twice to remove the remainder of the equilibrium solution, then either stored moist or freeze dried.

5.3.3 Specific Surface Area and Porosity

The SSA and porosity of ferrihydrite, adsorptive complexes and coprecipitates were analyzed by adsorption and desorption isotherms (25 adsorption and 24 desorption points) of N_2 at 77 K at partial pressure regions of 0.01 to 0.995 P/P_0, with a Micromeritics 3000 surface area and porosity analyzer. Freeze-dried samples were weighed into sample cells and outgassed under vacuum (10^{-3} mbar) at 298 K for 24 h at the instrument degas station to avoid structural transformation of the poorly crystalline ferrihydrite. We are aware that this is a compromise between complete water removal and the necessity to avoid mineral transformations. Multipoint (12 points) specific surface area (SSA) was determined by the BET equation (Brunauer et

al., 1938) from the relative pressures of 0.05 to 0.3. The micropore (<2 nm) volumes were analyzed by the Dubinin–Astakhov method (Ravkovitch & Meimark, 2001). The mesopore volume was obtained by the BJH model (Barrett et al., 1951) from the desorption branch at partial pressure of 0.3 to 0.95, assuming slit-like geometry. All analyses were performed at least in duplicate.

5.3.4 Ultraviolet–visible Spectroscopy

To characterize the fractionation process of DOM in the course of adsorption and coprecipitation with ferrihydrite, the initial DOM solution and the filtrates, after adsorption and coprecipitation, were analyzed by UV-vis spectroscopy with a Shimadzu UV-Probe PC2501 UV–Vis spectrophotometer (Columbia, MD). Prior to measurement, the OC content of these solutions was diluted with DI water to 10 mg L^{-1} to ensure comparability of all OM samples. Absorbances were recorded at 254, 280 and 365 nm. The specific UV absorbance at 280 nm, calculated as the ratio between absorption intensity at 280 nm and the OC concentration of the sample, is an index of aromaticity (Traina et al., 1990; Kalbitz et al., 2003). Scheel et al. (2007) found a linear relationship between UV absorbance at 280 nm and the aromatic C content as revealed by ^{13}C nuclear magnetic resonance spectroscopy. The ratio of absorbance at 254 nm to that at 365 nm (E_2/E_3) serves as an index of the relative molecular size of a material and was calculated based on the respective absorption values at 254 and 365 nm (Polubesova et al., 2008). The E_2/E_3 ratio can provide a proxy of molar mass, with

low values generally associated with high molecular weights (Peuravuori and Pihlaja, 1997; Guo and Chorover, 2003).

5.3.5 Desorption Experiment

Desorption of organic matter from the adsorptive complexes and coprecipitates of varying organic matter loadings was conducted 24 hours after sorption using 0.1 M NaH_2PO_4, 0.1 M NaOH, and 0.1 M $Na_4P_2O_7$. 10 ml of the desorptive solutions were added to the moist solid-phase products. After 24 hours of shaking at 60 rpm at 298K, the suspension was centrifuged at 2000 g for 30 minutes, the supernatant was removed, pressure-filtered through 0.2-μm membrane filters, and the DOC concentration was analyzed using a TOC analyzer. This step was repeated once and the total amount of desorbed OC was calculated by the summation of OC released in each step. We calculated the apparent fraction of desorbable OC as the ratio of the cumulative amount of OC released to the amount of OC previously bound to the solid phases.

5.4 Results and Discussion

5.4.1 OC Adsorption versus Coprecipitation

For both adsorption and coprecipitation experiments, the amount of OC adsorbed or coprecipitated increased linearly with initial C:Fe ratio at smaller ratios, followed by a gradual approach to a maximum at larger C:Fe ratios. On a mass basis, the maximum adsorption observed in this study was 314 mg C/g ferrihydrite at pH 4

and 288 mg C/g ferrihydrite at pH 7, respectively (Fig.5.1a). This corresponds to surface area normalized OC loadings of 1.64 mg m^{-2} at pH 4 and 1.44 mg m^{-2} at pH 7, respectively (Fig.5.1b). The maximum adsorption observed here exceeds the value found for adsorption of DOM on ferrihydrite (maximum 170 mg C g^{-1}) by Eusterhus et al (2011), but agrees well with the data (maximum 318 mg C g^{-1}) reported by Kaiser et al (2007). The inconsistency in maximum adsorption could be attributed to the difference in reactivity of the dissolved organic matter and the synthesized ferrihydrite in each study. The achieved maximum surface loadings in this study fit into the range of values observed for surface loadings reported for sediments and soils (Mayer & Xing, 2001; Wagai et al., 2009). Greater adsorption of OC at low pH, which is commonly observed for OM adsorption on Fe oxides (e.g. Kang & Xing, 2008), can be explained by considering the electrostatic interactions between the acidic functional moieties of DOM and the ferrihydrite surface. When the pH decreases, the ferrihydrite surfaces become more positvely charged and thus more likely to react with acidic functional groups in solution.

At comparable initial C:Fe ratios, the difference between the amount of adsorbed and coprecipitated OC is obviously small at lower initial C:Fe ratios, while the amount of coprecipitated OC is much greater than the adsorbed OC above the initial C:Fe ratio of 1 (Fig.5.1). Coprecipitation results in maximum mass-based solid phase OC values of ca. 486 mg/g ferrihydrite or 3.38 mg C m^{-2} ferrihydrite, when related to the specific surface area of 280 m^2 g^{-1} of the pure ferrihydrite for the

coprecipitates (assuming complete Fe precipitation). Coprecipitation of the DOM with ferrihydrite yielded a much higher maximum OC loading than for adsorption.

5.4.2 Micropore (<2 nm) and Mesopore (2-50 nm) Volumes and Mineral Specific Surface Area (SSA)

The adsorbed and coprecipitated OM associated with ferrihydrite resulted in a strong decrease in the N_2-accessible micro- and mesopore volume of (Fig.5.2a & 5.2b). The decrease in pore volume was linear at smaller OC loadings and leveled off at larger ones. Filling of micropores is unlikely because of the size constraints of OM (Buffle et al., 1998; Kaiser and Guggenberger, 2007), while sorption at the openings of micropores and thus clogging and rendering them inaccessible to N_2 is more reasonable. In contrast, most of the mesopore space of minerals could be filled with OM. In the case of coprecipitation, coprecipitaed OM resulted in complete loss of micro-and mesopores with loadings of 0.61 mg C m^{-2} and 0.78 mg C m^{-2}, respectively. Adsorption of OM to ferrihydrite also led to complete loss of micropores with ~0.6 mg C m^{-2} (Fig.5.2b), while the decrease in mesopore volume reached a maximum for adsorption at loadings of ~ 0.87-0.95 mg C m^{-2} (Fig.5.2b). However at the greatest decline, ferrihydrite lost 79% and 72% of its mesopore volume for adsorption at pH 4 and pH 7, respectively. In addition, greater reduction of mesopore volume was found for coprecipitation than adsoprtion at comparable OC loadings. These results suggest that micropores are equally important for OM retention by adsorption and coprecipitation, whereas more C could be associated with mesopores in the process of

coprecipitation than adsorption. In addition, these mineral micro- and mesopores are subjected to saturation of organic matter. Excess adsorbed and coprecipitated OM at higher loadings is not associated with these small pores and therefore might not be efficiently stabilized by these small mineral pores.

For both adsorption and coprecipitation, with increasing amounts of OC associated with ferrihydrite, the SSA of the ferrihydrite-OM complexes decreased strongly (Fig.5.2c). The decline was linear (r^2 = 0.94-0.98). Reduced accessibility of minerals surfaces for N_2 by OM has been frequently observed for sediments, soils and minerals (Mayer & Xing, 2001; Wagai et al., 2009; Kaiser & Guggenberger, 2003 2007; Kaiser et al, 2007). This has been attributed to the small SSA of the mineral-associated OM and the clogging of micropores and small mesopores by sorbed OM. A linear correlation was found between SSA and micro- and mesopore volumes in this study (Fig.C.1). The SSA accessible for N_2 dropped from 280 to 1.5 $m^2 g^{-1}$, which is similar to the SSA of organic matter (~ 1-2 $m^2 g^{-1}$), for coprecipitates with 0.97 mg C m^{-2} (Fig.5.2a). This indicates coprecipitation leads to complete C coverage on ferrihydrite at loadings of 0.97 mg C m^{-2}. The SSA finally decline to 6.8 and 9.3 $m^2 g^{-1}$ for adsorption with 0.95 and 0.88 mg C m^{-2} at pH 4 and pH 7, respectively, indicating adsorption was able to coat ~97-98% of the ferrihydrite surface. We can conclude that, in spite of adsorption and coprecipitation, OM achieved almost full coverage on ferrihydrite at loadings of 0.88-0.97 mg C m^{-2}, which is in the range of monolayer equivalent (ME) levels of OC (0.6 - 1.5 mg OC m^{-2}) (Mayer, 1994; Keil et al., 1994). Above the full coverage on ferrihydrite with C loadings of 0.88-0.97 mg C m^{-2},

additional adsorbed and coprecipitated C did not affect the SSA. These results imply that with increasing surface loading, an increasing amount of the organic matter associated with OM-ferrihydrite complexes, does not attach to mineral surfaces directly but forms organic multilayers as a result of hydrophobic interaction, bridging by polyvalent cations between organic ligands of adsorbed/coprecipitated and the organics in solution, or organic metal complex formation. In the case of adsorption, because potassium was the dominant cation in the initial DOM solution, the formation of organic multilayers by a cation bridging or organic metal complex formation is unlikely, while hydrophobic interactions between adsorbed and dissolved OM may control this process. However, in the case of coprecipitation, it is possible that a portion of added Fe^{3+} does not completely precipitate to ferrihydrite but forms a bridge between the copreciptated OM and dissolved OM. Therefore, the formation of organic multilayers by coprecipitation is not only controlled by hydrophobic interactions but is also due to the formation of Fe^{3+}-OM complexes via bridging between OM coprecipitated and dissolved OM. Besides bridging organic molecules, OM-Fe(III) cation complexes could be also possibly formed in case of coprecipitation. Above the full coverage of OC on ferrihydrite, the increasing amount of the organic matter which does not attach to mineral surfaces directly, might not be well stabilized by mineral surfaces.

5.4.3 DOM Fractionation: E_2/E_3 and Specific UV Adsorption at 280 nm

The OM remaining in solution after adsorption and coprecipitation was characterized by E_2/E_3 ratios and specific UV adsorption at 280 nm. The extent of molecular weight fractionation appears to be greatly influenced by the percentage of OC removed from the DOM solution (Fig.5.3a). At higher C/Fe ratios, where there was $< 65\%$ OC removal from solution, the E_2/E_3 ratios of the remaining DOM solution were nearly equivalent with the initial E_2/E_3 of the original DOM solution (Fig.5.3a). This suggests no preferential removal of organic matter compounds by adsorption and coprecipitation. However, at lower C/Fe ratios, where a larger portion of OM was removed from solution, the ratio increased strongly from 3.15 to 15.12 after coprecipitation, and finally to 14 and 7 for adsorption at pH 4 and pH 7, respectively (Fig.5.3a). This indicates preferential uptake of higher-molecular-weight compounds, consistent with previous observations (Chorover and Amistadi, 2001; Oren and Chefetz, 2012). The extent of molecular weight fractionation appears to be increasing with increasing OC removal from solution and therefore with decreasing C/Fe ratios. High-molecular-weight compounds were most enriched in OM-ferrihydrite complexes formed at small C/Fe ratios. At the comparable OC removal rate, the extent of increase in the E_2/E_3 ratio after adsorption and coprecipitation followed the trend: coprecipitation at pH 7> adsorption at pH 4> adsorption at pH 7. This indicates that high-molecular-weight organic compounds are more selectively uptake by coprecipitation than adsorption and are more preferentially adsorbed at lower pH.

Similar to the E_2/E_3 ratio, at higher C/Fe ratios, where OC removal from solution was <53% for coprecipitation and adsorption, the specific UV absorbance value ($SUVA_{280}$) in the remaining DOM showed no changes compared to the initial DOM solution (Fig.5.3b), indicating no preferential removal of the organic compounds. However, at lower C/Fe ratios, where larger portions of OC were removed from solution, the $SUVA_{280}$ decreased in the DOM solutions from 2.2 to 0.32 after coprecipitation with 80% OC removal from solution, and finally to 0.22 and 0.3 for adsorption with 84 and 82 % of OC removed from solution respectively (Fig.5.3b), indicating preferential adsorption and coprecipitaton of more complex and aromatic moieties, which matches well with previous studies (e.g., Chorover and Amistadi, 2001). The decrease in specific UV absorbance after coprecipitation and adsorption became more pronounced with increasing C removal from solution and therefore with decreasing C/Fe ratios, suggesting that aromatic C was most enriched in OM-ferrihydrite complexes formed at small C/Fe ratios. At a comparable OC removal rate, coprecipitation at pH 7 resulted in a similar extent of reduction of $SUVA_{280}$ to adsorption at pH 4, while adsorption at pH 4 reduced $SUVA_{280}$ to a larger extent (on average, 24-54%) than at pH 7 (on average, 9-30%). This reflects a more selective adsorption of aromatic compounds at lower pH.

5.4.4 Stability of the Adsorbed and Coprecipitated OC against Desorption

To give an estimation of the importance of adsorption and coprepitation processes in the preservation of OM by ferrihydrite, we carried out desorption

experiments on the respective complexes following adsorption and coprecipitation. Desorption with a high concentration (0.1 M) of inorganic oxyanion $H_2PO_4^-$, which is known to compete with OM for binding sites, resulted in a considerable release of OM (9-47%) (Fig.5.4a). Greater desorption was achieved with NaOH and $Na_4P_2O_7$, which removed 18-64% and 20-76% respectively, of the OC complexed with ferrhydrite (Fig 5.4b & 5.4c). The strong desorption by NaOH and $Na_4P_2O_7$ might be caused by the high pH (10-13) of these reagents. However, even under these harsh alkaline conditions, a large fraction of the adsorbed and coprecipitated OC did not desorb, suggesting strong association between OM and ferryhydrite. Largely irreversible sorption of OM on ferrihydirte and other Al and Fe oxides has been reported in previous observations (Kaiser and Guggenberger, 2007; Mikutta et al., 2007). This could be attributed to the strong bonding between OM and the mineral surface and the roles of small pores in the C sequestering process.

For both adsorption and coprecipitation, fractional OC desorption, irrespective of the desorptive reagent, increased significantly with increasing OC surface loadings on ferrihydrite and reached its maximum value at OC loadings of 0.88-0.97 mg C m^{-2}, where there was almost complete coverage of OC on ferrihydrite. Above the full OC coverage on ferrihydrite, additional adsorbed and coprecipitated C did not affect the extent of desorption. The higher chemical stability of OM on ferrihydrite at lower C loadings might be related to the strong chemical bonds formed between C and Fe by a ligand exchange mechanism, which is investigated in a companion paper part II. Another possible explanation is association of OM with mineral meso- and

micropores. Preferential retention of more recalcitrant compounds at lower C loadings is also a likely contributing factor. Collectively, these results suggest that potential stabilization at mineral surfaces is limited to those organic molecules that sorb to surfaces at small surface loadings. The OM sorbed in excess may not be efficiently protected. This result may also at least partly explain the frequently reported slow turnover of mineral-associated organic matter in subsoils that contain small quantities of organic matter. The small amounts of organic matter sorbed in subsoils might thus be more effectively preserved than the large amounts of organic matter bound in the topsoil.

The extent of C desorption from the adsorptive complexes was slightly less at pH 4 than at pH 7 at all C loadings. This appears consistent with the fact that a pH increase may cause the weakening of mineral-organic bonds, thus promoting OM desorption. At comparable OC loadings, coprecipitates released significantly less OC than did the adsorption complexes for all the desorptive reagents, indicating that the chemical stability of coprecipitated OC is much greater than adsorbed OC. Coprecipitation may result in stronger bonding between OM and ferrihydrite than adsorption, as examined in part II. More C occluded in the mesopores during coprecipitation may also contribute to greater stability. More preferential precipitation of high molecular weight compounds might be another reason for the larger stabilization of the coprecipitates when compared with the adsorptive complexes. Our study demonstrated for the first time that coprecipitation of OM with iron can lead to stronger C stabilization than adsorption, which might contribute to long-term C

sequestration in soils. Collectively, the stability of C bound with minerals is dependent not only on the surface loadings but also on how the OM-mineral complexes are formed. The effect of DOM -mineral interaction on C stabilization could not be reliably assessed when the formation process is unknown.

5.5 Implications

Association of carbon with minerals results in stabilization. The stability of solid-bound C depends on the extent of C coverage on ferrihydrite (referred as C loadings) for both adsorption and coprecipitation processes. This study shows the stability of C is greater at low C loadings. At higher C loadings, a portion of C is not directly associated with mineral surfaces and small pores and therefore the stability decreases. A greater importance of stabilized C can be expected in subsoil horizons where there may be less C coverage on minerals due to lower OC contents. Excessive accumulation of OC on minerals in surface soils may not be efficiently stabilized.

Although the importance of iron oxides for C retention has been long been known, only recently has the role of coprecipitation of OM with iron for C storage been shown to be quantitatively important on a global scale (Lalonde et al., 2012). Our study demonstrated that coprecipitation resulted in a significantly greater amount of C retained with the solid phase and greater C stability than adsorption, supporting the conclusion that coprecipitation might be an important process contributing to the accumulation and stabilization of OM in natural environments Future research should

also address the dynamics of precipitated OM in situ in the natural field that experiences significant changes in either redox or pH conditions.

REFERENCES

Andrew, R. Z.; Keith W. G.; Chorover, J.; Komarnenic, S.; Brantley, S. L., Mineral mesopore effects on nitrogenous organic matter adsorption. *Org. Geochem*. **2004**, 35, 355-375.

Baldock, J. A.; Skjemstad, J. O., Role of the soil matrix and minerals in protecting natural organic materials against biological attack. *Org. Geochem.* **2000**, 31, 697-710.

Barrett, E. P.; Joyner, L. G.; Halenda, P. P., The determination of pore volume and area distributions in porous substances. I. Computations from nitrogen isotherms. *J. Am. Chem. Soc.* **1951**, 73, 373-380.

Brunauer, S.; Emmett, P. H.; Teller, E., Adsorption of gases in multimolecular layers. *J. Am. Chem. Soc*. **1938**, 60, 309-319.

Buffle, J.; Wilkinson, K. J.; Stoll, S.; Filella, M.; Zhang, J., A generalized description of aquatic colloidal interactions: The three colloidal component approach. *Environ. Sci. Technol.* **1998**, 32, 2887-2899.

Chorover, J.; Amistad, M. K., Reaction of forest floor organic matter at goethite, birnessite and smectite surfaces. *Geochim. Cosmochim. Acta* **2001**, 65(1), 95-109.

Eusterhues, K.; Rennert, T.; Knicker, H.; Kögel-Knabner, I.; Totsche, K. U.; Schwertmann, U., Fractionation of Organic Matter Due to Reaction with Ferrihydrite: Coprecipitation versus Adsorption. *Environ. Sci. Technol.* **2011**, *45,* 527-533.

Eusterhues, K.; Rumpel, C.; Kögel-Knabner, I., Organomineral associations in sandy acid forest soils: importance of specific surface area, iron oxides and micropores. *Eur. J. Soil Sci.* **2005**, 56, 753-763.

Gu, B.; Schmitt, J.; Chen, Z.; Liang, L.; McCarthy J. F., Adsorption and desorption of different organic matter fractions on iron oxide. *Geochim. Cosmochim. Acta,* **1995**, 59, 219-229.

Guo, M.; Chorover, J., Transport and fractionation of dissolved organic matter in soil columns. *Soil Sci.* **2003**, 168, 108-118.

Hennberry, Y. K.; Kraus, T. E. C.; Nico, P. S.; Horwath, W. R., Structural stability of coprecipitated natural organic matter and ferric iron under reducing conditions. *Org. Geochem*. **2012**, 48, 81-89.

Jones, D.L.; Edwards, A.C., Influence of sorption on the biological utilization of two simple carbon substrates. *Soil Biol. Biochem.* **1998**, 30, 1895-1902.

Kaiser, K.; Guggenberger, G., The role of DOM sorption to mineral surfaces in the preservation of organic matter in soils. *Org. Geochem*. **2000**, 31, 711-725.

Kaiser, K.; Guggenberger, G., Mineral surfaces and soil organic matter. *Eur. J. Soil Sci.* **2003**, 54 (2), 219-236.

Kaiser, K.; Guggenberger, G., Sorptive stabilization oforganicmatter bymicroporous goethite: sorption into small pores vs. surface complexation. *Eur. J. Soil Sci.* **2007**, 58, 45-59.

Kaiser, K.; Mikutta, R.; Guggenberger, G., Increased Stability of Organic Matter Sorbed to Ferrihydrite and Goethite on Aging. *Soil Sci. Soc. Am. J.* **2007**, 71, 711-719.

Kaiser, K.; Zech, W., Release of natural organic matter sorbed to oxides and a subsoil. *Soil Sci. Soc. Am. J.* **1999**, 63(5), 1157-1166.

Kalbitz, K.; Kaiser, K., Contribution of dissolved organic matter to carbon storage in forest mineral soils. *J. Plant Nutr. Soil Sci.* **2008**, 171, 52-60.

Kalbitz, K.; Schwesig, D., Stabilization of dissolved organic matter by sorption to the mineral soil. *Soil Biol. Biochem.* **2005**, 37 (7), 1319-1331.

Kang, S.; Xing, B.S., Humic Acid Fractionation upon Sequential Adsorption onto Goethite. *Langmuir* **2008**, 24*,* 2525-2531

Keil, R. G.; Montlucon, D. B.; Prahl, F. R.; Hedges, J. I., Sorptive preservation of labile organic matter in marine sediments. *Nature* **1994**, 370, 549-552.

Kleber, M.; Mikutta, R.; Torn, M. S.; Jahn, R., Poorly crystalline mineral phases protect organic matter in acid subsoil horizons. *Eur. J. Soil Sci.* **2005**, 56:717-

725.

Kögel-Knabner, I.; Guggenberger, G.; Kleber, M.; Kandeler, E.; Kalbitz, K.; Scheu, S.; Eusterhues, K.; Leinweber, P., Organo-mineral associations in temperate soils: integrating biology, mineralogy, and organic matter chemistry. *J. Plant Nutr. Soil Sci.* **2008**, 171, 61-82.

Lalonde K.; Mucci, A.; Quellet, A.; Gélinas, Y., Preservation of organic matter in sediments promoted by iron. *Nature* **2012**, 483, 198-200.

Mayer, L.M., Relationships between mineral surfaces and organic carbon concentrations in soils and sediments. *Chem. Geol.* **1994**, 114, 347-363.

Mikutta, C.; Lang, F.; Kaupenjohann, M., Soil organic matter clogs mineral pores: Evidence from H-1-NMR and N-2 adsorption. *Soil Sci. Soc. Am. J.* **2004**, 68, 1853-1862.

Mikutta, R.; Mikutta, C.; Kalbitz, K.; Scheel, T.; Kaiser, K.; Jahn, R., Biodegradation of forest floor organic matter bound to minerals via different binding mechanisms. *Geochim. Cosmochim. Acta* **2007**, 71(10), 2569-2590.

Neff, J. C.; Asner, G. P., Dissolved organic carbon in terrestrial ecosystems: synthesis and a model. *Ecosystems* **2001**, 4, 29-48.

Nierop, K.G.J.; Jansen, B.; Verstraten, J. A., Dissolved organic matter, aluminium and iron interactions: precipitation induced by metal/carbon ratio, pH and competition. *Sci. Total Environ.* **2002**, 300, 201-211.

Oren, A.; Chefetz, B., Sorptive and desorptive Fractionation of dissolved organic matter by mineral soil matrices. *J. Environ. Qual.* **2012**, 41, 526-533.

Peuravuori, J.; Pihlaja, K., Molecular size distribution and spectroscopic properties of aquatic humic substances. *Anal. Chim. Acta* **1997**, 337, 133-149.

Polubesova, T.; Chen, Y.; Navon, R.; Chefetz, B., Interactions of hydrophobic fractions of dissolved organic matter with Fe^{3+}- and Cu^{2+}-montmorillonite. *Environ. Sci. Technol.* **2008**, 42, 4797-4803.

Ravkovitch, P. I.; Meimark, A. V., Characterization of nanoporous materials from adsorption and desorption isotherms. *Colloid Surface A* **2001**, 187/188, 11-21.

Scheel, T.; Dörfler, C.; Kalbitz, K., Precipitation of dissolved organic matter by aluminum stabilizes carbon in acidic forest soils. *Soil Sci. Soc. Am. J.* **2007**, 71, 64-74.

Schneider, M. P. W.;, Scheel, T.; Mikutta, R.; van Hees, P.; Kaiser, K.; Kalbitz, K., Sorptive stabilization of organic matter by amorphous Al hydroxide. *Geochim. Cosmochim. Acta* **2010**, 74, 1606-1619.

Schwertmann, U.; Cornell, R. M., *Iron Oxides in the Laboratory: Preparation and Characterization*, 2nd ed.; Wiley-VCH VerlagGmbH: Weinheim, **2000**.

Shang, C.; Tiessen, H., Organic matter stabilization in two semiarid tropical soils: size, density, and magnetic separations. *Soil Sci. Soc. Am. J.* **1998**, 62, 1247-1257.

Torn, M. S.; Trumbore, S. E.; Chadwick, O. A.; Vitousek, P. M.; Hendricks, D. M., Mineral control of soil organic carbon storage and turnover. *Nature* **1997**, 389, 170-173.

von Lützow, M.; Kögel-Knabner, I.; Ekschmitt, K.; Matzner, E.; Guggenberger, G.; Marschner, B.; Flessa, H., Stabilization of organic matter in temperate soils: mechanisms and their relevance under different soil conditions-a review. *Eur. J. Soil Sci.* **2006,** 57, 426-445**.**

Wagai, R.; Mayer, L. M.; Kitayama, K., Extent and nature of organic coverage of soil mineral surfaces assessed by a gas sorption approach. *Geoderma* **2009,** 149, 152-160.

Zimmerman, A.; Goyne, K. W.; Chorover, J.; Komarneni, S.; Brantley, S. L., Mineral mesopore effects on nitrogenous organic matter adsorption. Org. Geochem. **2004,** 35, 355-375.

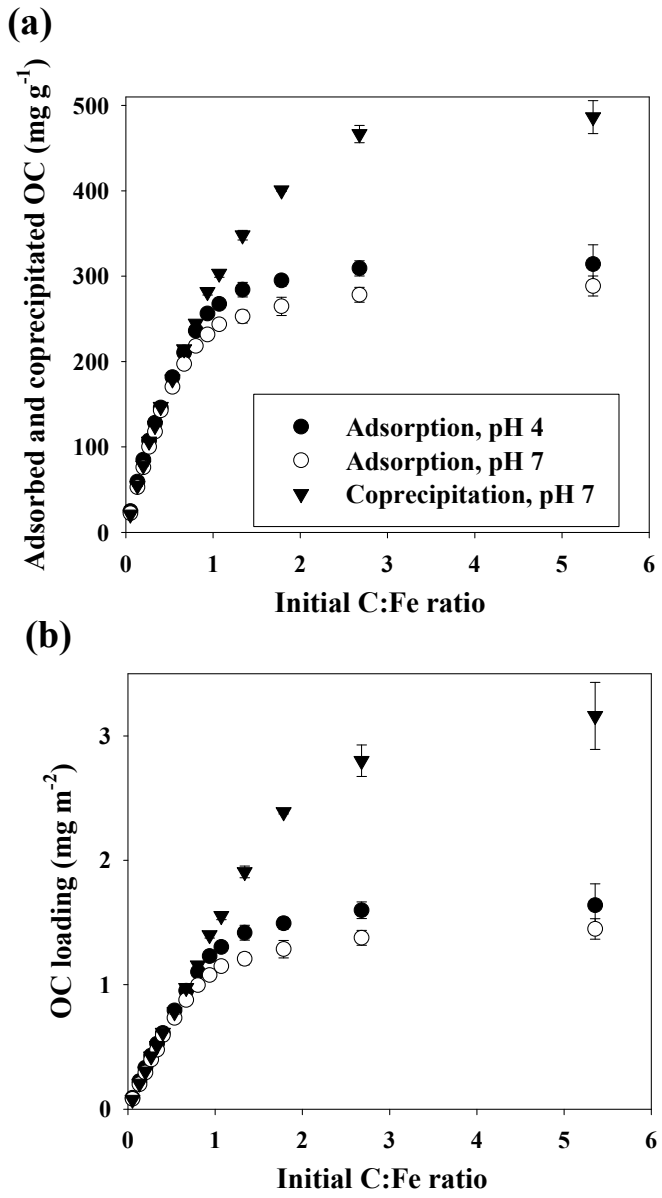

Figure 5.1 Adsorption and coprecipitation of dissolved organic carbon as a function of the initial C:Fe ratio. Adsorption and coprecipitation are given as the relation between the mass of the adsorbed and coprecipitated OC, normalized to the mass of the ferrihydrite (Figure 5.1a) or to the initial surface area of the ferrihydrite (Figure 5.1b), and the added mass of C normalized to initial mass of Fe. Complete Fe precipitation is assumed in the case of coprecipitation. Bars are standard errors; n = 3.

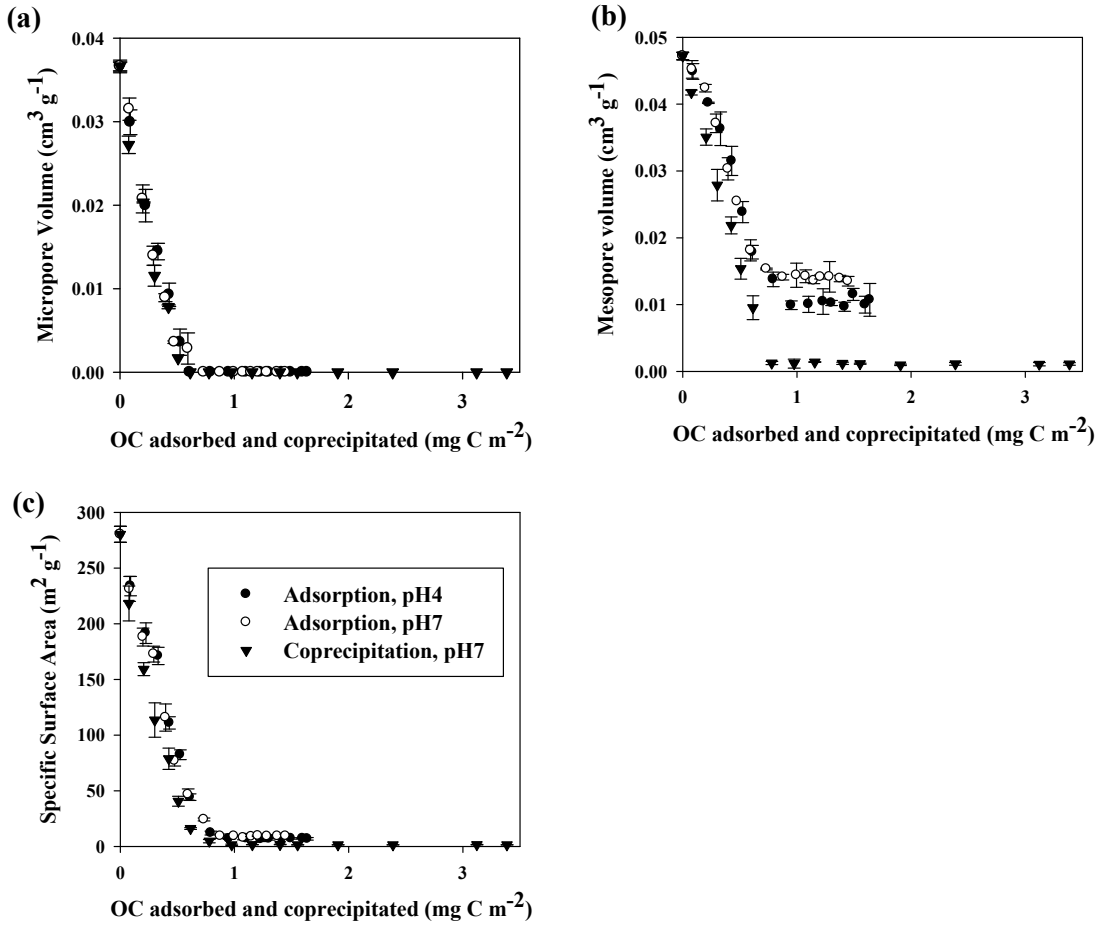

Figure 5.2 Changes in micropore (< 2 nm) and mesopore (2-50 nm) volumes and specific surface area accessible to N_2 with increasing amounts of organic matter adsorbed to and coprecipitated with ferrihydrite for the ferrhydrite-OM complexes. Bars are standard errors; n = 3.

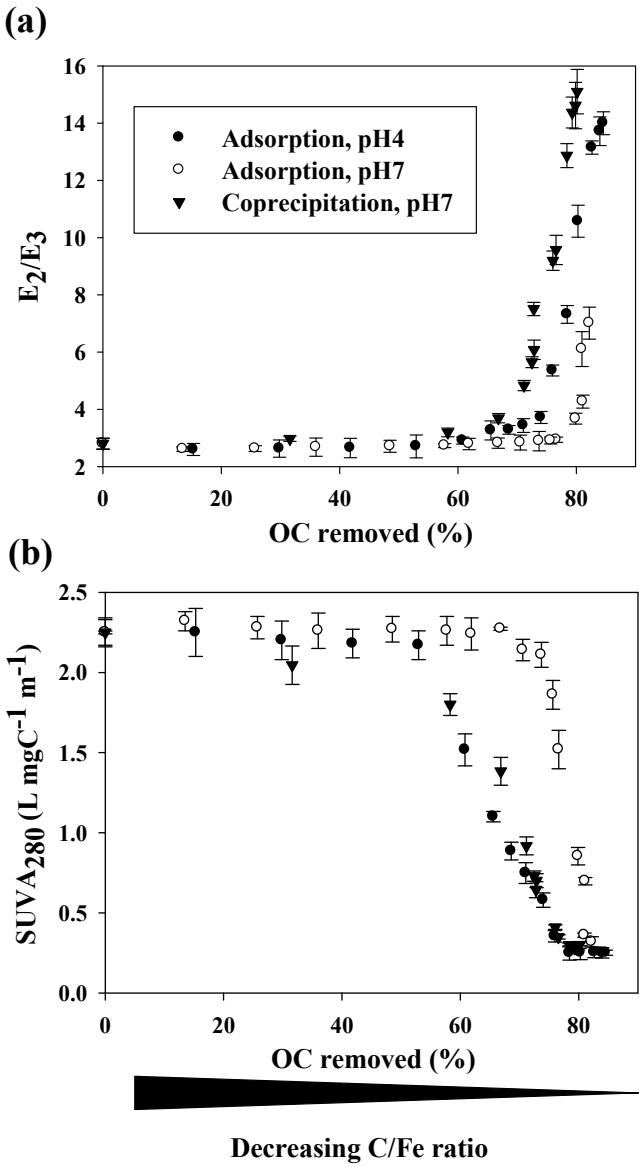

Figure 5.3 Changes in E_2/E_3 ratio and specific UV adsorption at 280 nm of the organic matter remaining in solution followed by adsorption at pH 4 and pH 7 and coprecipitation at pH 7, as related to the portion of organic carbon uptake from solution. Error bars indicate the standard error of the mean of three replicates.

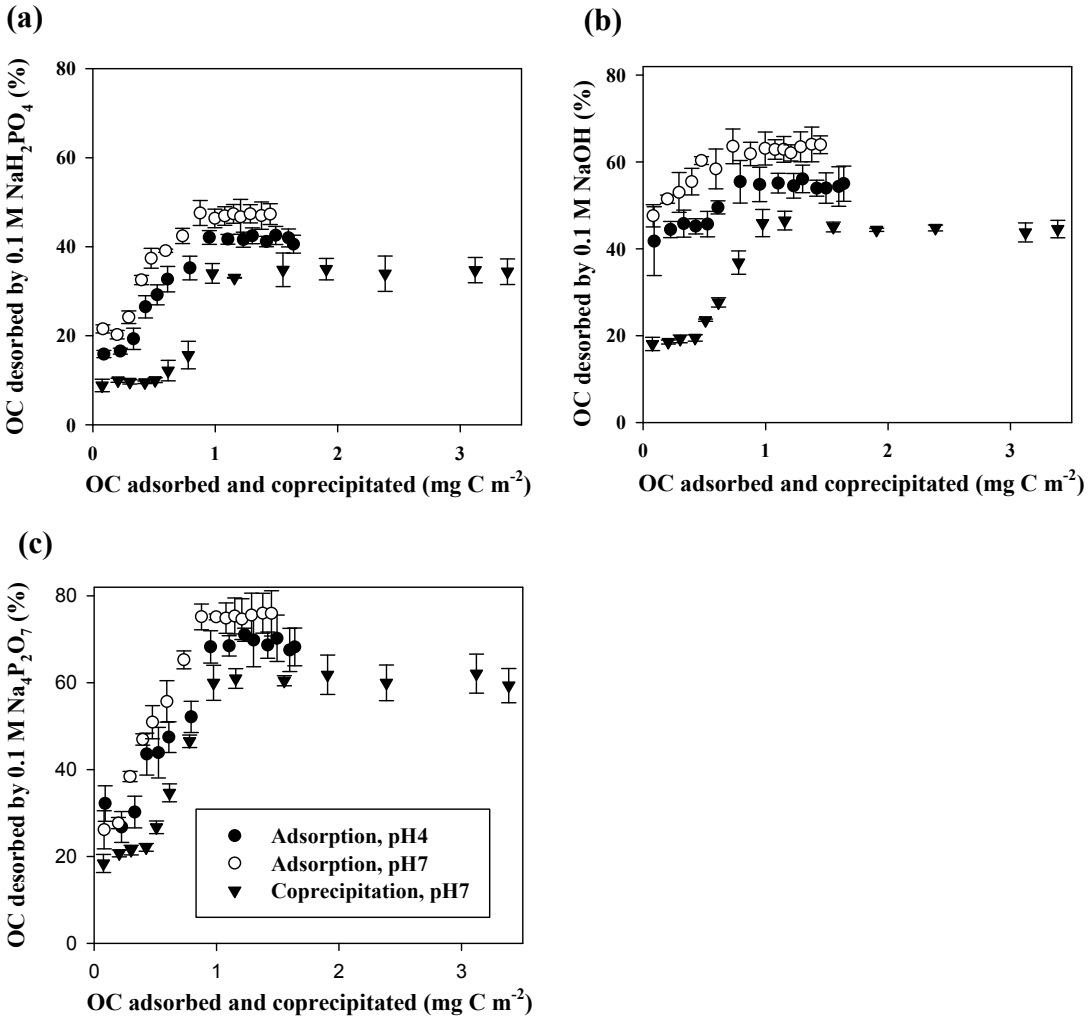

Figure 5.4 OC desorption (in % of the initial amount of OC bound with the solid phase) from the adsorbed and coprecipitated OC on ferrihydrite by using 0.1 M NaH_2PO_4, 0.1 M NaOH and 0.1 M $Na_4P_2O_7$, at different OC loadings. Error bars indicate the standard error of the mean of three replicates.

Chapter 6

RETENTION OF DISSOLVED ORGANIC MATTER BY ADSORPTION AND COPRECIPITATION WITH FERRIHYDRITE II: SPECTROSCOPIC AND MICROSCOPIC ANALYSIS

6.1 Abstract

This study investigated the interactive mechanisms of organic matter and ferrhydrite via adsorption and coprecipitation using Fe K-edge extended X-ray adsorption fine structure (EXAFS) spectroscopy, Fourier-transform infrared (FTIR) and Scanning Transmission X-ray microscopy (STXM) coupled with near edge X-ray absorption fine structure (NEXAFS) spectroscopy. Fe EXAFS measurements revealed that coprecipitation of OM with Fe led to the formation of OM-Fe(III) cation complexes in the solid phase by suppressing ferrihydrite formation, which might be related to a significantly greater maximum organic carbon (OC) retention for coprecipitation than adsorption, which was observed in part I. Formation of strong complexes between carboxyl C functional groups and ferrihydrite via a ligand exhange mechanism was evidenced by FTIR and C (1s) NEXAFS analysis for both adsorption and coprecipitation. Both FTIR and C (1s) NEXAFS analysis showed that aromatic C is preferentially removed with adsorption and coprecipitation at lower C loadings but no fractionation of aromatic C occurred at higher C loadings. The STXM analysis

demonstrated that at lower C loadings, C showed continuous homogenous distribution on ferrihydrite and C spatially correlated well with Fe, whereas there were localized concentrated C "hotspots" on ferrihydrite and the correlation between C and Fe was lower at higher C loadings.

6.2 Introduction

Organic Matter (OM)-ferrihydrite complexes could be formed by adsorption and coprecipitation (Kaiser et al., 2007; Eusterhues et al., 2011; Henneberry et al., 2012). These complexes can play an important role in immobilizing dissolved organic matter (DOM) and stabilizing it against microbial degradation (Torn et al., 1997; Baldock & Skjemstad, 2000; von Lützow et al., 2006). The DOM retention capacities via adsorption and coprecipitation were investigated in a companion paper (part I). The results reported in part I indicated that coprecipitation could result in greater C retention capacity than adsorption. However, the microscopic and molecular mechanisms involved during adsorption and coprecipitation are still poorly understood. Surface complexation by ligand exchange between carboxyl and phenolic fuctional organic groups and surface hydroxyls may control the binding of OM to Fe oxides (Gu et al., 1994; Kaiser et al., 1997; Chorover and Amistadi, 2001; Kaiser and Guggenberger, 2007). Despite the progress in the characterization of the adsorptive interactions between OM and Fe oxides, there is limited knowledge about the coprecipitation of organic matter with iron. In addition, it is still unclear why the coprecipitation process is responsible for greater C retention and stability

demonstrated in part I of this investigation. Furthermore, investigation on spatial carbon distribution on ferrihydrite via adsorption and coprecipitation is lacking.

The two primary objectives of this study were to: (1) study the interactive mechanisms of OM and ferrihydrite via adsorption and coprecipitation using Fourier-transform infrared (FTIR), C (1s) near edge X-ray absorption fine structure (NEXAFS), and Fe K-edge extended X-ray adsorption fine structure (EXAFS) spectroscopic techniques and (2) investigate the spatial distribution of organic matter at the iron-water interface at the nanometer-scale by scanning transmission X-ray microscopy (STXM) coupled with NEXAFS.

6.3 Materials and Methods

6.3.1 Iron K-edge Extended X-ray Adsorption Fine Structure Spectroscopy (EXAFS)

Samples for Fe EXAFS measurements included pure ferrihydrite, adsorptive complexes, coprecipitate samples with different amounts of organic matter, and organic matter-Fe(III) cation complexes. The Section of Materials and Methods in part I provides a detailed description of the adsorption and coprecipitation experiments. For preparing the organic matter-Fe(III) cation complex sample, 0.2 g $Fe(NO_3)_3 \cdot 9H_2O$ was mixed with 200ml of a DOM solution 750 mg C L^{-1}, generating C:Fe ratio (g/g) of 5.35. After 1 h of shaking the suspensions on a shaker at 60 rpm, the suspensions

were centrifuged at 2000 g for 30 minutes. The settled material was washed twice to remove the remainder of the equilibrium solution, and then freeze dried.

Iron K-edge extended X-ray absorption fine structure (EXAFS) spectra were collected on beamline 4-1 at the Stanford Synchrotron Radiation Facility (SSRL) and on beamline X11A at the National Synchrotron Light Source (NSLS). Samples were mounted as thin powders between Kapton tape. Mounted samples were placed in a He-purged sample chamber at room temperature and two to six replicate spectra were collected using a Lytle detector with energy calibrated against an Fe(0) foil (7112 eV). X-ray energy resolution was maintained by a crystal Si(220) and Si(111) monochromator at SSRL and NSLS, respectively. The monochromator was detuned by 50% of the maximum intensity in order to reduce the higher harmonic content in the beam.

The Sixpack program was used for standard background subtraction and edge-height normalization (Webb, 2005). Linear combination fitting (LCF) analysis was applied to quantify the contributions of ferrihydrite and organic matter- Fe(III) complexes in the coprecipitates. The fitting was performed using the Sixpack program on the k^3-weighted spectra. No energy shift was included in the LCF and the sum of the fitted fractions was not constrained (LCF data are presented normalized to 100%).

6.3.2 FTIR Analysis

The FTIR spectra for the original DOM solution before reaction, freshly prepared adsorption complexes and coprecipitates after freeze-drying were recorded

with a Thermo Nico Fourier transform infrared spectrometer equipped with an MCT detector. Samples were scanned over the 4000-400 cm^{-1} range. Spectra resolution was 2 cm^{-1}. An automatic baseline correction and normalization was applied to each spectrum. To obtain spectra of OM associated with mineral phases, the baseline-corrected and normalized spectrum of pure ferrhydrite was subtracted from the spectra of the adsorbed and coprecipitated OM-ferrihydrite complexes. Spectral analysis was performed using the OMNIC spectroscopy software suite (Thermo Scientific).

6.3.3 Scanning Transmission X-ray Microscopy Coupled with Near Edge X-ray Absorption Fine Structure Spectroscopy (STXM-NEXAFS)

Samples for STXM-NEXAFS analysis were prepared by depositing 1-2 µl of an aqueous suspension of freshly prepared adsorption complexes and coprecipitates onto a Si_3N_4 window (75 nm thick), which was then air-dried. The samples were analyzed at the STXM spectromicroscopy beamline 10ID-1 at the Canadian Light Source (CLS), a 2.9 GeV third-generation synchrotron source (Kaznatcheev et al., 2007). All measurements were performed using a 25 nm Fresnel zone plate, which provided a maximum spatial resolution of ~30 nm and the samples were kept under 1/6 atm of He during data collection. The samples were raster scanned with synchronized detection of transmitted X-rays to generate images. The C NEXAFS measurements were obtained from 280 to 310 eV with dwell times of 1-1.2 ms to avoid potential beam damage and with pixel sizes of 40nm. Two Fe images were recorded with the same dwell time and pixel size to determine Fe distribution: one

measured at the energy of a strong characteristic absorption feature and the other measured at the energy below the onset of absorption for Fe.

The aXis2000 software package was used for image and spectra processing (Hitchcock, 2000). The energy scale of C-1s spectra was calibrated by using the CO_2 absorption peak (C 3p) at 294.96 eV by measuring CO_2 gas spectra before or after the measurements (Ma et al., 1991). The total concentration of a given species was mapped by the difference between two images, one measured at the energy of a strong characteristic absorption feature and the other measured at the energy below the onset of absorption for the specific element. The image difference map was made quantitative by converting the change in the optical density (ΔOD) scale to effective thickness (in nm) using a scale factor determined from the linear absorbance (optical density per nm) for a specific compound at the top photon energies. The energies and scaling factor used for the quantification of the image difference maps (on-resonance minus off-resonance) for C and Fe are listed in Table D.1.

6.4 Results and Discussion

6.4.1 Iron EXAFS

Linear combination fitting (LCF) of Fe K-edge EXAFS spectra was applied to determine the formation of ferrihydrite and organic matter complexed Fe(III) cation in the coprecipitates. Pure ferrihydrite and organic matter-Fe(III) cation complex was employed as fit component. Fig.6.1 shows the LCFs of the Fe K-edge EXAFS spectra

and the relative proportions of Fe contained in the ferrihydrite and organic matter-Fe(III) cation complex is shown on the right side of this figure. For coprecipitate samples with C loadings of 0.5 - 1 mg C m^{-2} SA, all iron was precipitated as ferrihydrite, and no organic matter-Fe(III) cation complex was formed in the coprecipitates. However, at higher C loadings, a portion of Fe(III) cation did not precipitate as ferrihydrite but forms complexes with organic matter in the coprecipitates. In addition, the proportion of Fe in organic matter-Fe(III) cation complexes increased with increasing amounts of organic matter associated with the coprecipitates. For the coprecipitate sample with C loading of around 3.1 mg C m^{-2} SA, OM-Fe(III) cation complexes accounted for 36% of total Fe. These results indicate that coprecipitation of organic matter with iron produces OM-Fe(III) cation complexes by inhibiting ferrihydrite formation. This is in accordance with the results presented by Karlsson and Persson (2012), showing that strong complexation between Fe(III) cation and Suwannee river natural organic matter suppresses ferrihydrite precipitation. A study by Mikutta (2011) also suggested that natural organic matter can effectively suppress ferrihydrite precipitation as they kinetically control the availability of inorganic Fe(III) species for nucleation and/or polymerization reactions. For the adsorptive complexes, there is no OM-Fe(III) cation complexes formed even at the high C loading (Fig.D.1), due to the fact that solubility of ferrihydrite at pH 4 is limited. In contrast to adsorption of DOM onto ferrihydrite, the formation of organic matter-Fe(III) cation complexes in the process of coprecipitation might account for greater maximum C loadings in the coprecipitates, which was observed in part I.

Fe(III) cation can promote intra- or intermolecular linkages within OM, causing precipitation of organic substances (Nierop et al., 2002; Henneberry et al., 2012; Riedel et al., 2012). This process could help retain organic matter in soils and sediments in the natural environments. Schwertmann et al. (1986) reported that complexation of Fe(III) ions with dissociated functional groups on organic matter can occur in soil micro-environments with high amounts of iron (III) and decomposed and humified materials. Petersen (1976) and Wada (1995) reported that precipitation of these complexes is an important stabilization mechanism in volcanic and acid leached subsurface soils. Riedel et al (2013) found that a large portion of DOM can be rapidly precipitated by iron after aeration of anoxic pore water.

6.4.2 FTIR

Fourier transform infrared spectra of freeze-dried samples of dissolved organic matter prior to reaction and of organic matter bound in different amounts to ferrihydrite by adsorption and coprecipitation were determined. The spectra of the bound organic matter were calculated by the difference between the FTIR spectra of ferrihydrite with and without associated organic matter. The FTIR spectra of the unreacted DOM and bound fractions of DOM with ferrihydrite in the course of adsorption and coprecipitation are presented in Fig.6.2.

Spectra of the ferrihydrite-associated OM (adsorbed or coprecipitated) clearly differ from the initial unreacted DOM (Fig.6.2). Upon adsorption and coprecipitation, the symmetric COO^- band at 1400 cm^{-1} became sharper and shifted to a lower

wavenumber of 1378-1389 cm^{-1} (Fig.6.2) and the peak area of this band increased (Table D.3). The shift, distortion, or increase of this band is related to carboxylate-metal bond formation via a ligand exchange mechanism (Gu et al., 1994, Chorover and Amistadi, 2001; Kaiser and Guggenberger 2007; Heckman et al., 2011). In addition, adsorption and coprecipitation led to a significant decrease in the band of asymmetric carboxyl groups at 1595 cm^{-1} and the appearance (emergence) of a new band at 1615 cm^{-1} (Fig.6.2), probably also suggesting asymmetric carboxyl C function groups are involved in strong complexes with ferrihydrite. Strong complexes of carboxylic groups with soil minerals via ligand exchange have been repeatedly demonstrated using FTIR spectroscopy (Gu et al., 1994, Chorover and Amistadi, 2001; Kaiser and Guggenberger 2007; Oren and Chefetz, 2012). Notably, at comparable amounts of OC associated with ferrihydrite, although the difference is not very large, coprecipitation yielded a larger shift in the 1400 cm^{-1} band and greater increase in peak area than adsorption (Fig.6.2 & Table D.3), implying coprecipitation may lead to stronger C-O-Fe bonding than adsorption. The stronger chemical C-O-Fe bonds may contribute to greater stability of the coprecipitated OC than the adsorbed OC against desorption, which was observed in part I.

At higher C loadings, the decrease in the asymmetric COO^- band at 1595 cm^{-1} and the shift or increase of the symmetric COO^- band at 1400 cm^{-1} became smaller (Fig.6.2 & Table D.3), suggesting weaker associations between carboxyl C and iron as C loading increases. Therefore, the strength of the interactions depends on C loadings. The large C loadings could result in fewer carboxyl groups per molecule involved in

the formation of bonds between carbon and mineral, which might be explained by a decrease in bonding sites, as the more OM is associated with minerals (Podoll et al., 1987, Kaiser 1997, Kaiser & Guggenbeger 2007). In addition, the analysis of mineral surface area and small pores in part I, indicated that ferrihydrite achieved almost full coverage at C loadings of around 0.9 mg C m^{-2} SA. Increasing amounts of organic matter associated with ferrihydrite may not form direct bonds between C and Fe, but result in association with the organic matter already sorbed on ferrihydrite through other weaker interactions such as hydrophobic interactions. This indirect association could in turn contribute to the weaker bonding between C and Fe at higher C loadings. These results could also explain the greater fractional C desorbed at higher C loadings in part I.

At lower C loadings, the aromatic band at 1515 cm^{-1} becomes stronger for bound OM than for DOM prior to reaction (Fig.6.2), indicating the aromatic group is preferentially removed with adsorption and coprecipitation. However, this selective uptake of aromatic C does not occur at higher C loadings. It also matches the trend recorded in the SUVA280 measurements in part I. Another important observation is that the peak intensity of the absorbance bands at 1270, 1130, 1080 and 1050 cm^{-1} significantly decreased after adsorption and coprecipitation, which clearly indicates phenolics and carbohydrates seem to be less important for the adsorption and coprecipitation of DOM on Fe oxides. This agrees with weak sorption to soil minerals of OM rich in carbohydrates (Kaiser & Guggenberger 2007, Chorover and Amistadi, 2001; Oren and Chefetz, 2012). In contrast, Eusterhues et al. (2011), studying the

sorption of forest-floor-extracted DOM and lignin on ferrihydrite, observed sorbed fractions that were rich in carbohydrate peaks.

6.4.3 STXM-NEXAFS Measurements

6.4.3.1 Carbon NEXAFS

Figure 6.3 presents the NEXAFS spectra of the OM-ferrihydrite complexes via adsorption and coprecpitation and of the initial DOM solution before reaction. The spectra of the unreacted DOM show two peaks at 285.1 and 286.6 eV and a major band at 288.4 eV. These features correspond to aromatic ($\pi^*_{C=C}$, 285.1 eV), phenolic ($\pi^*_{C=C-O}$, 286.6 eV), and carboxylic carbon ($\pi^*_{C=O}$, 288.4 eV) as labeled in figure 6.3 (Wan et al., 2007; Lehmann et al., 2008). The two peaks at 297.2 and 299.8 eV are due to potassium. Upon adsorption and coprecipitation, the two peaks for K disappeared (Fig.6.3), indicating potassium is not involved with organic matter and mineral interactions.

The ligand exchange (or bond formation) between COO^- functional groups of DOM and ferrihydrite was also shown in the NEXAFS spectroscopic studies. Compared to the unreacted DOM solution, the peak for carboxylic C at 288.4 eV after adsorption and coprecipitation dramatically declines, suggesting that the COO^- functional groups of DOM have complexed with the ferrihydrite. The involvement of carboxylic functional groups in ligand-exchange complexation reactions with hydroxylated Fe- and Al-oxide surfaces is considered a major interaction pathway by

several groups (Parfitt et al., 1977; Tipping, 1981; McKnight et al., 1992; Gu et al., 1994; Kaiser et al., 1997; Chorover and Amistadi, 2001; Kaiser and Guggenberger, 2007)

An increase in the aromatic C peak at 285.1 eV was observed at lower C loadings after adsorption and coprecipitation (Fig.6.3), indicating aromatic C is preferentially removed by adsorption and coprecipitation. However, no fractionation of aromatic C (Fig.6.3) is visible at greater C loadings. These results agree well with the $SUVA_{280}$ results and FTIR analysis. The peak for phenolic C significantly decreased after adsorption and coprecipitation (Fig.6.3), suggesting no selective uptake of phenolic C occurred. This is in line with FTIR analysis.

6.4.3.2 Spatial Distribution of Organic Matter on Ferrihydrite

To show explicitly the spatial correlation between C and Fe, C and Fe distribution maps (Fig D.3-6) were aligned to common reference features and overlayed. The color-coded composite maps are shown in Figure 6.4. To determine the correlation coefficients between C and Fe, elemental thickness values on a pixel-by-pixel basis were compared. Plots of C and Fe correlations are shown in Figure 6.5.

The color-coded composite maps of C and Fe show C is highly spatially correlated with Fe for both adsorptive complexes and coprecipitates (Fig.6.4, Fig.D.7-10c). There is no separate phase of C and Fe. This is in contrast to the results presented by Heneberry et al (2012), showing the presence of concentrated C spots with no detectable Fe after coprecipitation of DOM with iron. At lower C loadings, C

distribution on ferrihydrite is continuous and relatively uniform for both adsorptive complexes and coprecipitates (Fig.6.4a-b, Fig.D.7-8c), whereas there are localized concentrated C "hot spots" at higher C loadings (Fig.6.4c-d, Fig.D.9-10c). In addition, C correlates well with Fe at lower C loadings with a correlation coefficient up to 0.98 at lower C loadings (Fig.6.5a-b, Fig.D.7-8d). However, this correlation is lower at higher C loadings (Fig.6.5c-d, Fig.D.9-10d). These results may support the idea that C is directly associated on ferrihydrite at lower C loadings, whereas with increasing C loading an increasing amount of the organic matter associated with OM-ferrihydrite complexes does not attach to mineral surfaces directly but forms organic multilayers by interacting with the orginally sorbed OM, which is also evidenced by mineral surface area analysis in part I. Kleber et al (2007) proposed a conceptual model, which suggests that soil organic matter sorbs to mineral surfaces in a discrete zone sequence: (1) in the *contact zone,* the particularly strong organo-mineral associations are formed via ligand exchange between polar organic functional groups of amphiphiles and singly coordinated mineral hydroxyls*;* (2) Exposed hydrophobic portions of amphiphilic molecules adsorbed directly to mineral surfaces would be shielded from the polar aqueous phase through association with hydrophobic moieties of other amphiphilic molecules. This process can create a membrane-like bilayer containing a *hydrophobic zone*, whose components may exchange more easily with the surrounding soil solution than those in the contact zone, but which are still retained with considerable force; and (3) Sorbed to the hydrophilic exterior of hemimicellar coatings, or to adsorbed proteins, are organic molecules forming an outer region, or

kinetic zone, that is loosely retained by cation bridging, hydrogen bonding, and other interactions. Organic material in the kinetic zone may experience high exchange rates with the surrounding soil solution, leading to short residence times for individual molecular fragments. The STXM analysis in this study might imply that, in case of association of organic matter with ferrhydrite, the contact zone of OM on ferrihydrite is continuous and more uniform, whereas the hydrophobic/kinetic zone is, at least partially, localized.

6.5 Implications

In this study we found that direct chelation of Fe(III) cation with organic matter in the solid phase occurred in the process of coprecipitation. This chelation of Fe(III) with organic matter might track DOM in pore water or streams and play a significant role in C storage in the natural environments. Lalonde et al (2012) estimated that 21.5 ± 8.6% of the organic carbon buried in surface marine sediments (150×10^{15} g of organic carbon), or a global mass of $(19–45) \times 10^{15}$ g of organic carbon, is preserved as a result of direct chelation or co-precipitation of macromolecular OC-Fe structures. The strong chemical C-O-Fe bonds formed in the process of adsorption and coprecipitation and selective uptake of aromatic C might contribute to stabilizing organic matter by minerals. This study also demonstrated the spatial distribution of C on ferrhydrite at the nanometer scale for the first time. Although previous studies on natural soils have shown that C displays heterogeneous distribution on soil minerals, this study showed that C distribution on ferrihydrite was

relatively uniform at lower surface loadings. However, at higher C loadings, the spatial distribution of C on ferrihydrite became more heterogeneous. This study also provided possible microscopic evidence for the formation of organic multilayers on minerals at higher C loadings, which supplements specific surface area analysis in part I.

REFERENCES

Baldock, J. A.; Skjemstad, J. O., Role of the soil matrix and minerals in protecting natural organic materials against biological attack. *Org. Geochem.* **2000**, 31, 697-710.

Chorover, J.; Amistad, M. K., Reaction of forest floor organic matter at goethite, birnessite and smectite surfaces. *Geochim. Cosmochim. Acta* **2001**, 65(1), 95-109.

Eusterhues, K.; Rennert, T.; Knicker, H.; Kögel-Knabner, I.; Totsche, K. U.; Schwertmann, U., Fractionation of Organic Matter Due to Reaction with Ferrihydrite: Coprecipitation versus Adsorption. *Environ. Sci. Technol.* **2011**, 45, 527-533.

Gu, B. H.; Schmitt, J.; Chen, Z.; Liang, L. Y.; McCarthy, J. F., Adsorption and desorption of natural organic matter on iron oxide: mechanisms and models. *Environ. Sci. Technol.* **1994**, 28, 38-46.

Heckman, K.; Vazquez-Ortega, A.; Gao, X.; Chorover, J.; Rasmussen, C., Changes in water extractable organic matter during incubation of forest floor material in the presence of quartz, goethite and gibbsite surfaces. *Geochim. Cosmochim. Acta* **2011**, 75: 4295-4309.

Hennberry, Y. K.; Kraus, T. E. C.; Nico, P. S.; Horwath, W. R., Structural stability of coprecipitated natural organic matter and ferric iron under reducing conditions. *Org. Geochem.* **2012**, 48, 81-89.

Hitchcock, A. P., aXis-2000 is an IDL-based analytical package. **2000.** http://unicorn.mcmaster.ca.

Morikawa, E.; Roy, A.; Scott, J., Nuclear Instruments & Methods in Physics Research Section A-Accelerators Spectrometers Detectors and Associated Equipment, *Nucl. Instrum. Methods* **2007**, 582, 93-95.

Kaiser, K.; Guggenberger, G., Sorptive stabilization of organic matter by microporous goethite: sorption into small pores vs. surface complexation. *Eur. J. Soil Sci.* **2007**, 58, 45-59.

Kaiser, K.; Guggenberger, G.; Haumaier, L.; Zech, W., Dis-solved organic matter sorption on subsoils and minerals studied by 13C-NMR and DRIFT spectroscopy. *Eur. J. Soil Sci.* **1997**, 48:301-310.

Karlsson, T.; Persson, P., Complexes with aquatic organic matter suppress hydrolysis and precipitation of Fe(III). *Chem. Geol.* **2012**, 322/323, 19-27.

Kaznatcheev, K. V.; Karunakaran, C.; Lanke, U. D.; Urquhart, S. G.; Obst, M.; Hitchcock, A. P., Soft X-ray spectromicroscopybeamline at the CLS: commissioning results. *Nucl. Instrum. Methods Phys. Res. Sect. A-Accel. Spectrom. Dect. Assoc. Equip.* **2007**, 582, 96-99.

Kleber, M.; Sollins, P.; Sutton, R., A conceptual model of organo-mineral interactions in soils: self-assembly of organic molecular fragments into zonal structures on mineral surfaces. *Biogeochem.* **2007**, 85, 9-24.

Lalonde, K.; Mucci, A.; Quellet, A.; Gélinas, Y., Preservation of organic matter in sediments promoted by iron. *Nature* **2012**, 483, 198-200.

Lehmann, J.; Solomon, D.; Kinyang, J.; Dathe, L.; Wirick, S.; Jacobsen, S., Spatial complexity of soil organic matter forms at nanometer scales. *Nature Geosci*. **2008**, 1, 238-242.

McKnight, D. M.; Bencala, K. E.; Zellweger, G. W.; Alken, G. R.; Feder, G. L.; Thorn, K. A., Sorption of dissolved organic carbon by hydrous aluminum and iron oxides occurring at the confluence of Deer Creek with the Snake River, Summit County, Colorado. *Environ. Sci. Technol.* **1992**, l26, 1388-1398.

Mikutta, C., X-ray absorption spectroscopy study on the effect of hydroxybenzoic acids on the formation and structure of ferrihydrite. *Geochim. Cosmochim. Acta* **2011**, 75, 5122-5139.

Nierop, K. G. J.; Jansen, B.; Verstraten, J. M., Dissolved organic matter, aluminum, and iron interactions: precipitation induced by metal/carbon ratio, pH, and competition. *Sci. Total Envir.* **2002**, 300, 201-211.

Oren, A.; *Chefetz*, B., *Sorptive and desorptive fractionation of dissolved organic matter* by mineral soil matrices. *J. Environ. Qual.* **2012**, 41, 526-533.

Petersen, L., Podzols and Podzolization. DSR Forlag, Copenhagen **1976**.

Parfitt, R. L.; Fraser, A. R.; Farmer, V. C., Adsorption on hydrous oxides. III. Fulvic acid and humic acid on goethite, gibbsite and imogolite. *J. Soil Sci.* **1977**, 28, 289-296.

Podoll, R. T.; Irwin, K. C.; Brendlinger, S., Sorption of water-soluble oligomers on sediments. *Environ. Sci. Technol*. **1987**, 21, 562-568.

Regier, T.; Krochak, J.; Sham, T. K.; Hu, Y. F.; Thompson, J.; Blyth, R. I. R., Performance and capabilities of the Canadian Dragon: the SGM beamline at the Canadian Light Source. *Nucl. Instrum. Methods Phys. Res. Sect. A-Accel. Spectrom.Dect. Assoc. Equip.* **2007**, 582(1), 93-95.

Riedel, T.; Biester, H.; Dittmar, T., Molecular fractionation of dissolved organic matter with metal salts. *Environ. Sci. Technol.* **2012**, 46(8), 4419-4426.

Riedel, T.; Zak, D.; Biester, H.; Dittmar, T., Iron traps terrestrially derived dissolved organic matter at redox interfaces. www.pnas.org/cgi/doi/10.1073/pnas.1221487110

Schwertmann, U.; Kodama, H.; Fischer, W. R., Mutual interactions between organics and iron oxides. In: Huang, P.M., Schnitzer, M., (Eds.), Interactions of Soil Minerals with Natural Organics and Microbes. *Soil Sci. Soc. Am. Spec.* 17, Madison, WI, **1986**, 223-250.

Torn, M. S.; Trumbore, S. E.; Chadwick, O. A.; Vitousek, P. M.; Hendricks, D. M., Mineral control of soil organic carbon storage and turnover. *Nature* **1997**, 389, 170-173.

von Lützow, M.; Kögel-Knabner, I.; Ekschmitt, K.; Matzner, E.; Guggenberger, G.; Marschner, B.; Flessa, H., Stabilization of organic matter in temperate soils: mechanisms and their relevance under different soil conditions-a review. *Eur. J. Soil Sci.* **2006**, 57, 426-445.

Wada, K., Role of aluminium and iron in the accumulation of organic matter in soils with variable charge. In: Huang, P.M. et al. (Eds.), Environmental Impact of Soil Component Interactions, vol. 1. CRC Lewis, Boca Raton, FL, **1995**, 47-58.

Wan, J. M.; Tyliszczak, T.; Tokunaga, T. K., Organic carbon distribution, speciation, and elemental correlations with soil micro aggregates: applications of STXM and NEXAFS spectroscopy. *Geochim. Cosmochim. Acta* **2007**, 71(22), 5439-5449.

Webb, S. M., SIXPack a graphical user interface for XAS analysis using IFEFFIT. *Phys. Scr.* **2005**, T115.

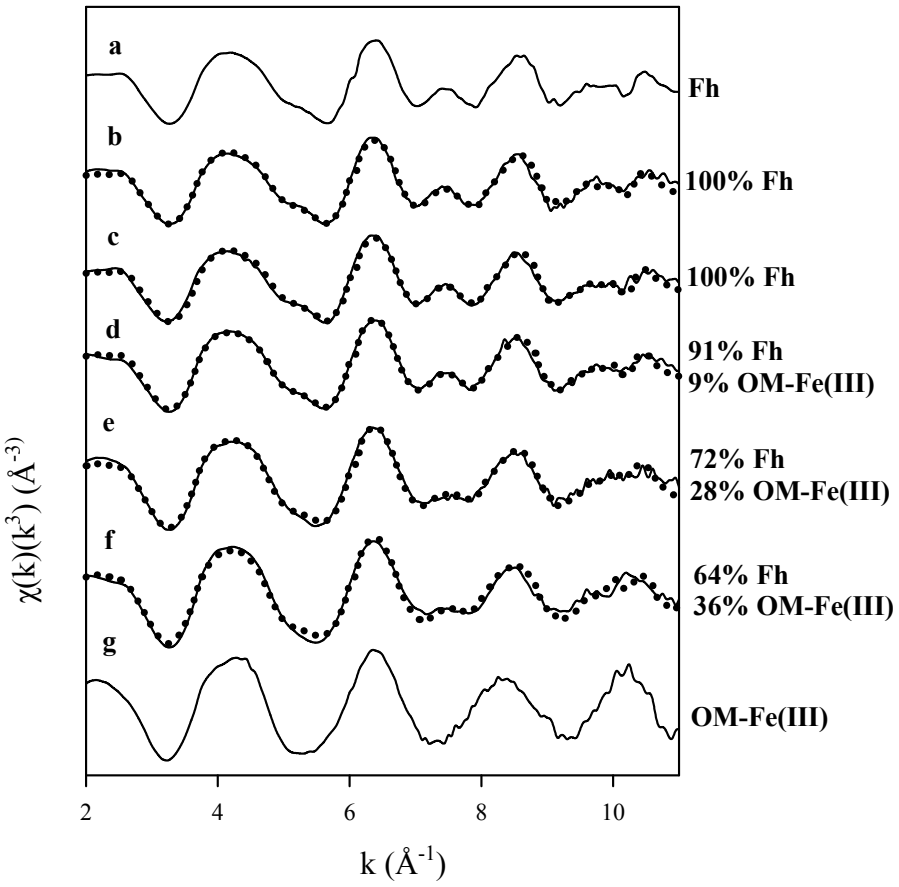

Figure 6.1 Iron k^3-weighted EXAFS spectra of (a) pure ferrihydrite (Fh), coprecipitate samples with C loadings of (b) 0.51, (c) 0.98, (d) 1.58, (e) 2.81 and (f) 3.13 mg C m^{-2} SA, and (g) organic matter-Fe(III) complexes. Dotted lines show linear combination fits over a *k*-range of 2-11 $Å^{-1}$ using (a) pure ferrihydrite and organic matter-Fe(III) complex as fit components. The numbers to the right of the spectra give the corresponding linear-combination-fitting (LCF) results of EXAFS.

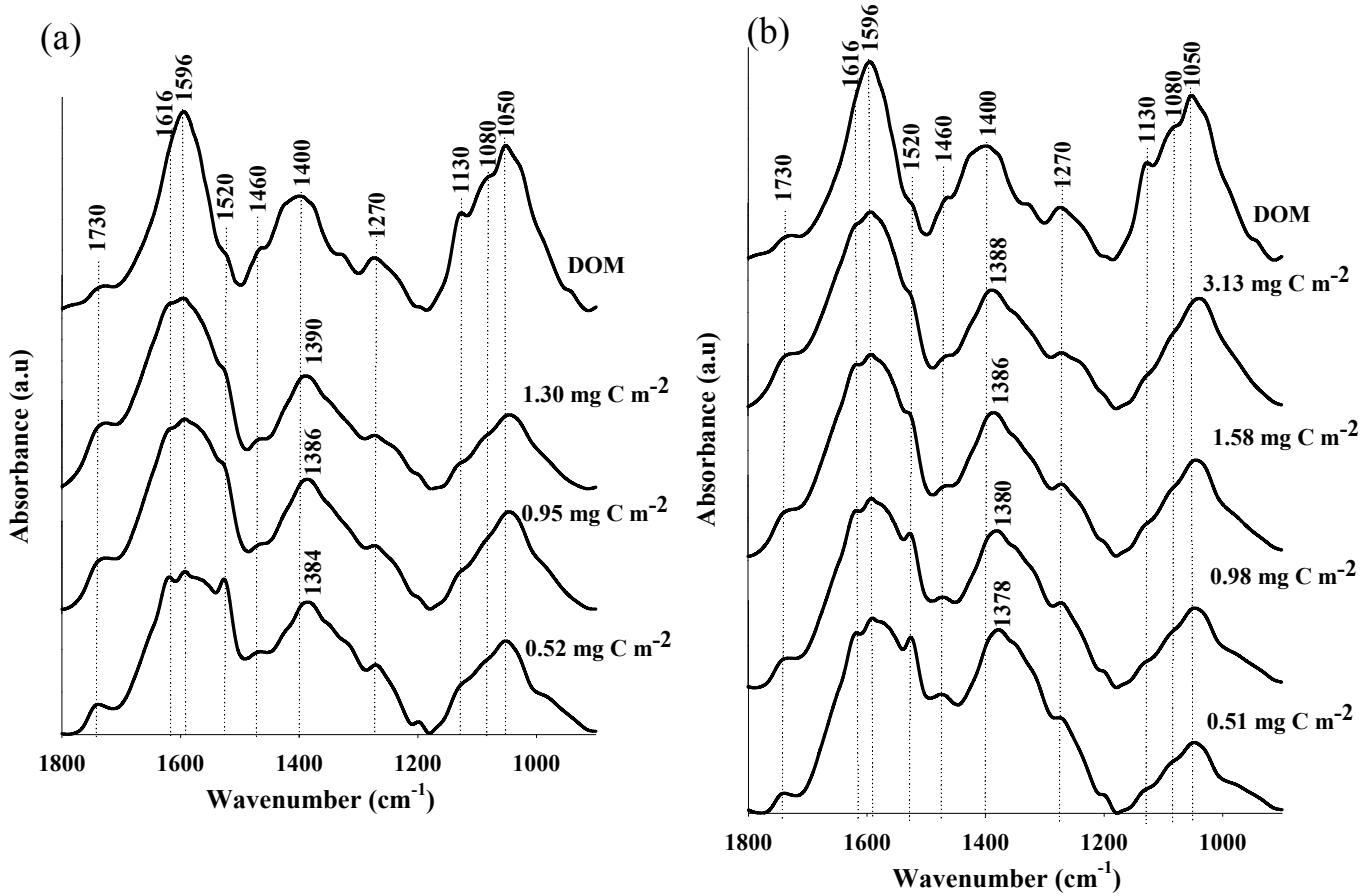

Figure 6.2 FTIR spectra of the (a) adsorbed and (b) coprecipitated organic matter in comparison to the original unreacted dissolved organic matter (DOM). Numbers to the right of the spectra give the C loadings: normalized C concentration to the specific surface area of pure ferrihydrite. Table A6.2 of the supporting information summarizes the peak assignments for organic matter.

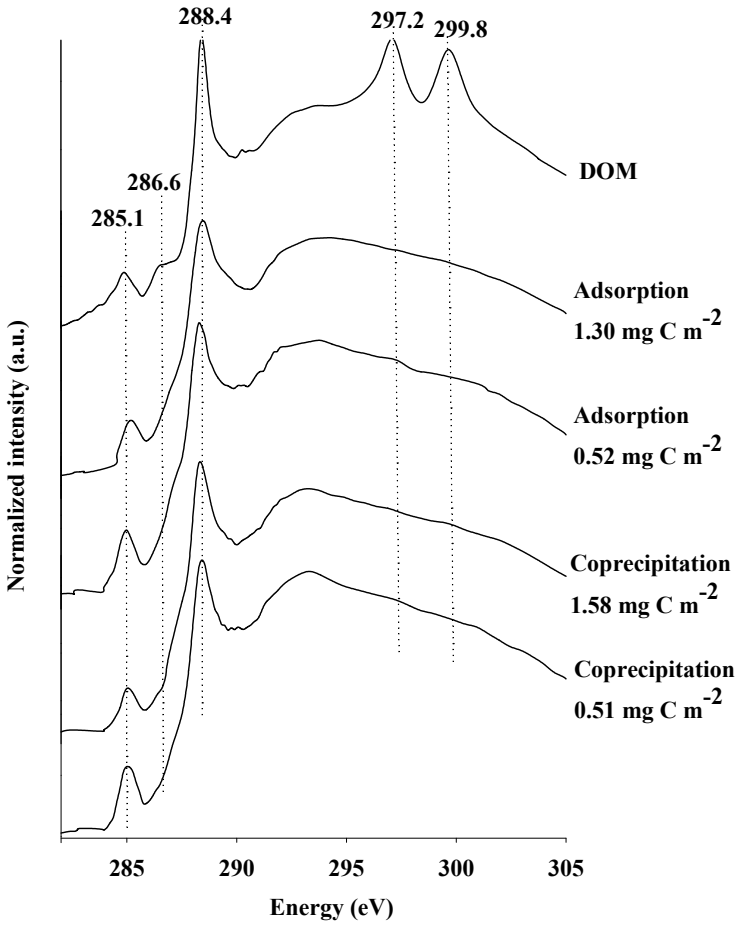

Figure 6.3 C 1s NEXAFS spectra of the adsorbed and coprecipitated OM, compared to the original DOM before reaction. The numbers to the right of the spectra give the C loadings: normalized C concentration by specific surface area of the pure ferrihydrite.

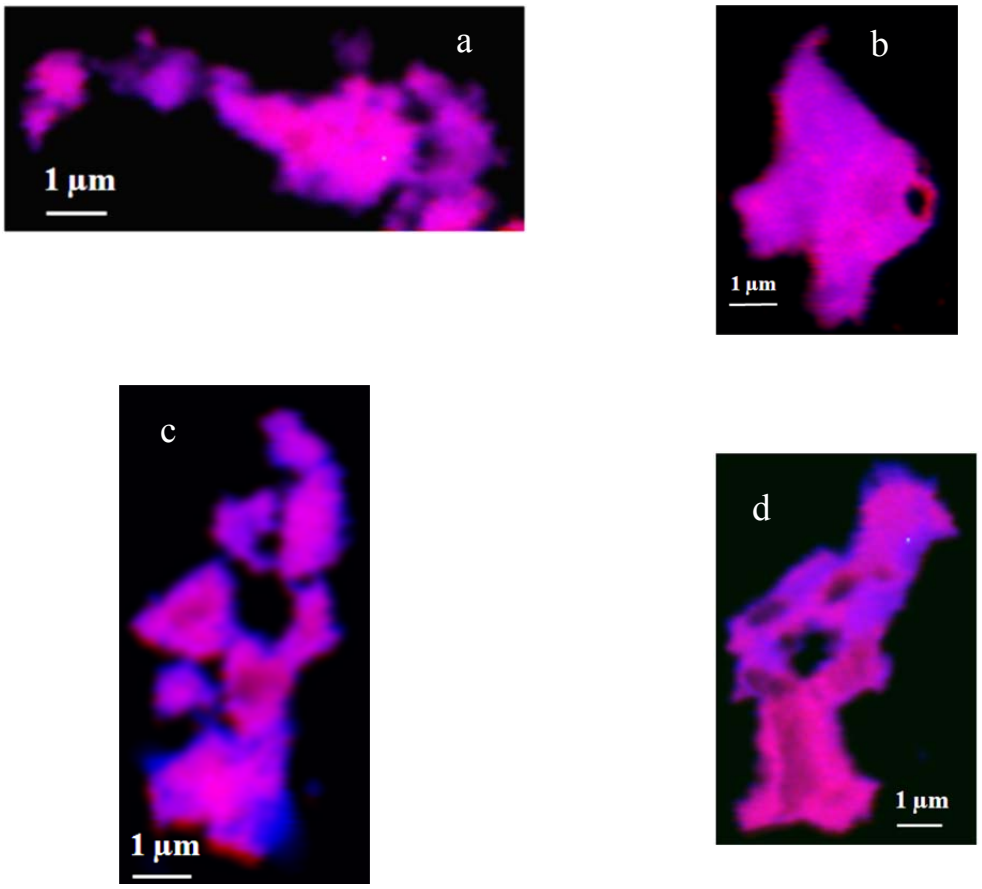

Figure 6.4 Color-coded composite maps of carbon and iron (carbon, blue; iron, red) for the (a) adsorptive complexes with C loadings of 0.52 mg C m^{-2} SA, (b) coprecipitates with C loadings of 0.51 mg C m^{-2} SA, (c) the adsorptive complexes with C loadings of 1.30 mg C m^{-2} SA and (d) coprecipitates with C loadings of 1.58 mg C m^{-2} SA.

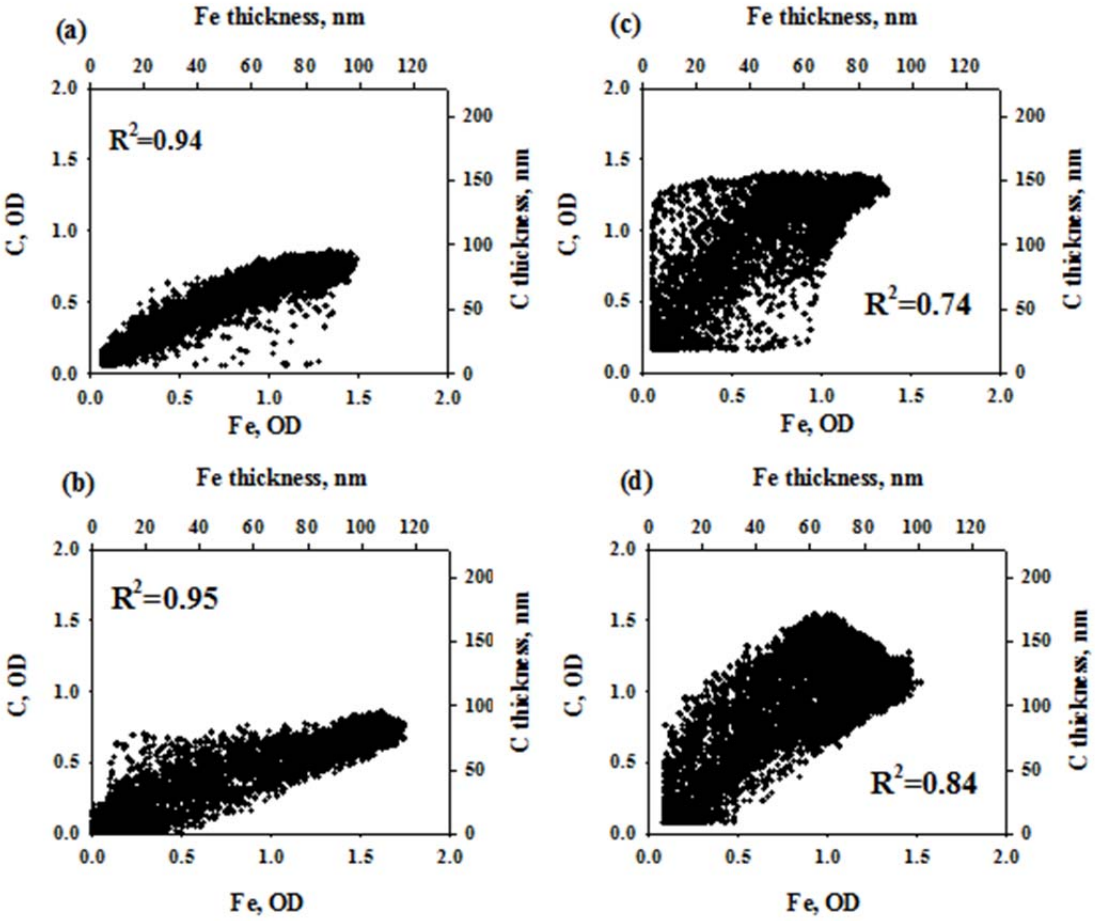

Figure 6.5 Correlation plots of thickness values of C and Fe obtained from STXM elemental distribution maps of the (a) the adsorptive complexs with C loadings of 0.52 mg C m^{-2} SA, (b) coprecipitates with C loadings of 0.51 mg C m^{-2} SA, (c) the adsorptive complexes with C loadings of 1.30 mg C m^{-2} SA and (d) coprecipitates with C loadings of 1.58 mg C m^{-2} SA. Correlation coefficients (R^2) are provided on the plots.

Chapter 7

IRON-ORGRANIC MATTER COPRECIPITATION IMPACTS ON THE CHARACTERISTICS AND FE(II)-CATALYZED TRANSFORMATION OF FERRIHYDRITE

7.1 Abstract

The poorly crystalline Fe(III) hydroxide ferrihydrite is considered one of the most important sinks for organic matter (OM), nutrients and contaminants within soils, sediments and waters. The ripening of ferrihydrite to more stable and hence less reactive phases such as goethite is catalyzed by surface reaction with aqueous Fe(II). While ferrihydrite within most natural environments contains high concentrations of co-precipitated organic matter, little is known regarding the impact of this OM on Fe(II)-induced transformation of ferrihydrite to secondary phases. In this study, we investigated the structural characteristics of OM-Fe coprecipitates and explored the extent, pathways and products of Fe(II)-induced secondary mineralization of OM-Fe coprecipitates by reacting aqueous Fe(II) (0.2 and 2.0 mM) with ferrihydrite containing a range of coprecipitated OM loadings (0-21% C). XRD and Mössbauer results indicated that the coprecipitated OM decreased crystallinity of ferrihydrite . Regardless of Fe(II) concentration, OM copreciptated with ferrihydrite resulted in diminished secondary mineralization and preservation of ferrihydrite and the degree of

ferrihydrite preservation increased with increasing OM loadings. The secondary mineral profiles upon Fe(II) reaction with ferrihydrite are a function of OM surface loadings and Fe(II) concentrations. At lower Fe(II) levels, the coprecipitated OM impeded goethite formation, while magnetite nucleation, in addition to goethite formation, was inhibited by OM. These findings provide insight into mechanisms that may be responsible for ferrihydrite preservation and low levels of secondary magnetite typically found in sedimentary environments. Considering the preponderance of organic matter on ferrihydrite in soils and sediments, the reactivity of natural (compromised) ferrihydrites and the subsequent impact on mineral evolution needs to be more fully explored.

7.2 Introduction

Ferrihydrite, an amorphous Fe oxyhydroxide, is ubiquitous in soils and sediments (Jambor and Dutrizac, 1998; Cornell and Schwertmann, 2003). Ferrihydrite, with its high surface area and intrinsic reactivity, serves as an important sink for many nutrients, metals and organic matter. Ferrihydrite is a precursor phase for many well-crystalline Fe phases such as goethite (a-FeOOH), hematite (a-Fe_2O_3), or mixed valence phases like magnetite (Fe_3O_4). Understanding the structure and reactivity of ferrihydrite and its controlling factors is therefore essential to predict the environmental stability of ferrihydrite.

While effects of inorganic constituents such as bicarbonate, silicate, or phosphate on the structure and stability of ferrihydrite have been extensively studied

in the past (Cornell and Schwertmann, 2003), equivalent studies with organic compounds are scarce (Nesterova et al., 2000; Rancourt et al., 2005; Schwertmann et al., 2005; Eusterhues et al., 2008). This knowledge, however, is required in order to predict the mineral's biogeochemical reactivity in soils and sediments. In natural environments, ferrihydrite often forms in the presence of dissolved organic matter (DOM), which leads to coprecipitation of organic matter (OM) with ferrihydrite. The coprecipitation of Fe and DOM is common in soils and sediment that experience fluctuating pH and redox conditions (Fuller et al., 1993; Pokrovsky and Schott, 2002). Therefore, OM–Fe coprecipitates represent an important class of structures whose chemistry and reactivity require further understanding under different environmental conditions since Fe speciation and mobility affect the availability, cycling, and transport of metals, OM and nutrients. When OM is bound to the surface of ferrihydrite, organic chelates may retard crystal growth, thus limiting the structural intermediate and long-range order (>Å), or they can alter the Fe coordination at the sub-nanometer scale. Studies of OM-contained Fe (hydr)oxide structures have found greater structural disorder in the coprecipitated Fe phases vs. organic-free or synthetic ferrihydrite (Eusterhues et al., 2008; Cismasu et al., 2011; Mikutta, 2011). Therefore, the reactivity of natural ferrihydrites will often differ from their synthetic counterparts, formed in the absence of OM. However the implications of these structural changes on biogeochemical processes remain unresolved.

Ferrihydrite is thermodynamically unstable with respect to more stable phases, such as goethite and hematite, and will therefore ripen to these phases over time. This

'ripening' of ferrihydrite to more stable (crystalline) Fe(III) (hydr)oxides is catalyzed by reductive dissolution by chemical reductants like Fe(II) (Jang et al., 2003; Hansel et al., 2005; Pedersen et al., 2005; Yee et al., 2006). The products of Fe(II)-induced ferrihydrite transformations have received considerable attention recently in an attempt to understand the microbial and geochemical controls on Fe mineralization pathways in soils and sediments (Benner et al., 2002; Zachara et al., 2002; Hansel et al., 2003, 2004, 2005; Pedersen et al., 2005; Yee et al., 2006; Jones et al., 2009; Tufano et al., 2009; Pallud et al.,2010a).The rate of conversion and ultimate Fe(III) mineral species formed, however, is a function of competing mineralization pathways induced by aqueous conditions including Fe(II) concentration and flux, ligand composition, and pH (Zachara et al., 2002; Hansel et al., 2003, 2004, 2005; Jang et al., 2003; Tufano et al., 2009; Pallud et al., 2010a,b). The sequence of precipitation and subsequent stability of the secondary phases also varies with the aqueous environment, such that certain phases can serve as either a transient intermediate or a stable end product (e.g., lepidocrocite) under appropriate conditions (Hansel et al., 2003, 2005; Tufano et al., 2009). Previous studies have also demonstrated that organic compounds can kinetically retard and in some instances completely prevent, the transformation of Fe(III) minerals to more crystalline, thermodynamically stable forms of Fe(III) in the absence of Fe(II) (Cornell and Schwertmann, 1979; Cornell and Schneider, 1989). Most of the studies used simple or synthesized organic compounds such as citric and tartaric acids and oxalate rather than more complex, naturally occurring OM. In addition, despite the prevalence of OM-ferrihydrite coprecipitation in natural

environments, the role of OM coprecipitation on ferrihydrite transformation in the presence of Fe(II) is not well understood. However, such knowledge is critical to predicting the fate of poorly crystalline Fe (hydr)oxides in the environments such as wetlands that experience significant variations in either pH or redox conditions.

Accordingly, the goals of this study were to: (1) characterize organic matter-ferrihydrite coprecipitates by X-ray diffraction (XRD) and Mössbauer and Extended X-ray Adsorption Fine Structure (EXAFS) spectroscopic techniques; and (2) investigate the impact of OM coprecipitation on the extent, pathways and products of Fe(II)-induced secondary mineralization of 2-line ferrihydrite.

7.3 Materials and Methods

7.3.1 Synthesis of OM-free ferrihydrite and OM-ferrihydrite coprecipitates

Dissolved organic matter for the adsorption and coprecipitation experiments was extracted from field-fresh samples of a forest floor layer by mixing organic materials with deionized water for 24 h. The dominant tree species were beech (*Fagus grandifolia*), red and black oak (*Quercus rubra and Q. velutina*), and tulip poplar (*Liriodendron tulipifera*). The suspension was stirred periodically, centrifuged at 20000 g for 20 min and subsequently isolated by pressure filtration through 0.2-μm polysulfone membrane filters. The extraction was carried out just before the experiments.

Two-line ferrihydrite was produced by titrating a 0.01M $Fe(NO_3)_3$ solution with 0.1M KOH to a pH of 7 (*Schwertmann and Cornell, 2000*). Organic matter-ferrihydrite coprecipitates were prepared by dissolving the $Fe(NO_3)_3$ in a solution containing dissolved organic matter and then raising the pH afterward to 7. Coprecipitates with different OM loadings were produced by varying the C/Fe ratio of the initial solution. The precipitates were separated by centrifugation, washed twice with deionized water and analyzed by XRD and Mössbauer and EXAFS spectrocopy.

7.3.2 Transformation Experiment Setup

Fe(II) catalyzed transformation of ferrihydrite and OM-ferrihydrite coprecipitates was studied by reaction with $FeSO_4$. The OM-free ferrihydrite and OM-ferrihydrite coprecipitates were washed with anaerobic deionized water three times and resuspended in anaerobic PIPES buffer. Five (OM-) ferrihydrite samples containin C contenst ranging from 0% to 21%, which corresponds 0 to 0.98 mg C m^{-2} SA by normalizing to the mineral surface area of OM-free ferihydrite, were prepared. Reactions were performed in 125 ml serum vials. Each vial contained 1% Fe by weight as an (OM-) ferrihydrite slurry in 100 ml of anaerobic PIPES (1,4-piperazinediethanesulfonic acid) buffer (10 mM, pH 7.2). Ferrous sulfate (as $FeSO_4 \cdot 7H_2O$) was added to the vials to obtain the final Fe(II) concentration s of 0.2 or 2.0 mM. Experiments were performed in a glovebox with 95% N_2 and 5% H_2. Kinetics studies were performed by using a series of reaction vials and sacrificing vials at each time point. Vials were equilibrated and maintained at pH 7.2 under N_2

atmosphere and gently shaken to minimize diffusion effects. Aqueous samples were extracted in the glove box using a sterile syringe and analyzed for Fe(II) concentration and pH. Fe(II) was monitored spectrophotometrically at 562 nm using the ferrozine assay (Stookey, 1970). After reaction, solids were rinsed twice with anaerobic deionized water. All the solids were analyzed by Fe K-edge extended X-ray adsorption fine structure (EXAFS) spectroscopy. The resulting solids sampled after three months reaction were also analyzed by XRD.

7.3.3 Solid Analysis

7.3.3.1 X-ray Diffraction

All the synthesized precipitates and the solid products after reacting with Fe(II) for three months were freeze-dried for XRD analysis. All X-ray diffractograms were recorded with a Rigaku Miniflex X-ray diffractometer equipped with Cu-Kα radiation generated at 35 kV and 10 mA. The XRD patterns were recorded from 2 to 70° 2θ with 0.05° 2θ step-size and 2s acquisition time.

7.3.3.2 Iron K-edge X-ray Absorption Spectroscopy

Samples for XAS measurements included all the precipitates and the products following reaction with Fe(II). Homogeneous sample films were prepared by vacuum filtration of mineral slurries onto cellulose nitrate filters that were subsequently sealed between two layers of Kapton tape. Iron K-edge X-ray absorption spectra were recorded at the National Synchrotron Light Source (NSLS) on beamline X11A and

Stanford Synchrotron Radiation Lightsource (SSRL) on beamline 4-1. Fe K-edge EXAFS spectra were collected using a Si(111) monochromator on beamline X11A and using a Si(220) monochromator crystal set on beamline 4-1. The monochromator was detuned 50% for harmonic rejection. Four scans of each sample were collected either in transmission mode using an ion chamber or fluorescence mode using a Lytle detector. Scans were obtained from 100 eV below to 1000 eV above the Fe K-edge at 7111 eV. Data reduction and linear combination k^3-weighted EXAFS spectral fitting were performed using SIXPACK (Webb, 2005). To quantify the secondary Fe phases, linear-combination fitting of k^3-weighted EXAFS spectra with a set of reference standards for Fe was performed from 2 to 11.5 $Å^{-1}$. Reference compounds used for fittings were considered based on XRD data and the known reaction pathways of ferrihydrite transformation.

7.3.3.3 Mössbauer Spectroscopy

Mössbauer measurements were also performed at the Environmental Molecular Science Laboratory (EMSL) at Pacific Northwest National Laboratory on the synthesized precipitates. Samples were prepared by mixing approximately 50-80 mg of samples with vaseline in a Cu Mössbauer sample holder (0.95 cm by 1.27 cm). The holder was entirely filled with the sample mixture and sealed with Scotch tape. An oxygen impermeable polymer film (aluminized Mylar) was used as an outer seal on the ends of the holder. Both the tape and polymer were snapped into the holder with rings made of carbonized-polyethyletherketone (PEEK) polymer to ensure

tightness. Mössbauer spectra were collected using a 50-mCi (initial strength) 57Co/Rh source. The velocity transducer MVT- 1000 (WissEL) was operated in a constant acceleration mode (23 Hz, ±12 mm/s). An Ar–Kr proportional counter was used to detect the radiation transmitted through the holder, and the counts were stored in a multichannel scalar (MCS) as a function of energy (transducer velocity) using a 1024 channel analyzer. Data were folded to 512 channels to give a flat background and a zero-velocity position corresponding to the center shift (CS or d) of a metal iron foil at room temperature (RT). Calibration spectra were obtained with a 25-lm-thick a-Fe(m) foil (Amersham, England) placed in the same position as the samples to minimize errors due to geometry changes. A closed-cycle cryostat (ARS, Allentown, PA) was employed below RT measurements. The Mössbauer data were modeled with the Recoil software using a Voight-based structural filtering routine (Rancourt and Ping, 1991).

7.4 Results and Discussion

7.4.1 Structural Characteristics of (OM-)Ferrihydrite by XRD and Mössbauer Spectroscopy

The XRD data for the OM-free ferrihydrite and coprecipitate samples are shown in Figure 7.1.The XRD of the OM-free sample showed the usual peaks of 2-line ferrihydrite (Fig.7.1). With an increasing OM surface loading, the two main peaks broadened (Fig.7.1). The observed broadening indicates a decreasing size of coherent

scattering domains or an increase of stacking disorder in the anionic layers. Based on EXAFS, Waychunas et al. (1993) suggested that the precipitation process of ferrihydrite starts with the formation of small chains of Fe octahedra, continues by linking these chains via their edges to plate-like dioctahedral and trioctahedral chains, and only then proceeds by cross-linking the chains at their octahedral corners. In the presence of bound organic matter, frequent reactions between Fe (O, OH)6 octahedra and organic molecules may prevent cross-linking and result in a structural disorder of ferrihydrite.

Figure 7.2 shows Mössbauer spectra of pure ferrihydrite and coprecipitates. All spectra recorded at room temperature showed broadened electric quadrupole doublets (Fig.7.2). The broadening of the doublets can be attributed to a distribution of electric field gradients. None of the spectra contained a quadrupole doublet component representing iron that does not exhibit a magnetic splitting, as has been reported by Schwertmann et al. (2005). No Fe(II) doublets were observed in any of the samples (Fig.7.2), indicating the absence of detectable amounts of Fe(II)-containing phases. As the temperature decreased, the doublets gradually transferred to broadened sextets, indicating progressive magnetic ordering at low temperatures. Transformation of doublets to sextets started from 77K for pure ferrihydrite, while doublets begun to transfer to sextets at 45K and 25 K for the ferrihydrite with 12% and 21% of C, respectively (Fig.7.2) This indicates that magnetic ordering temperature (transformation of doublet feature (paramagnetic) to sextet feature (magnetic)) of ferrihydrite decreased with increasing OM loadings on ferrihydrite. Such a decrease

can be explained by decreasing particle size and crystallinity or by decreasing interparticle interaction (Mikutta et al., 2008; Eusterhues et al., 2008). Decreasing particle size was observed in previous studies (Eusterhues et al., 2008), decreasing crystallinity is shown by XRD, and decreasing interparticle interactions is plausible because of the increasing amounts of diamagnetic organic materials between individual ferrihydrite particles. The nature of the functional groups of organic matter that are involved in the interaction with Fe was revealed by NEXAFS and FTIR spectroscopy. Carboxylic C may account for interaction between organic matter and iron oxides by forming strong Fe-O-C chemical binds.

Collectively, Mössbauer and XRD results show that the coprecipitated OM hasa clear impact on the structure of the precipitated ferrihydrite. Natural ferrihydrites must, therefore, be expected to differ in many properties from their synthetic analogues.

7.4.2 Effects of the Coprecipitated Organic Matter on Fe(II)-catalyzed Transformation of Ferrihydrite

To determine the impacts of OM-Fe coprecipitation on Fe(II)-induced conversion of ferrihydrite, we reacted ferrihydrite minerals containing different amounts of coprecipitated OM with two concentrations of ferrous Fe(II). XRD patterns of the secondary mineral phases after 90 days of reaction are shown in figs. 7.3 and 7.4. Quantitative speciation of the final product was determined by Fe K-edge

EXAFS and linear combination fitting of the sample spectrum with reference mineral spectra. The results of the linear combination fits are presented in figs.7.5-7.

Following 90 days of reaction with Fe(II) concentrations (0.2 mM Fe(II); ~0.66 mmol Fe(II)/g ferrihydrite), pure ferrihydrite is converted to goethite (Figs.7.3 and 7.5). At higher Fe(II) levels (2.0 mM; ~6.6 mmol Fe(II)/g ferrihydrite), magnetite, in addition to goethite, is formed (Figs.7.4 and 7.5). These results are consistent with that observed previously (Hansel et al., 2005). The secondary mineral phases and their proportions varied substantially as a function of OM surface loading (Figs.7.3-5). Regardless of the concentration of Fe(II), the presence of OM on the ferrihydrite resulted in diminished secondary mineralization and the preservation of ferrihydrite, and the degree of preservation increased with an increasing OM surface loadings. Coprecipitation with 21% C resulted in complete ferrihydrite preservation (Fig.7.3-5).

7.4.2.1 Reaction with Low levels of Fe(II)

Upon reaction with low Fe(II) levels for 90 days, OM-containing ferrihydrite was converted mainly to lepidocrocite, with only minor amounts of goethite in the sample with 3% C (Figs.7.3 and 7.5). This is in contrast with the data observed for pure ferrihydrite where goethite was the sole secondary mineral phase (Figs.7.3 and 7.5). In contrast to pure ferrihydrite and ferrihydrite coprecipitated with 3% C, higher OM loadings resulted in incomplete ferrihydrite mineralization (Figs.7.3 and 7.5). In fact, for OM-Fe coprecipitates with 20% C, ferrihydrite was completely preserved (Figs.7.3 and 7.5). Ferrihydrite is a highly reactive Fe hydroxide that is

thermodynamically unstable and has a propensity to transform to thermodynamically stable crystalline phases (an Oswald ripening process) (Cornell and Schwertman, 1996). While ferrihydrite transformation often takes months to years at room temperaute and near-neutral pH (Schwertmann et al., 2004), Fe(II) reaction with ferrihydrite can accelerate Ostwald ripenning at neutral pH (Zachara et al., 2002; Hansel et al., 2005 20011; Pedersen et al., 2005). The conversion of ferrihydrite to lepidocrocite and goehtite is attributed to a traditional ripening process. Reaction of Fe(II) with the ferrihydrite surface results in Fe(II) adsorption (Tronc et al., 1992) or exchange of Fe(II) for Fe(II) in terminal octahedral positions (Pedersen et al., 2005) and subsequent electron transfer from bound Fe(II) to bulk Fe(III). Increased electron density within ferrihydrite enhances the rate of dissolution and leads to an increased rate of reprecipitation to secondary phases (Rosso et al., 2010). The Fe(II)-induced reductive dissolution of ferrihydrite solubilizes aqueous Fe(III), which rapidly precipitates as a more thermodynamically stable Fe(III) (hydr)oxide (Pedersen et al., 2005), either lepidocrocite or goethite under these conditions. The presence of OM impedes the conversion of ferrihydrite to goethite. The presence of 3% C resulted in a 88% decline in ferrihydrite conversion to goethite, which is accounted for by a corresponding increase in lepidocrocite precipitation (Figs.7.3 and 7.5). Further increasing C concentration to 8 % on ferrihydrite resulted in complete inhibition of goethite formation (Figs.7.3 and 7.5). The level of lepidocrocite significantly decreased with C loadings and instead ferrihydrite was preserved at the expense of lepidocrocite formation (Fig.7.5).

The progression/pathway of Fe(II)-induced secondary mineralization of ferrihydrite is also altered by the presence of OM. Following 18 hours of reaction of pure ferrihydrite with 0.2 mM Fe(II), almost equivalents amounts of lepidocrocite and goethite were formed as major secondary phases (Fig.7.6). However, the relative abundance of lepidocrocite was significantly reduced at 6 days and completely disappeared at 90 days (Fig.7.6). These results indicate that goethite observed at later time points forms at the expense of lepidocrocite, similar to that observed previously (Hansel et al., 2005 2011; Tufano et al., 2009). The influence of a lepidocrocite precursor phase was also found for ferrihydrite coprecipitated with 3% C. Twelve percent of goethite at 90 days was formed from the transformation of lepidocrocite (Fig.7.6). In contrast, transformation from lepidocrocite to goethite was completely inhibited in the presence of higher OM surface loadings (5% C, 10% C) (Fig.7.6). Lepidocrocite is metastable with respect to goethite (Cornell and Schewertmann, 2003). The diminished formation of goethite from lepidocrocite with increasing OM loadings suggests that the presence of OM inhibits the mineral ripening process. .It has been shown before that for aging in the absence of catalyst Fe(II), sorption of ligands suppresses dissolution, internal ordering and aggregation of ferrihydrite, thus inhibiting its transformation to goethite and hematite (Cornell and Schewertmann, 2003).

7.4.2.2 Reaction with High Levels of Fe(II)

Reaction of 2.0 mM Fe(II) with ferrihydrite containing a range of coprecipitated OM also resulted in inhibited ferrihydrite conversion and secondary mineralization.(Figs.7.4 and 7.5). The impact of OM loadings at high Fe(II) levels with ferrihydrite is as great as that observed for low Fe(II) reactions. Similar to low Fe(II) levels, the presence of OM also favored the conversion of ferrihydrite to lepidocrocite rather than goethite at higher Fe(II) concentrations (Figs.7.4 and 7.5). However, it is notable that that in the presence of the coprecipitated OM, the extent of lepidocrocite accumulation was significantly lower at higher Fe(II) levels than at lower Fe (II) concentrations, accompanied by a corresponding increase in goethite formation at higher Fe(II) levels (Fig.7.5). This suggests that continued lepidocrocite precipitation is impeded by the formation of, or conditions leading to goethite. Lepidocrocite and goethite levels decreased with OM loadings because of an increasing degree of ferrihydrite preservation (Fig.7.5). Magnetite is an additional secondary product of Fe(II)-induced conversion of pure ferrihydrite at high Fe(II) concentrations (Figs.7.4 and 7.5), as observed previously (Hansel et al 2005 2011; Tufano et al., 2009). The proportion of magnetite formed declined dramatically with the presence of OM on ferrihydrite. About 30% magnetite was formed for pure ferrihydrate upon reaction for 90 days, while the presence of OM resulted in only 7-10% of magnetite nucleation (Fig.7.5). Magnetite nucleation from ferrihydrite has been primarily attributed to a surface atomic rearrangement (topotactic conversion) of ferrihydrite to magnetite (Zachara et al., 2002). Ferric Fe in tetrahedral coordination

on the surface of ferrihydrite would allow for a solid state conversion mechanism, although there are conflicting reports on the presence of tetrahedral Fe(III) in ferrihydrite and this remains a matter of debate (Michel et al., 2007; Manceau, 2009). Previous investigations revealed that nucleation of magnetite on lepidocrocite and goethite was not observed and it was therefore suggested magnetite nucleated on ferrihydrite followed by continued crystal growth, supported by an Fe(III) flux from lepidocrocite and goethite dissolution (Hansel et al., 2005). Therefore OM-inhibited magnetite nucleation could not be attributed to a shift in the mineralization to lepidocrocite rather than goethite, since the solubility of lepidocrocite is greater than that of goethite. Inhibition of magnetite in the presence of OM on the surface is attributed to a shift in mineralization pathways. Instead, inhibition of magnetite is at the expense of ferrihydrite preservation by organic matter.

Organic matter also affected ferrihydrite mineralization pathways. After reacting pure ferrihydrite with high Fe(II) levels for 18 hours, about 60% of the goethite with 13% magnetite was precipitated (Fig.7.7). As reaction time increased, the relative abundance of goethite remained unvaried, while magnetite continued to increase at the expense of ferrihydrite (Fig.7.7). This suggests that magnetite precipitates directly from ferrihydrite instead of goethite. The accumulation of high goethite concentrations (>40%) has been shown to inhibit the precipitation of magnetite (Hansel et al., 2003; Tufano et al., 2009). This inhibition has been attributed to the passivation of the ferrihydrite surface (Hansel et al., 2003) and consumption of tetrahedral Fe(III) centers within ferrihydrite that are presumed necessary for the

nucleation of magnetite via a solid-state conversion of ferrihydrite to magnetite (Tufano et al., 2009). It is unlikely that the same inhibition processes are operative here, however, since after 18 hours, equivalent goethite concentrations are present, yet magnetite precipitation continued to ensue (Fig.7.7). After reaction of ferrihydrite with 3-8% C with Fe(II) for 18 hours, only 7-10% of magnetite formed and the relative abundance of magnetite remained constant with reaction time, while goethite and lepidocrocite continued to accumulate at the expense of ferrihydrite as reaction time increased, implying that the initial nucleation of magnetite on ferrihydrite was somehow inhibited by organic matter.

While we cannot confirm the mechanism(s) responsible for the diminished Fe(II)-induced conversion of OM-ferrihydrite coprecipitates to more stable hydroxides or inhibition of magnetite nucleation, considering that electron transfer between Fe(II) and Fe(II) or surface rearrangement is requisite for ferrihydrite transformation and secondary mineral formation, the diminished (in some cases completely) mineralization of OM-ferrihydrite may be due to blocking of surface sites by OM. The specific surface area of the precipitated ferrihydrite has been shown to decrease with increasing OM loading, supporting the idea that the surface sites of ferrihydrite are blocked by organic matter. This site blocking may therefore result in a lower electron exchange between aqueous Fe(II) and solid Fe(III) in the mineral.

7.5 Environmental implications

The dominant role of aqueous Fe(II) concentrations in dictating the mineralization pathways of ferrihydrite has been observed both in batch and dynamic flow conditions (Fredrickson et al., 1998; Benner et al., 2002; Zachara et al., 2002; Hansel et al., 2003, 2005; Tufano et al.,2009). Furthermore, model simulations exploring the Fe(II)-induced ferrihydrite transformations along diffusive gradients reproduced the observed secondary mineral profiles by changing only the aqueous Fe(II) concentration in the employed rate expressions (Tufano et al., 2009). Here, we show that coprecipitated OM on ferrihydrite will dramatically affect its structure and the secondary mineralization profiles upon reaction with Fe(II). OM stabilizes ferrihydrite, impeding its transformation to more thermodynamically stable products, particularly goethite and magnetite. Furthermore, here we observe a linear ($R^2 = 0.93$) increase in ferrihydrite concentrations with increasing OM loadings on ferrihydrite (see Fig.7.8). Based on this linear trend, OM levels above 21% C will result in completely inhibited ferrihydrite transformation. The findings of this study may provide an explanation for the preservation of ferrihydrite and minor levels of secondary magnetite frequently found within most soils and sedimentary environments. Considering the preponderance of organic matter bound with ferrihydrite in soils and sediments, the reactivity of natural ferrihydrites and the subsequent impact on mineral evolution needs to be more fully explored.

REFERENCES

Benner, S. G.; Hansel, C. M.; Wielinga, B. W.; Barber, T. M.; Fendorf, S., Reductive dissolution and biomineralization of iron hydroxide under dynamic flow conditions. *Environ. Sci. Technol.* **2002**, 36, 1705-1711.

Cismasu, A. C.; Michel, F. M.; Tcaciuc, A. P.; Tyliszczak, T.; Brown, J.; Gordon, E.; Brown, Jr. G. E., Composition and structural aspects of naturally occurring ferrihydrite. *CR. Geosci.* **2011**, 343, 210-218.

Cornell, R. M.; Schneider, W., Formation of goethite from ferrihydrite at physiological pH under the influ*ence* of cysteine: *Polyhedron* **1989**, 8, 149-155.

Cornell, R. M.; Schwertmann, U., The iron oxides: Structure, properties, reactions, occurrences and uses, 2nd edition. Wiley-VCH. **2003**.

Cornell, R. M.; Schwertmann, U., The iron oxides: structure, properties, reactions, occurrences and uses. Wiley–VCH, Weinheim. **1996**.

Eusterhues, K.; Wagner, F. E.; Ha¨usler, W.; Hanzlik, M.; Knicker, H.; Totsche, K. U.; Ko¨gel-Knabner, I.; Schwertmann, U., Characterization of ferrihydrite-soil organic matter coprecipitates by X-ray diffraction and Mo¨ssbauer spectroscopy. *Environ. Sci. Technol*. **2008**, 42, 7891-7897.

Fredrickson, J. K.; Zachara, J. M.; Kennedy, D. W.; Dong, H.; Onstott, T. C.; Hinman, N. W.; Li, S. M., Biogenic iron mineralization accompanying the dissimilatory reduction of hydrous ferric oxide by a groundwater bacterium. *Geochim. Cosmochim. Acta* **1998**, 62, 3239-3257.

Fuller, C. C.; Davis, J. A.; Waychunas, G. A., Surface-chemistry of ferrihydrite. 2. Kinetics of arsenate adsorption and coprecipitation. *Geochim. Cosmochim. Acta* **1993**, 57, 2271-2282.

Hansel, C. M.; Benner, S. G.; Neiss, J.; Dohnalkova, A.; Kukkadapu, R. K.; Fendorf S., Secondary mineralization pathways induced by dissimilatory iron reduction of ferrihydrite under advective flow. *Geochim. Cosmochim. Acta* **2003**, 67, 2977-2992.

Hansel, C. M.; Benner, S. G.; Nico, P.; Fendorf, S., Structural constraints of ferric (hydr)oxides on dissimilatory iron reduction and the fate of Fe(II). *Geochim. Cosmochim. Acta* **2004**, 68, 3217-3229.

Hansel, C. M.; Benner, S. G.; Fendorf, S., Competing Fe(II)-induced mineralization pathways of ferrihydrite. *Environ. Sci. Technol*. **2005**, 39, 7147-7153.

Jambor, J. L.; Dutrizac, J. E., Occurrence and constitution of natural and synthetic ferrihydrite, a wide spread iron oxyhydroxide. *Chem. Rev.* **1998**, *98*, 2549-2585.

Jang, J. H.; Dempsey, B. A.; Catchen, G. L.; Burgos, W. D., Effects of Zn(II), Cu(II), Mn(II), Fe(II), NO_3^-, or $SO4^{2-}$at pH 6.5 and 8.5 on transformations of hydrous ferric oxide (HFO) as evidenced by Mossbauer spectroscopy. *Colloids Surf. A: Physicochem. Eng. Aspects* **2003**, 221, 55-68.

Jones, A. M.; Collins, R. N.; Rose, J.; Waite, T. D., The effect of silica and natural organic matter on the Fe(II)-catalysed transformation and reactivity of Fe(III) minerals. *Geochim. Cosmochim. Acta* **2009**, 73, 4409-4422.

Manceau, A., Evaluation of the structural model for ferrihydrite derived from real-space modeling of high-energy X-ray diffraction data. *Clay Miner.* **2009**, 44, 19-34.

Michel, F. M.; Ehm, L.; Antao, S. M.; Lee, P. L.; Chupas, P. J.; Liu, G.; Strongin, D. R.; Schoonen, M. A. A.; Phillips, B. L.; Parise, J. B., The structure of ferrihydrite, a nanocrystalline material. *Science* **2007**, 316, 1726-1729.

Mikutta, C., X-ray absorption spectroscopy study on the effect of hydroxybenzoic acids on the formation and structure of ferrihydrite. *Geochim. Cosmochim. Acta* **2011**, 75, 5122-5139.

Mikutta, C.; Mikutta, R.; Bonneville, S.; Wagner, F.; Voegelin, A.; Christl, I.; Kretzschmar, R., Synthetic coprecipitates of exopolysaccharides and ferrihydrite. Part 1: Characterization. *Geochim. Cosmochim. Acta* **2008**, 72(4), 1111-1127.

Nesterova, N. V.; Walton, S. A.; Webb, J., Nanoscaleiron(III) oxyhydroxy aggregates formed in the presence of functional water-soluble polymers: models for iron(III) biomineralization processes. *J. Inorg. Biochem*. **2000**, 79, 109-118.

Pallud, C.; Kausch, M.; Fendorf, S.; Meile, C., Spatial patterns and modeling of reductive ferrihydrite transformation observed in artificial soil aggregates. *Environ. Sci. Technol.* **2010a**, 44, 74-79.

Pallud, C.; Masue-Slowey, Y.; Fendorf, S., Aggregatescale spatial heterogeneity in reductive transformation of ferrihydrite resulting from coupled biogeochemical and physical processes. *Geochim*. *Cosmochim*. *Acta* **2010b**, 74, 2811-2825.

Pedersen, H. D.; Postma, D.; Jakobsen, R.; Larsen, O., Fast transformation of iron oxyhydroxides by the catalytic action of aqueous Fe(II). *Geochim*. *Cosmochim*. *Acta* **2005**, 69, 3967-3977.

Pokrovsky, O.S.; Schott, J., Iron colloids/organic matter associated transport of major and trace elements in small boreal rivers and their estuaries (NW Russia). *Chem. Geol.* **2002**, 190, 141-179.

Rancourt, D. G.; Ping, J. Y., Voigt-based methods for arbitrary-shape static hyperfine parameter distributions in mossbauer spectroscopy. *Nucl. Instrum. Methods Phys. Res., Sect. B* **1991**, 58, 85-97.

Rancourt, D. G.; Thibault, P.-J.; Mavrocordatos, D.; Lamarche, G., Hydrous ferric oxide precipitation in the presence of nonmetabolizing bacteria: constraints on the mechanism of a biotic effect. *Geochim*. *Cosmochim. Acta* 2005, 69, 553-577.

Rosso, K. M.; Yanina, S. V.; Gorski, C. A.; Larese-Casanova, P.; Scherer, M. M., Connecting observations of hematite (alpha-Fe2O3) growth catalyzed by Fe(II). *Environ. Sci. Technol*. **2010**, 44, 61-67.

Schwertmann U. and Cornell R. M., Iron Oxides in the Laboratory: Preparation and Characterization. Wiley-VCH, NY. **2000**.

Schwertmann, U.; Stanjek, H.; Becher, H. H., Long-term in vitro transformation of 2-line ferrihydrite to goethite/hematite at 4, 10, 15 and 25 _C. *Clay Miner.* **2004**, 39, 433-438.

Schwertmann, U.; Wagner, F.; Knicker, H., Ferrihydrite–humic associations: magnetic hyperfine interactions. *Soil Sci. Soc. Am. J.* **2005**, 69, 1009-1015.

Stookey, L. L., Ferrozine – A new spectrophotometric reagent for iron. *Anal. Chem*. **1970**, 42, 779-781.

Tronc, E.; Belleville, P.; Jolivet, J. P., Livage, J., Transformation of ferric hydroxide into spinel by Fe(II) adsorption. *Langmuir* **1992**, 8, 313-319.

Tufano, K. J.; Benner, S. G.; Mayer, K. U.; Marcus, M. A.; Nico, P. S.; Fendorf, S., Aggregate-scale heterogeneity in iron (hydr)oxide reductive transformations. *Vadose Zone J.* **2009**, 8, 1004-1012.

Waychunas, G. A.; Rea, B. A.; Fuller, C. C.; Davis, J. A., Surfacechemistry of ferrihydrite 0.1. EXAFS studies of the geometry of coprecipitated and adsorbed arsenate. *Geochim. Cosmochim. Acta* **1993**, *57*, 2251-2269.

Webb, S. M., SIXPack a graphical user interface for XAS analysis using IFEFFIT. *Phys. Scr.* **2005**, T115.

Yee, N.; Shaw, S.; Benning, L. G.; Nguyen, T. H., The rate of ferrihydrite transformation to goethite via the Fe(II) pathway. *Am. Miner.* **2006**, 91, 92-96.

Cornell, R. M.; Schwertmann, U., Influence of organic anions on the crystallization of ferrihydrite. *Clays Clay Miner.* **1979**, 27, 402-410.

Zachara, J. M.; Kukkadapu, R. K.; Fredrickson, J. K.; Gorby, Y. A.; Smith, S. C., Biomineralization of poorly crystalline Fe(III) oxides by dissimilatory metal reducing bacteria (DMRB). *Geomicrobiol. J.* **2002**, 19, 179-207.

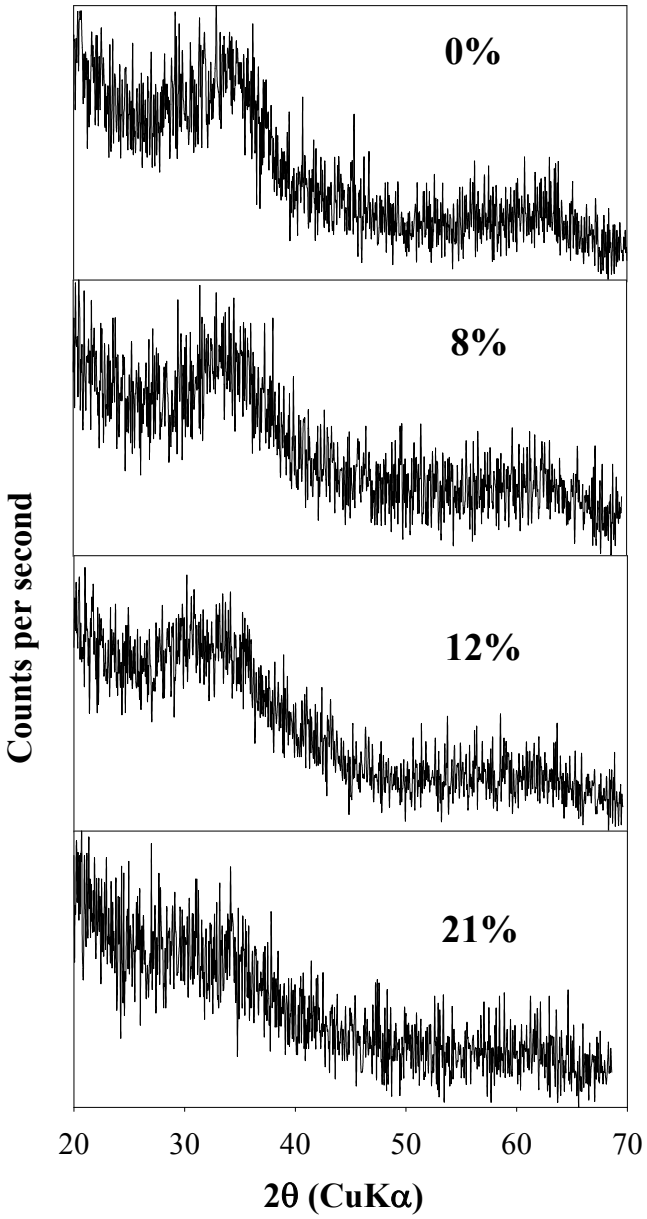

Figure 7.1 XRD patterns of ferrihydrite coprecipitated with 0-21% C.

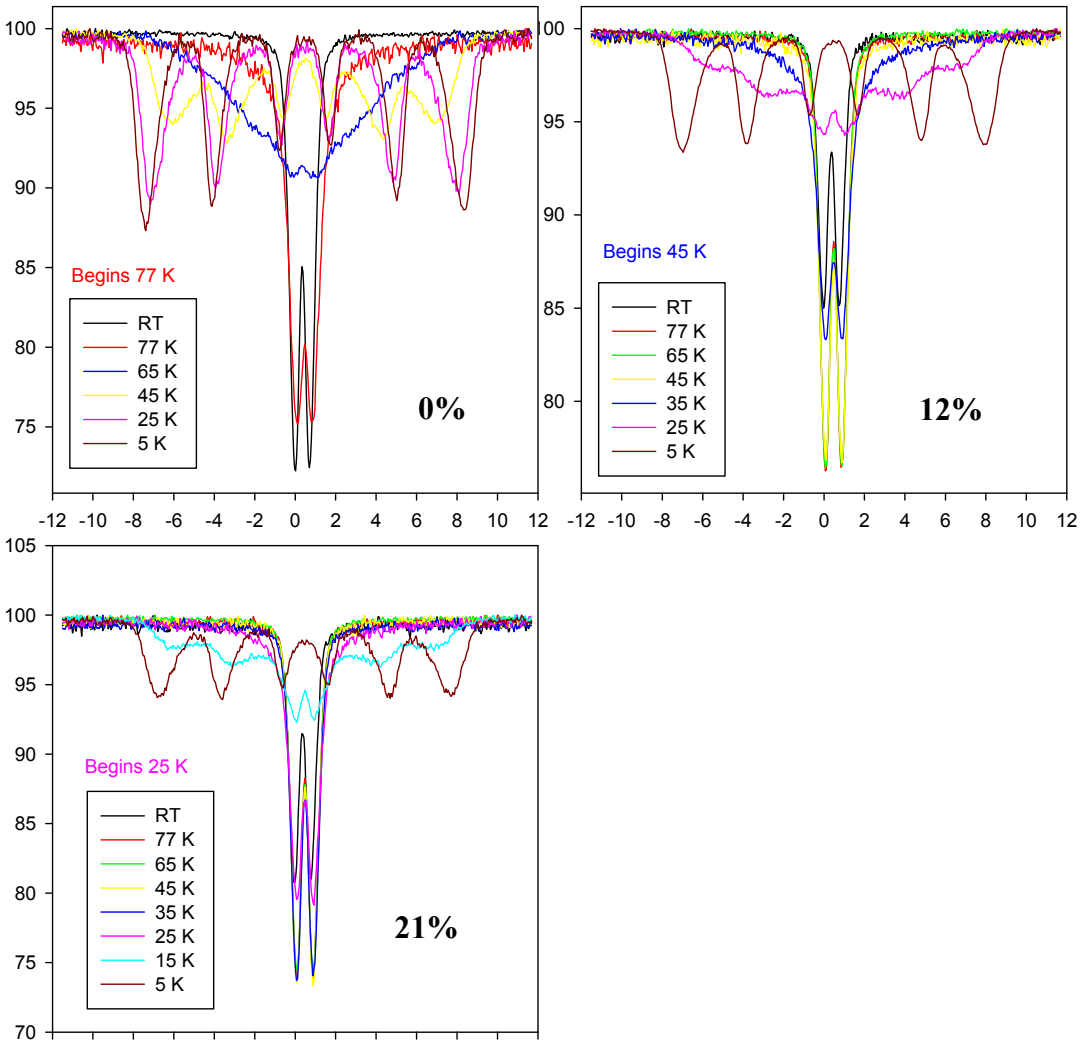

Figure 7.2 Mössbauer spectra of ferrihydrite coprecipitated with 0-21% of C at varying temperatures.

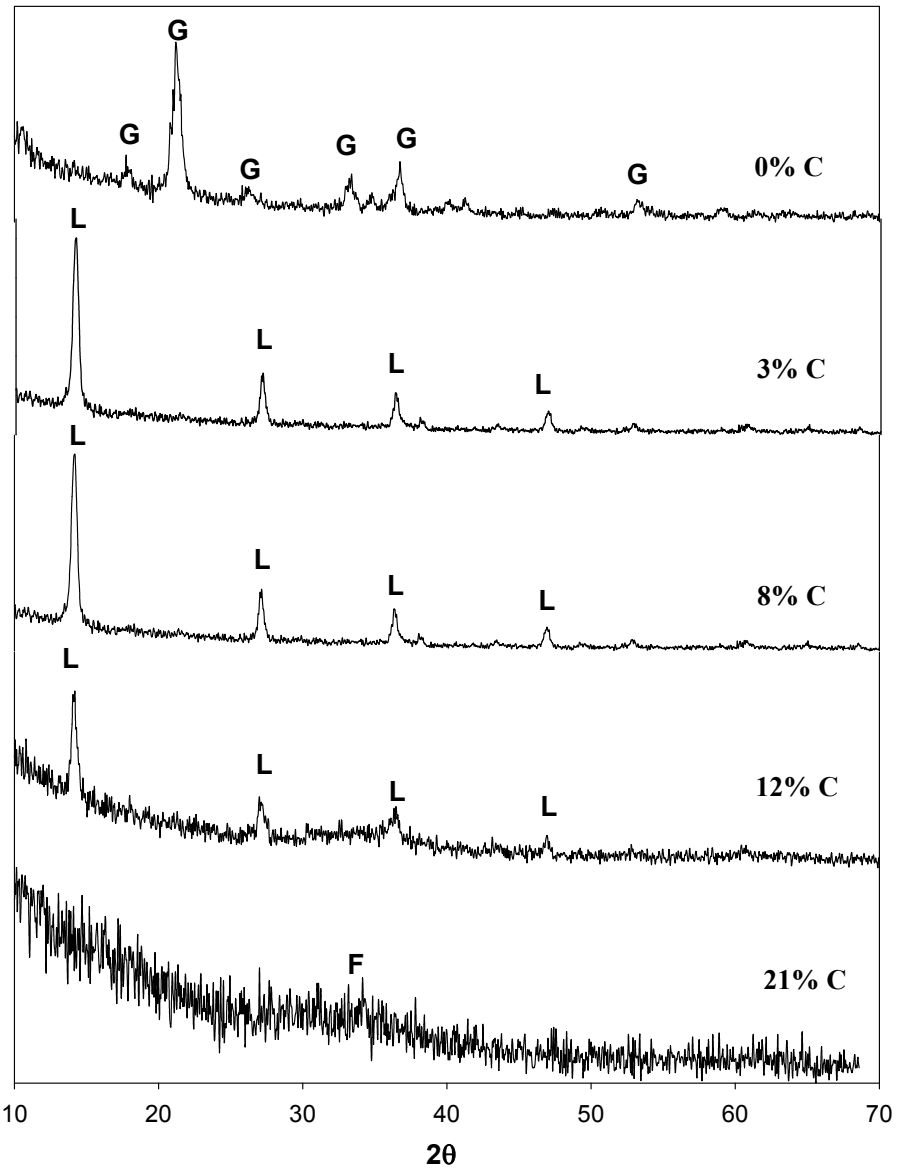

Figure 7.3 XRD patterns of the secondary minerals formed following 90 days of reaction of 0.2mM Fe(II) with ferrihydrite coprecipitated with 0-21% C. F: Ferrihydrite; L, Lepidocrocite; G, Goethite.

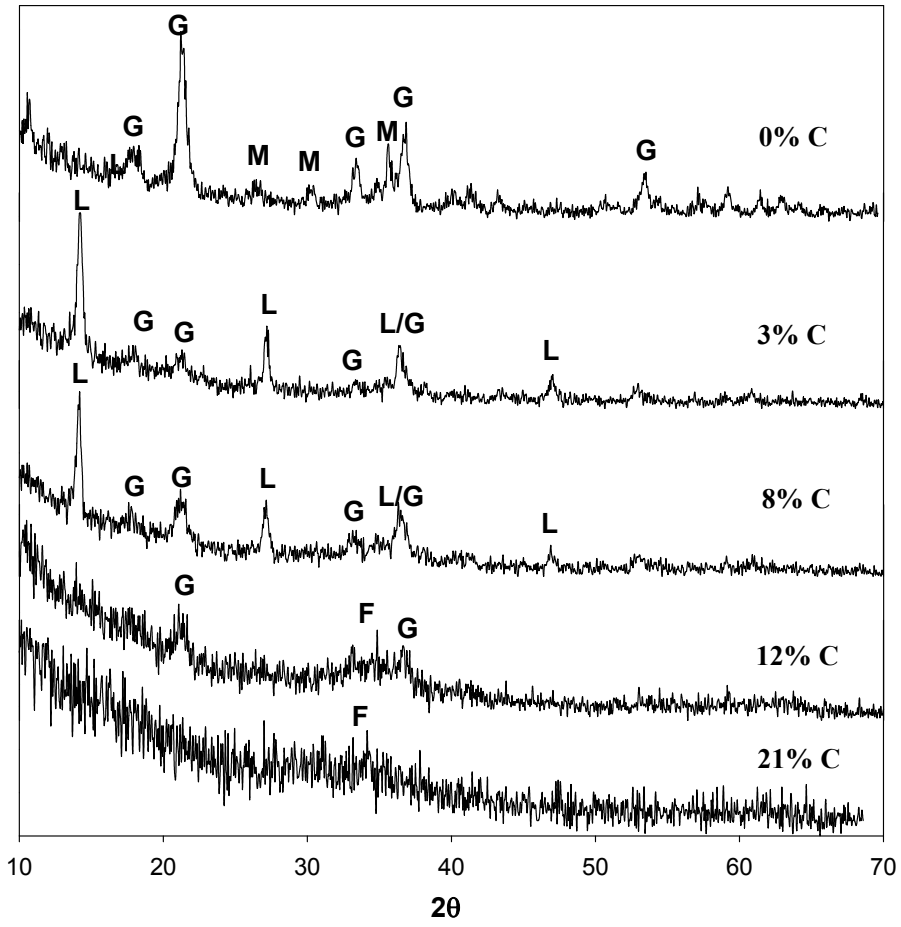

Figure 7.4 XRD patterns of the secondary minerals formed following 90 days of reaction of 2.0 mM Fe(II) with ferrihydrite coprecipitated with 0-21% C. F: Ferrihydrite; L, Lepidocrocite; G, Goethite; M, Magnetite.

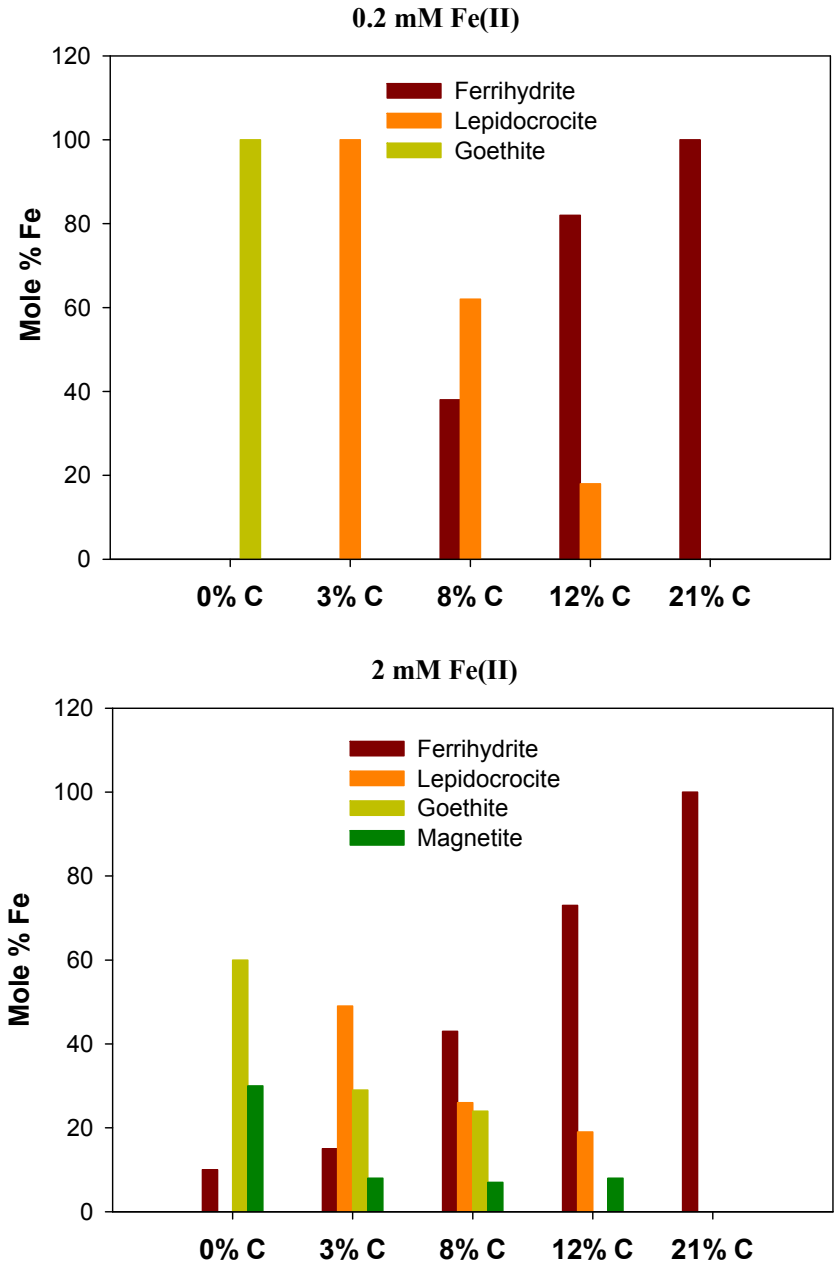

Figure 7.5 Secondary minerals formed following 90 days of reaction of 0.2 and 2.0 mM Fe(II) with ferrihydrite coprecipitated with 0-21% C. Mineral percents were obtained via linear combination fitting of Fe K-edge EXAFS spectra with reference minerals.

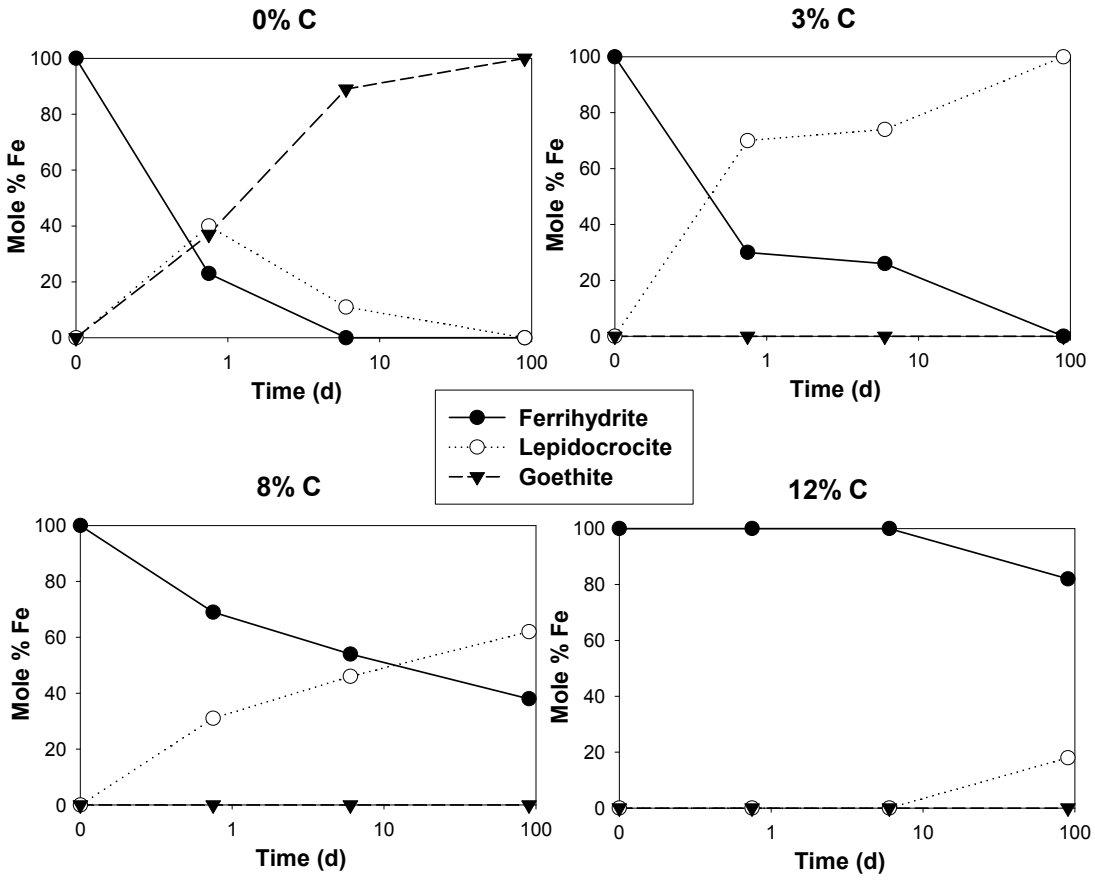

Figure 7.6 Temporal mineral distribution for the conversion of ferrihydrite coprecipitated with 0-21% of C, upon reaction with 0.2 mM Fe(II). Mineral percentages were obtained via linear combination fitting of Fe K-edge EXAFS spectra with reference minerals.

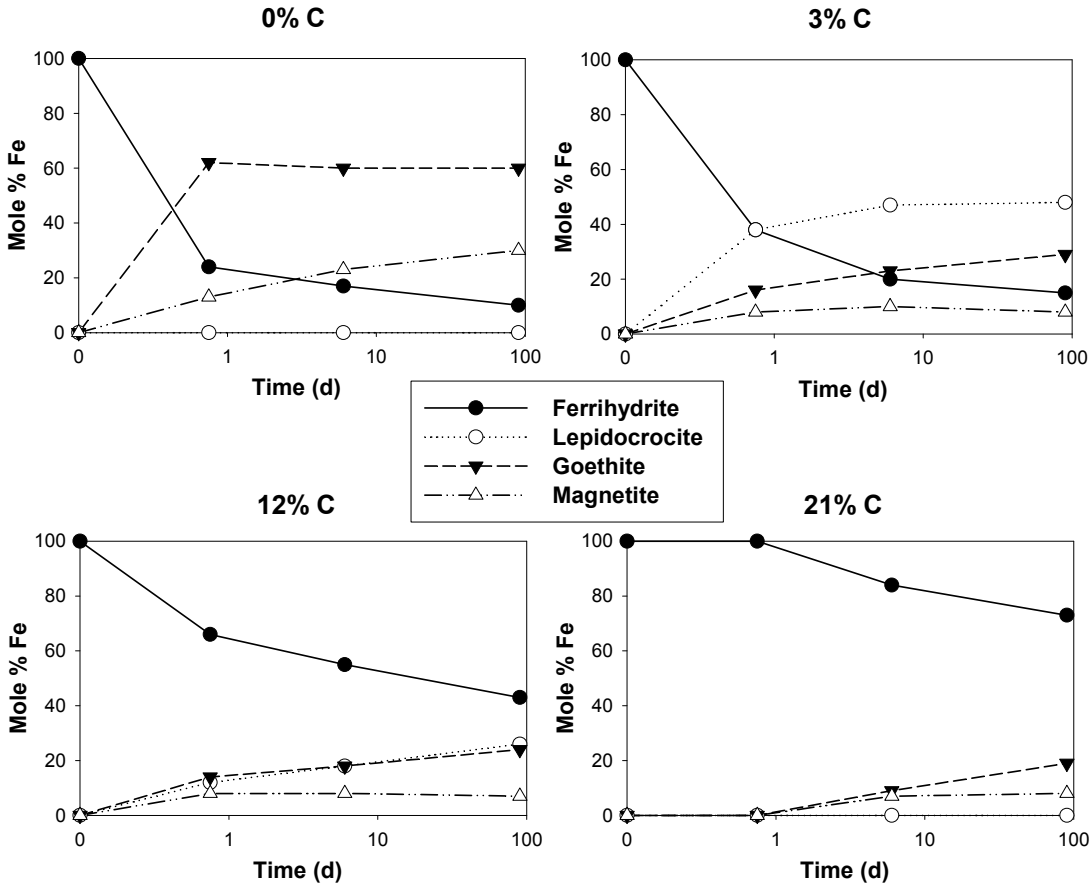

Figure 7.7 Temporal mineral distribution for the conversion of ferrihydrite coprecipitated with 0-21% of C, upon reaction with mM Fe(II). Mineral percentages were obtained via linear combination fitting of Fe K-edge EXAFS spectra with reference minerals.

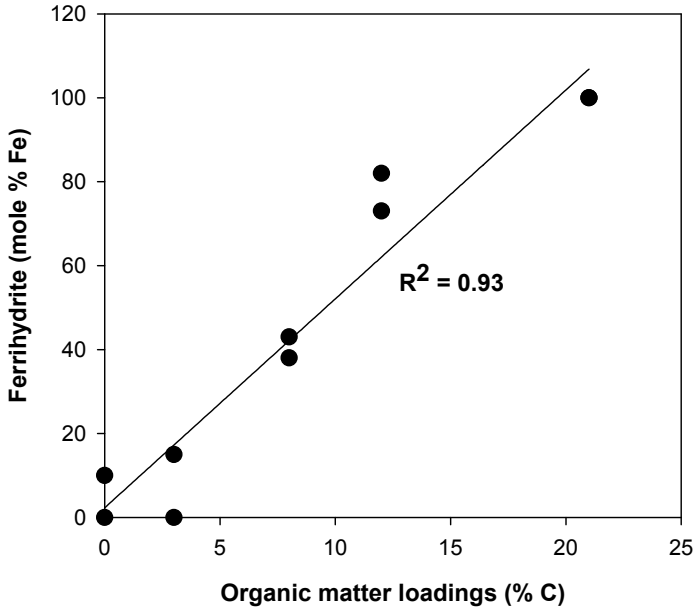

Figure 7.8 Preservation of ferrihydrite as a function of organic matter loadings on ferrihydrite, following 90 days of reaction with 0.2 and 2.0 mM Fe(II).

Chapter 8

CONCLUSIONS

8.1 Summary

The soil's ability to accumulate and retain C has received increasing interest, as the concerns about climate change grow. Organic carbon bound to minerals is considered relatively stable (Torn et al., 1997, 2005; Kalbitz et al., 2005; Mikutta et al., 2006) and controls the long-term sequestration of organic matter in soils. Organic matter stabilization by minerals has been envisioned as a combined effect of the mineralogical properties (surface area and charge) and the composition of the OM involved, with aromatic structure being most resistant to microbial decomposition (Kalbitz et al., 2005; Mikutta et al., 2007).

Whereas the chemical composition of soil OM has been subject to numerous studies, little is known about the structural changes of SOM as a function of landscape topographic position. In this study, we combined NEXAFS spectroscopy and Py-FIMS to characterize SOM at different soil depths and landscape topographic positions along a pasture hillslope. These two techniques were able to reveal common trends among soil depths and landscape topographic locations. The relative amount of recalcitrant aromatic C compounds and lignin materials, including alkylaromatics and

phenols and lignin monmers, increased with soil depth, while the proportions of lipid-like compounds such as alkanes, alkenes, n-alkyl esters, sterols and fatty acids decreased with soil depth. In addition, the poorly-drained footslope soil was enriched in recalcitrant aromatic C compounds and lignin materials including alkylaromatics and phenols and lignin monomers. Carbohydrates, N-containing compounds, and phenols and lignin monomers showed increasing thermal stability at deeper depths and poorly-drained footslope locations. Collectively, this study suggests that organic compounds are more recalcitrant and stable in the subsoils and depressional landscape locations.

Scanning transmission X-ray microscopy (STXM) of high spatial resolution, combined with NEXAFS spectroscopy, represents the most direct way to observe organic matter-mineral interactions (Wan et al., 2007). It enables direct assessment of distribution and speciation of C and major cations and their associations in organo-mineral assemblages. In this study, STXM-NEXAFS at the C1s, Ca 2p, Fe 2p, Al 1s and Si 1s edges was used to investigate C associations with Ca, Fe, Al and Si species in soil clay fractions from a .pasture hillslope. Bulk techniques including Fe EXAFS and XRD were also applied to provide supplementary information. The C NEXAFS results clearly demonstrated that aromatic C=C, carboxyl and polysaccharides were the major C functional groups intimately associated with soil mineral phases, despite variability in the distribution of C species on mineral surfaces. This study suggests the importance of Ca in organo-metal-mineral interactions and/or organo-metal cation omplexation, although no definite conclusion could be drawn on the specific role of

Ca in OM-mineral interactions. The mineral matrix in these soils was composed of Fe(III) oxides (hematite, goethite, and ferrihydrite), quartz and phyllosilicates, including hydroxyl-interlayered vermiculite, illite and kaolinite. C showed similar correlation with Fe to Al and Si. This study is among the first spectromicroscopic investigations of organo-mineral assemblages in soils. Overall, our results show the progress towards examining, at the sub-micron-level, compositional chemistry and associative interactions between organic matter and the mineral matrix.

Iron oxides are important in OM-mineral interactions because of their abundance and reactivity. Iron oxides with short-range crystal order and small particle sizes contain more reactive surface area compared to other bulk Fe-oxides (Cornell and Schwertmann, 2003; Bonneville et al., 2004). Soil redox conditions affect not only the amount but also the mineralogical composition of Fe mineral phases. This research applied EXAFS and Mössbauer spectroscopy to characterize Fe mineral phases in a floodplain soil profile with spatially sharp redox gradients. Results showed that soil redox conditions had an important control on soil Fe mineralogy. The permanent reducing conditions led to a complete reductive dissolution of Fe(III) oxides. Therefore, the importance of Fe oxides in OM-mineral interactions would be expected to decrease with decreasing redox levels. In addition, the reducing conditions resulted in a strong reduction in the structural Fe(III) in the phyllosilicates. The impacts of redox cycling of structural Fe in phyllosilicates on carbon and metal cycling remain largely unknown and need to be further explored.

Poorly-crystalline Fe oxy-hydroxide ferrihydrite, because of its prevalence in the environment and high surface area, is of particular importance in organic matter retention. In soils, poorly-crystalline Fe oxides like ferrihydrite, often precipitates from solutions containing varying amounts of dissolved organic matter. This leads to coprecipitation of OM with ferrihydrite. In contrast to adsorption studies, the coprecipitation process has received relatively little attention. In this study, we compared ferrihydrite-OM complexes formed via adsorption and coprecipitation with dissolved organic matter extracts from a forest litter layer. Our study demonstrated that coprecipitation resulted in a significantly greater amount of C retained with the solid phase and greater C stability than adsorption, supporting the contention that coprecipitation might be an important process contributing to the accumulation and stabilization of OM in natural environments. Iron EXAFS measurements revealed that coprecipitation of OM with Fe led to the formation of OM-Fe(III) cation complexes in the solid phase by suppressing ferrihydrite formation, which might be related to a significantly greater organic carbon (OC) retention for coprecipitation than adsorption, The strong chemical C-O-Fe bonds formed in the process of adsorption and coprecipitation and selective uptake of aromatic C might contribute to stabilizing organic matter by minerals. This study also demonstrated the spatial distribution of C on ferrhydrite at the nanometer scale for the first time. Although studies on natural soils have shown that C displays a heterogeneous distribution on soil minerals, this study showed that C distribution on ferrihydrite was relatively uniform at lower surface loadings. However, at higher C loadings, the spatial distribution of C on

ferrihydrite became heterogeneous. This study also provided possible evidence for the formation of organic multilayers on minerals at higher C loadings.

The ripening of ferrihydrite to more stable and hence less reactive phases such as goethite is catalyzed by surface reaction with aqueous Fe(II) (Hansel et al., 2005). While ferrihydrite within most natural environments contains high concentrations of co-precipitated organic matter, little is known regarding the impact of this OM on the reactivity of ferrihydrite. In this study, we investigated the structural characteristics of OM-Fe coprecipitates and explored the extent, pathways and products of Fe(II)-induced secondary mineralization of OM-Fe coprecipitates by reacting with aqueous Fe(II) (0.2 and 2.0 mM). Results indicated that the coprecipitated OM decreased crystallinity of ferrihydrite. Organic matter stabilizes ferrihydrite, impeding its transformation to more thermodynamically stable products. We observed a linear ($R^2 = 0.93$) increase in ferrihydrite preservation with increasing OM loadings on ferrihydrite .OM levels above 21% C will result in completely inhibited ferrihydrite transformation. At low Fe(II) levels, the coprecipitated OM impeded goethite formation, while magnetite nucleation, in addition to goethite formation, was inhibited by OM at high Fe(II) levels. These findings provide insight into mechanisms that may be responsible for ferrihydrite preservation and low levels of secondary magnetite typically found in sedimentary environments. Considering the preponderance of organic matter on ferrihydrite in soils and sediments, the reactivity of natural (compromised) ferrihydrites and the subsequent impact on mineral evolution needs to be more fully explored.

8.2 Recommended Future Research

8.2.1 Investigating the role of Ca in organic matter-mineral interactions in soils

The STXM-NEXAFS analysis of pasture soils in this study demonstrated good C-Ca correlations and carbonate was not detected, suggesting that Ca plays an important role in organo-mineral assemblage formation in these soils. Organic anions are normally repelled from negatively charged surfaces in soils. Calcium can facilitate binding of organic compounds to permanently negative-charged siloxane surfaces or to the hydroxyls of phyllosilicates and oxides via "cation bridging". In addition, dissolved organic matter can also be precipitated by metal ions such as Ca^{2+} (von Lützow et al., 2006) and thus organic matter- Ca precipitates might also be present in the soils. Organic-metal ion (such as Ca^{2+}) complexation has been considered as potentially stabilizing soil OM (Baldock & Skjemstad, 2000). Therefore, the good C-Ca correlation could be a result of Ca-bridging and/or OM-Ca^{2+} precipitates in soils. It is uncertain which mechanism would play the major role based on the current study. Thus, the specific interactive mechanisms of organic matter, calcium and the soil mineral matrix need to be assessed in future studies. Investigating the role of Ca in OM-mineral interactions in agricultural soil is particularly important, since application of Ca amendments such as calcite and dolomite to soils has been a common agricultural practice to counteract natural acidifying processes. It remains largely unknown how and by which mechanism(s) the Ca amendments affect the OM-mineral interactions.

8.2.2 Assessing the importance of Fe oxides in organic matter-mineral interactions along wide redox and mineralogical gradients

Soil redox conditions affect not only the amount, but also the mineralogical composition of Fe mineral phases. This study showed that anoxic conditions led to a reductive dissolution of Fe(III) oxides. The degree of reduction increased with decreasing redox levels, and thus the amount of Fe oxides decreased with decreasing redox levels. At permanent anoxic conditions, complete reductive dissolution of Fe oxides occurred. Therefore one could hypothesize that the importance of Fe oxides in OM-mineral interactions would decrease with decreasing redox levels. However, under intermediate redox levels, where Fe oxides were partially reduced, Fe oxides with smaller particle size and lower crystallinity were relatively enriched. This makes the assessment of the importance of Fe oxides under varying redox conditions more complicated. The direct assessment of the role of Fe oxides in OM-mineral interactions under different redox condtions is lacking and deserves further study.

STXM analysis of pasture soils showed that C was associated with both phyllosilicates and Fe(III) oxides with Fe(III) oxides being slightly more prominent than phyllosilicates in C-mineral association, as inferred from a better correlation of C with Fe than with Al and Si. In these Utisols, the Fe(III) oxide content was low (< 2%). In addition, most of the Fe(III) oxides were crystalline goethite and hematite This is probably why we only observed a slightly better correlation of C with Fe than with Al and Si as amorphous and poorly crystalline minerals (e.g,. ferrihydrite) are more powerful in stabilizing OC in the soils. In order to fully investigate the role of Fe(III)

oxides in C-mineral associations in soils, further study on soils with varying Fe oxide content and crystallinity is highly recommended. For example, tropical soils usually contain very high amounts of Fe oxides mainly as hematite, whereas poorly-crystalline Fe oxides such as ferrihydrite are dominant in Andosols. Of particular interest for future research is to expand this investigation by including soils with a wider range of mineralogical composition such as tropical soils and Andosols. Such a study will help to develop a clearer understanding of specific OM-mineral associations in a wide variety of soil types.

8.2.3 Examining the impacts of organic matter associations on Fe oxides on the mobility of metal(oid)s

Associations of organic matter on Fe(III) oxides is universal in soils. The structure and reactivity of Fe oxides in natural soils are influenced by organic matter. This study indicated that organic matter association with poorly-crystalline ferrihydrite impeded its transformation to more stable Fe oxide phases, after reacting with reductants such as Fe(II). Previous studies have also demonstrated that organic compounds can kinetically retard, and in some instances, completely prevent, the transformation of Fe(III) minerals to more crystalline, thermodynamically stable forms of Fe(III) in the absence of Fe(II) (Cornell and Schwertmann, 1979; Cornell and Schneider, 1989; Mayer and Jarrell, 1996; Schwertmann and Thalmann, 1976). Dissolved humic substances have been shown to stimulate microbial reduction of poorly soluble Fe(III) minerals by acting as electron shuttles between cells and

minerals (Kappler et al., 2004). However, the effect of solid-phase associated organic matter on the microbial transformation of iron minerals remains largely unknown. Metal(oid)s, such as arsenic desorption from soils/sediments, is primarily controlled by the reductive dissolution of Fe(III) oxides (Smedley and Kinniburgh, 2002; Ahmed et al., 2004). The rate and extent of Fe oxide dissolution and transformation are critical to the fate of metal(oid)s. Owing to its reactivity and propensity to transform, metal(oid) retention/release upon microbial reduction of ferrihydrite is of particular importance. Despite the prevalence of organic matter associations with Fe oxides in natural environments, the role of the bound organic matter on ferrihydrite reduction and metal(oid) release is not well understood and deserves future exploration.

REFERENCES

Bonneville, S.; Van Cappellen, P.; Behrends, T. Microbial reduction of iron(III) oxyhydroxides: effects of mineral solubility and availability, *Chem. Geol.* **2004**, 212, 255-268.

Cornell, R. M.; Schwertmann, U. The iron oxides: characterization. In: *The Iron Oxides,*R.M. Cornell and U. Schwertmann, Eds, VCH, New York, NY, **2003**.

Kalbitz, K.; Schwesig, D.; Rethemeyer, J.; Matzner, E. Stabilization of dissolved organic matter by sorption to the mineral soil. *Soil Biol. Biochem.* **2005**, 37, 1319-1331.

Mikutta, R.; Kleber, M.; Torn, M. S.; Jahn, R. Stabilization of soil organic matter: Association with minerals or chemical recalcitrance? *Biogeochem*. **2006**, 77(1), 25-56.

Mikutta, R.; Mikutta, C.; Kalbitz, K.; Scheel, T.; Kaiser, K.; Jahn, R. Biodegradation of forest floor organic matter bound to minerals via different binding mechanisms. *Geochim. Cosmochim. Acta* **2007**, 71, 2569-2590.

Torn, M. S.; Trumbore, S. E.; Chadwick, O. A.; Vitousek, P. M.; Hendricks, D. M. Mineral control of soil organic carbon storage and turnover. *Nature*, **1997**, 389, 170-173.

Wan, J. M.; Tyliszczak, T.; Tokunaga, T. K., Organic carbon distribution, speciation, and elemental correlations with soil micro aggregates: applications of STXM and NEXAFS spectroscopy. *Geochim. Cosmochim. Acta*, **2007**, 71(22), 5439-5449.

von Lützow, M.; Kögel-Knabner, I.; Ekschmitt, K.; Matzner, E.; Guggenberger, G.; Marschner, B.; Flessa, H. Stabilization of organic matter in temperate soils: mechanisms and their relevance under different soil conditions - a review. *Eur. J. Soil Sci*. **2006**, 57, 426-445.

Appendix A

ADDITIONAL STXM-NEXAFS, FE K-EDGE EXAFS AND C & N BULK NEXAFS DATA OF CHAPTER 3

Materials and Methods

Site description

The watershed has a long history of human impacts starting with agricultural expansion during the colonial era. Currently, 23% of the watershed is covered with forests (Newbold et al., 1997). Approximately 52% of the watershed area is in pasture for horses and cattle, and 22% is tilled primarily for maize, soybeans and winter wheat or hayed (alfalfa).The remaining land (~3%) is in residential use, a commercial catering establishment, and the Stroud Water Research Center (Newbold et al., 1997).

STXM Data Analysis

Energy Scale Calibration: The energy scale of C-1s spectra was calibrated by using the CO_2 absorption peak (C 3p) at 294.96 eV by measuring CO_2 gas spectra before or after the measurements. The Ca-2p spectra were calibrated internally using the main $2p_{1/2} \rightarrow 3d$ resonance peak at 352.6 eV (Benzerara et al., 2004). The absolute energy scale in the Fe 2p region was set by assigning the energy of the second peak in the $Fe2p_{3/2}$ signal of $FeCl_3 \cdot 6H_2O$ to 709.8 eV (Dynes et al., 2006); for Al 1s, the 1s-4p

peak of muscovite was set to 1570.4 eV (Yoon et al., 2004); and for Si 1s, the t_2 peak of muscovite was set to 1846.4 eV (Li et al., 1995).

Reference Spectra for Cation (Ca, Fe, Al and Si) Speciation: Calcite ($CaCO_3$), sorbed Ca on EPS and calcium phosphate ($CaHPO_4 \cdot 2H_2O$) were used as Ca 2p reference compounds. Reference spectra of $FeCl_3.6H_2O$ (Fe(III)) and $FeCl_2.4H_2O$ (Fe(II)) were collected. The Al 1s and Si1s reference spectra of muscovite were determined using a muscovite sample from the Stanford Mineral Collection. A density of 2.82 g $cm^{-3}$and a structural formula of $KAl_2(AlSi_3O_{10})(OH)_2$ were used. The other Si 1s reference spectrum was coesite (SiO_2) (d=3 g cm^{-3}).

Characteristics of Bulk Soils

The soil was air-dried, ground, and passed through a 2 mm sieve. The particle size measurements and cation exchange capacity were analyzed for < 2 mm samples (Table A3.4) at the Soil Testing Lab at the University of Delaware. Particle size distribution was determined using the hydrometer method with a standard hydrometer (ATSM152H); Cation Exchange Capacity (CEC) was determined by a method described by Sumner and Miller (1996); and exchangeable cations (Ca, Mg, Na, K) were measured by inductively coupled plasma atomic emission spectroscopy (ICP-AES, Thermo Intrepid II XSP ICP) after extracting the soil with a 1M NH_4OAc solution at pH 7.

Chemical Analysis of Soil Clay Fractions

Carbon concentration was analyzed by dry combustion with a C/N elemental analyzer. The different Fe fractions in the soils were determined by extraction methods. The

crystalline and poorly crystalline Fe oxides (Fe_d) were extracted from 0.2 g of the freeze-dried soil clays with 0.4 g sodium dithionite dissolved in 30 ml of a 0.57 M sodium citrate solution for 12 hours (Soil Survey Laboratory Methods Manual, 2004). The poorly crystalline Fe oxides were extracted with 0.275 M ammonium oxalate in darkness at pH 3.25. Total Fe (Fe_t) and elemental concentrations were measured using EPA 3051 microwave digestion. The extracts and digestion were analyzed by ICP-AES.

Soil Clay Mineralogy Characterization by XRD

X-ray diffraction (XRD) analyses were conducted on the clay fractions. Clay samples were oriented and mounted on glass slides with the following standard treatment: Mg-saturation, Mg-Glycerol saturation, K-saturation, and heat treatment of K-saturated samples at 300 ºC and 550ºC (Soil Survey Laboratory Methods Manual, 2004). XRD analyses were made with a Rigaku D/Max 2200 diffractometer producing Cu-kα radiation with a wavelength of 0.154 nm. The scan range was from 5º to 35º with a step size of 0.05º. The mineral identification and semi-quantitative estimates of clay mineral compositions were made according to the XRD parameters of common soil minerals (Soil Survey Laboratory Methods Manual, 2004).

Bulk Carbon and Nitrogen NEXAFS Spectroscopy

The bulk C and N *K*-edge NEXAFS data were acquired at the SGM beamline located at the Canadian Light Source (CLS), Saskatoon, Canada. The soil clay samples were mixed with C-free nanopure water and then deposited onto gold-coated silicon wafers. C (1s) and N (1s) NEXAFS spectra of the samples were recorded from 270 to 312 eV

and from 390 to 420 eV, respectively, in steps of 0.1eV using a dwell time of 500 ms. Exit slit gap was 50 μm. Background measurements were collected by measuring an empty gold-coated silicon wafer. A Ti filter was used in the beamline to reduce the effects of second order oxygen in the pre-edge region. In order to minimize beam damage to organic matter, we collected only one spectrum from one spot. Six spectra were collected from each sample and averaged. The C NEXAFS spectra were energy calibrated using the 1s $\rightarrow \pi^*_{C=O}$ transition of glutaric acid at 288.6 eV (Kim et al., 2003) and the 1s $\rightarrow \pi^*$ vibrational manifold of N_2 gas at 400.8 eV evolved from $(NH_4)_2SO_4$ was used for the N edge calibration (Gillespie et al., 2008).

Fe K-edge X-ray absorption spectroscopy

Method. Soil clay fraction samples from the summit and footslope were examined by X-ray absorption spectroscopy (XAS) to determine Fe speciation. Iron K-edge extended X-ray absorption fine structure (EXAFS) spectra were collected on beamline 4-1 at the Stanford Synchrotron Radiation Facility (SSRL). Samples and reference standards were mounted as thin powders between Kapton tape. Mounted samples were placed in a He-purged sample chamber at room temperature and four to six replicate spectra were collected using a Lytle detector with energy calibrated against an Fe(0) foil (7112 eV). X-ray energy resolution was maintained by a crystal Si(220) monochromator. The Sixpack program was used for standard background subtraction and edge-height normalization (Webb, 2005). Iron speciation of the samples was quantified by least squares fitting (LCF) of k^3-weighted EXAFS oscillations in the 2–11$Å^{-1}$ range, to selected reference standards using the Sixpack program. LCF analysis

of the sample spectra was started with the reference spectrum giving the lowest R-factor (Kelly et al., 2008). A best-fit involving n+1 components was only considered to be superior to the best n-component fit if the R-factor decreased by more than 10% (relative). No energy shift was included in the LCF and the sum of the fitted fractions was not constrained (LCF data are presented normalized to 100%).

Reference Spectra. For the analysis of the Fe-K EXAFS spectra of soil clay fractions by linear combination fitting, the reference compounds listed below were considered.

Illite (IMt-1): from Source Clays Repository, Clay Minerals Society

Fe(III)-Oxalate ($Fe_2(C_2O_4)_3$): Aldrich 98% pure

Fe(III)-Citrate Hydrate ($C_6H_5FeO_7$): Aldrich 98% pure

Nontronite (NAu-1): from Source Clays Repository, Clay Minerals Society

Smectite (SWy-2): from Source Clays Repository, Clay Minerals Society

Vermicullite (VTx-1): from Source Clays Repository, Clay Minerals Society

Ferrihydrite ($Fe(OH)_3$): synthesized from $Fe(NO_3)_3.9H_2O$ and KOH according to the 2-line ferrihydrite method of Schwertmann and Cornell (1991).

Goethite (FeOOH): synthesized from $Fe(NO_3)_3.9H_2O$ and KOH according to the method of Schwertmann and Cornell (1991).

Lepidocrocite (FeOOH): synthesized from $FeCl_2.4H_2O$ and NaOH according to the method of Schwertmann and Cornell (1991).

Hematite (Fe_2O_3): synthesized from $Fe(NO_3)_3.9H_2O$ according to the precipitation method of Schwertmann and Cornell (1991).

Results and Discussion

Bulk C and N near edge X-ray absorption fine structure (NEXAFS) spectroscopy

The challenge with STXM is that we can only image small portions of soil samples. This limits our ability to compare C speciation in soils as influenced by landscape topography. Compared to STXM, the SGM beamline is a bulk beamline, and with a beam spot size of 1000 μm × 100μm, allows one to perform bulk C and N near-edge X-ray absorption fine structure (NEXAFS) analyses on soil samples. Another great advantage of this technique is that it allows one to characterize in-situ soil organic matter without extraction. Soil organic matter extraction techniques are controversial, and may cause alterations and artifacts.

Fig.A.11 shows C NEXAFS spectra collected at the bulk SGM beamline. The summit and footslope soils displayed major features at 288.5 eV for aromatic C, 288.6 eV for carboxyl C and 289.5 eV for polysaccharides. This agrees with C NEXAFS results from the STXM technique, suggesting results from the STXM technique may represent the whole soil, although it only images a small portion of soil samples. A minor peak at 287.4 eV for aliphatic C was present in the summit soil but disappeared in the footslope soil. In addition, compared to the summit soil, the footslope soil was slightly enriched in aromatic C. These results suggest a selective preservation of recalcitrant aromatic C in the footslope soil. According to the field observation, the footslope soil may experience poorly-drained conditions after heavy rainfall. Due to

periodic O_2 deficiency, decomposition of aromatic lignin material may be limited at the footlsope soil, compared to the summit soil.

The N NEXAFS spectra in Fig.A.12 showed features at 398.7 eV (i), an intensive feature at 401.2 eV (ii) and a broad peak at 405.8 eV (iii). These peaks are assigned to aromatic C in six-membered rings (pyridines, pyrazines) and/or non-peptide C=N as in aliphatic imines (i), and amide (protein) N (ii) (Leinweber et al., 2007). The broad feature (iii) can be assigned to overlapping 1s→σ* transition of various N moieties (Leinweber et al., 2007). The summit and footslope soils showed similar N NEXAFS spectra. There was a very small peak at 398.7 eV (i) in both soils, indicating a small contribution of aromatic pyridines, pyrazines and/or aliphatic imines to soil total nitrogen. N NEXAFS spectra of both soils showed a strong feature at 401.2 eV, indicating amide (protein) N dominates in these soils. The dominance of the amide N feature agrees with previous N NEXAFS studies from soils and soil related materials (Gillespie et al., 2009; Gillespie et al., 2011; Leinweber et al., 2010a; Leinweber et al., 2010b). Protein and amide N is widely reported to be the largest soil N pool (Stevenson 1982; Schulten & Schnitzer, 1998).

References in Appendix A

Benzerara, K.; Yoon, T. H.; Tyliszczak, T.; Constantz, B.; Spormann, A. M; Brown, G. E., Scanning transmission X-ray microscopy study of microbial calcification. *Geobiology* **2004**, 2, 249-259.

Burt, R., (Ed.), Soil Survey Laboratory Methods Manual, Soil Survey Investigations Report No. 42 Version 4.0. Lincoln, NE: Natural Resources Conservation Service, U.S. Department of Agriculture. **2004**.

Dynes, J. J.; Tyliszczak, T.; Araki, T.; Lawrence, J. R.; Swerhone, G. D. W.; Leppard, G. G.; Hitchcock, A. P., Speciation and quantitative mapping of metal species in microbial biofilms using scanning transmission X-ray microscopy. *Environ. Sci. Technol*. **2006**, 40(5), 1556-1565.

Gillespie, A.W.; Walley, F. L.; Farrell, R. E.; Regier, T.Z.; Blyth, R.I.R., Calibration method at the N K-edge using interstitial nitrogen gas in solid-state nitrogen-containing inorganic compounds. *J. Synchrotron Radiat.* **2008**, 15, 532-534.

Gillespie, A.W;.Walley, F.L.; Farrell, R.E.; Leinweber, P.; Schlichting, A.; Eckhardt, K.U.;Regier, T.Z.; Blyth, R.I.R., Profiling rhizosphere chemistry: evidence from carbon and nitrogen K-Edge XANES and Pyrolysis-FIMS. *Soil Sci. Soc. Am. J.* **2009**, 73, 2002-2012.

Gillespie, A.W.; Farrell, R.E.; Walley, F.L.; Ross, A.R.S.; Leinweber, P.; Eckhardt, K.U.; Regier, T. Z.; Blyth, R.I.R., Glomalin-related soil protein contains non-mycorrhizal-related heat-stable proteins, lipids and humic materials. *Soil Biol. Biochem.* **2011**, 43, 766-777.

Kelly S. D.; Hesterberg D.; Ravel B., Analysis of soilsand minerals using X-ray absosrption spectroscopy. In Methodsof Soil Analysis Part 5 – Mineralogical Methods (eds. A. L.Ulery and R. Drees). Soil Science Society of America. **2008**.

Kim, J.S.; Ree, M.; Lee, W.S.; Oh, W.; Baek, S.; Lee, B.; Shin, T.J.; Kim, K.J.; Kim, B.; Luning, J., NEXAFS spectroscopy study of the surface properties of zinc glutarate and its reactivity with carbon dioxide and propylene oxide. *J. Catal.* **2003**, 218, 386-395.

Leinweber, P.; Kruse, J.; Walley, F. L.; Gillespie, A.; Eckhardt, K. U.; Blyth, R. I. R.; Regier, T. Z. Nitrogen K-edge XANES – an overview of reference compounds used to identify 'unknown' organic nitrogen in environmental samples. *J. Synchrotron Radiat.* **2007**, 14, 500-511.

Leinweber, P.; Kruse, J.; Walley, F. L.; Gillespie, A.W.; Eckhardt, K. U.; Blyth, R. I. R.; Regier, T. Z., Nitrogen compounds in dissolved and solid environmental samples. B. Singh, M. Gräfe (Eds.), Developments in Soil Science – Synchrotron-Based Techniques in Soils and Sediments, vol. 34 Elsevier, Oxford (2010), **2010a**, 55-288.

Leinweber, P.; Jandl, G.; Eckhardt, K.U.; Kruse, J.; Walley, F. L.; Khan, M. J.; Blyth, R. I. R.; Regier, T. Z.; Nitrogen speciation in fine and coarse clay fractions of a Cryoboroll – new evidence from pyrolysis-mass spectrometry and nitrogen K-edge XANES. *Can. J. Soil Sci.* **2010b,** 90, 309-318.

Li, D.; Bancroft, G, M.; Fleet, M. E.; Feng, X. H., Silicon K-edge XANES spectra of silicate minerals. *Phys. Chem. Miner.* **1995,** 22, 115-122.

Newbold, J. D.; Bott, R. L.; Kaplan L. A.; Sweeney, B. W.; Vannote, R. L., Organic matter dynamics in White Clay Creek, Pennsylvania, USA. *J. North Am. Benthological Soc*. **1997**, 16(1), 46-50.

Schulten, H. R.; Schnitzer, M., The chemistry of soil organic nitrogen: a review. *Biol. Fert. Soils* **1998**, 26, pp. 1-15.

Stevenson, F. J., Nitrogen in Agricultural Soils. Agronomy Monograph 22, American Society of Agronomy, Wisconsin, Madison. **1982**.

Sumner, M. E.; Miller, W. P., Cation exchange capacity and exchangecoefficients. p. 1201–1229. *In* D.L. Sparks (ed.) Methods of soil analysis.Part 3. Chemical analysis. SSSA Book Ser. 5. SSSA, Madison, WI. **1996**.

Schwertmann, U.; Cornell, R. M., Iron oxides in the laboratory: Preparation and characterization, 137 p. Weinheim, New York. **1991**.

Webb S. M., SIXPack a graphical user interface for XASanalysis using IFEFFIT. Phys. Scr. T115. **2005**.

Yoon, T. H.; Johnson, S. B.; Benzerara, K.; Doyle, C. S.; Tyliszczak, T.; Shuh, D. K.; Brown, G. E. Jr., In situ characterization of aluminum coating mineral-microorganism aqueous suspensions using scanning transmission x-ray microscopy. *Langmuir* **2004**, 20, 10361-10366.

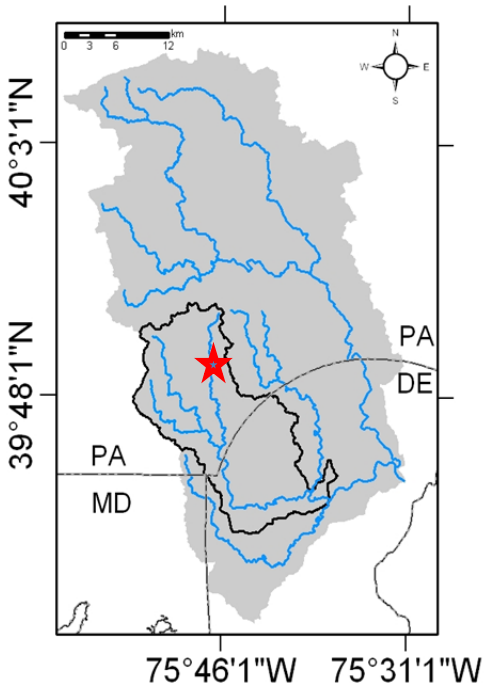

Figure A.1 Map of Christina River Basin (~1440 km^2). The study area of Stroud Watershed is marked by the pentagram symbol.

Figure A.2 Picture of the sampled pasture hillsope transect.

Table A.1 X-ray energies, difference between mass attenuation coefficients above and below the absorption edge (μ), and approximate resonance enhancements (RE) used for elemental mapping, according Wan et al. (and references therein).

Edge	Pre-edge (eV)	Above-edge (eV)	μ (g^{-1} cm^2)	RE	ρ(g cm^{-3})	f(g g^{-1})
C 1s	280.0	289.0	51400	1	1.4	0.58

ρ is density.
f is the mass fraction of the element of interest within its solid phase.

Table A.2 Energies, scaling factor and reference compounds used to map the total concentration of Ca, Fe, Al and Si using image difference maps.

Edge	Pre-edge (eV)	Peak (eV)	Scale factor (nm^{-1})	Reference compound
Ca 2p	350.3	352.6	0.025	$CaHPO_4 \cdot 2H_2O$
Fe 2p	704.0	709.8	0.015	$FeCl_3 \cdot 6H_2O$
Al 1s	1555.0	1570.4	0.002	Muscovite ($KAl_2(AlSi_3O_{10})(OH)_2$)
Si 1s	1830.0	1846.4	0.0014	Muscovite ($KAl_2(AlSi_3O_{10})(OH)_2$)

Table A.3 Carbon content in bulk soils and their different fractions (sand, silt and clay).

Location	C content ($g\ kg^{-1}$)				Fraction of total C associated with clay fraction (%)
	Bulk	Sand	Silt	Clay	
Summit	30.6 (0.3)	12.6 (0.9)	25.0 (0.1)	72.5 (0.1)	47.4
Footslope	27.6 (0.6)	9.9 (0.3)	22.0 (0.4)	68.7 (0.1)	59.7

Standard deviation errors shown in parentheses.

Table A.4 The characteristics of bulk soils.

Location	pH	Sand (%)	Silt (%)	Clay (%)	Texture class	Exch. Cations (meq/100g)				CEC @ pH7 (meq/100g)
						Ca	K	Mg	Na	
Summit	5.5	41	39	20	loam	6.53	0.35	1.66	0.06	17.40
Footslope	5.7	35	41	24	loam	5.51	0.21	1.72	0.02	15.89

Table A.5 Soil clay mineralogy by X-ray diffraction. X-ray diffractograms are shown in Figure A.13.

Location	Hydroxy-Interlayered Vermiculite (%)	Illite (%)	Kaolinite (%)
Summit	36	30	34
Footslope	25	29	46

Table A.6 Fe content from selective extractions and total digestion of soil clay fractions.

Location	Fe_t (%)	Fe_d (%)	Fe_o (%)	Fe_t-Fe_d (%)	Fe_d/Fe_t	Fe_o/Fe_d
Summit	5.85 (0.12)	2.50 (0.08)	0.51 (0.03)	3.35	0.43	0.20
Footslope	5.10 (0.10)	2.10 (0.06)	0.71 (0.05)	3.00	0.41	0.34

Fe_t, Fe_d and Fe_o refer to total Fe, dithionite and oxalate extractable Fe, respectively. Standard deviation errors shown in parentheses.

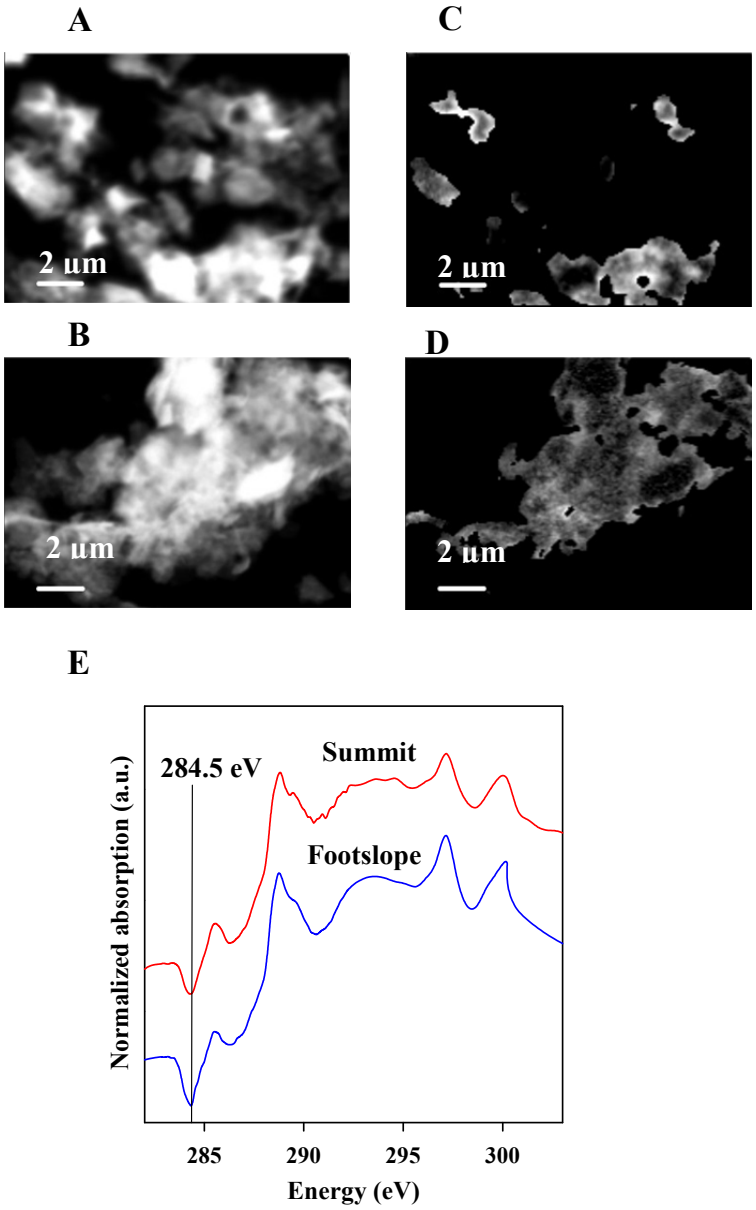

Figure A.3 Carbon pre-edge images at 282 eV of the (A) summit and (B) footslope soil clay particles. Carbon image difference maps (OD_{289}-OD_{282}) of the thick regions from the (C) summit and (D) footslope soil clay particles. (E) C 1s NEXAFS spectra extracted from the selected thick regions from the summit and footslope soil clay particles.

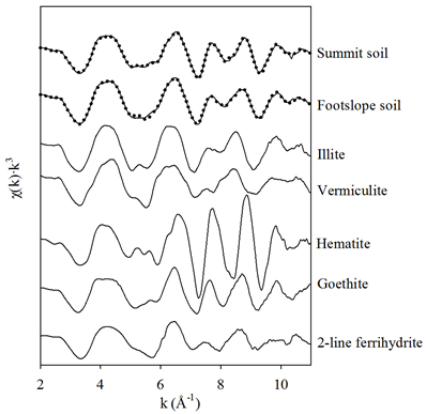

Figure A.4 Iron k^3-weighted chi spectra of the summit and footslope soil clay fractions and selected reference compounds. Solid lines are the collected data and dotted lines show the best linear combination fits.

Table A.7 Summary of Fe mineralogy of the summit and footslope soil clay fractions based on EXAFS linear combination fitting over a *k*-range of 2-11 $Å^{-1}$.

	Fe(III)-aluminosilicates		Fe(III) oxides			R-factor
	Vermiculite (%)	Illite (%)	2-line ferrihydrite (%)	Goethite (%)	Hematite (%)	
Summit	35	15	9	18	23	0.0078
Footslope	32	12	16	24	16	0.0086

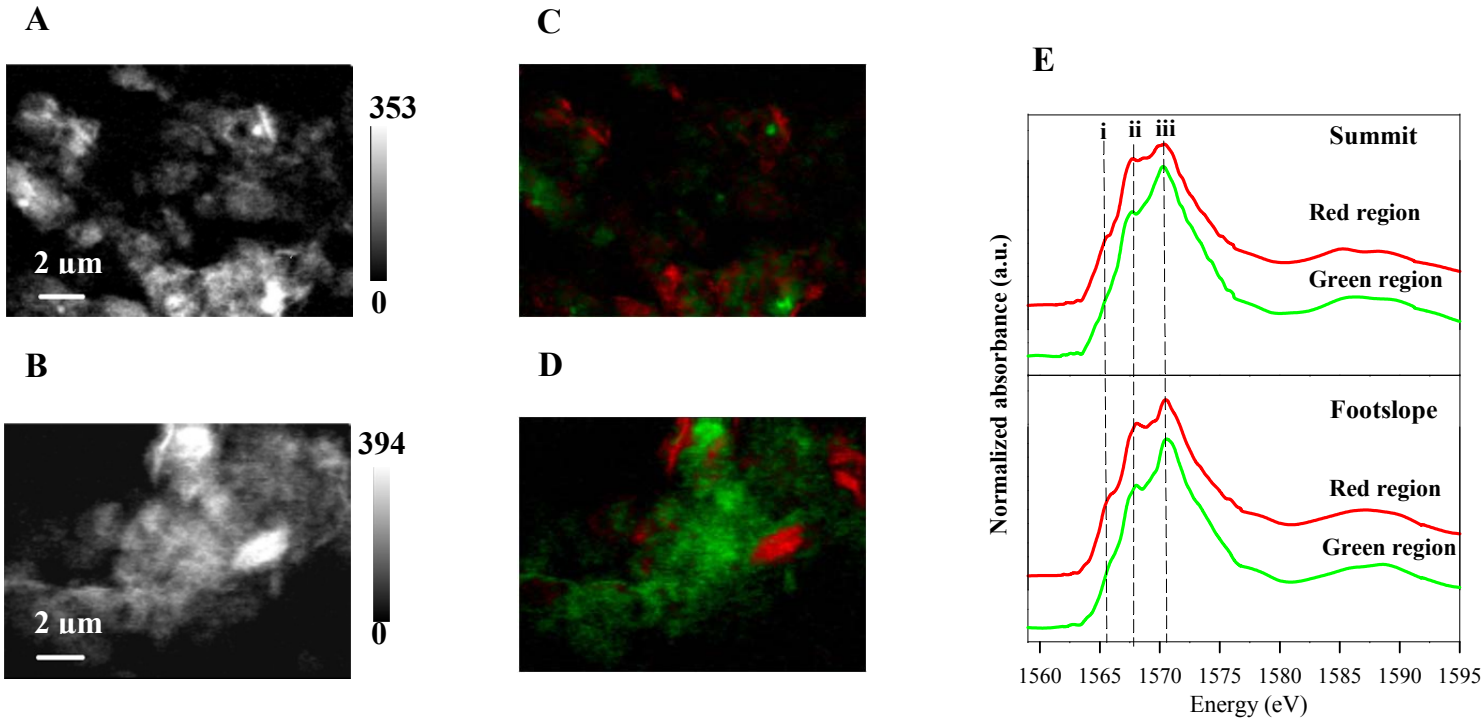

Figure A.5 Al distribution map ($OD_{1570.4}$-$OD_{1555.0}$) of the (A) summit and (B) footslope soil clay particles. The gray scale indicates thickness in nanometers. Al 1s cluster indices map showing the distribution of Al species in the (C) summit and (D) footslope soil clay particles with two distinct regions (red and green), respectively. (E) The Al 1s NEXAFS spectra were extracted from the regions in the cluster indices maps for the summit and footslope soil clay particles, respectively. Note the color of the spectra and the region's color from which they were extracted are the same. The vertical dashed lines correspond to (i) 1565.6, (ii) 1567.7, and (iii) 1570.4 eV.

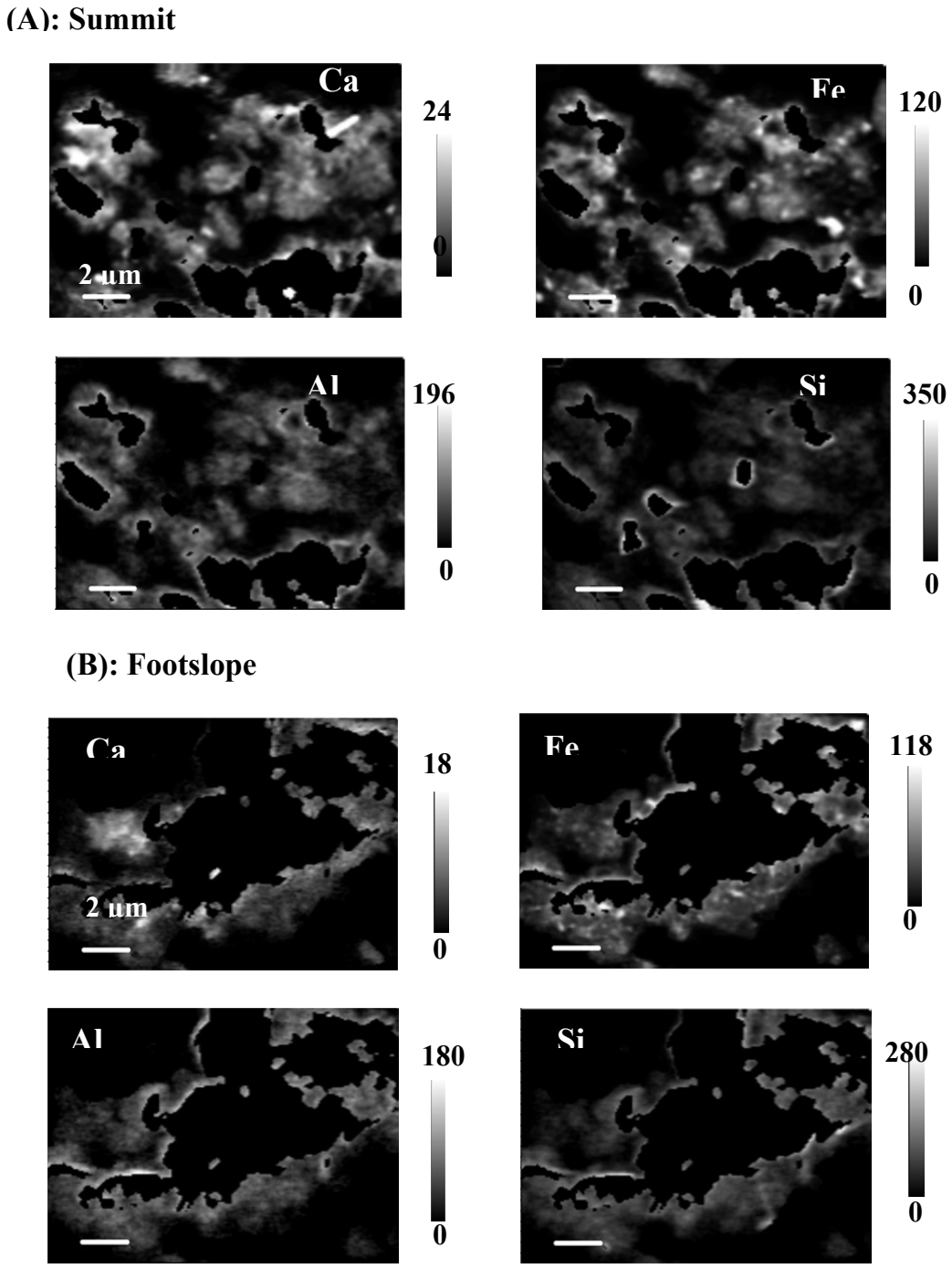

Figure A.6 Ca, Fe, Al and Si distribution maps of the thin regions from the (A) summit and (B) footslope soil clay particles. The gray scale indicates thickness in nanometers.

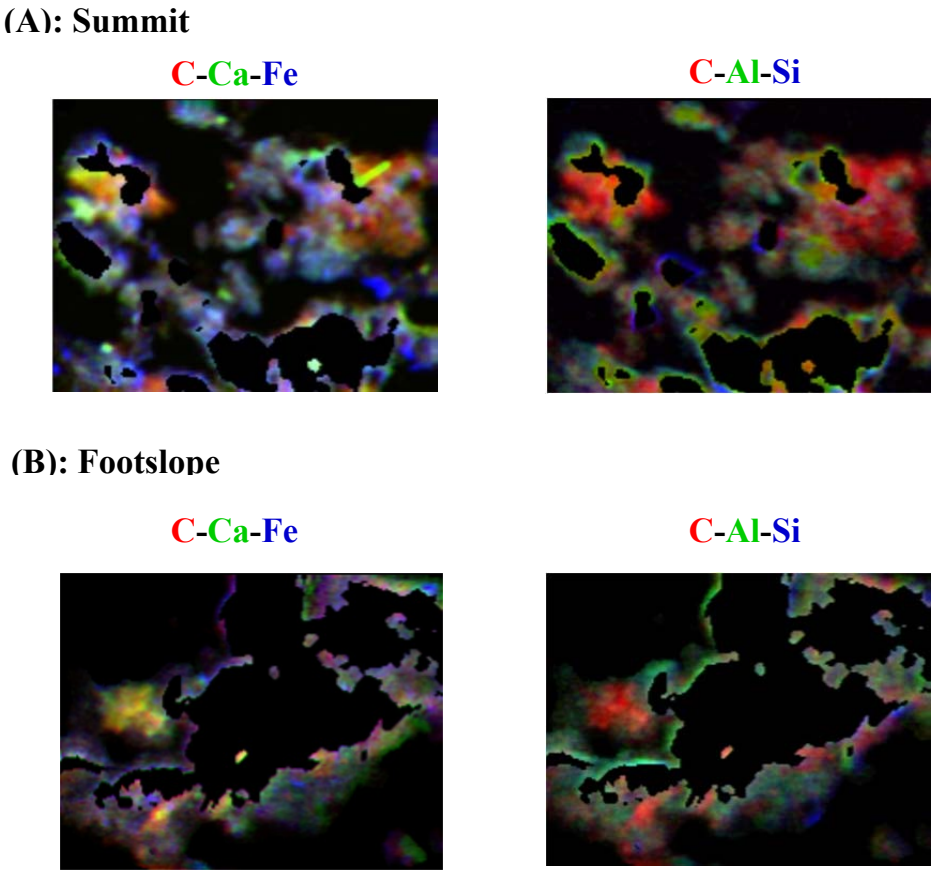

Figure A.7 Rescaled color-coded composite maps of C-Ca-Fe and C-Al-Si derived from image difference maps of the thin regions for the summit (A) and footslope (B) soil clay particles. The color of the symbol (e.g., C) is the color of the layer.

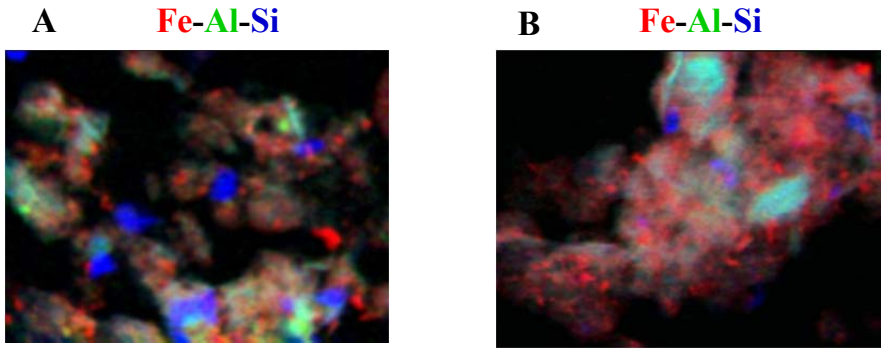

Figure A.8 Rescaled color-coded composite maps of Fe-Al-Si derived from image difference maps for the summit (A) and footslope (B) soil clay particles. The color of the symbol (e.g., Fe) is the color of the layer.

(A): Summit

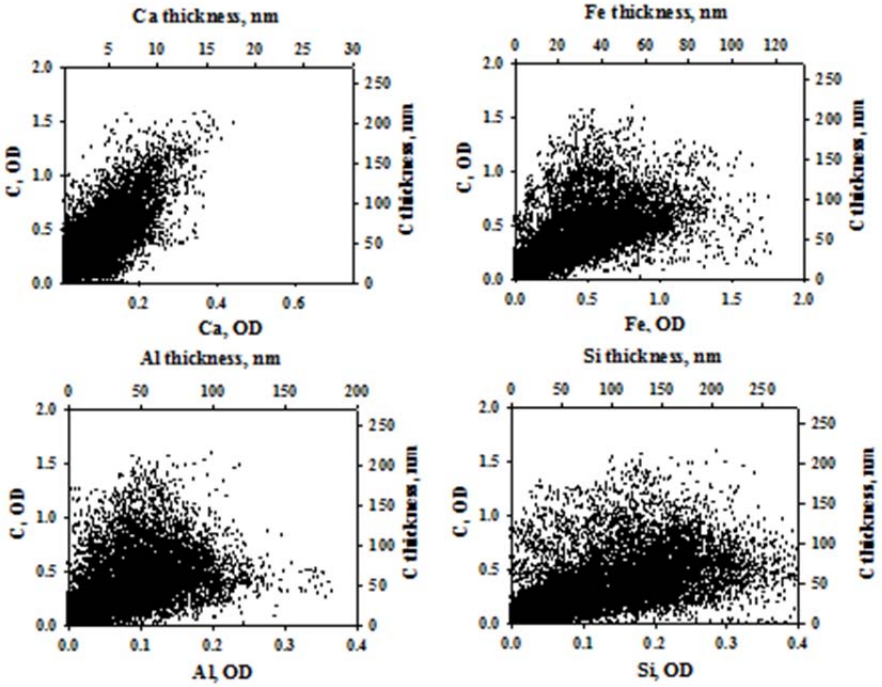
Ca thickness, nm
Ca, OD
C, OD
C thickness, nm
Fe thickness, nm
Fe, OD
Al thickness, nm
Al, OD
Si thickness, nm
Si, OD

(B): Footslope

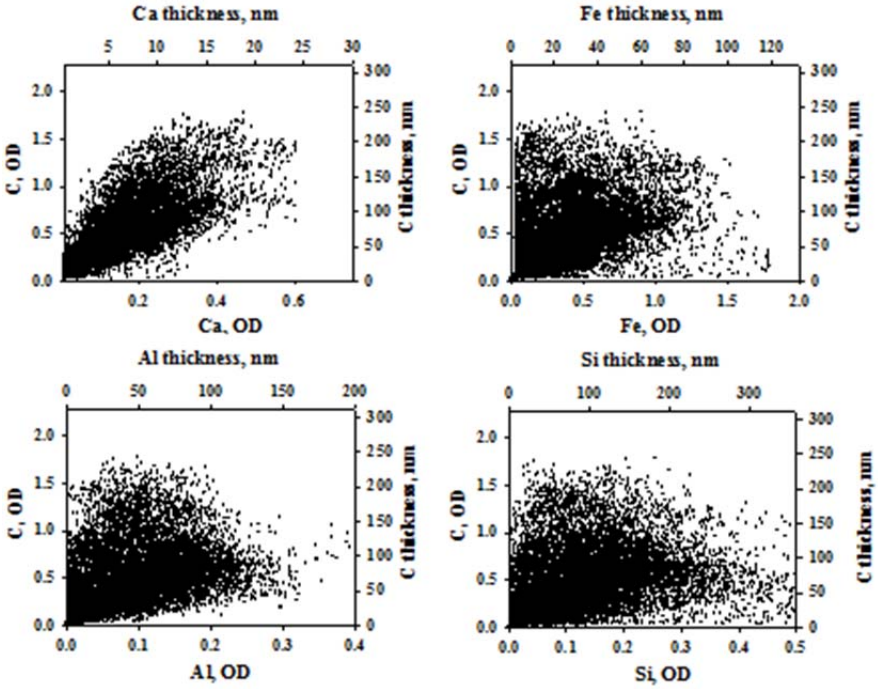

Figure A.9 C-Ca, C-Fe, C-Al and C-Si correlation plots of thickness values obtained from STXM elemental distribution maps of the thin regions (as shown in Figure 1A-B and Figure A.6A-B) from the (A) summit and (B) footslope soil clay particles. Linear correlation coefficients for these plots and other elemental relations are provided in Table 3.1.

(A): Summit

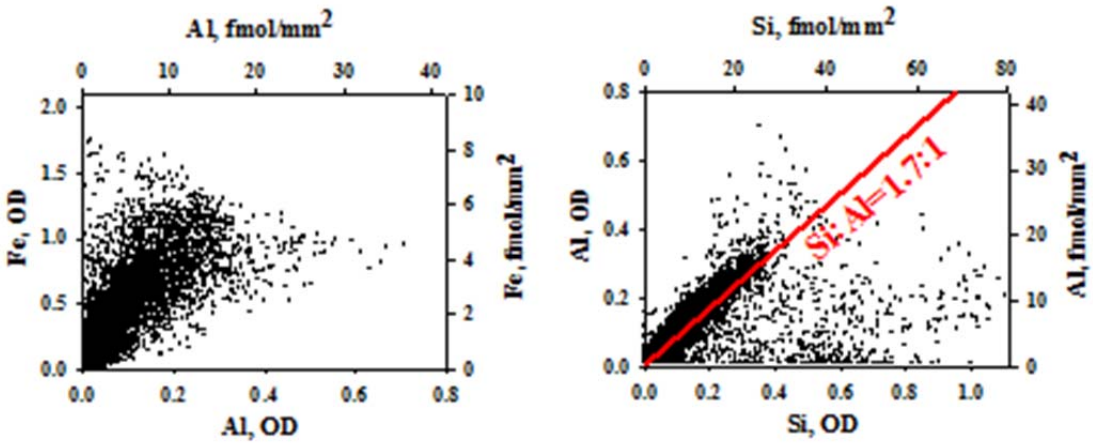

(B): Footslope

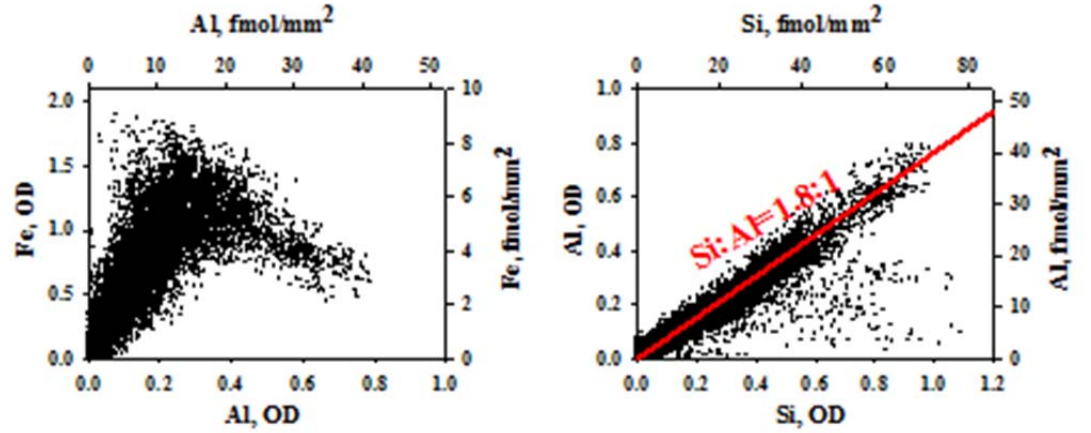

Figure A.10 Fe-Al and Al-Si correlation plots of thickness values obtained from STXM elemental distribution maps (as shown in Fig.3.3A-B, Fig.3.4A-B, and Fig.A.5A-B) from the (A) summit and (B) footslope soil clay particles. Linear correlation coefficients for these plots and other elemental relations are provided in Table 3.1.

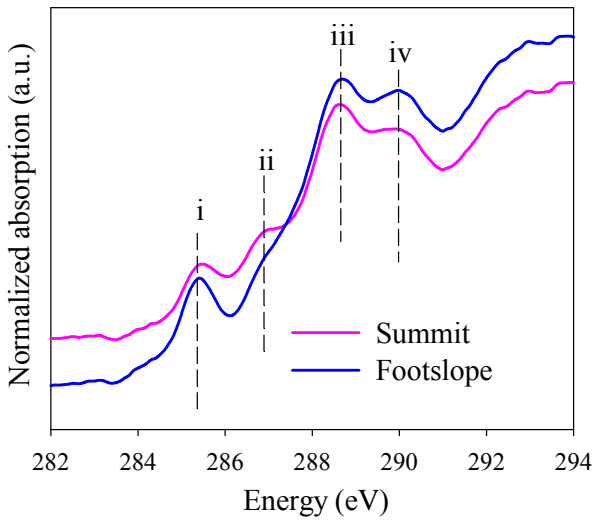

Figure A.11 Bulk C 1s NEXAFS spectra of the summit and footslope soil clay fractions from SGM beamline: (i) 285.5 eV; (ii) 287.4 eV; (3) 288.6 eV; (4) 289.5 eV.

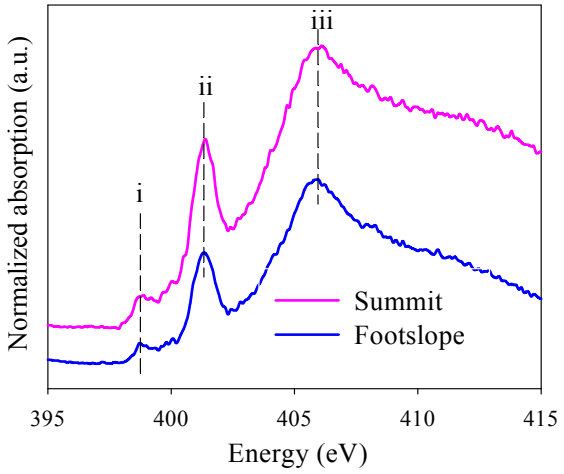

Figure A.12 Bulk N NEXAFS spectra of the summit and footslope soil clay fractions from SGM beamline: (i) 398.7 V; (ii) 401.2 eV; (iii) 405.8 eV.

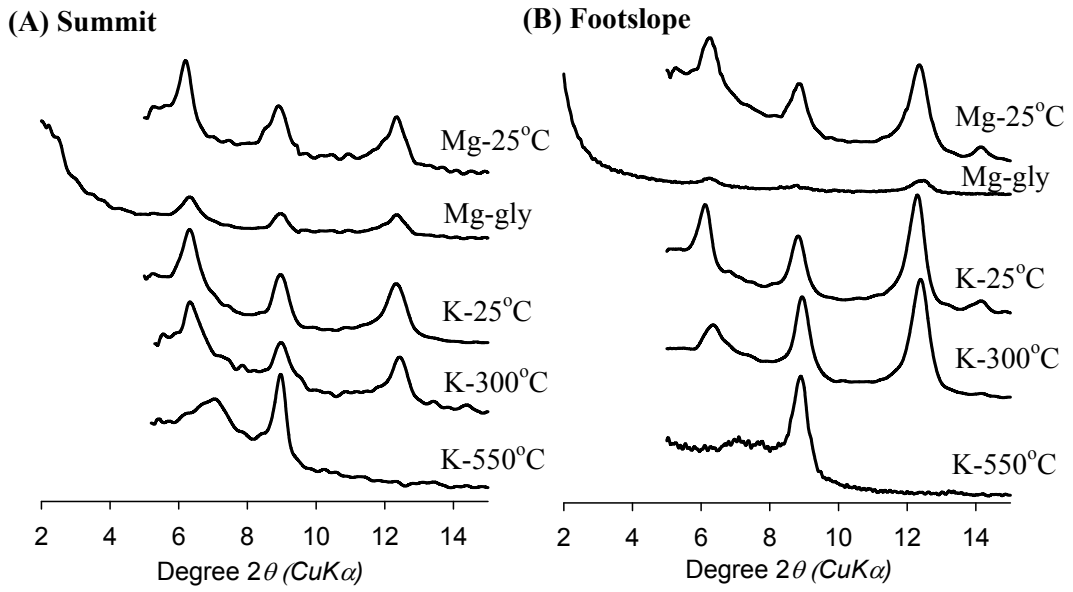

Figure A.13 The X-ray diffractograms of the (A) summit and (B) footslope soil clay fractions.

Appendix B

ADDITIONAL FIGURE OF CHAPTER 4

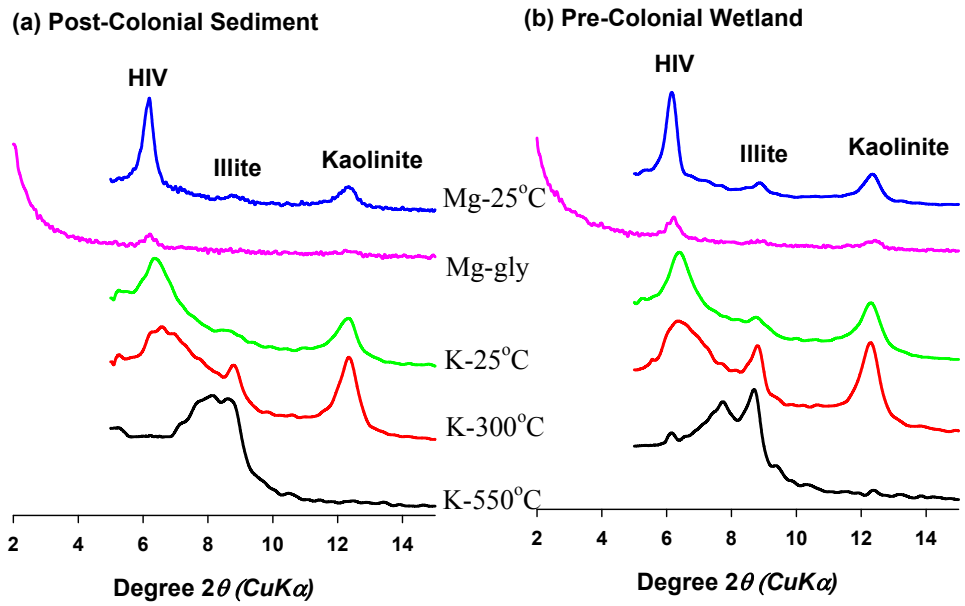

Figure B.1 X-ray diffractograms of the clay fractions separated from the post-colonial sediment and the pre-colonial buried wetland.

Appendix C

ADDITIONAL FIGURES OF CHAPTER 5

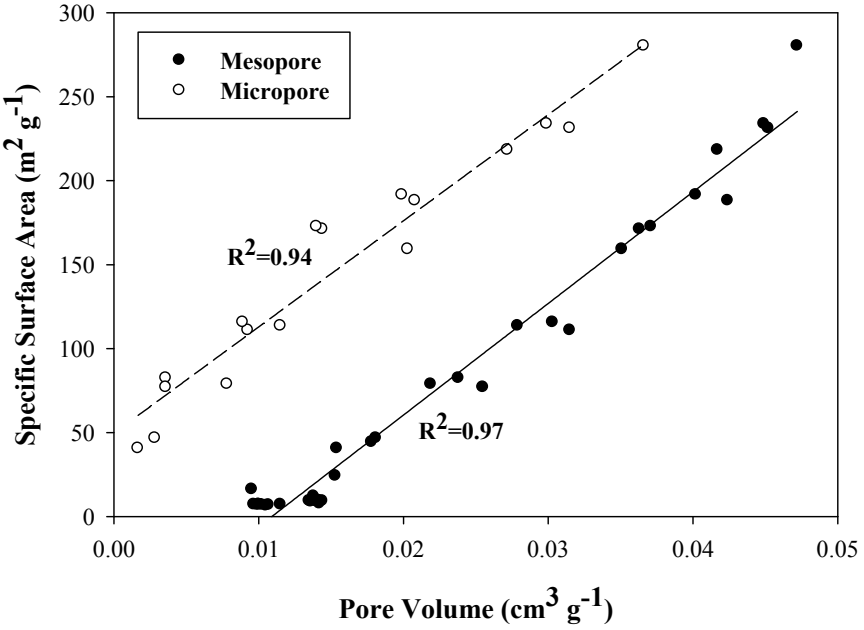

Figure C.1 Correlation between specific surface area and micro- and mesopore volumes. The correlation coefficients (R^2) were shown on the plots.

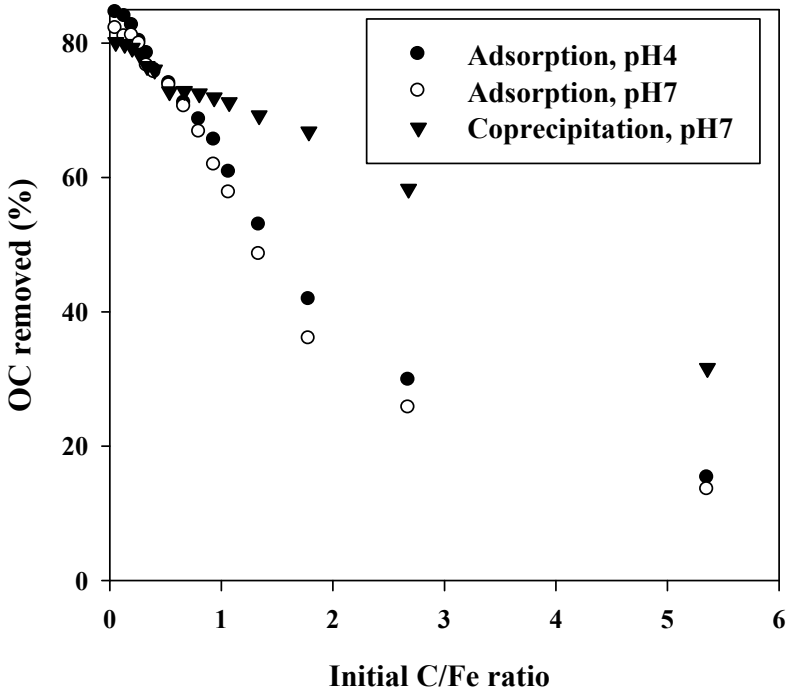

Figure C.2 The portion of organic carbon uptake from solution by coprecipitation and adsorption as a function of the initial C/Fe ratio.

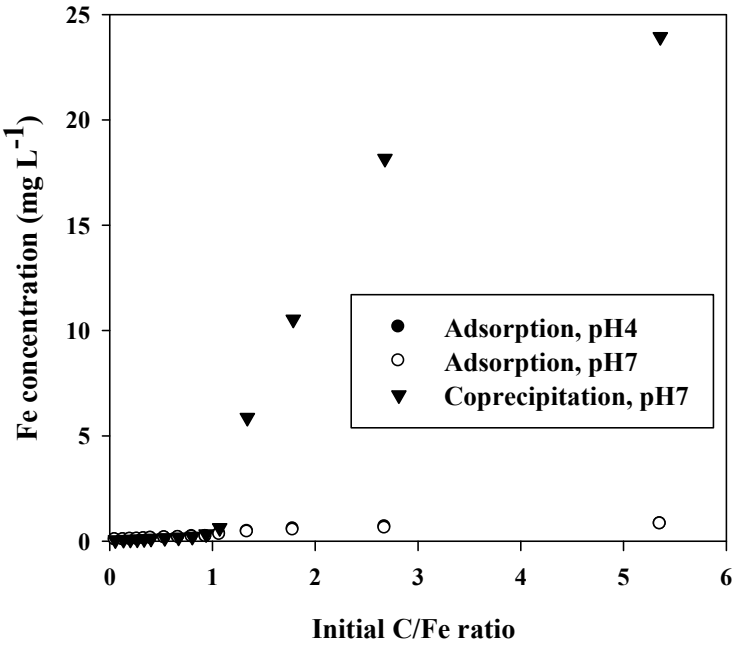

Figure C.3 Fe concentration in the remaining solution after coprecipitation and adsorption as a functional of the initial C/Fe ratio.

Appendix D

ADDITIONAL TABLES AND FIGURES OF CHAPTER 6

Table D.1 Energies, scaling factor and reference compounds used to map the total concentration of C and Fe using image difference maps.

Edge	Pre-edge (eV)	Peak (eV)	Scale factor (nm^{-1})	Reference compound
C 1s	282.0	288.4	0.0091	albumin
Fe 2p	704.0	709.8	0.015	$FeCl_3 \cdot 6H_2O$

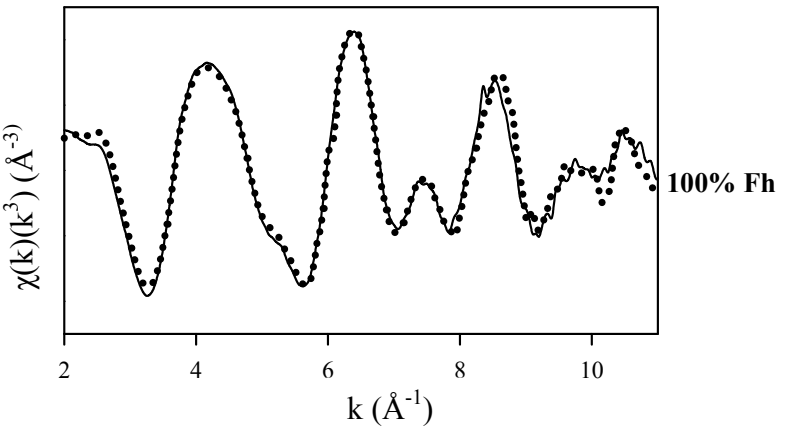

Figure D.1 Iron k^3-weighted EXAFS spectra of the adsorptive complexes with C loadings of 1.30 mg C m^{-2} SA. Dotted lines show linear combination fits over a *k*-range of 2-11 $Å^{-1}$ using pure ferrihydrite (Fh) and organic matter-Fe(III) complex as fit components. The numbers to the right of the spectrum give the corresponding linear-combination-fitting (LCF) results of EXAFS.

Table D.2 Peak assignments for FTIR spectra of organic matter samples according to Gu et al., Swift, Chorover and Amistadi, Fu and Quan, Artz et al., Heckman et al., Oren and Chefetz (and references therein).

Peak position (cm^{-1})	Assignment
1730	Symmetric C=O stretch of esters
1596-1616	Asymmetric COO^- stretch
1520	Aromatic C=C stretching
1460	CH_2 scissoring
1400	Symmetric COO^-stretch
1378-1390	COO-metal stretch
1270	O–H stretching of phenolic OH
1130	C–O stretch of carbohydrates
1080	C–O stretch of carbohydrates
1050	C–O stretch of carbohydrates

Table D.3 FTIR peak areas of the symmetric COO^- band.

	C loadings (mg C m^{-2} SA)	Peak position (cm^{-1})	Peak Area
Unreacted DOM		1400	18.5
Adsorptive complexes	0.52	1384	28.8
	0.95	1386	26.3
	1.30	1390	25.3
Coprecipitates	0.51	1378	36.2
	0.98	1380	34.0
	1.58	1386	30.7
	3.31	1388	29.5

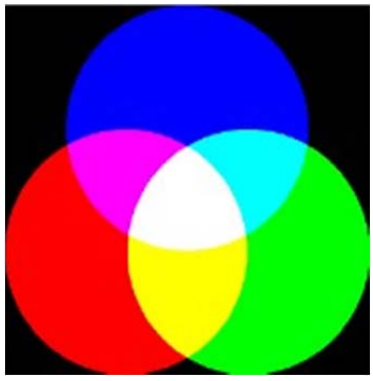

Figure D.2 Color indications of Red-Green-Blue (RGB) composite maps.

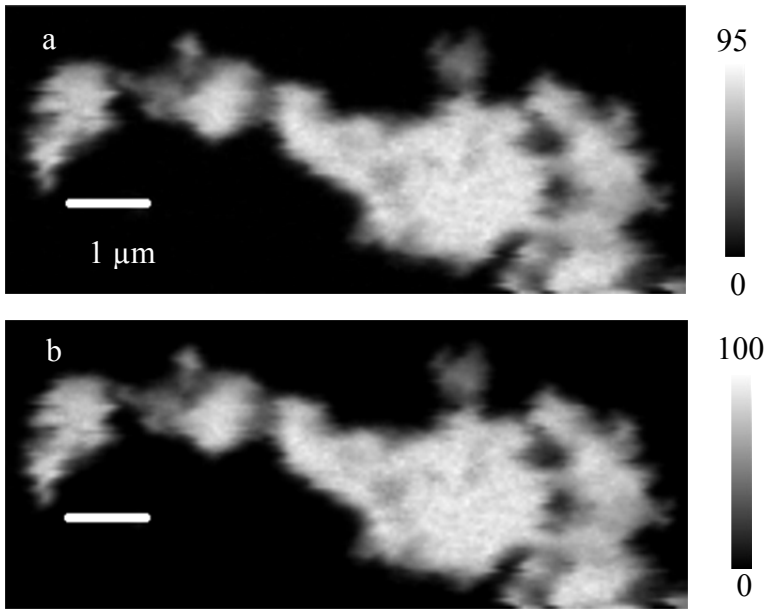

Figure D.3 STXM elemental distribution maps of (a) carbon and (b) iron for the adsorptive complexes with C loadings of 0.52 mg C m^{-2} SA. The gray scale indicates thickness in nanometers.

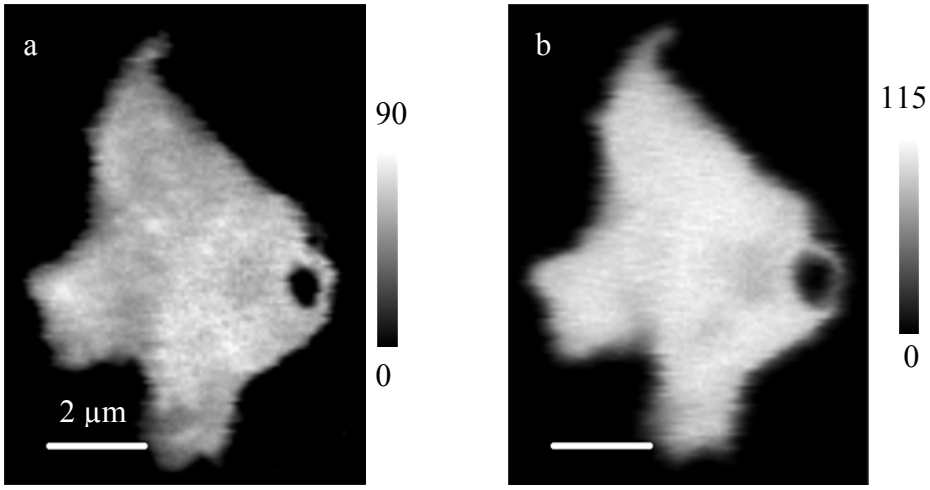

Figure D.4 STXM elemental distribution maps of (a) carbon and (b) iron for the coprecipitates with C loadings of 0.51 mg C m^{-2} SA. The gray scale indicates thickness in nanometers.

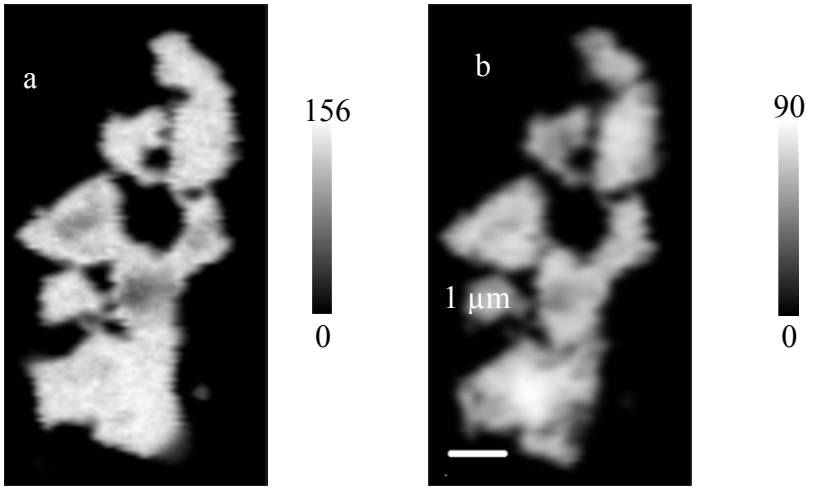

Figure D.5 STXM elemental distribution maps of (a) carbon and (b) iron for the adsorptive complexes with C loadings of 1.30 mg C m^{-2} SA. The gray scale indicates thickness in nanometers.

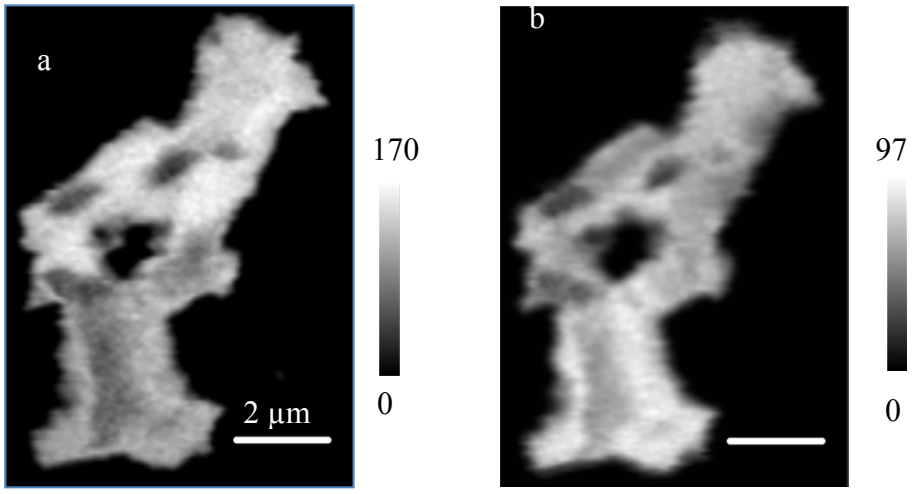

Figure D.6 STXM elemental distribution maps of (a) carbon and (b) iron for the coprecipitates with C loadings of 1.58 mg C m^{-2} SA. The gray scale indicates thickness in nanometers.

Additional elemental distribution and color-coded composite maps and correlation plots of carbon and iron from STXM technique.

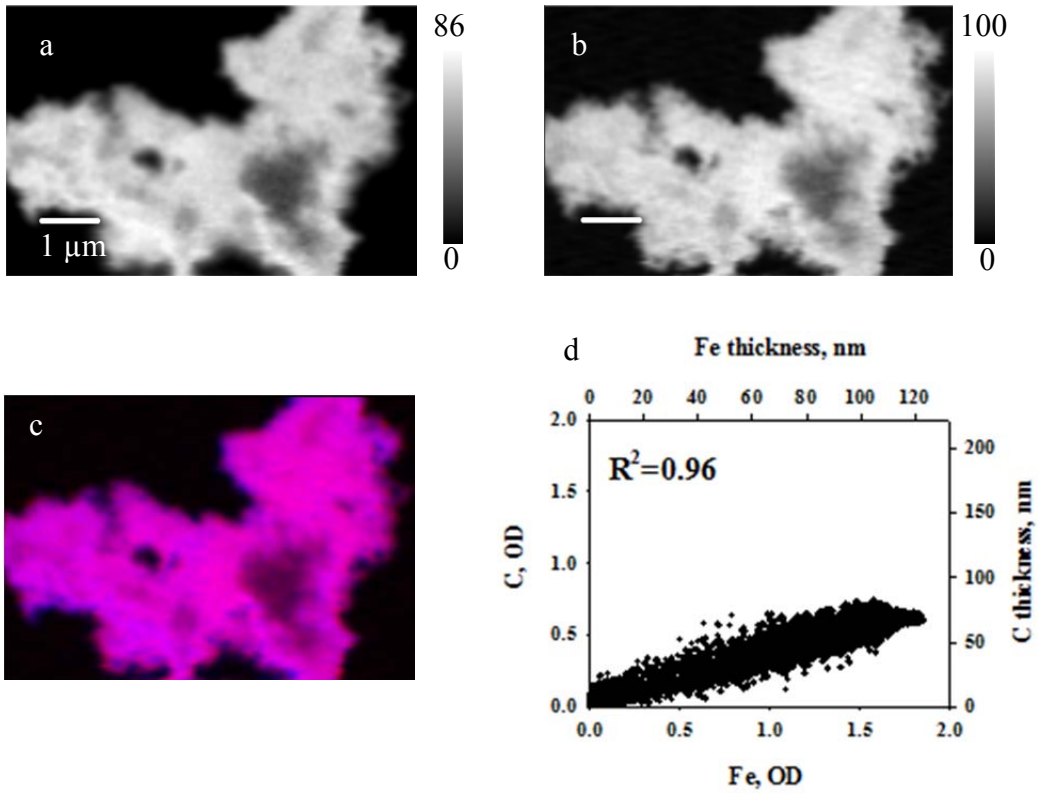

Figure D.7 STXM elemental distribution maps of (a) carbon and (b) iron for the adsorptive complexes with C loadings of 0.52 mg C m^{-2} SA. The gray scale indicates thickness in nanometers. (c) Color-coded composite maps of (a) carbon and (b) iron (Carbon, blue; Iron, red). (d) Correlation plots of thickness values of (a) carbon and (b) iron obtained from STXM elemental distribution maps. Correlation coefficients (R^2) are provided on the plots.

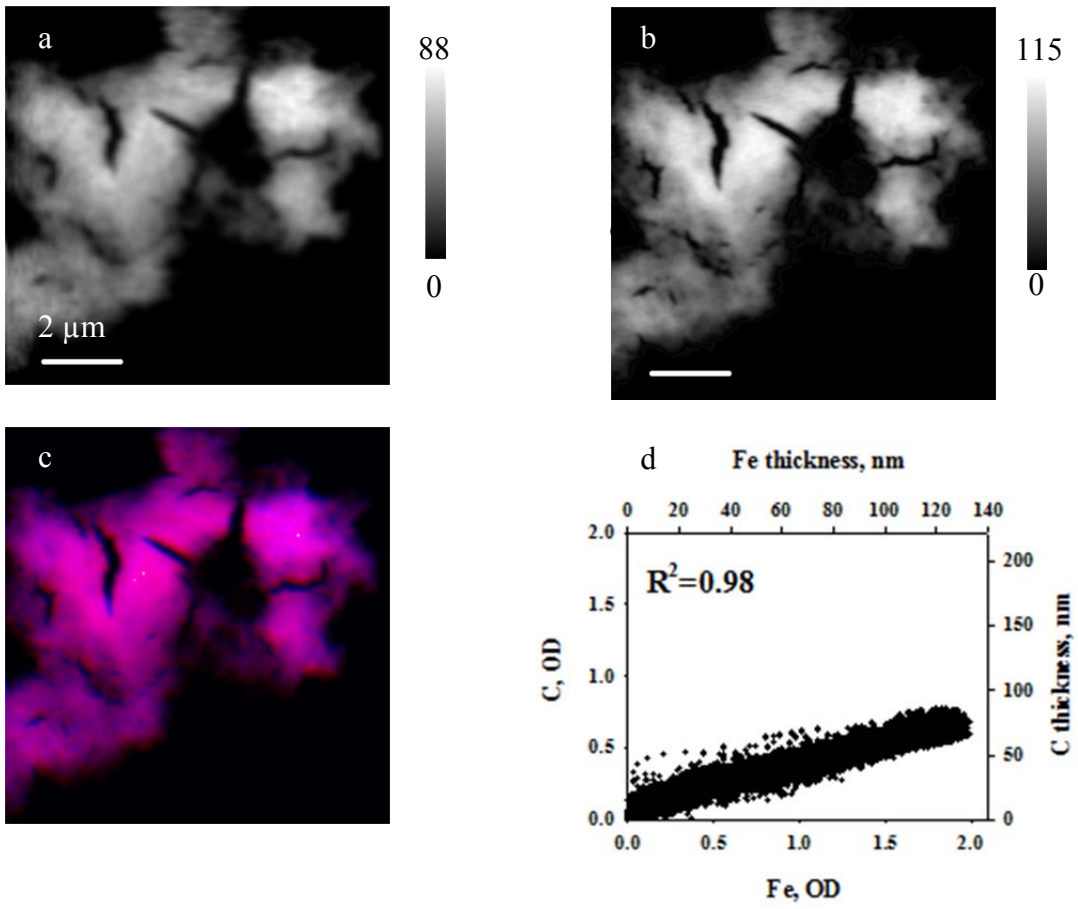

Figure D.8 STXM elemental distribution maps of (a) carbon and (b) iron for the coprecipitates with C loadings of 0.51 mg C m^{-2} SA. The gray scale indicates thickness in nanometers. (c) Color-coded composite maps of (a) carbon and (b) iron (Carbon, blue; Iron, red). (d) Correlation plots of thickness values of (a) carbon and (b) iron obtained from STXM elemental distribution maps. Correlation coefficients (R^2) are provided on the plots.

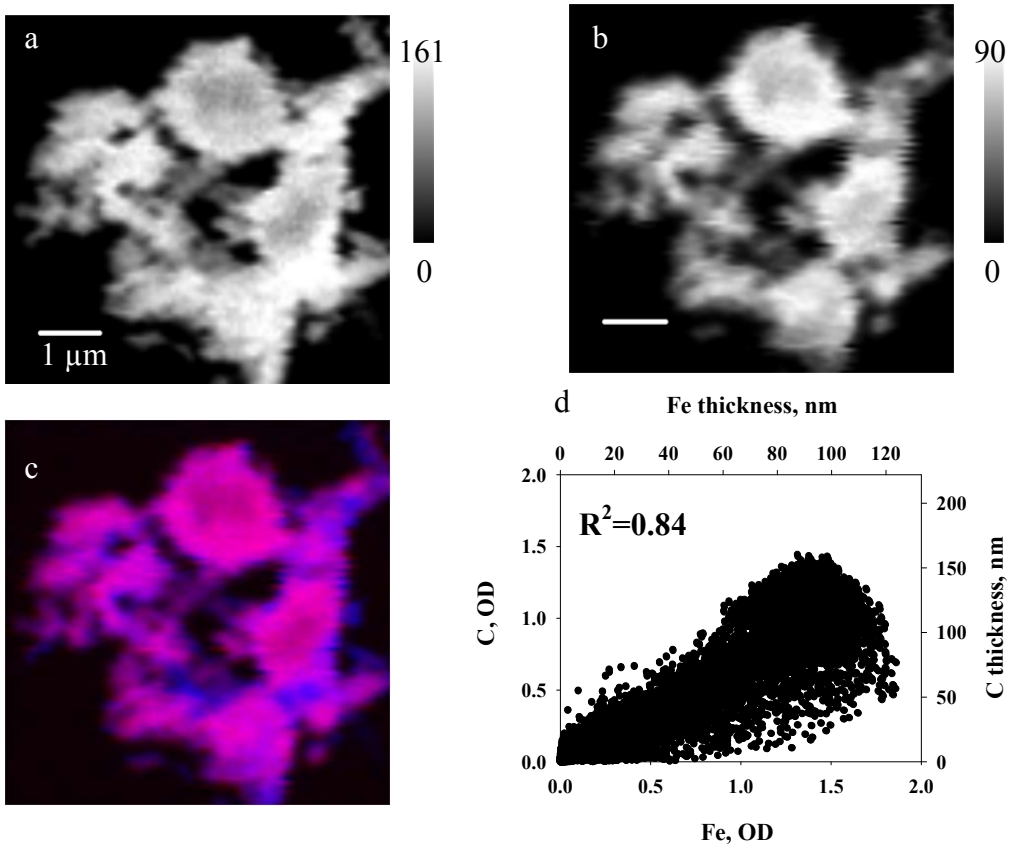

Figure D.9 STXM elemental distribution maps of (a) carbon and (b) iron for the adsorptive complexes with C loadings of 1.30 mg C m^{-2} SA. The gray scale indicates thickness in nanometers. (c) Color-coded composite maps of (a) carbon and (b) iron (Carbon, blue; Iron, red). (d) Correlation plots of thickness values of (a) carbon and (b) iron obtained from STXM elemental distribution maps. Correlation coefficients (R^2) are provided on the plots.

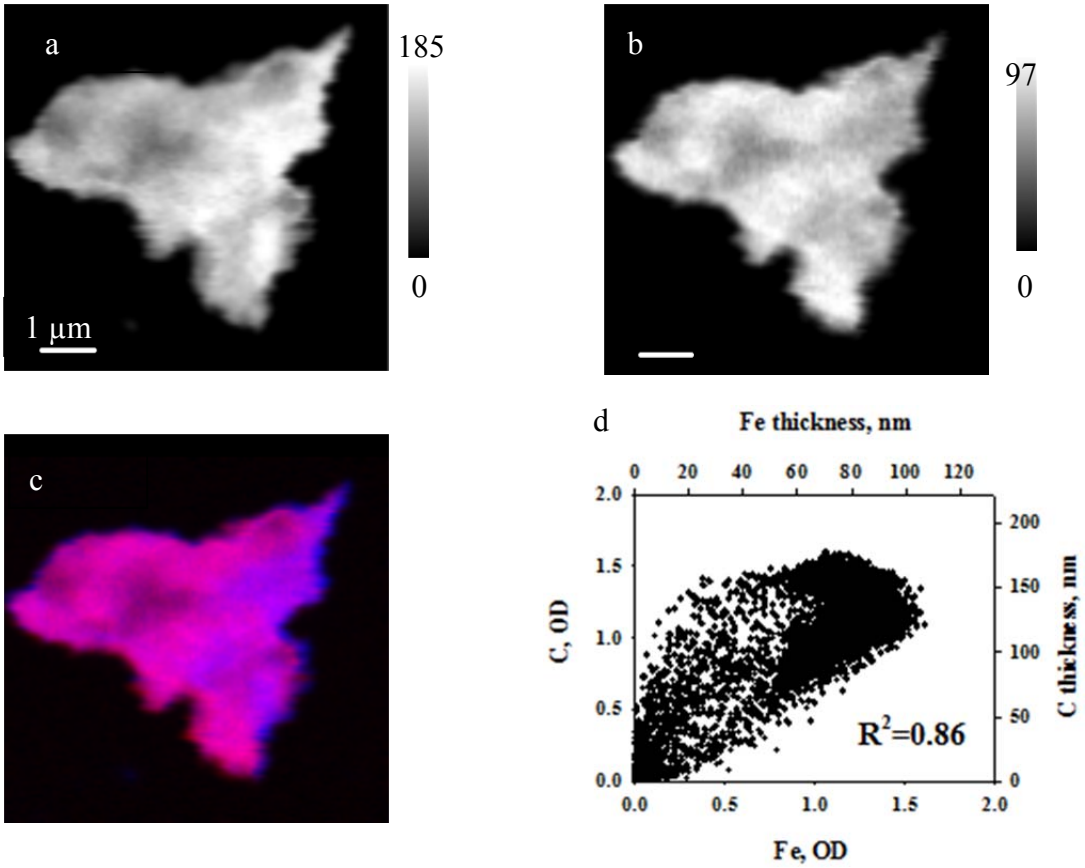

Figure D.10 STXM elemental distribution maps of (a) carbon and (b) iron for the coprecipitates with C loadings of 1.58 mg C m^{-2} SA. The gray scale indicates thickness in nanometers. (c) Color-coded composite maps of (a) carbon and (b) iron (Carbon, blue; Iron, red). (d) Correlation plots of thickness values of (a) carbon and (b) iron obtained from STXM elemental distribution maps. Correlation coefficients (R^2) are provided on the plots.

References in Appendix D

Gu, B.; Schmitt, J.; Chen, Z.; Liang, L; McCarthy, J. F., Adsorption and desorption of natural organic matter on iron oxide: mechanisms and models. *Environ. Sci. Technol*. **1994**, 28, 38-46.

Gu, B.; Schmitt, J.; Chen, Z.; Liang, L.; McCarthy, J. F., Adsorption and desorption of different organic matter fractions on iron oxide. *Geochim. Cosmochim. Acta* **1995**, 59(2), 219-229.

Swift, R. S., Organic matter characterization. In Methods of Soil Analysis: Part 3, Chemical Methods, SSSA Book Series 5 (ed. D. L. Sparks et al.). Soil Science Society of America, Madison, WI, **1996**, pp. 1018-1020.

Chorover, J.; Amistadi, M. K., Reaction of forest floor organic matter at goethite, birnessite and smectite surfaces. *Geochim. Cosmochim. Acta* **2001**, 65(1), 95-109.

Fu, H.; Quan, X., Complexes of fulvic acid on the surface of hematite, goethite, and akaganeite: FTIR observation. *Chemosphere* **2006**, 63, 403-410.

Artz, R. R. E.; Chapman, S. J.; Robertson, A. H. J.; Potts, J. M.; Laggoun-Defarge, F.; Gogo S.; Comont, L.; Disnar, J. R.; Francez, A. J., FTIR spectroscopy can be used as a screening tool for organic matter quality in regenerating cutover peat lands. *Soil Biol. Biochem.* **2008**, 40, 515-527.

Heckman, K.; Vazquez-Ortega, A.; Gao, X.; Chorover, J.; Rasmussen, C., Changes in water extractable organic matter during incubation of forest floor material in the presence of quartz, goethite and gibbsite surfaces. *Geochim. Cosmochim. Acta* **2011**, 75, 4295-4309.

Oren, A.; Chefetz, B., Sorptive and Desorptive Fractionation of Dissolved Organic Matter by Mineral Soil Matrices. *J. Environ. Qual.* **2012**, 41, 526-533.